



*Research Project Number TPF-5(193) Supplement #75
NDOR Sponsoring Agency Code RHE-08*

LENGTH OF NEED AND MINIMUM SYSTEM LENGTH FOR F-SHAPE PORTABLE CONCRETE BARRIER

Submitted by

Robert W. Bielenberg, M.S.M.E., E.I.T.
Research Associate Engineer

Dylan T. Meyer
Undergraduate Research Assistant

Ronald K. Faller, Ph.D., P.E.
Research Associate Professor
MwRSF Director

John D. Reid, Ph.D.
Professor

MIDWEST ROADSIDE SAFETY FACILITY

Nebraska Transportation Center
University of Nebraska-Lincoln
130 Whittier Research Center
2200 Vine Street
Lincoln, Nebraska 68583-0853
(402) 472-0965

Submitted to

NEBRASKA DEPARTMENT OF ROADS
1500 Nebraska Highway 2
Lincoln, Nebraska 68502

SMART WORK ZONE DEPLOYMENT INITIATIVE
Iowa State University
2711 S. Loop Drive, Suite 4700
Ames, Iowa 50010-8664

Sponsored by

NEBRASKA DEPARTMENT OF ROADS
Research Project No. TPF-5(193) Supplement #75

SMART WORK ZONE DEPLOYMENT INITIATIVE
(TPF-5(295) Contract No. 16346)

MwRSF Research Report No. TRP-03-337-17

May 3, 2017

TECHNICAL REPORT DOCUMENTATION PAGE

1. Report No. TRP-03-337-17	2.	3. Recipient's Accession No.	
4. Title and Subtitle Length of Need and Minimum System Length for F-Shape Portable Concrete Barrier		5. Report Date May 3, 2017	
		6.	
7. Author(s) Bielenberg, R.W., Meyer, D.T., Faller, R.K., and Reid, J.D.		8. Performing Organization Report No. TRP-03-337-17	
9. Performing Organization Name and Address Midwest Roadside Safety Facility (MwRSF) Nebraska Transportation Center University of Nebraska-Lincoln 130 Whittier Research Center 2200 Vine Street Lincoln, Nebraska 68583-0853		10. Project/Task/Work Unit No.	
		11. Contract © or Grant (G) No. NDOR: TPF-5(193) Supplement #75 SWZDI TPF-5(295) Contract No. 16346 FHWA Pooled Fund Study TPF-5(081) InTrans Project No. 15-535	
12. Sponsoring Organization Name and Address <div style="display: flex; justify-content: space-between;"> <div>Nebraska Department of Roads 1500 Nebraska Highway 2 Lincoln, Nebraska 68502</div> <div>Smart Work Zone Deployment Initiative Iowa Department of Transportation 800 Lincoln Way Ames, Iowa 50010</div> </div> Federal Highway Administration U.S. Department of Transportation 1200 New Jersey Avenue SE Washington, DC 20590		13. Type of Report and Period Covered Final Report: 2014 – 2017	
		14. Sponsoring Agency Code	
15. Supplementary Notes Prepared in cooperation with U.S. Department of Transportation, Federal Highway Administration. Visit www.intrans.iastate.edu/smartwz/ for color pdfs of this and other Smart Work Zone Deployment Initiative research reports.			
16. Abstract <p>Portable concrete barrier (PCB) systems are often used to redirect errant vehicles through a combination of inertial resistance, lateral friction loads, and tensile loads developed from the mass and friction of the barrier segments. State departments of transportation (DOTs) and other end users may wish to utilize minimal length PCB installations to shield a hazard or work zone or limit the number of barriers required on the upstream and downstream ends to reduce overall system length. However, concerns with the performance of shorter PCB installations include increased lateral deflections and working widths and barrier pocketing. Additionally, no impact testing has been performed near the upstream or downstream ends of the free-standing PCB system to determine the limits of the length of need (LON) of the system. These impacts may increase the potential for gating through the system, pocketing, rapid deceleration, and/or vehicle instability.</p> <p>The objective of this research study was to investigate and evaluate the safety performance of a previously developed F-shape PCB system to determine minimum system length and the number of barriers required for the beginning and end of the LON. LS-DYNA simulation modeling was applied to determine potential beginning and end of LON points on reduced system lengths to select a configuration for full-scale testing and evaluation of a minimum length PCB system. A 100-ft long PCB installation was selected, and full-scale crash testing was conducted on the beginning and end of LON of the reduced length system. Test no. NELON-1 was conducted to MASH test designation 3-35 criteria on the beginning of LON of the 100-ft long PCB installation, and the vehicle was safely redirected. Test no. NELON-2 was conducted to modified MASH test designation no. 3-37 criteria on the end of LON of the 100-ft long PCB installation, but the test was deemed a failure as the vehicle demonstrated a roll angle in excess of 75 degrees. Review of the crash test results suggested that a nine barrier or 112.5-ft long PCB installation would perform acceptably.</p>			
17. Document Analysis/Descriptors Highway Safety, Crash Test, Roadside Appurtenances, Compliance Test, Portable Concrete Barrier, Work Zone, F-Shape, Length of Need, LON, Concrete Protection Barrier		18. Availability Statement No restrictions. Document available from: National Technical Information Services, Springfield, Virginia 22161	
19. Security Class (this report) Unclassified	20. Security Class (this page) Unclassified	21. No. of Pages 225	22. Price

DISCLAIMER STATEMENT

This report was completed with funding from the Federal Highway Administration, U.S. Department of Transportation, the Midwest States Smart Work Zone Deployment Initiative (SWZDI), and the Nebraska Department of Roads. The contents of this report reflect the views and opinions of the authors who are responsible for the facts and the accuracy of the data presented herein. The contents do not necessarily reflect the official views or policies of SWZDI, the Nebraska Department of Roads, the Federal Highway Administration, or the U.S. Department of Transportation. This report does not constitute a standard, specification, regulation, product endorsement, or an endorsement of manufacturers.

ABOUT SWZDI

Iowa, Kansas, Missouri, and Nebraska created the Midwest States Smart Work Zone Deployment Initiative in 1999 and Wisconsin joined in 2001. Through this pooled-fund study, researchers investigate better ways of controlling traffic through work zones. Their goal is to improve the safety and efficiency of traffic operations and highway work. The project is now administered by Iowa State University's Institute for Transportation.

UNCERTAINTY OF MEASUREMENT STATEMENT

The Midwest Roadside Safety Facility (MwRSF) has determined the uncertainty of measurements for several parameters involved in standard full-scale crash testing and non-standard testing of roadside safety features. Information regarding the uncertainty of measurements for critical parameters is available upon request by the sponsor and the Federal Highway Administration.

INDEPENDENT APPROVING AUTHORITY

The Independent Approving Authority (IAA) for the data contained herein was Ms. Karla Lechtenberg, Research Associate Engineer.

QUALITY ASSURANCE STATEMENT

The Federal Highway Administration (FHWA) provides high-quality information to serve Government, industry, and the public in a manner that promotes public understanding. Standards and policies are used to ensure and maximize the quality, objectivity, utility, and integrity of its information. The FHWA periodically reviews quality issues and adjusts its programs and processes to ensure continuous quality improvement.

IOWA DEPARTMENT OF TRANSPORTATION STATEMENTS

Federal and state laws prohibit employment and/or public accommodation discrimination on the basis of age, color, creed, disability, gender identity, national origin, pregnancy, race, religion, sex, sexual orientation or veteran's status. If you believe you have been discriminated against, please contact the Iowa Civil Rights Commission at 800-457-4416 or the Iowa Department of Transportation affirmative action officer. If you need accommodations because of a disability

to access the Iowa Department of Transportation's services, contact the agency's affirmative action officer at 800-262-0003.

The preparation of this report was financed in part through funds provided by the Iowa Department of Transportation through its "Second Revised Agreement for the Management of Research Conducted by Iowa State University for the Iowa Department of Transportation" and its amendments.

The opinions, findings, and conclusions expressed in this publication are those of the authors and not necessarily those of the Iowa Department of Transportation or the U.S. Department of Transportation Federal Highway Administration.

ACKNOWLEDGEMENTS

The authors wish to acknowledge several sources that made a contribution to this project: (1) Nebraska Department of Roads and the Smart Work Zone Deployment Initiative for sponsoring this project and (2) MwRSF personnel for assisting in the completion of this project.

This research was conducted under the Smart Work Zone Deployment Initiative (SWZDI) and Federal Highway Administration (FHWA) Pooled Fund Study TPF-5(081), involving the following state departments of transportation:

- Iowa (lead state)
- Kansas
- Missouri
- Nebraska
- Wisconsin

The authors would like to thank the FHWA, the Iowa Department of Transportation (DOT), and the other pooled fund state partners for their financial support and technical assistance.

Acknowledgement is also given to the following individuals who made a contribution to the completion of this research project.

Midwest Roadside Safety Facility

J.C. Holloway, M.S.C.E., E.I.T., Test Site Manager
K.A. Lechtenberg, M.S.M.E., E.I.T., Research Associate Engineer
S.K. Rosenbaugh, M.S.C.E., E.I.T., Research Associate Engineer
J.D. Schmidt, Ph.D., P.E., Research Assistant Professor
C.S. Stolle, Ph.D., Research Assistant Professor
A.T. Russell, B.S.B.A., Shop Manager
S.M. Tighe, Laboratory Mechanic
D.S. Charroin, Laboratory Mechanic
M.A. Rasmussen, Laboratory Mechanic
E.W. Krier, Laboratory Mechanic
Undergraduate and Graduate Research Assistants

Nebraska Department of Roads

Phil TenHulzen, P.E., Design Standards Engineer
Jim Knott, P.E., State Roadway Design Engineer
Jodi Gibson, Research Coordinator

Federal Highway Administration

John Perry, P.E., Nebraska Division Office
Danny Briggs, Nebraska Division Office

Iowa State University

Keith Knapp, Iowa LTAP Director, Smart Work Zone Deployment Initiative (SWZDI)

EXECUTIVE SUMMARY

Portable concrete barrier (PCB) systems are often used to redirect errant vehicles through a combination of inertial resistance, lateral friction loads, and tensile loads developed from the mass and friction of the barrier segments. Unfortunately, recommendations on minimum PCB system lengths have generally been limited to the 200-ft (61-m) length or longer in order to preserve the as-tested system deflections and impact behavior. In addition, guidance on the beginning and end of the length of need (LON) of these systems is typically given as a minimum of 100 ft (30.5 m) in order to preserve performance similar to existing crash tests.

State departments of transportation (DOTs) and other end users may wish to use shorter PCB installations to shield a hazard or work zone or limit the number of barriers required on the upstream and downstream ends to reduce overall system length. However, concerns with the performance of shorter PCB installations must be considered, including increased lateral deflections, working widths, and barrier pocketing, which could lead to vehicle instability or excessive decelerations. Additionally, no impact testing has been performed near the upstream or downstream ends of the free-standing PCB system to determine the limits of the LON of the system. Impacts at or near the barriers at the ends of a free-standing barrier system could produce very different barrier performance, and may include the potential for gating of the vehicle through the system, pocketing, rapid deceleration, and/or vehicle instability.

The objective of this research effort was to investigate and evaluate the safety performance of the previously developed F-shape PCB system in order to determine minimum system length and the number of barriers required for the beginning and end of the LON. LS-DYNA simulation was used to model MASH TL-3 impacts with a 2270P vehicle at varied locations along the PCB installation to determine the beginning and end of LON for a 200-ft (61-m) long system. Next, models impacting the selected beginning and end of LON points were conducted on reduced system lengths to select a configuration for full-scale testing and evaluation. A 100-ft (30.5-m) long PCB installation was selected, and full-scale crash testing was conducted at the beginning and end of LON of the reduced length system. Test no. NELON-1 was conducted according to MASH test designation no. 3-35 on the beginning of LON of the 100-ft (30.5-m) long PCB installation, and the vehicle was safely redirected. Test no. NELON-2 was conducted according to a modified MASH test designation no. 3-37 on the end of LON of the 100-ft (30.5-m) long PCB installation, however, the test was deemed a failure as the vehicle demonstrated a roll angle in excess of 75 degrees. Review of the crash test results suggested that a nine barrier or 112.5-ft (34-m) long PCB installation would perform acceptably. Additional computer simulation modeling was conducted to provide guidance for deflections and working widths of intermediate length installations as well as for impacts at the 85th percentile impact severity.

TABLE OF CONTENTS

TECHNICAL REPORT DOCUMENTATION PAGE	i
DISCLAIMER STATEMENT	ii
ABOUT SWZDI	ii
UNCERTAINTY OF MEASUREMENT STATEMENT	ii
INDEPENDENT APPROVING AUTHORITY	ii
QUALITY ASSURANCE STATEMENT	ii
IOWA DEPARTMENT OF TRANSPORTATION STATEMENTS	ii
ACKNOWLEDGEMENTS	iv
EXECUTIVE SUMMARY	vi
TABLE OF CONTENTS	vii
LIST OF FIGURES	x
LIST OF TABLES	xv
ACRONYMS, ABBREVIATIONS, AND SYMBOLS	xvi
1 INTRODUCTION	1
1.1 Problem Statement	1
1.2 Objectives	2
1.3 Scope	2
2 COMPONENT TESTING OF PCB FRICTION COEFFICIENTS	4
2.1 Purpose	4
2.2 Scope	4
2.3 Equipment and Instrumentation	5
2.3.1 Tensile-Load Cells	5
2.3.2 Digital Photography	5
2.4 Data Processing	5
3 FRICTION TESTING RESULTS AND DISCUSSION	7
3.1 Test No. TCBFA-1	7
4 BASELINE MODEL OF F-SHAPE PCB SYSTEM	9
4.1 PCB Model	9
4.2 Vehicle Models	11
4.3 Baseline Model Simulations	11
4.3.1 Chevy Silverado V3 Simulations	12

4.3.2 Chevy Silverado V3r Simulations	16
4.3.3 Chevy Silverado V2 Simulations.....	16
4.3.4 Baseline Model Conclusions.....	17
5 EVALUATION OF LENGTH OF NEED.....	23
5.1 Beginning of Length of Need Simulations	23
5.2 End of Length of Need Simulations.....	37
5.3 Selection of Beginning and End of LON for 16 PCB Simulations.....	49
6 EVALUATION OF REDUCED SYSTEM LENGTHS.....	51
6.1 Seven Barrier F-Shape PCB System Simulations.....	51
6.2 Eight-Barrier F-Shape PCB System Simulations	58
6.3 Selection of System Length for Full-Scale Testing	64
7 DESIGN DETAILS	65
8 TEST REQUIREMENTS AND EVALUATION CRITERIA	75
8.1 Test Requirements	75
8.2 Evaluation Criteria.....	76
9 TEST CONDITIONS.....	78
9.1 Test Facility	78
9.2 Vehicle Tow and Guidance System.....	78
9.3 Test Vehicles.....	78
9.4 Simulated Occupant	83
9.5 Data Acquisition Systems	83
9.5.1 Accelerometers	83
9.5.2 Rate Transducers.....	83
9.5.3 Retroreflective Optic Speed Trap	84
9.5.4 Digital Photography	84
10 FULL-SCALE CRASH TEST NO. NELON-1	89
10.1 Weather Conditions	89
10.2 Test Description	89
10.3 Barrier Damage	91
10.4 Vehicle Damage.....	92
10.5 Occupant Risk.....	93
10.6 Discussion	94
11 FULL-SCALE CRASH TEST NO. NELON-2	112
11.1 Weather Conditions	112
11.2 Test Description	112
11.3 Barrier Damage	114
11.4 Vehicle Damage.....	115
11.5 Occupant Risk.....	118
11.6 Discussion	119
12 DISCUSSION OF FULL-SCALE TEST RESULTS	136

13 ANALYSIS OF BARRIER DEFLECTIONS 142

 13.1 Simulation Calibration with Full-Scale Crash Test 142

 13.2 TL-3 PCB Deflections for Intermediate System Lengths 148

 13.3 85th Percentile Impact Severity PCB Deflections for Intermediate System
 Lengths 149

 13.4 Discussion 152

14 SUMMARY, CONCLUSIONS, AND RECOMMENDATIONS..... 156

 14.1 Recommendations 160

15 REFERENCES 161

16 APPENDICES 164

 Appendix A. Material Specifications 165

 Appendix B. Vehicle Center of Gravity Determination..... 175

 Appendix C. Vehicle Deformation Records..... 178

 Appendix D. Accelerometer and Rate Transducer Data Plots, Test No. NELON-1 191

 Appendix E. Accelerometer and Rate Transducer Data Plots, Test No. NELON-2.... 208

LIST OF FIGURES

Figure 1. Quasi-Static Pull Test Setup, Test No. TCBFA-1	4
Figure 2. Load Cell Arrangement, Test No. TCBFA-1	5
Figure 3. Force vs. Time, Test No. TCBFA-1	8
Figure 4. F-Shape PCB: (a) Actual and (b) Finite Element Model	10
Figure 5. Chevy Silverado 2270P Truck Model Variations	12
Figure 6. Crash Sequence - Standard Chevy Silverado V3 Model and Test No. 2214TB-2.....	14
Figure 7. Crash Sequence - Standard Chevy Silverado V3 Model and Test No. 2214TB-2.....	15
Figure 8. Overhead Sequential Views, Chevy Silverado V2 Model and Test No. 2214TB-2	18
Figure 9. Overhead Sequential Views, Chevy Silverado V2 Model and Test No. 2214TB-2	19
Figure 10. Downstream Sequential Views, Chevy Silverado V2 Model and Test No. 2214TB-2	20
Figure 11. Downstream Sequential Views, Chevy Silverado V2 Model and Test No. 2214TB-2	21
Figure 12. RSVVP Results, Chevy Silverado V2 Impact with F-Shape PCB Model	22
Figure 13. Simulation of Beginning of LON for 16-Barrier F-Shape PCB System, Overhead View, t=0.000 sec	25
Figure 14. Simulation of Beginning of LON for 16-Barrier F-Shape PCB System, Overhead View, t=0.400 sec	26
Figure 15. Simulation of Beginning of LON for 16-Barrier F-Shape PCB System, Overhead View, t=0.800 sec	27
Figure 16. Simulation of Beginning of LON for 16-Barrier F-Shape PCB System, Overhead View, t=1.100 sec	28
Figure 17. Simulation of Beginning of LON for 16-Barrier F-Shape PCB System, Downstream View, t=0.000 sec	29
Figure 18. Simulation of Beginning of LON for 16-Barrier F-Shape PCB System, Downstream View, t=0.400 sec	30
Figure 19. Simulation of Beginning of LON for 16-Barrier F-Shape PCB System, Downstream View, t=0.800 sec	31
Figure 20. Simulation of Beginning of LON for 16-Barrier F-Shape PCB System, Downstream View, t=1.100 sec	32
Figure 21. Beginning of LON Simulations, Maximum Lateral Barrier Deflections	33
Figure 22. Beginning of LON Simulations, Maximum Longitudinal Displacement of Barrier No. 1	34
Figure 23. Beginning of LON Simulations, Maximum Longitudinal Displacement of Barrier No. 16	35
Figure 24. Beginning of LON Connection Pin Deformation Comparison	36
Figure 25. Simulation of End of LON for 16-Barrier F-Shape PCB System, Overhead View, t=0.000 sec	38
Figure 26. Simulation of End of LON for 16-Barrier F-Shape PCB System, Overhead View, t=0.400 sec	39
Figure 27. Simulation of End of LON for 16-Barrier F-Shape PCB System, Overhead View, t=0.800 sec	40
Figure 28. Simulation of End of LON for 16-Barrier F-Shape PCB System, Overhead View, t=1.100 sec	41

Figure 29. Simulation of End of LON for 16-Barrier F-Shape PCB System, Downstream View, t=0.000 sec	42
Figure 30. Simulation of End of LON for 16-Barrier F-Shape PCB System, Downstream View, t=0.400 sec	43
Figure 31. Simulation of End of LON for 16-Barrier F-Shape PCB System, Downstream View, t=0.800 sec	44
Figure 32. Simulation of End of LON for 16-Barrier F-Shape PCB System, Downstream View, t=1.100 sec	45
Figure 33. End of LON Simulations, Maximum Lateral Barrier Deflections	46
Figure 34. End of LON Simulations, Maximum Longitudinal Displacement of Barrier No. 1	47
Figure 35. End of LON Simulations, Maximum Longitudinal Displacement of Barrier No. 16	48
Figure 36. End of LON Connection Pin Deformation Comparison	50
Figure 37. Simulation of Beginning of LON for 7-Barrier F-Shape PCB System, Overhead View	52
Figure 38. Simulation of Beginning of LON for 7-Barrier F-Shape PCB System, Downstream View	53
Figure 39. Simulation of Beginning of LON for 7-Barrier F-Shape PCB System, Barrier Knee Impact at Barrier Nos. 5 and 6 Joint	54
Figure 40. Simulation of End of LON for 7-Barrier F-Shape PCB System, Overhead View	55
Figure 41. Simulation of End of LON for 7-Barrier F-Shape PCB System, Downstream View	56
Figure 42. Simulation of End of LON for 7-Barrier F-Shape PCB System, Final Barrier Impact on Driver-Side Door	57
Figure 43. Simulation of Beginning of LON for 8-Barrier F-Shape PCB System, Overhead View	59
Figure 44. Simulation of Beginning of LON for 8-Barrier F-Shape PCB System, Downstream View	60
Figure 45. Simulation of Beginning of LON for 8-Barrier F-Shape PCB System, Barrier Knee Impact at Barrier Nos. 5 and 6 Joint	61
Figure 46. Simulation of End of LON for 8-Barrier F-Shape PCB System, Overhead View	62
Figure 47. Simulation of End of LON for 8-Barrier F-Shape PCB System, Downstream View	63
Figure 48. Simulation of End of LON for 8-Barrier F-Shape PCB System, Barrier Knee Impact at Barrier Nos. 6 and 7 Joint	64
Figure 49. System Layout, Test No. NELON-1	66
Figure 50. System Layout, Test No. NELON-2	67
Figure 51. Portable Concrete Barrier, Test Nos. NELON-1 and NELON-2	68
Figure 52. Portable Concrete Barrier Profile Detail, Test Nos. NELON-1 and NELON-2	69
Figure 53. Bill of Bars – Portable Concrete Barriers, Test Nos. NELON-1 and NELON-2	70
Figure 54. Connection Pin Detail, Test Nos. NELON-1 and NELON-2	71
Figure 55. Bill of Materials, Test Nos. NELON-1 and NELON-2	72
Figure 56. Test Installation Photographs, Test No. NELON-1	73
Figure 57. Test Installation Photographs, Test No. NELON-2	74
Figure 58. Test Vehicle, Test No. NELON-1	79
Figure 59 Vehicle Dimensions, Test No. NELON-1	80

Figure 60. Test Vehicle, Test No. NELON-2	81
Figure 61. Vehicle Dimensions, Test No. NELON-2	82
Figure 62. Target Geometry, Test No. NELON-1	85
Figure 63. Target Geometry, Test No. NELON-2	86
Figure 64. Camera Locations, Speeds, and Lens Settings, Test No. NELON-1	87
Figure 65. Camera Locations, Speeds, and Lens Settings, Test No. NELON-2	88
Figure 66. Summary of Test Results and Sequential Photographs, Test No. NELON-1	95
Figure 67. Additional Sequential Photographs, Test No. NELON-1	96
Figure 68. Additional Sequential Photographs, Test No. NELON-1	97
Figure 69. Documentary Photographs, Test No. NELON-1	98
Figure 70. Documentary Photographs, Test No. NELON-1	99
Figure 71. Impact Location, Test No. NELON-1	100
Figure 72. Vehicle Final Position and Trajectory Marks, Test No. NELON-1	101
Figure 73. System Deflection and Damage, Test No. NELON-1	102
Figure 74. Barrier Nos. 1 and 2 Damage, Test No. NELON-1	103
Figure 75. Barrier No. 3 Damage, Test No. NELON-1	104
Figure 76. Barrier No. 4 Damage, Test No. NELON-1	105
Figure 77. Barrier No. 5 Damage, Test No. NELON-1	106
Figure 78. Barrier No. 6 Damage, Test No. NELON-1	107
Figure 79. Barrier Nos. 7 and 8 Damage, Test No. NELON-1	108
Figure 80. Vehicle Damage, Test No. NELON-1	109
Figure 81. Vehicle Damage, Test No. NELON-1	110
Figure 82. Occupant Compartment Damage, Test No. NELON-1	111
Figure 83. B-Pillar Deformation, Test No. NELON-2	118
Figure 84. Summary of Test Results and Sequential Photographs, Test No. NELON-2	120
Figure 85. Additional Sequential Photographs, Test No. NELON-2	121
Figure 86. Additional Sequential Photographs, Test No. NELON-2	122
Figure 87. Documentary Photographs, Test No. NELON-1	123
Figure 88. Documentary Photographs, Test No. NELON-2	124
Figure 89. Impact Location, Test No. NELON-2	125
Figure 90. Vehicle Final Position and Trajectory Marks, Test No. NELON-2	126
Figure 91. System Deflection and Damage, Test No. NELON-2	127
Figure 92. Barrier Nos. 1 through 3 Damage, Test No. NELON-2	128
Figure 93. Barrier No. 4 Damage, Test No. NELON-2	129
Figure 94. Barrier No. 5 Damage, Test No. NELON-2	130
Figure 95. Barrier No. 6 Damage, Test No. NELON-2	131
Figure 96. Barrier Nos. 7 and 8 Damage, Test No. NELON-2	132
Figure 97. Vehicle Damage, Test No. NELON-2	133
Figure 98. Vehicle Damage, Test No. NELON-2	134
Figure 99. Occupant Compartment Damage, Test No. NELON-2	135
Figure 100. PCB System Comparison, Overhead View	137
Figure 101. PCB System Comparison, Overhead View	138
Figure 102. PCB System Comparison, Downstream View	139
Figure 103. PCB System Comparison, Downstream View	140
Figure 104. Vehicle Roll Angle Comparison for PCB Testing	141
Figure 105. Nine Barrier Segment Reduced Length PCB System	141
Figure 106. Test No. NELON-1 vs. LS-DYNA Simulation, Overhead View	144

Figure 107. Test No. NELON-1 vs. LS-DYNA Simulation, Overhead View.....	145
Figure 108. Test No. NELON-1 vs. LS-DYNA Simulation, Downstream View.....	146
Figure 109. Test No. NELON-1 vs. LS-DYNA Simulation, Downstream View.....	147
Figure 110. Lateral Barrier Deflections for Intermediate PCB System Lengths, MASH TL-3	149
Figure 111. NCHRP 22-17 IS Distribution for Freeways.....	151
Figure 112. Lateral Barrier Deflections for Intermediate PCB System Lengths, 85 th Percentile IS	151
Figure 113. F-Shape PCB Lateral Deflection Guidance, MASH TL-3	154
Figure 114. F-Shape PCB Lateral Deflection Guidance, 85 th Percentile IS	155
Figure A-1. ½-in. (13-mm) Dia., 146-in. (3,708-mm) Long Longitudinal Steel Bars, Test Nos. NELON-1 and NELON-2.....	167
Figure A-2. ½-in. (13-mm) Dia., 72-in. (1,828-mm) Long Form Bar, Test Nos. NELON-1 and NELON-2.....	168
Figure A-3. ¾-in. (19-mm) Dia. Connection Loop Bar, Test Nos. NELON-1 and NELON-2...169	
Figure A-4. ¾-in. (19-mm) Dia. Connection Loop Bar, Test Nos. NELON-1 and NELON-2...170	
Figure A-5. 5/8-in. (16-mm) Dia. Longitudinal Bar, Test Nos. NELON-1 and NELON-2	171
Figure A-6. ¾-in. (19-mm) Dia. Anchor Loop Bar, Test Nos. NELON-1 and NELON-2	172
Figure A-7. Concrete Strength Values, Test Nos. NELON-1 and NELON-2.....	173
Figure A-8. 1¼-in. (32-mm) Dia., 28-in. (71-mm) Long Connector Pin, Test Nos. NELON-1 and NELON-2.....	174
Figure B-1. Vehicle Mass Distribution, Test No. NELON-1	176
Figure B-2. Vehicle Mass Distribution, Test No. NELON-2	177
Figure C-1. Floor Pan Deformation Data - Set 1, Test No. NELON-1	179
Figure C-2. Floor Pan Deformation Data - Set 1, Test No. NELON-2	180
Figure C-3. Floor Pan Deformation Data - Set 2, Test No. NELON-1	181
Figure C-4. Floor Pan Deformation Data - Set 2, Test No. NELON-2	182
Figure C-5. Occupant Compartment Deformation Data - Set 1, Test No. NELON-1.....	183
Figure C-6. Occupant Compartment Deformation Data - Set 1, Test No. NELON-2.....	184
Figure C-7. Occupant Compartment Deformation Data - Set 2, Test No. NELON-1.....	185
Figure C-8. Occupant Compartment Deformation Data - Set 2, Test No. NELON-2.....	186
Figure C-9. Exterior Vehicle Crush (NASS) - Front, Test No. NELON-1	187
Figure C-10. Exterior Vehicle Crush (NASS) - Front, Test No. NELON-2	188
Figure C-11. Exterior Vehicle Crush (NASS) - Side, Test No. NELON-1	189
Figure C-12. Exterior Vehicle Crush (NASS) - Side, Test No. NELON-2	190
Figure D-1. 10-ms Average Longitudinal Deceleration (SLICE-1), Test No. NELON-1	192
Figure D-2. Longitudinal Occupant Impact Velocity (SLICE-1), Test No. NELON-1	193
Figure D-3. Longitudinal Occupant Displacement (SLICE-1), Test No. NELON-1	194
Figure D-4. 10-ms Average Lateral Deceleration (SLICE-1), Test No. NELON-1.....	195
Figure D-5. Lateral Occupant Impact Velocity (SLICE-1), Test No. NELON-1.....	196
Figure D-6. Lateral Occupant Displacement (SLICE-1), Test No. NELON-1	197
Figure D-7. Vehicle Angular Displacements (SLICE-1), Test No. NELON-1	198
Figure D-8. Acceleration Severity Index (SLICE-1), Test No. NELON-1	199
Figure D-9. 10-ms Average Longitudinal Deceleration (SLICE-2), Test No. NELON-1	200
Figure D-10. Longitudinal Occupant Impact Velocity (SLICE-2), Test No. NELON-1	201
Figure D-11. Longitudinal Occupant Displacement (SLICE-2), Test No. NELON-1	202
Figure D-12. 10-ms Average Lateral Deceleration (SLICE-2), Test No. NELON-1.....	203

Figure D-13. Lateral Occupant Impact Velocity (SLICE-2), Test No. NELON-1.....	204
Figure D-14. Lateral Occupant Displacement (SLICE-2), Test No. NELON-1	205
Figure D-15. Vehicle Angular Displacements (SLICE-2), Test No. NELON-1	206
Figure D-16. Acceleration Severity Index (SLICE-2), Test No. NELON-1	207
Figure E-1. 10-ms Average Longitudinal Deceleration (SLICE-1), Test No. NELON-2.....	209
Figure E-2. Longitudinal Occupant Impact Velocity (SLICE-1), Test No. NELON-2.....	210
Figure E-3. Longitudinal Occupant Displacement (SLICE-1), Test No. NELON-2.....	211
Figure E-4. 10-ms Average Lateral Deceleration (SLICE-1), Test No. NELON-2	212
Figure E-5. Lateral Occupant Velocity (SLICE-1), Test No. NELON-2	213
Figure E-6. Lateral Occupant Displacement (SLICE-1), Test No. NELON-2	214
Figure E-7. Vehicle Angular Displacements (SLICE-1), Test No. NELON-2	215
Figure E-8. Acceleration Severity Index (SLICE-1), Test No. NELON-2.....	216
Figure E-9. 10-ms Average Longitudinal Deceleration (SLICE-2), Test No. NELON-2.....	217
Figure E-10. Longitudinal Occupant Impact Velocity (SLICE-2), Test No. NELON-2.....	218
Figure E-11. Longitudinal Occupant Displacement (SLICE-2), Test No. NELON-2.....	219
Figure E-12. 10-ms Average Lateral Deceleration (SLICE-2), Test No. NELON-2	220
Figure E-13. Lateral Occupant Impact Velocity (SLICE-2), Test No. NELON-2	221
Figure E-14. Lateral Occupant Displacement (SLICE-2), Test No. NELON-2.....	222
Figure E-15. Vehicle Angular Displacements (SLICE-2), Test No. NELON-2	223
Figure E-16. Acceleration Severity Index (SLICE-2), Test No. NELON-2.....	224

LIST OF TABLES

Table 1. Summary of F-shape PCB Baseline Model Simulations	13
Table 2. MASH TL-3 Crash Test Conditions for Terminals and Crash Cushions	75
Table 3. MASH Evaluation Criteria for Terminals and Crash Cushions	77
Table 4. Weather Conditions, Test No. NELON-1	89
Table 5. Sequential Description of Impact Events, Test No. NELON-1	89
Table 6. Maximum Occupant Compartment Deformations by Location	93
Table 7. Summary of OIV, ORA, THIV, PHD, and ASI Values, Test No. NELON-1	94
Table 8. Weather Conditions, Test No. NELON-2	112
Table 9. Sequential Description of Impact Events, Test No. NELON-2	112
Table 10. Maximum Occupant Compartment Deformations by Location	116
Table 11. B-Pillar Deformation, Test No. NELON-2	117
Table 12. Summary of OIV, ORA, THIV, PHD, and ASI Values, Test No. NELON-2	118
Table 13. Summary of Safety Performance Evaluation Results, Test Nos. NELON-1 and NELON-2	158
Table 14. Comparison of Test Results, Test Nos. NELON-1 and NELON-2	159
Table 15. Bill of Materials, Test Nos. NELON-1 and NELON-2	166

ACRONYMS, ABBREVIATIONS, AND SYMBOLS

Acronym	Definition
AASHTO	- American Association of State Highway and Transportation Officials
AOS	- AOS Technologies AG
ASI	- Acceleration Severity Index
ASTM	- American Society for Testing and Materials
B.S.B.A.	- Bachelor of Science in Business Administration
c.g.	- center of gravity
CIP	- Critical Impact Point
CPU	- central processing unit
deg.	- degree
DOT	- Department of Transportation
DTS	- Diversified Technical Systems, Incorporated
E.I.T.	- Engineer in Training
FHWA	- Federal Highway Administration
ft	- foot
ft/s	- feet per second
g's	- g-force, acceleration due to gravity at the Earth's surface
GP	- GoPro
GB	- gigabyte
h	- hour
Hz	- Hertz
i.e.	- id est (that is)
IAA	- Independent Approving Authority
in.	- inch
IS	- impact severity
JVC	- Victor Company of Japan, Limited
kg	- kilogram
kip-in.	- thousand pounds-force inches
kips	- thousand pounds-force
kJ	- kilojoules
km	- kilometer
km/h	- kilometers per hour
kN	- kilonewton
lb	- pound(s)
LED	- light-emitting diode
LON	- length of need
m/s	- meters per second
m	- meter
mm	- millimeter

MASH	- Manual for Assessing Safety Hardware
mm	- millimeter
mph	- miles per hour
M.S.C.E.	- Master of Science in Civil Engineering
M.S.M.E.	- Master of Science in Mechanical Engineering
<i>mV</i>	- millivolts
MwRSF	- Midwest Roadside Safety Facility
N	- Newton
NA	- not applicable
NCAC	- National Crash Analysis Center
NCHRP	- National Cooperative Highway Research Program
NDOR	- Nebraska Department of Roads
NHS	- National Highway System
no.	- number
nos.	- numbers
OIV	- occupant impact velocity
ORA	- occupant ridedown acceleration
PCB	- Portable Concrete Barrier
P.E.	- Professional Engineer
Ph.D.	- Doctor of Philosophy
PHD	- Post-Impact Head Deceleration
p.m	- post meridiem
R&D	- research and development
RSVVP	- Roadside Safety Simulation Verification and Validation Program
RWD	- rear-wheel drive
s	- second
SAE	- Society of Automotive Engineers
SBP	- slope break point
sec	- second
SIM	- Sensor Input Module
THIV	- Theoretical Head Impact Velocity
TL	- Test Level
TTI	- Texas A&M Transportation Institute
U.S.	- United States
US	- upstream
V	- volts
vs.	- versus
° F	- degrees Fahrenheit
'	- foot
”	- inch
%	- percent

μ	- vehicle-to-ground friction
σ_w	- yield strength of W-beam rail
t_w	- thickness of W-beam rail
D_b	- bolt diameter
F_v	- shear force

1 INTRODUCTION

1.1 Problem Statement

Portable concrete barrier (PCB) systems redirect errant vehicles through a combination of various forces and mechanisms, including inertial resistance developed by the acceleration of several barrier segments, lateral friction loads, and the tensile loads developed from the mass and friction of the barrier segments upstream and downstream of the impacted region. Typically PCB designs are evaluated and tested using 200-ft (61-m) long system lengths. It has generally been assumed that this length of system provides vehicle redirection, resulting system deflections, and working widths that are representative of longer PCB installations. Unfortunately, recommendations on minimum PCB system lengths have generally been limited to the 200-ft (61-m) length or longer in order to preserve the as-tested system deflections and impact behavior. In addition, guidance on the beginning and end of the length of need (LON) of these systems is typically given as a minimum of 100 ft (30.5 m) (i.e., eight barrier segments of 12.5 ft (3.8 m) long) in order to preserve performance similar to existing crash tests.

Many instances exist where state departments of transportation (DOTs) and other end users wish to use shorter PCB installations to shield a hazard or work zone or limit the number of barriers required on the upstream and downstream ends to reduce the overall system length. Shorter barrier lengths are associated with lower accident frequencies and provide improved cost and safety benefits as long as they retain their ability to safely contain and redirect errant vehicles. However, concerns with the performance of shorter PCB installations must be considered. First, shorter PCB systems would be expected to have higher deflections and working widths than installations of 200 ft (61 m) or more due to the reduction of upstream and downstream barrier mass and friction forces. Second, PCB systems may not develop sufficient longitudinal resistance at shorter system lengths and may form a pocket in front of an impacting vehicle, which could lead to vehicle instability or excessive decelerations. Finally, no impact testing has been performed near the upstream or downstream ends of free-standing PCB systems to determine the limits of the LON of the system. Impacts at or near the barriers at the ends of a free-standing barrier system may produce very different barrier performance than impacts near the center of the system, and the results may include the potential for gating of the vehicle through the system, pocketing, rapid deceleration, and/or vehicle instability.

Thus, a desire exists to install PCB systems shorter than 200 ft (61 m) and to more accurately define the beginning and end of the LON for these systems. Further study on the minimum effective length of PCB systems, their associated deflections and working widths, as well as a determination of the LON of these systems is warranted in order to provide more efficient and safe PCB installations.

Midwest Roadside Safety Facility (MwRSF) previously developed and full-scale vehicle crash tested a 12.5-ft (3.8-m) long F-shape portable concrete barrier system for use in both free-standing and tie-down applications. This temporary barrier design is currently used by the Nebraska Department of Roads (NDOR). Full-scale crash testing of this barrier system was conducted under both the National Cooperative Highway Research Program (NCHRP) Report 350 [1] and *Manual for Assessing Safety Hardware* (MASH) [2] Test Level 3 (TL-3) safety requirements [3-4]. During the MASH TL-3 full-scale crash test, test no. 2214TB-2, the F-shape

PCB system exhibited a dynamic deflection of 79.6 in. (2,022 mm) when impacted near the middle of a sixteen barrier segment test system with an overall length of 200 ft (61 m).

PCB installations shorter than the tested length would likely result in increased dynamic deflections as well as the potential for barrier pocketing. It is believed that the potential exists for shorter runs of free-standing F-shape PCBs to safely redirect errant vehicles. However, no existing research effort has been done to date to quantify the increased deflections and potential safety issues associated with shorter system lengths.

In order to effectively determine minimum system lengths and the required beginning and end of the LON for the free-standing F-shape PCB system, analysis of three main factors must be considered. These factors include the number of barriers required on the upstream end of the system, the number of barriers required on the downstream end of the system, and the overall system length. A minimum number of barrier segments are required on the upstream end of the system or beginning of LON to provide sufficient anchorage to safely redirect impacting vehicles with a reasonable dynamic deflection. Similarly, a minimum number of barrier segments is required on the downstream end of the system (i.e., end of the LON). However, the number of required barriers may be different on the upstream and downstream ends. In addition, the number of barrier segments required on the ends of the system will likely be affected by the overall length of the system. For example, the number of barrier segments required on the upstream end of a long PCB installation (i.e., higher downstream barrier resistance) may be different than the number of barriers required for a short system length that allows increased PCB movement downstream of the beginning of LON. Thus, determination of safe system lengths and beginning and end of the LON requirements for free-standing F-shape PCBs would require consideration of all of these factors.

1.2 Objectives

The objective of this research effort was to investigate and evaluate the safety performance of the previously developed F-shape PCB system in order to determine the minimum system length and the number of barriers required for the beginning and end of the LON. The minimum system length was evaluated through full-scale crash testing at the beginning and end of the LON. The full-scale crash testing was conducted and evaluated according to the TL-3 criteria set forth in MASH.

1.3 Scope

The research objective was achieved through completion of several tasks. First, a simple friction test to determine the coefficient of friction between the PCB and asphalt paving was conducted for comparison with previous PCB and concrete friction testing. Next, LS-DYNA computer simulation of the F-shape PCB system was conducted in order to analyze PCB system length and the beginning and end of the LON requirements. The simulation analysis provided guidance with respect to the potential minimum system length, number of barrier segments on the beginning and end of the LON, and critical impact points (CIP) for evaluation with full-scale crash testing. The proposed PCB system configuration was evaluated according to the MASH TL-3 safety criteria. Two full-scale crash tests were conducted to evaluate the system. The first test consisted of MASH test designation no. 3-35 to evaluate the effectiveness of the beginning of LON with a minimal system length. The second test consisted of a modified version of MASH test

designation no. 3-37 with the intent of assessing the end of the LON for the PCB system rather than maximizing vehicle snag and instability on a terminal or crash cushion. The full-scale vehicle crash tests were conducted, documented, and evaluated by MwRSF personnel in accordance with the MASH guidelines. Next, the test results were analyzed, evaluated, and documented. Following the full-scale crash testing, additional simulation analysis was conducted to provide guidance on PCB system deflections for intermediate system lengths. Finally, conclusions and recommendations were made that pertain to the safety performance of the LON for a free-standing, F-shape PCB system.

2 COMPONENT TESTING OF PCB FRICTION COEFFICIENTS

2.1 Purpose

Portable concrete barriers rely on friction between the bottom surface of the barrier and the roadway to develop resistance to longitudinal and lateral barrier motion and limit deflection. In previous research, Texas A&M Transportation Institute (TTI) conducted basic component testing of PCB segments on flat ground to determine coefficients of friction for PCB segments on concrete [5]. The results of those component tests estimated the coefficient of friction for PCB segments on concrete to be 0.40. MwRSF also conducted similar friction testing as part of a reduced deflection PCB study [6]. In that study, MwRSF identified static and kinetic coefficients of friction of 0.72 and 0.44, respectively, for the F-shape PCB used in this study on a concrete tarmac.

For this study, NDOR requested additional component testing of the barrier-to-ground friction mechanism to quantify barrier-to-ground friction values for the PCB segment on asphalt paving. Thus, a quasi-static pull test of the concrete barrier segment on the asphalt paving was conducted for comparison with the previously determined values for the PCB segment when loaded on concrete. The details of the quasi-static pull test for determination of the static and kinetic coefficients of friction between the PCB segment and an asphalt road surface are provided in subsequent sections.

2.2 Scope

One quasi-static pull test was conducted on an F-shape PCB segment installed on asphalt paving in order to determine the static and kinetic coefficients of friction between the PCB segment and an asphalt road surface. The test setup is shown in Figure 1. An existing F-shape PCB segment used in a previous research effort was utilized for the quasi-static pull test. The PCB was installed on a 4-in. (102-mm) thick by 4-ft (1.2-m) wide asphalt mow strip. The asphalt mow strip was constructed with a 52-34 grade binder typically utilized in highway shoulder construction in Nebraska.



Figure 1. Quasi-Static Pull Test Setup, Test No. TCBFA-1

2.3 Equipment and Instrumentation

Equipment and instrumentation utilized to collect and record data during the pull tests included a skid-steer, two tensile-load cells, standard-speed digital video, and a still camera.

2.3.1 Tensile-Load Cells

Two load cells were mounted in line with the pull cable to measure the tension in the cable for test no. TCBFA-1, as shown in Figure 2. The data from both load cells was processed and compared to ensure accuracy of the readings. The load cells were manufactured by Transducer Techniques and conformed to model no. TLL-50K with a load range up to 50 kips (222 kN). During testing, output voltage signals were sent from the load cells to a National Instruments data acquisition board, acquired with LabView software, and stored permanently on a personal computer. The data collection rate for the load cells was 1,000 samples per second (1,000 Hz).



Figure 2. Load Cell Arrangement, Test No. TCBFA-1

2.3.2 Digital Photography

One GoPro digital video camera was used to document this test. The GoPro camera had a frame rate of 120 frames per second. The camera was placed laterally from the barrier test segment, with a view perpendicular to the direction of pull. A Nikon D3100 digital still camera was also used to document pre- and post-test conditions for this test.

2.4 Data Processing

For test no. TCBFA-1, force data was measured with the load cell transducers and filtered using the SAE Class 60 Butterworth filter conforming to the SAE J211/1 specifications [7]. The pertinent voltage signal was extracted from the bulk of the data signal similar to the acceleration data. The filtered voltage data was converted to load using the following equation:

$$Load = \left[\frac{1}{Gain} \right] * \left[\frac{Filtered\ Load\ Cell\ Data}{\left(\frac{(Calibration\ Factor)(Excitation\ Voltage)}{Full - Scale\ Load} \right) * \left(\frac{1V}{1000\ mV} \right)} \right]$$

Details behind the theory and equations used for processing and filtering the load cell data are located in SAE J211/1. The gain and excitation voltage were recorded for each test. The calibration factor varied depending on the specific load cell being used. The load cell data was recorded in a data file and processed in a specifically-designed Excel spreadsheet. Force vs. time plots were created to describe the load imparted to the system.

3 FRICTION TESTING RESULTS AND DISCUSSION

Test no. TCBFA-1 was conducted to evaluate the barrier-to-ground friction coefficients for PCB segments on asphalt pavement. The component testing of the PCB segments sliding on concrete pavement was instrumented to estimate friction forces and coefficients. When the pulling force was initially applied to the barrier, a noticeable peak in the force vs. time graph was achieved. This peak force was used to calculate the static coefficient of friction between the surfaces by dividing the peak force by the weight of the barrier segment. Once the barrier began to slide on the pavement, the resistive force was reduced. The force readings taken while the barrier was in motion were averaged, and the average force was divided by the weight of the barrier segment to calculate the kinetic coefficient of friction.

3.1 Test No. TCBFA-1

In test no. TCBFA-1, a 4,796 lb (2,175 kg) F-shape PCB segment was pulled on the asphalt pavement using a skid-steer. The corresponding force vs. time data is shown in Figure 3. A peak force of 3.07 kips (13.7 kN) was measured prior to the onset of the PCB sliding. Once the PCB began to slide over the asphalt paving, an average force of 2.45 kips (10.9 kN) was measured during barrier motion. Calculation of the friction coefficients for the barrier based on these forces and the mass of the barrier yielded static and kinetic coefficients of friction between the PCB and asphalt road surface of 0.64 and 0.51, respectively.

The friction coefficients determined between the PCB and asphalt were similar to those obtained previously for the PCB on the concrete surface with the asphalt surface providing a slightly lower static coefficient of friction and a slightly higher dynamic coefficient of friction. This suggested that the design and evaluation of the PCB systems on concrete paving should provide relevant results for barriers installed on asphalt.

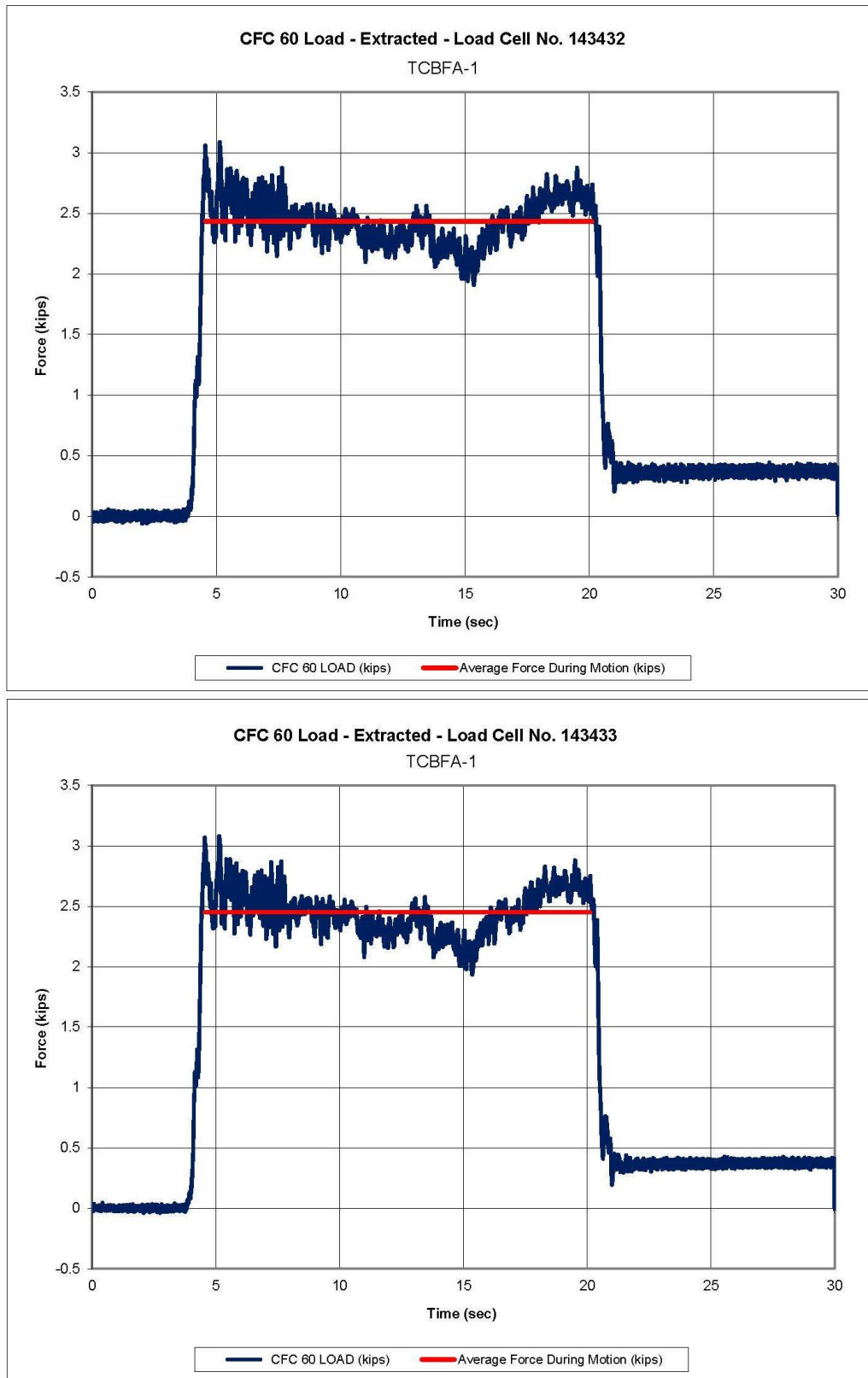


Figure 3. Force vs. Time, Test No. TCBFA-1

4 BASELINE MODEL OF F-SHAPE PCB SYSTEM

In order to evaluate impacts at the beginning and end of the LON and minimum system lengths, a baseline model of the free-standing, F-shape PCB system was created and compared to previous MASH TL-3 full-scale crash testing with the 2270P vehicle, test no. 2214TB-2 [4]. While previous simulation models of the F-shape PCB had been developed by the researchers, it was desired to further investigate the performance of the barrier model to promote improved results when analyzing the beginning and end of the LON and minimum system length. Thus, comparisons between the simulation model and the full-scale crash test were conducted based on dynamic barrier deflection, vehicle trajectory, and Roadside Safety Simulation Verification and Validation Program (RSVVP) analysis of vehicle transducer data [8]. Details for the baseline model development and the comparison with full-scale crash testing is detailed below.

4.1 PCB Model

The model of the F-shape portable concrete barrier was based on models developed previously at MwRSF for simulation of portable concrete barriers [9-6]. The model consisted of the F-shape barrier, the end connection loops, and the connection pins, as shown in Figure 4. The main body of the F-shape barrier model was created using shell elements with a rigid material definition. The rigid material definition allowed the proper mass and rotational inertias to be defined for the barrier even though it was essentially hollow. The barrier segments were assigned a mass of 4,976 lb (2,257 kg) based on measurements taken from actual barrier segments. The rotational inertias were determined based on SolidWorks models of the PCB segment. The SolidWorks models used tended to overestimate the mass and rotational inertia of the PCB segment as the solid model included the mass of the concrete body and the reinforcing steel, but did not account for the volume of concrete lost due to the reinforcing steel. Thus, the rotational inertias determined by the software were scaled down based on the ratio of the actual measured mass of the barrier segment to the software estimated mass of the segment. The use of the shell elements improved the overall contact of the barrier and the vehicle. In addition, the use of shell elements made it easier to fillet the corners and edges of the barrier. By rounding off the barrier edges, the edge contacts and penetrations were reduced, thus further improving the contact interface.

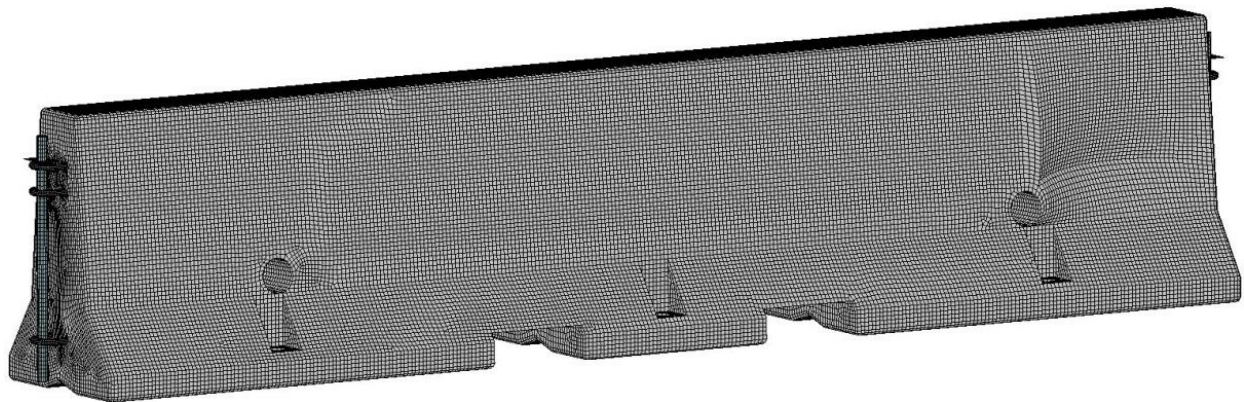
The loops in the barrier model consisted of two sets of three rebar loops. The connection loops were modeled with a rigid material as previous testing of the barrier in various configurations showed little to no deformation of the connection loops. The connection pin was modeled with the MAT_PIECEWISE_LINEAR_PLASTICITY material in LS-DYNA with the appropriate properties for A36 steel. The baseline barrier system model incorporated a total of sixteen barrier segments for a total barrier length of 200 ft (61.0 m).

A critical component of the baseline model of the free-standing, F-shape PCB was the definition of the barrier-to-ground friction. PCB systems use a combination of inertial resistance and longitudinal tension to redirect impacting vehicles. The longitudinal tension in the barrier system is largely developed by barrier-to-ground friction. Previous research at TTI and MwRSF measured the kinematic friction coefficient for a concrete PCB segment sliding on a concrete surface to be between 0.40 and 0.44 [6-5]. Testing to measure the kinematic friction coefficient for a concrete PCB segment sliding on an asphalt surface detailed in the previous chapters of this report found a kinematic friction coefficient of 0.51. The lower friction value of 0.40 was selected

for use in the analysis in order to better correlate with the road surface used in the full-scale testing and to maximize potential deflections. This friction value was applied in the LS-DYNA baseline model between the barrier segments and the shell element ground. In addition to providing appropriate friction coefficients, the barrier model needed to develop the correct weight or normal forces on the ground. This was accomplished by allowing the barriers in the simulation model to reach quasi-static equilibrium on the ground prior to being impacted. Damping was used to help the barriers reach a steady normal force on the ground and was turned off prior to vehicle impact.



(a)



(b)

Figure 4. F-Shape PCB: (a) Actual and (b) Finite Element Model

4.2 Vehicle Models

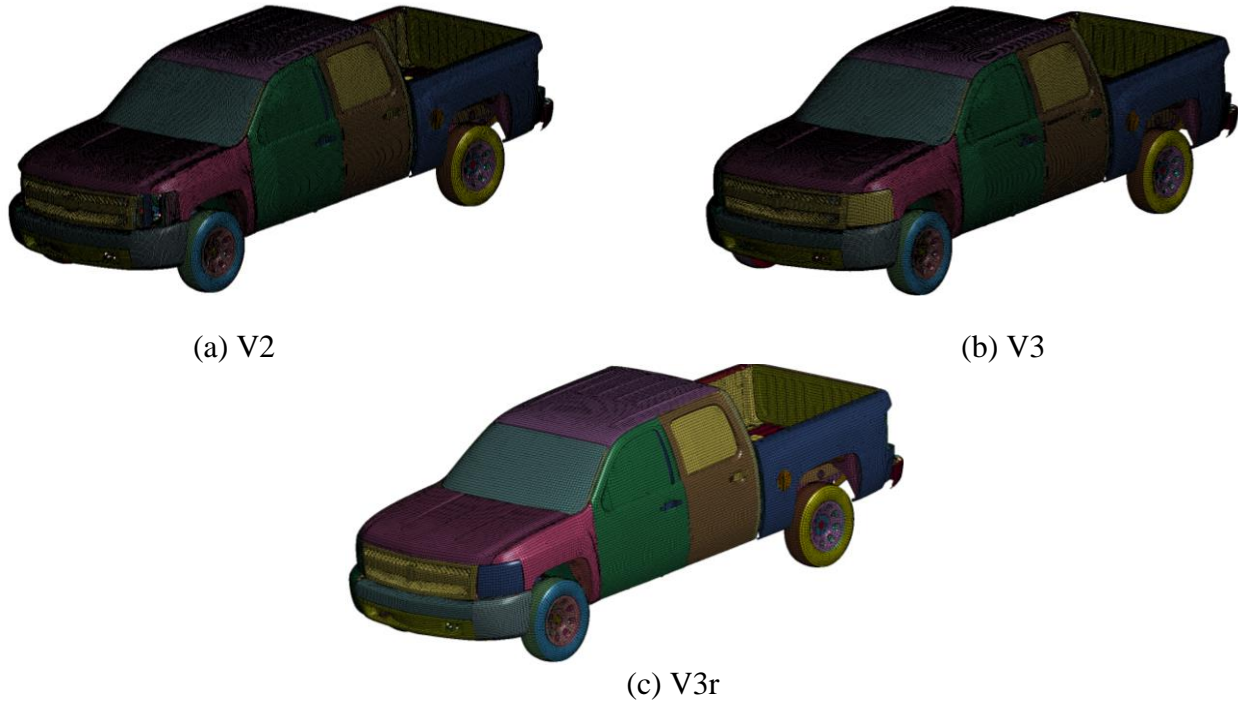
MASH denotes that a TL-3 longitudinal barrier such as the F-shape PCB utilized in this research must be subjected to impacts with the 2270P pickup truck and the 1100C small car. However, the 2270P test vehicle was deemed more critical than the 1100C small car due to the likelihood of increased barrier deflections, impact loading, and barrier pocketing. Further, vehicle instabilities have been exhibited during full-scale crash tests involving 2270P pickup trucks with F-shape PCB systems due to vehicle climb.

The Chevrolet Silverado quad cab vehicle model was chosen for the research and simulation study. The Silverado vehicle model was originally created by the National Crash Analysis Center (NCAC) and later modified by MwRSF personnel for use in roadside safety applications. Three versions of the Chevrolet Silverado vehicle model were investigated as part of the analysis of the baseline model: Version 2 (V2), Version 3 (V3), and Version 3 – Reduced (V3r). All three versions of the vehicle model represented the same Chevrolet Silverado quad cab vehicle, but there were differences in the tires, steering, vehicle-to-ground friction, and mesh size, among other factors. These differences are summarized in Figure 5.

The V3 and V3r models of the truck incorporated steering for the front wheels while the V2 model did not. The V2 model had a tire stiffness that correlated with the stiffness of actual truck tires, while the V3 and V3r models used significantly stiffer tire models. The meshes for all three versions of the truck model were different, with the main variation being the larger, coarser mesh of the reduced model. The coarser mesh of the V3r model improved its CPU efficiency, but may have had other effects in terms of contacts and vehicle deformation. Finally, the V3 and V3r models used default tire-to-ground friction values that were over twice as high as the default value for the V2 model. As such, it was believed that these differences in the vehicle models could contribute to the accuracy of the baseline model. Thus, all three vehicle models were used and compared when simulating the baseline model of the F-shape PCB system. Additional variations to the truck model that had been implemented by MwRSF over time were also investigated. These included the use of additional weld attachments between the truck box and frame in Version 3 that had previously been shown to improve stability and disengagement of the front wheels to represent suspension failure.

4.3 Baseline Model Simulations

The baseline model of the sixteen, free-standing, F-shape PCBs was simulated with a 2270P vehicle impacting the system at a speed of 62 mph (100 km/h) and at an angle of 25 degrees. The vehicle impacted the system 4.3 ft (1.3 m) upstream of the center of the joint between the eighth and ninth barrier segments. In order to evaluate the barrier model, a series of simulations were conducted using variations of the three Chevrolet Silverado vehicle models noted previously. This included simulations of the V2, V3 and V3r models and variations of those models, including changes in tire-to-ground friction, the use of front wheel disengagement, and the application of additional weld connections on the back end of the vehicle. The various models were compared to test no. 2214TB-2 based on the high-speed video comparison, dynamic deflection of the barrier system, and RSVVP comparison of transducer data. A summary of the model runs is shown in Table 1.



Version No.	Tire Stiffness	Steering	Vehicle-to-Ground Friction	Mesh
V2	Soft	No	$\mu = 0.40$	Fine
V3	Hard	Yes	$\mu = 0.90$	Fine
V3r	Hard	Yes	$\mu = 0.90$	Coarse

Figure 5. Chevy Silverado 2270P Truck Model Variations

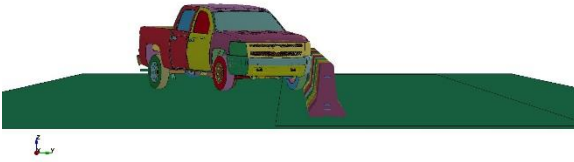
4.3.1 Chevy Silverado V3 Simulations

Analysis of the simulation of the F-shape PCB with the standard Chevy Silverado V3 found that the V3 model did not provide the best correlation with test no. 2214TB-2. Comparison of the high-speed video, shown in Figures 6 and 7, found that the V3 model displayed increased vehicle roll and pitch as compared to the full-scale test. This was confirmed by comparison of the rate gyro data between the simulation and testing. Additionally, the front wheels of the V3 model tended to steer away from the barrier, which was opposite of the steering behavior in test no. 2214TB-2. Comparison of the vehicle transducer data using the RSVVP program found that the standard Chevy Silverado V3 did not meet the single channel or multiple channel metric comparisons. The dynamic deflection of the PCB system in the V3 model was found to be 75.3 in. (1,912 mm) which was slightly less than the 79.6 in. (2,022 mm) deflection measured in the full-scale crash test. Review of the model suggested that the discrepancies between the simulation model behavior and the full-scale crash test were largely due to the combination of the V3 model's increased tire stiffness, higher tire-to-ground friction values, and the differences in the vehicle steering behavior. Vehicle tail slap with the barrier was also observed to be an issue with the V3 model due to the rigid rear axle assembly used on the vehicle. During vehicle tail slap with the PCBs, the axle assembly seemed to increase the severity of the tail slap and produce excess yaw and high lateral accelerations as compared to the full-scale testing.

Table 1. Summary of F-shape PCB Baseline Model Simulations

Run No.	Vehicle Model	Wheel Disengagement	Tire-Ground Friction	Additional Back End Welds	Dynamic Deflection (mm)	RSVVP CFC 180 (single channel)						RSVVP Multiple Channel	Notes
						X-acceleration	Y-acceleration	Z-acceleration	Yaw	Roll	Pitch		
Run 5	V3	No	0.9	No	1912	No	No	No	No	No	No	No	Did not meet RSVVP - no single channels or multi-channel. Vehicle tires initially steer away from barrier in model and towards barrier in test.
Run 6	V3	Yes	0.9	Yes	1995	NA	NA	NA	NA	NA	NA	NA	RSVVP not run. Truck trajectory has far too much roll and pitch motion near end of simulation. Better deflections. Vehicle tires initially steer away from barrier in model and towards barrier in test.
Run 7	V3	Yes	0.9	No	1961	NA	NA	NA	NA	NA	NA	NA	RSVVP not run. Truck trajectory has far too much roll and pitch motion near end of simulation. Better deflections. Extra back end welds reduced truck roll slightly. Vehicle tires initially steer away from barrier in model and towards barrier in test.
Run 8	V3	No	0.9	Yes	1965	No	No	No	No	No	No	No	Roll of vehicle increased compared to Run 5. Vehicle tires initially steer away from barrier in model and towards barrier in test. Extra back end welds increased truck roll slightly.
Run 9	V3r	No	0.9	NA	1554*	NA	NA	NA	NA	NA	NA	NA	RSVVP not run. Excessive body roll and model instability.
Run 10	V3	Yes	0.4	Yes	2015	No	No	No	No	No	No	No	Vehicle tires initially steer away from barrier in model and towards barrier in test. Roll and pitch motions near end of model much improved over Run 6. Much better RSVVP comparisons. Note that this and all previous models have good lateral acceleration comps but underestimate longitudinal deceleration. Potentially low vehicle to barrier friction issue.
Run 11	V2	No	0.4	NA	2061	No	Yes	No	No	No	No	Yes	V2 truck steering much closer to test - does not steer away. V2 truck does not allow steering. Accelerations much less "noisy". V-V comparisons much improved. Yaw better than V3 truck. Acceleration much closer even with CFC 180 comps. Softer tires and steering response appear to be a major factor. Tail slap seems to be over represented in severity leading to excess yaw and high lateral accelerations as compared to the test. Note that single channel comparisons improve greatly with CFC 60 accelerations. Velocity curves unchanged, but accelerations compare better (i.e. long accelerations pass).
Run 12	V2	Yes	0.4	NA	2057	No	Yes	No	No	No	No	Yes	Disconnect of wheel tends to increase roll and decrease climb as compared to Run 11. Appears that keeping the tire attached is a better representation of test even though tire detached in test.
Run 13	V3r	Yes	0.9	NA	1895	NA	NA	NA	NA	NA	NA	NA	RSVVP not run. V3r has much higher roll and vehicle instability than V3 or V2.
Run 14	V3	no	0.4	No	1976	No	No	No	No	No	No	No	Reduced pitch and roll motions as compared to Run 5. Vehicle tires initially steer away from barrier in model and towards barrier in test. Similar in improvement seen between Run 6 and Run 10. May suggest lower barrier to ground friction for all models. Still very early drop in yaw rate. Likely due to tailslap and potentially vehicle-barrier friction as noted above.
*simulation did not finish													

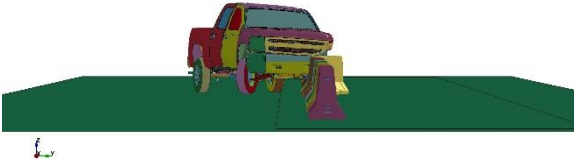
NDOR PCB LON - Baseline
Time = 35



Time = 0.000 sec



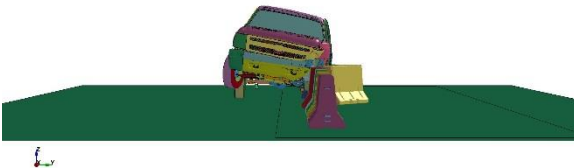
NDOR PCB LON - Baseline
Time = 135



Time = 0.100 sec



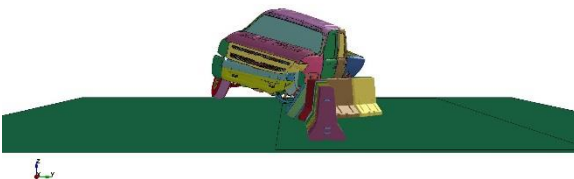
NDOR PCB LON - Baseline
Time = 235



Time = 0.200 sec



NDOR PCB LON - Baseline
Time = 335

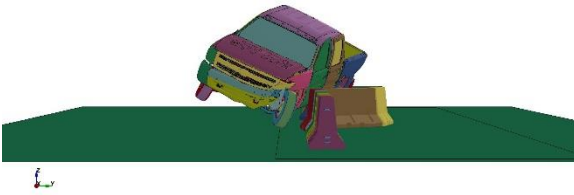


Time = 0.300 sec



Figure 6. Crash Sequence - Standard Chevy Silverado V3 Model and Test No. 2214TB-2

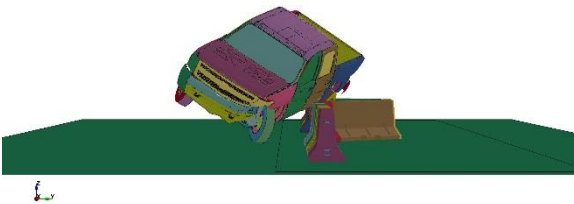
NDOR PCB LON - Baseline
Time = 435



Time = 0.400 sec



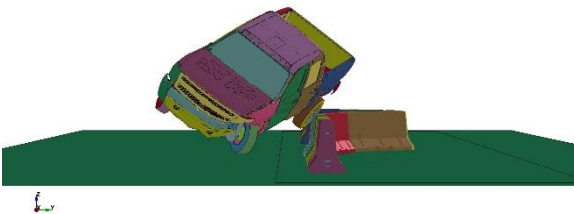
NDOR PCB LON - Baseline
Time = 535



Time = 0.500 sec



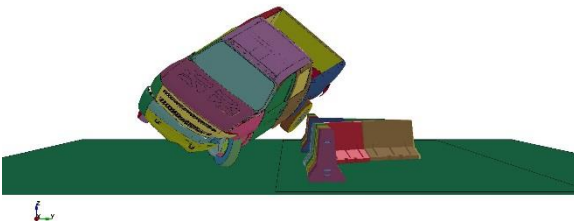
NDOR PCB LON - Baseline
Time = 635



Time = 0.600 sec



NDOR PCB LON - Baseline
Time = 735



Time = 0.700 sec



Figure 7. Crash Sequence - Standard Chevy Silverado V3 Model and Test No. 2214TB-2

Subsequent changes were made to the V3 model to investigate if the model performance improved. These changes included disengagement of the left-front wheel during impact with the PCBs, reduction of the tire-to-ground friction, and adding additional welds to connect the box to the truck frame. Disengagement of the left-front vehicle wheel was observed in full-scale crash test no. 2214TB-2, but adding similar wheel release to the V3 model impact with the F-shape PCB did not improve correlation. Wheel disengagement tended to further increase the vehicle roll and pitch motions. Reduction of the tire-to-ground friction improved the response of the V3 model impacting the F-shape PCB by providing decreased roll and pitch motions and slightly increasing lateral barrier deflections. However, the steering of the vehicle wheels still prevented the simulation from meeting the single channel and multiple channel RSVVP comparisons. Finally, analysis of the additional welds on the rear section of the vehicle found little to no effect on the results of the simulation of the F-shape PCB impact.

4.3.2 Chevy Silverado V3r Simulations

Another series of simulations was conducted using the Chevy Silverado V3r model impacting the F-shape PCB system. The reduced model of the Chevy Silverado displayed similar increased roll and pitch motions, reduced lateral deflections, and inaccurate steering behavior as the V3 model. Additionally, the V3r model developed instabilities during simulation that were likely due to the coarser mesh used in the model and corresponding problems with the contact algorithms. Based on these issues, the V3r version of the Chevy Silverado was not selected for use as part of the baseline analysis of the PCB system.

4.3.3 Chevy Silverado V2 Simulations

A final series of simulations was conducted using the Chevy Silverado V2 model impacting the F-shape PCB system. Recall that the V2 model of the Silverado had significantly softer tires and lower default tire-to-ground friction values, but it did not include steering of the front wheels like the V3 and V3r models. Simulation of the F-shape PCB system with the Chevy Silverado V2 model demonstrated better correlation with the full-scale test results than the previous simulations with the V3 and V3r vehicles. The softer tires and lower tire-to-ground friction resulted in vehicle climb and roll and pitch motions that corresponded well with test no. 2214TB-2. Additionally, the lack of steering in the V2 model provided better correlation with the motion of the front wheels in the full-scale test as it did not show the tires steering away from the barrier like the V3 and V3r models. Similarly, increased vehicle yaw and lateral accelerations during tail slap were observed with the V2 model as compared with the V3 and V3r models.

Comparison of the results from the Chevy Silverado V2 model impacting the F-shape PCB system are shown in sequential images in Figures 8 through 11. This comparison found good correlation between the V2 model simulation and test no. 2214TB-2 in terms of vehicle behavior and the barrier motions. The simulation of the PCB impact with the V2 model had a peak dynamic barrier displacement of 81.1 in. (2,061 mm) which was nearly identical to the 79.6 in. (2,022 mm) displacement observed in test no. 2214TB-2. Additionally, RSVVP comparisons of the vehicle acceleration and rotation data found that the V2 model provided the best correlation with the full-scale test as it passed the single channel correlations for the lateral acceleration and yaw rotation and met the multiple channel comparisons in RSVVP. The results of the RSVVP comparison are shown in Figure 12.

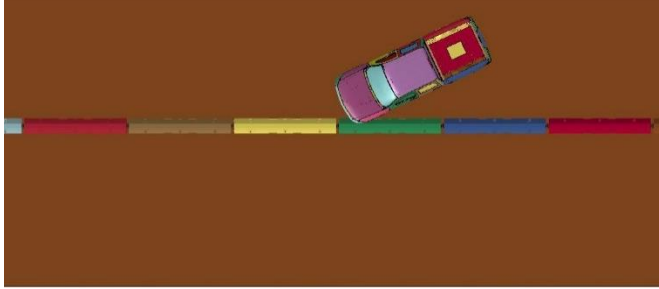
Additional simulations were conducted with the Chevy Silverado V2 model impacting the F-shape PCB system that included disengagement of the front wheel on the impact side as was observed in the test. The overall response of the Chevy Silverado V2 model with front wheel disengagement was very similar to the original V2 simulation in terms of vehicle deceleration and barrier displacement. Disengagement of the front wheel increased vehicle roll and decreased vehicle climb of the barrier as compared to test no. 2214TB-2. Additionally, disengagement of the front wheel tended to produce instabilities in some impact configurations due to the interaction of the disengaged tire and wheel with the barrier and ground later in the impact event.

4.3.4 Baseline Model Conclusions

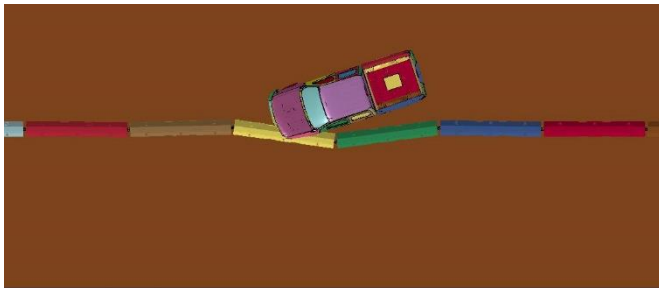
Review of the simulations of the TL-3 impacts with the various Chevy Silverado models into the F-shape PCB system led to several observations about the baseline simulation model. First, the stiff tires, steering, and tire-to-ground friction on the Chevy Silverado V3 and V3r models adversely affected the correlation of the model with the test results. The stiffer tires potentially improved simulation stability by deforming less under load, but the increased stiffness tended to over-exaggerate the tire interaction with the barrier. This led to increased roll and pitch motions and negatively affected vehicle accelerations. The inclusion of front-wheel steering in the V3 and V3r models did not improve model correlation even though it would seem to be more accurate to include vehicle steering. It is possible that the steering in the model may need to include the mechanical resistance to motion of an actual steering mechanism, reduce tire stiffness, or refine vehicle tire and wheel friction with the barrier segments in order to produce a more accurate steering response. The default tire-to-ground friction value also tended to degrade the model correlation with the full-scale crash test due to an observed increase in roll and pitch motions. Second, the tail slap event for all three of the vehicle models tended to be more severe than what is typically observed in physical crash tests with these types of barriers and caused increased vehicle yaw and lateral accelerations. It was noted that this could potentially be improved through the use of more deformable structures and connections in the current rigid rear axle assembly.

Disengagement of the front wheel was implemented with all three versions of the truck model. This tended to increase the instability in most cases and did not improve the correlation with the full-scale test. It was noted that wheel disengagement could be used to bracket the vehicle response if necessary later in the research effort.

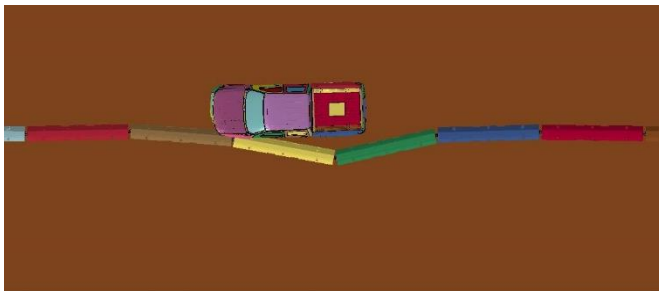
Finally, review of the results from all three truck models found that the Chevy Silverado V2 model of the impact with the F-shape PCB produced the best correlation with full-scale crash test no. 2214TB-2. Vehicle and barrier motions correlated well with the full-scale test based on high-speed video comparisons, and the dynamic lateral barrier deflection of the model was within 2 percent of that observed in the full-scale test. RSVVP analysis of the vehicle transducer data from the model and the test met two of the single channel comparisons and the multiple channel comparison. Thus, the baseline model for the simulation of the beginning and end of LON impacts on the F-shape PCB was selected to use the Chevy Silverado V2 vehicle model with the previously developed F-shape barrier model.



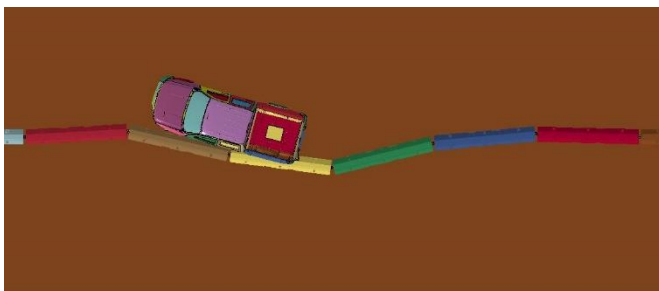
Time = 0.000 sec



Time = 0.100 sec

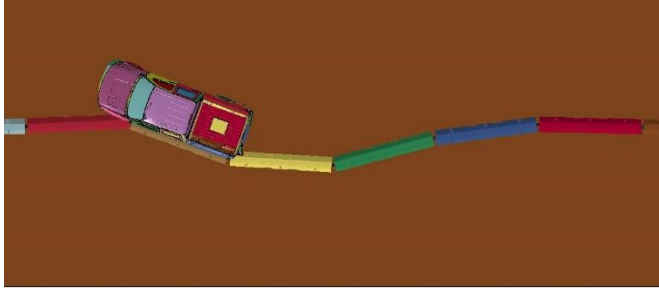


Time = 0.200 sec

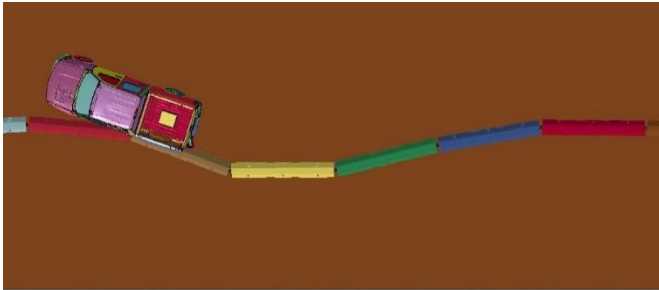


Time = 0.300 sec

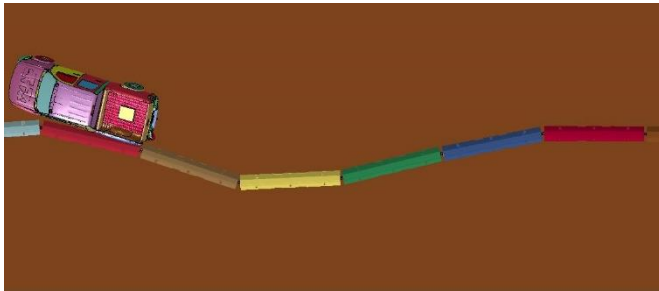
Figure 8. Overhead Sequential Views, Chevy Silverado V2 Model and Test No. 2214TB-2



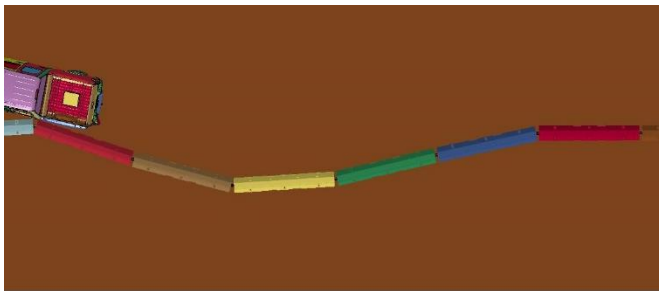
Time = 0.400 sec



Time = 0.500 sec



Time = 0.600 sec



Time = 0.700 sec

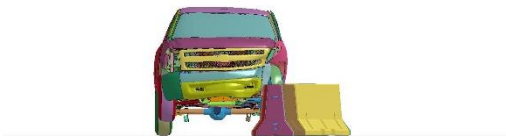
Figure 9. Overhead Sequential Views, Chevy Silverado V2 Model and Test No. 2214TB-2



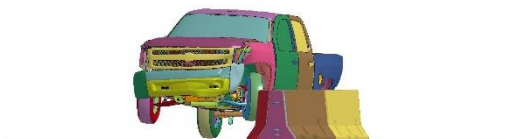
Time = 0.000 sec



Time = 0.100 sec



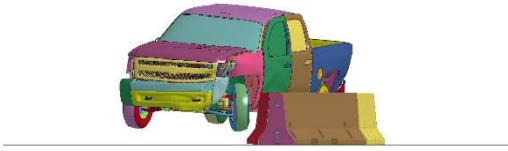
Time = 0.200 sec



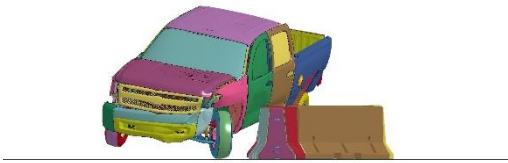
Time = 0.300 sec



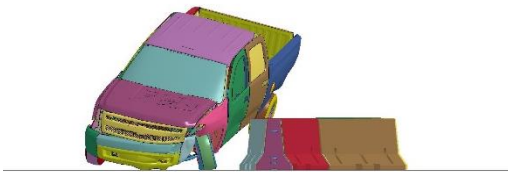
Figure 10. Downstream Sequential Views, Chevy Silverado V2 Model and Test No. 2214TB-2



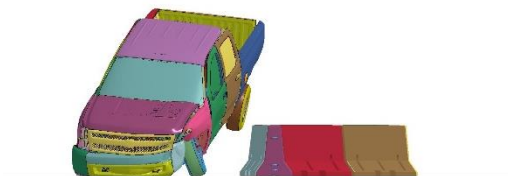
Time = 0.400 sec



Time = 0.500 sec



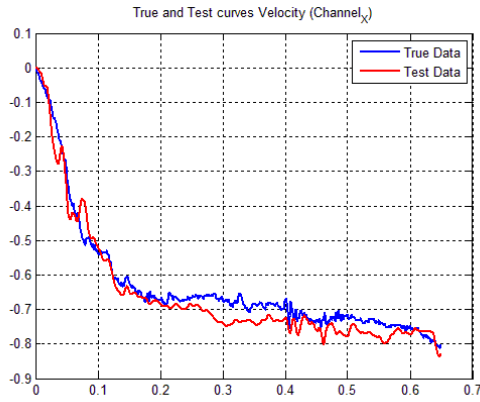
Time = 0.600 sec



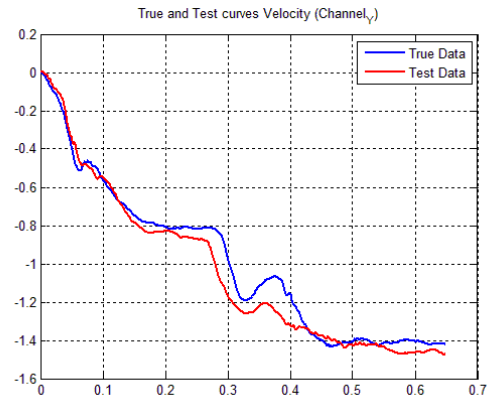
Time = 0.700 sec



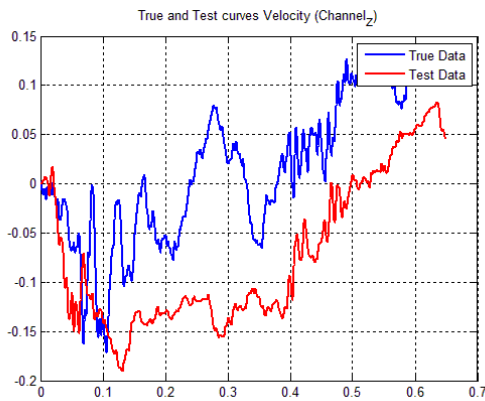
Figure 11. Downstream Sequential Views, Chevy Silverado V2 Model and Test No. 2214TB-2



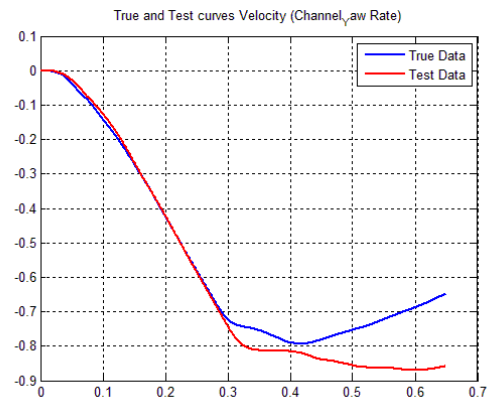
(a) Longitudinal Velocity



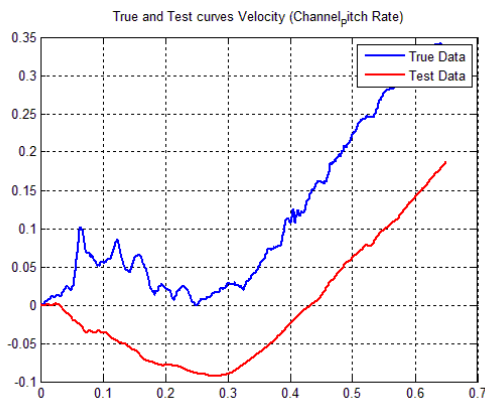
(b) Lateral Velocity



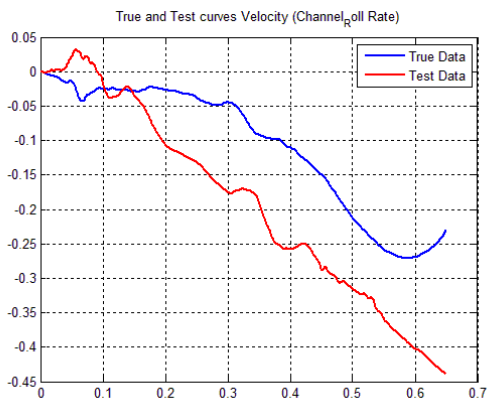
(c) Vertical Velocity



(d) Yaw Angle



(e) Pitch Angle



(f) Roll Angle

Figure 12. RSVVP Results, Chevy Silverado V2 Impact with F-Shape PCB Model

5 EVALUATION OF LENGTH OF NEED

With the baseline simulation model of the sixteen barrier, 200-ft (61-m) long F-shape PCB system successfully calibrated against full-scale crash test no. 2214TB-2, the researchers began to use the baseline model to investigate the limits of the LON for the barrier system. A series of models were simulated that impacted each of the sixteen barrier segments in the system at a target impact point 4.3 ft (1.3 m) upstream of the joint between the adjacent segments. Due to computation instabilities with the truck model as it impacted the first barrier joint downstream of impact, some models were run with an impact point 12 in. or 24 in. (305 mm or 610 mm) farther upstream in order to allow the simulations to run to completion. Barrier no. 16 was impacted midway along its length as there was no joint downstream of impact. The impact conditions for each simulation consisted of the 2270P vehicle impacting the barrier at a speed of 62 mph (100 km/h) and at an angle of 25 degrees. This corresponded to the MASH TL-3 impact conditions for test designation no. 3-11. Each of the simulations were analyzed to investigate a variety of parameters that would indicate the potential for safe vehicle redirection at that point along the length of the barrier system. These factors included:

1. Vehicle redirection
2. Vehicle climb
3. Vehicle stability (roll, pitch, and yaw)
4. Vehicle parallel time
5. Occupant risk (ORA and OIV)
6. Barrier pocketing – determined by the angle of the barrier prior to the vehicle contacting it
7. Displacement of the end barriers
8. Barrier roll (rotation of the barrier about its longitudinal axis)
9. Joint loads and pin deformation

The simulation of the various impact points was separated into two parts. Simulations of impacts along the first eight barrier segments of the 200-ft (61-m) long barrier system were conducted to evaluate the beginning of LON, while impacts along the last eight barrier segments were conducted to evaluate the end of LON. Details of that analysis are provided below.

5.1 Beginning of Length of Need Simulations

The results from all of the simulations impacting the first eight barrier segments of the sixteen barrier, 200-ft (61-m) long F-shape PCB system were compared to evaluate a potential beginning of LON point. Sequential photographs comparing the behavior of the PCB system at all eight impact points are shown in Figures 13 through 20. Review of the simulations found that the performance of the F-shape PCB system changed significantly when impacted closer to the upstream end of the barrier system. All of the impacts resulted in vehicle redirection. This was largely due to the inertial resistance of the barriers being sufficient to supply the primary redirective forces necessary to prevent gating of the barrier. Similarly, the time required for the vehicle to parallel the barrier during the impacts, the occupant risk values, and the vehicle climb of the barrier were consistent through all eight impacts. Vehicle stability for all of the impacts was acceptable, but vehicle roll tended to increase as the impact point moved upstream.

Barrier motions and deflections were directly affected as the impact of the vehicle neared the upstream end of the system. Maximum lateral barrier deflections, shown in Figure 21,

displayed only minor variations from impacts on the fifth through the eighth barriers in the PCB system. Impacts on the first four barriers of the system showed increasing lateral deflections as the impact approached the end of the system. This was a cause for concern due to increased lateral deflections potentially affecting vehicle stability as well as requiring larger clear areas behind the barrier system.

The maximum longitudinal displacement of the end barriers of the PCB system was also collected during the simulations, as shown in Figures 22 and 23. Large displacements of the end barriers indicated that the barrier system was potentially not providing sufficient tension upstream and downstream of the impact point and that barrier performance may be degraded. Longitudinal displacement of barrier no. 1 on the upstream end was most affected as the vehicle impacts approached the upstream end. Displacement of this barrier tended to increase as the impact point moved upstream. These increases were less severe when impacting barrier nos. 4 through 8, but became larger when impacting the first three barriers of the system. While there was no quantitative limit for the end barrier displacement, the displacements observed for the impacts on the first three barriers in the system were concerning as they effectively tripled the displacement of the end barrier observed for the baseline impact at the midspan of the system. Longitudinal displacement of barrier no. 16 was not as drastically affected, but it was noted that the displacement of this barrier decreased as the impact point of the vehicle moved upstream.

Pocketing of the barrier ahead of the vehicle was not noted even with the increased barrier deflections. This was largely due to the vehicle redirection occurring early in the impact event due to the inertial resistance of the barrier when barrier deflections were small.

Impacts near the upstream end of the system, particularly barrier nos. 1 through 3, produced high levels of deformation in the connecting pin between the barrier segments. A comparison of the connecting pin deformation for the baseline, midspan impact simulation, and the impact of the vehicle on barrier no. 1 is shown in Figure 24. The connection pin in the simulation of the impact on barrier no. 2 showed a large degree of deformation in the regions where it was loaded by the barrier connection loops. This level of deformation was not observed in the baseline, midspan simulation nor was it observed in full-scale crash testing. Thus, the deformation of the pin indicated that the loading of the barrier joints was increasing for impacts near the end of the system.

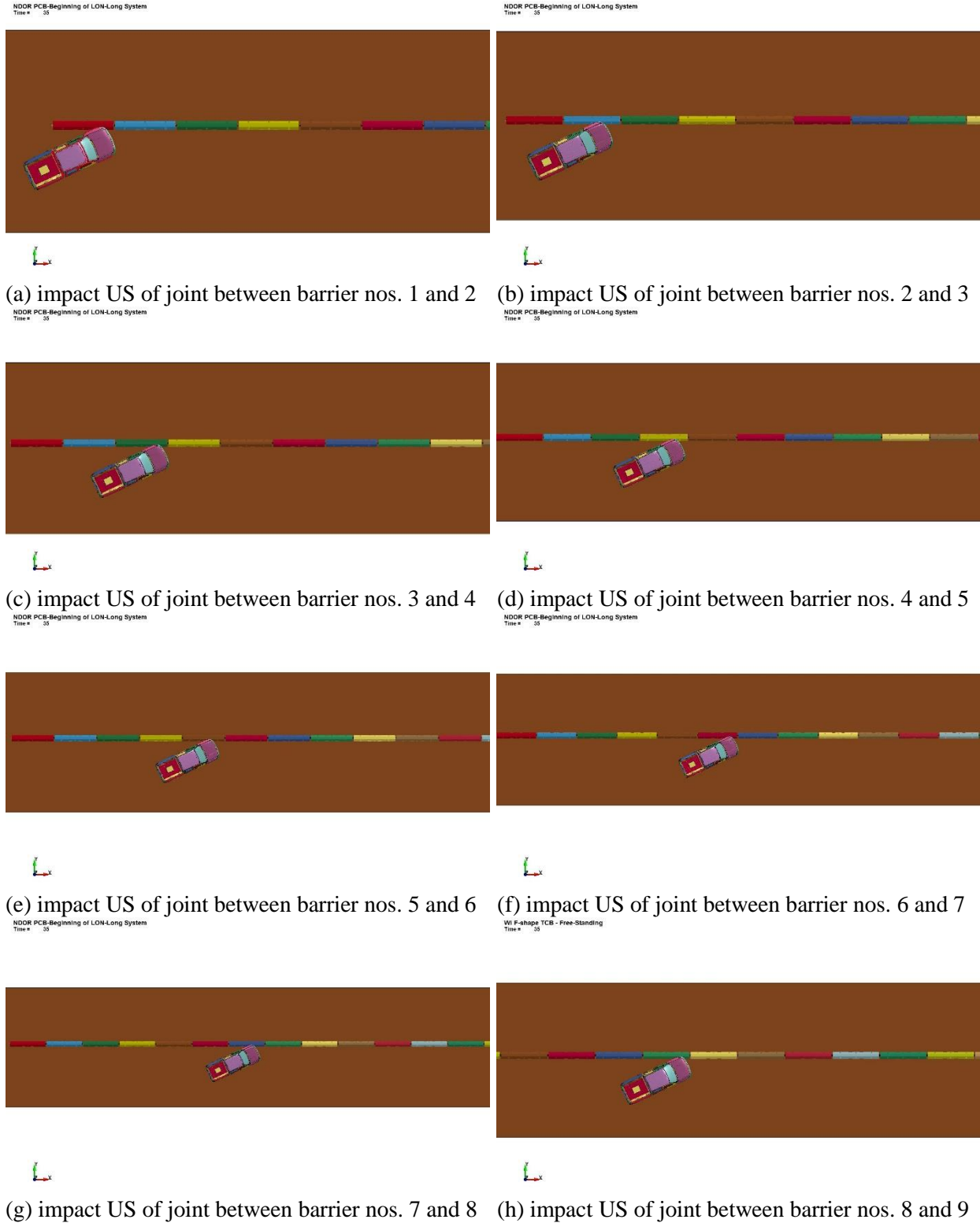


Figure 13. Simulation of Beginning of LON for 16-Barrier F-Shape PCB System, Overhead View, $t=0.000$ sec

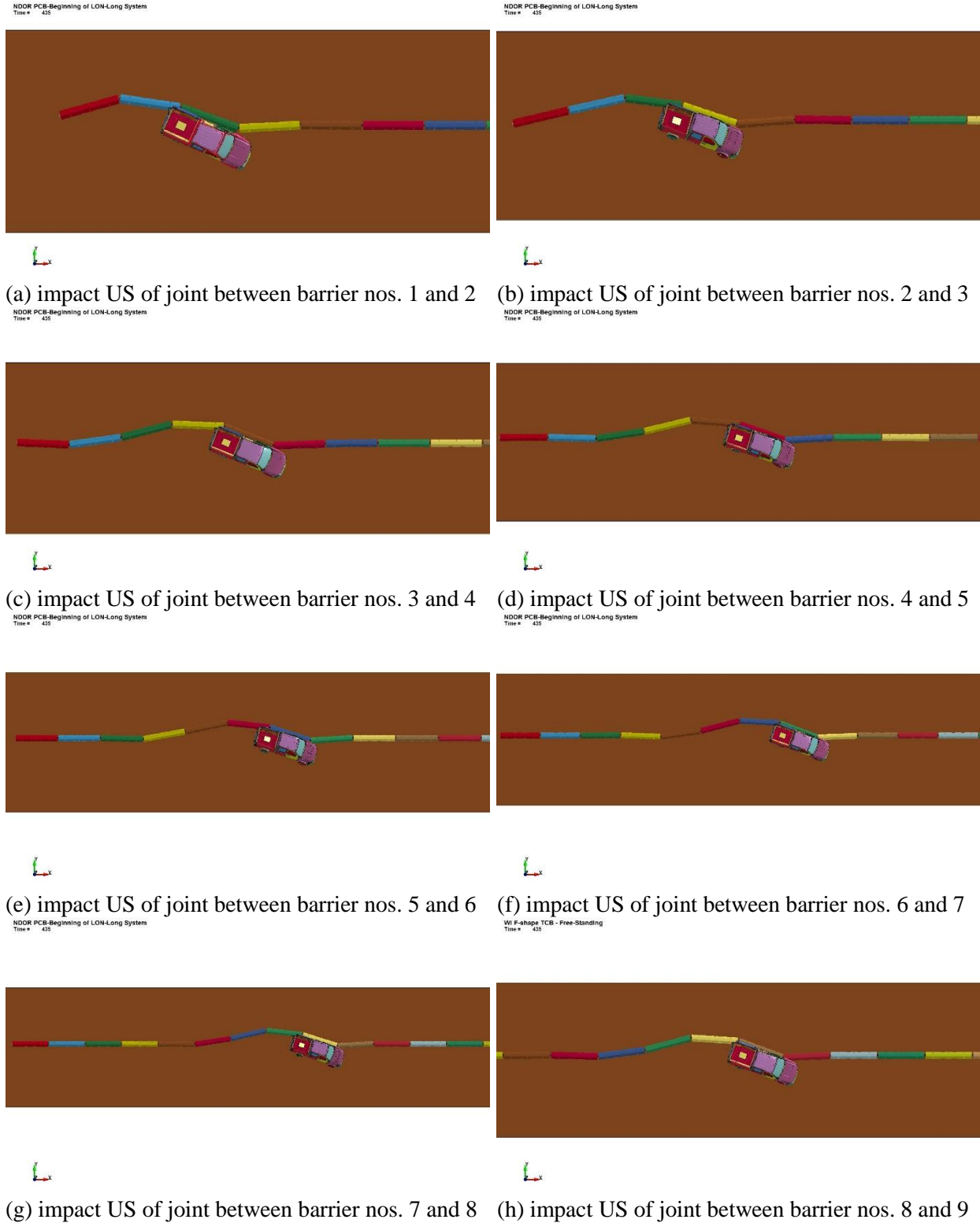


Figure 14. Simulation of Beginning of LON for 16-Barrier F-Shape PCB System, Overhead View, t=0.400 sec

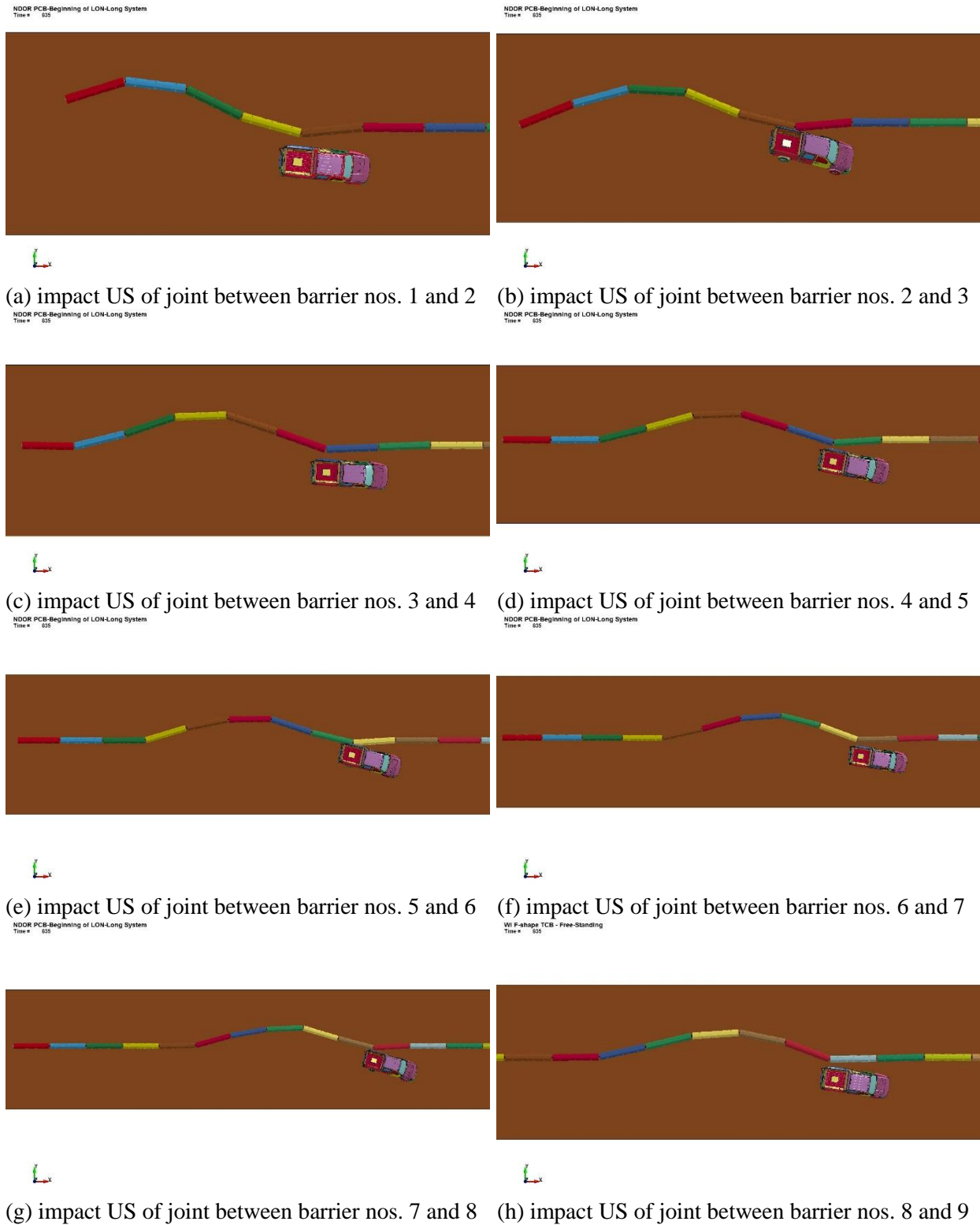


Figure 15. Simulation of Beginning of LON for 16-Barrier F-Shape PCB System, Overhead View, t=0.800 sec



Figure 16. Simulation of Beginning of LON for 16-Barrier F-Shape PCB System, Overhead View, $t=1.100$ sec

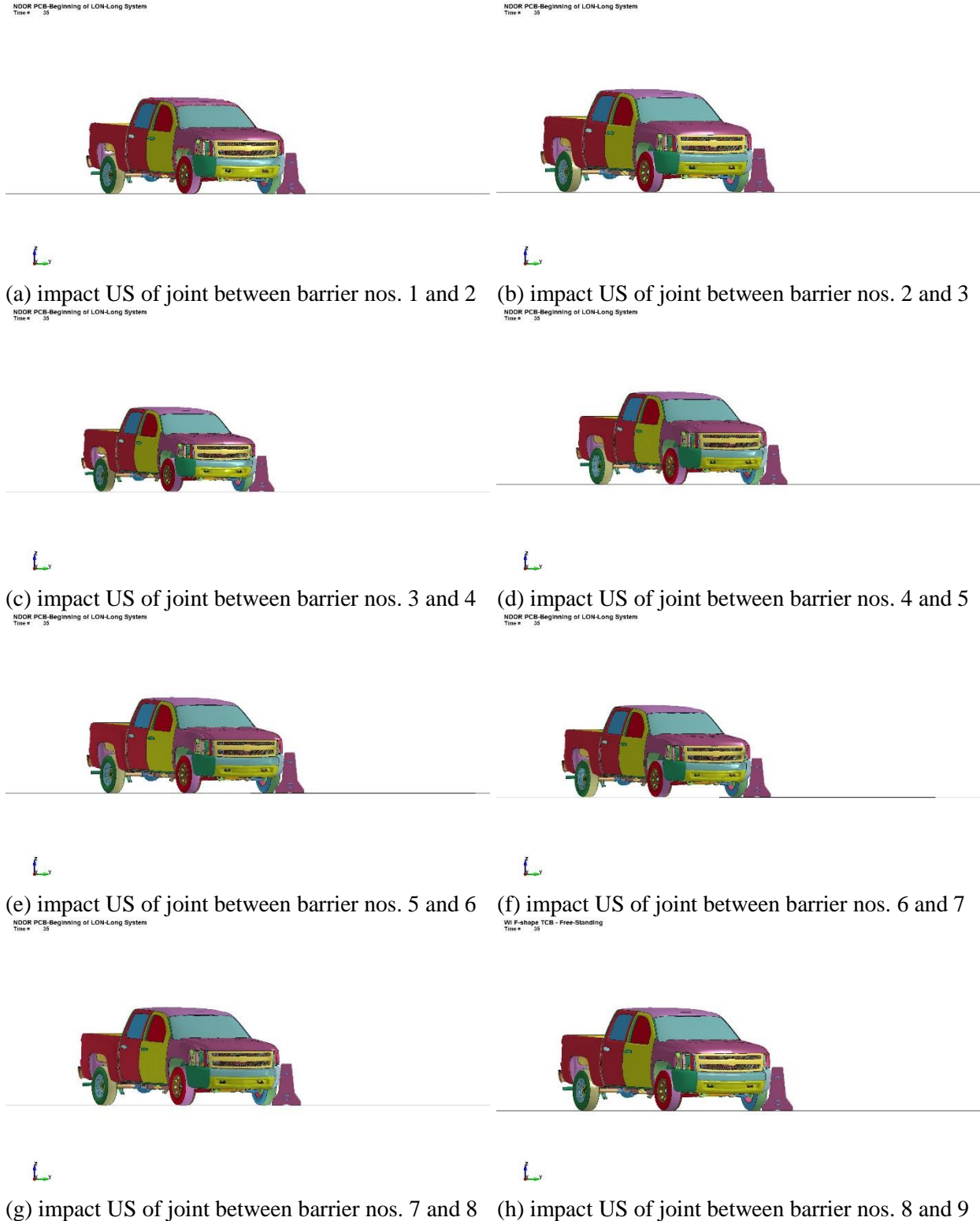
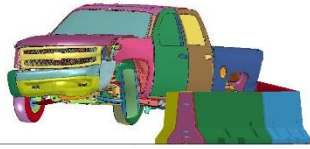
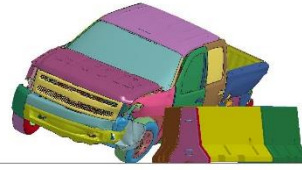


Figure 17. Simulation of Beginning of LON for 16-Barrier F-Shape PCB System, Downstream View, $t=0.000$ sec

NDOR PCB-Beginning of LON-Long System
Time = 435



NDOR PCB-Beginning of LON-Long System
Time = 435



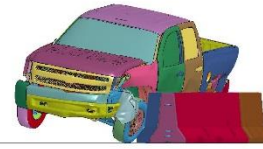
(a) impact US of joint between barrier nos. 1 and 2

(b) impact US of joint between barrier nos. 2 and 3

NDOR PCB-Beginning of LON-Long System
Time = 435



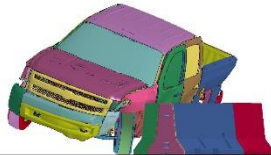
NDOR PCB-Beginning of LON-Long System
Time = 435



(c) impact US of joint between barrier nos. 3 and 4

(d) impact US of joint between barrier nos. 4 and 5

NDOR PCB-Beginning of LON-Long System
Time = 435



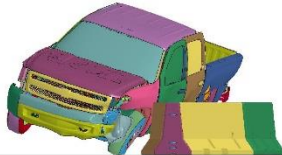
NDOR PCB-Beginning of LON-Long System
Time = 435



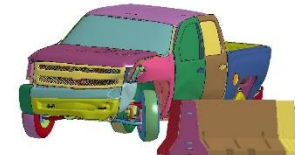
(e) impact US of joint between barrier nos. 5 and 6

(f) impact US of joint between barrier nos. 6 and 7

NDOR PCB-Beginning of LON-Long System
Time = 435



W1 F-shape TCB - Free-Standing
Time = 435



(g) impact US of joint between barrier nos. 7 and 8

(h) impact US of joint between barrier nos. 8 and 9

Figure 18. Simulation of Beginning of LON for 16-Barrier F-Shape PCB System, Downstream View, t=0.400 sec

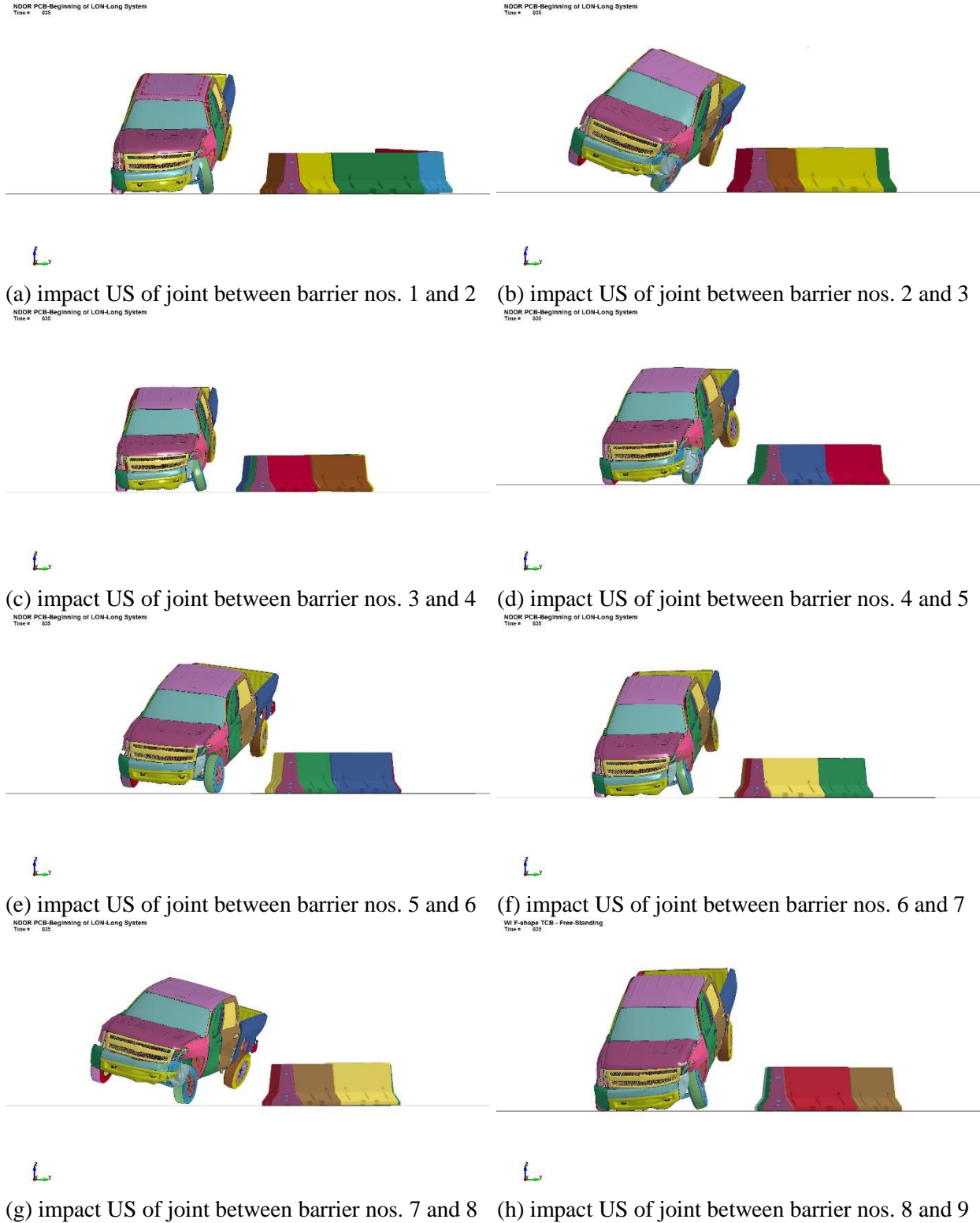


Figure 19. Simulation of Beginning of LON for 16-Barrier F-Shape PCB System, Downstream View, $t=0.800$ sec

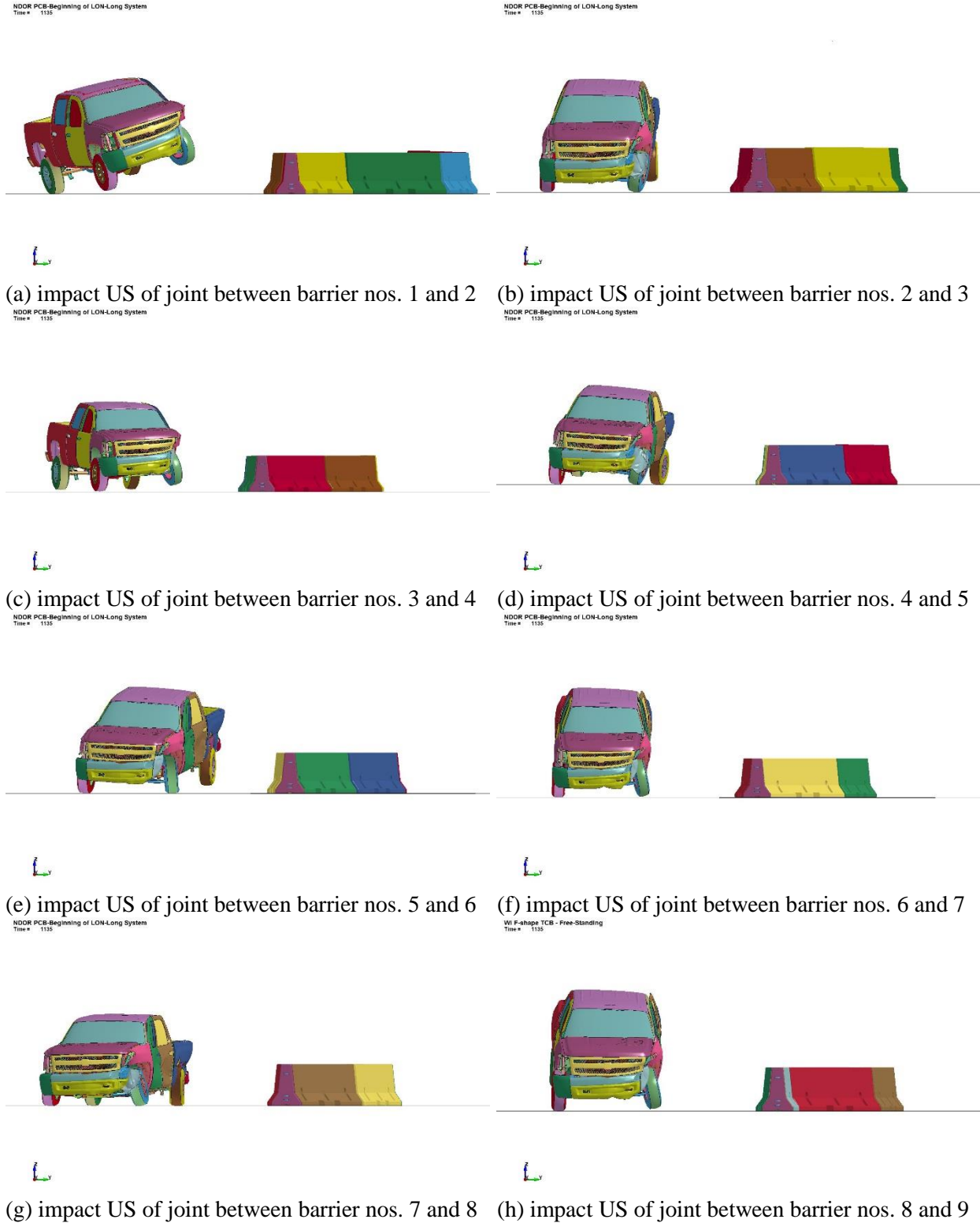


Figure 20. Simulation of Beginning of LON for 16-Barrier F-Shape PCB System, Downstream View, $t=1.100$ sec

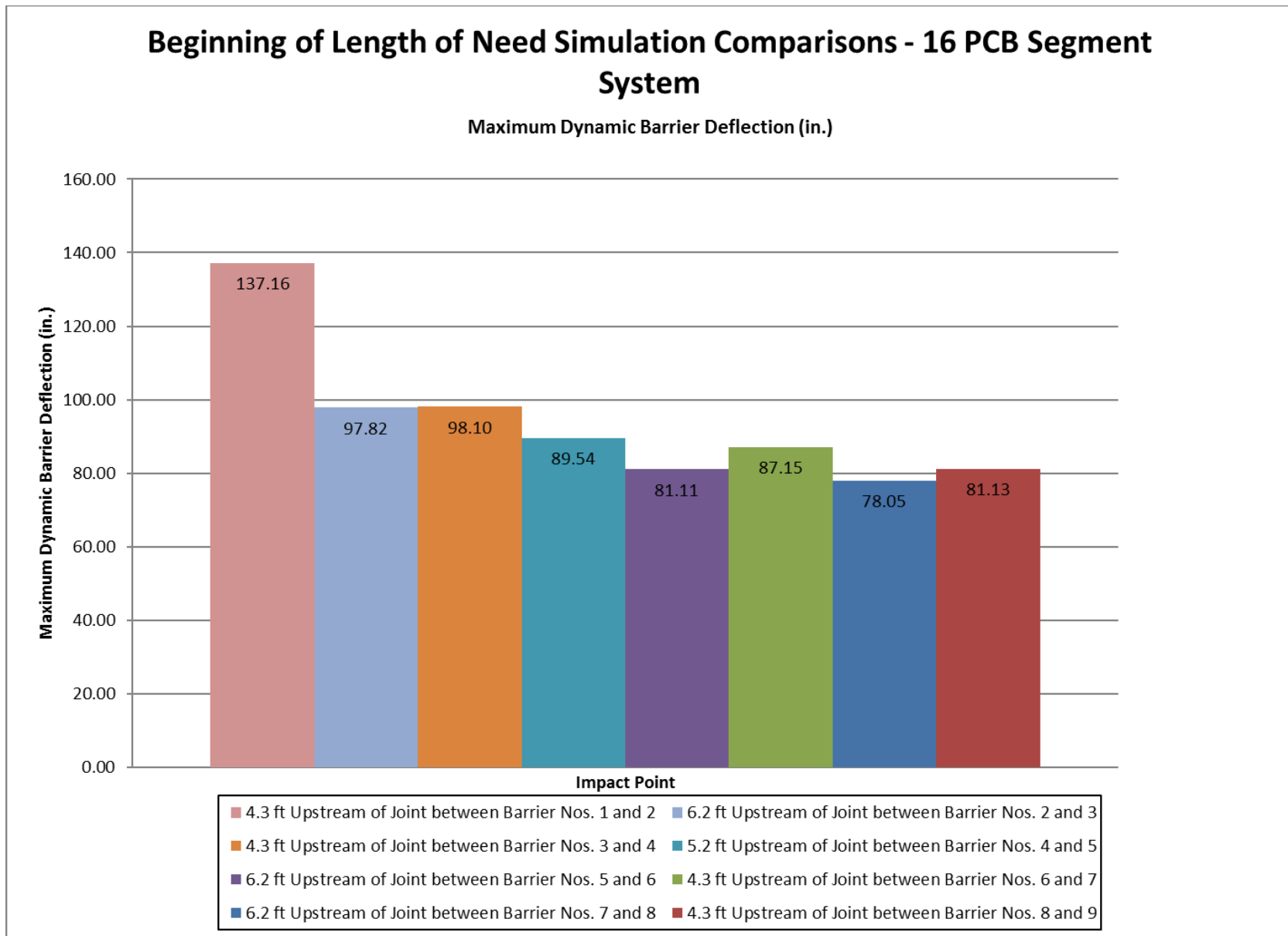


Figure 21. Beginning of LON Simulations, Maximum Lateral Barrier Deflections

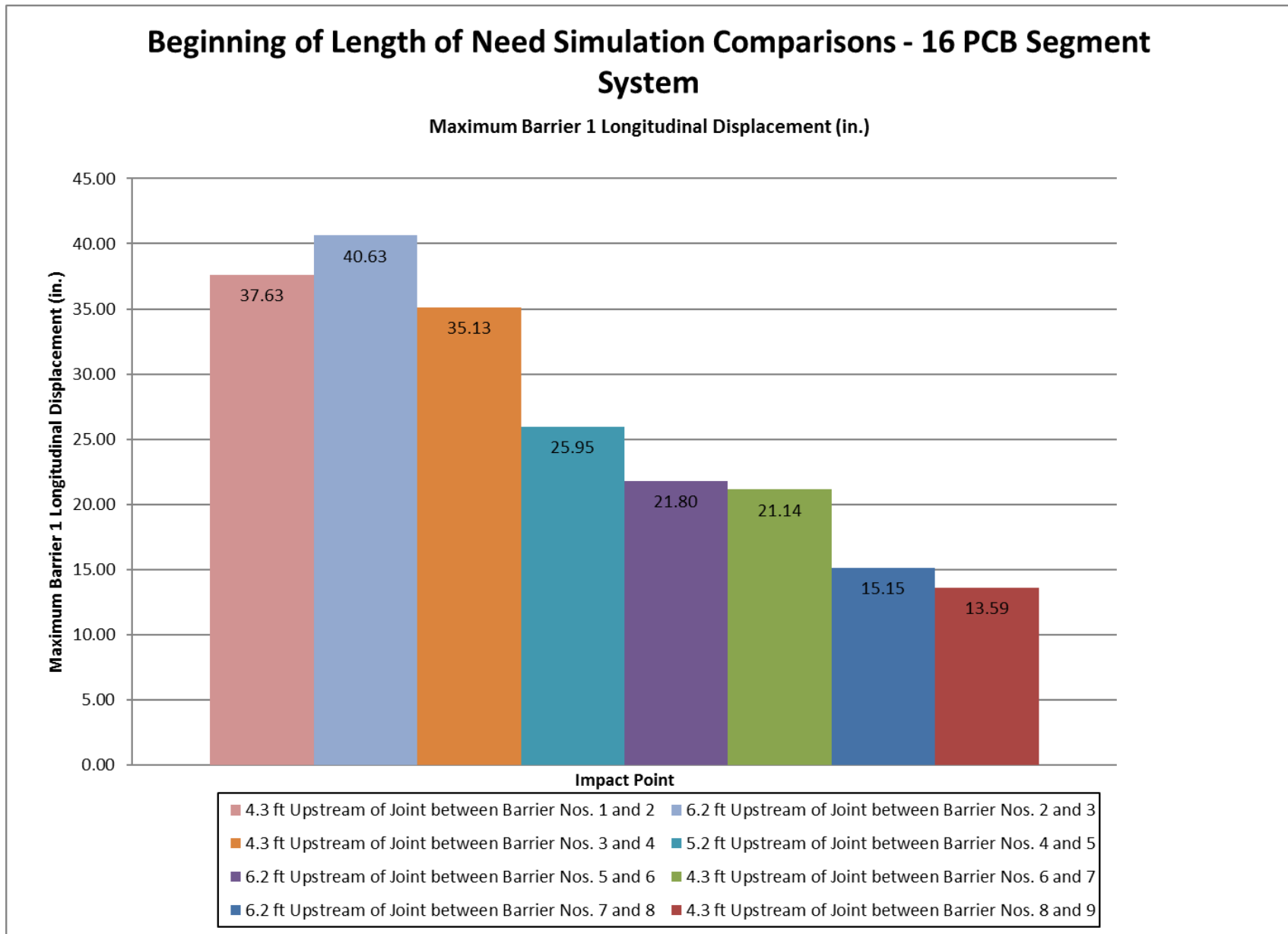


Figure 22. Beginning of LON Simulations, Maximum Longitudinal Displacement of Barrier No. 1

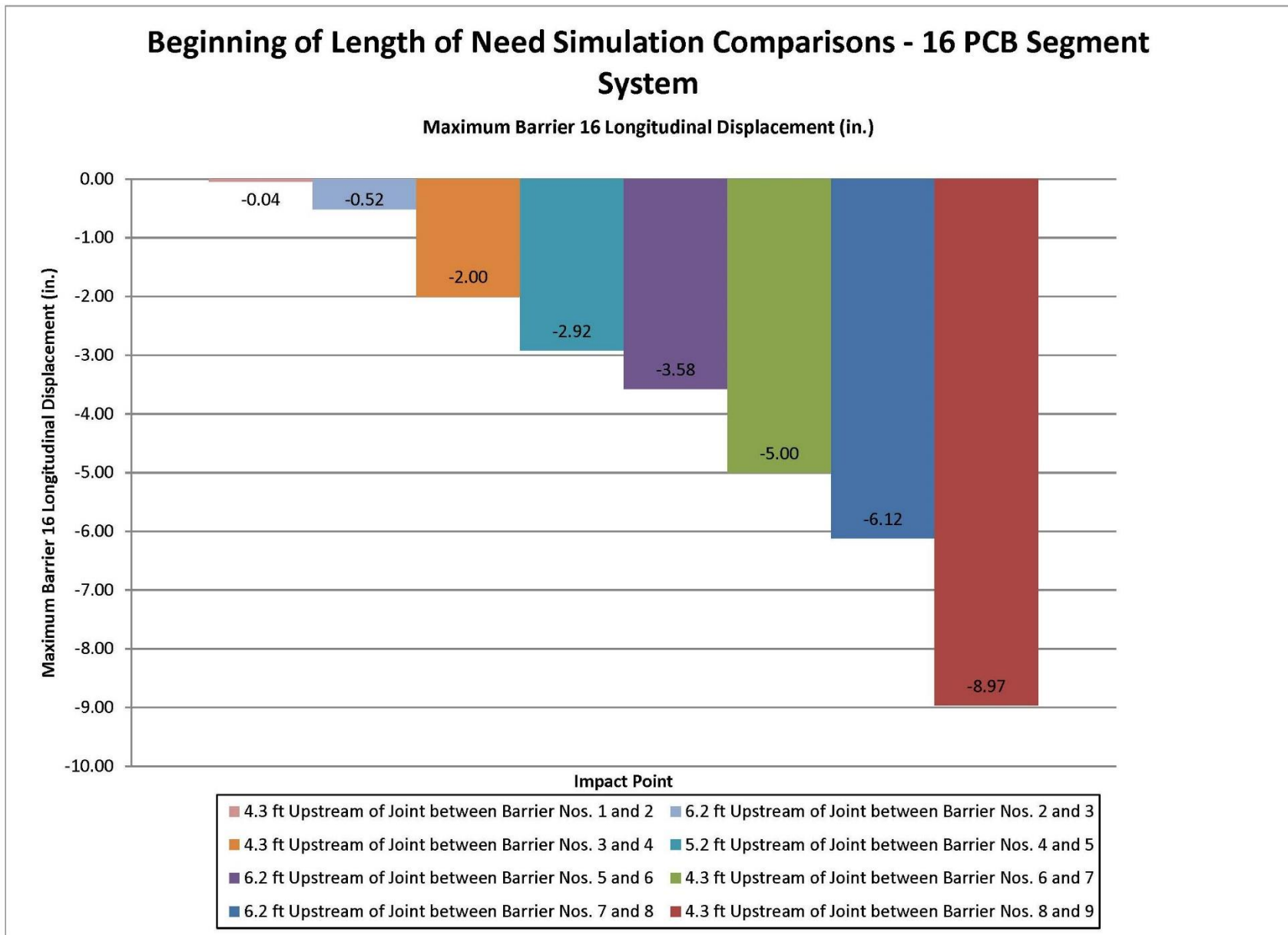
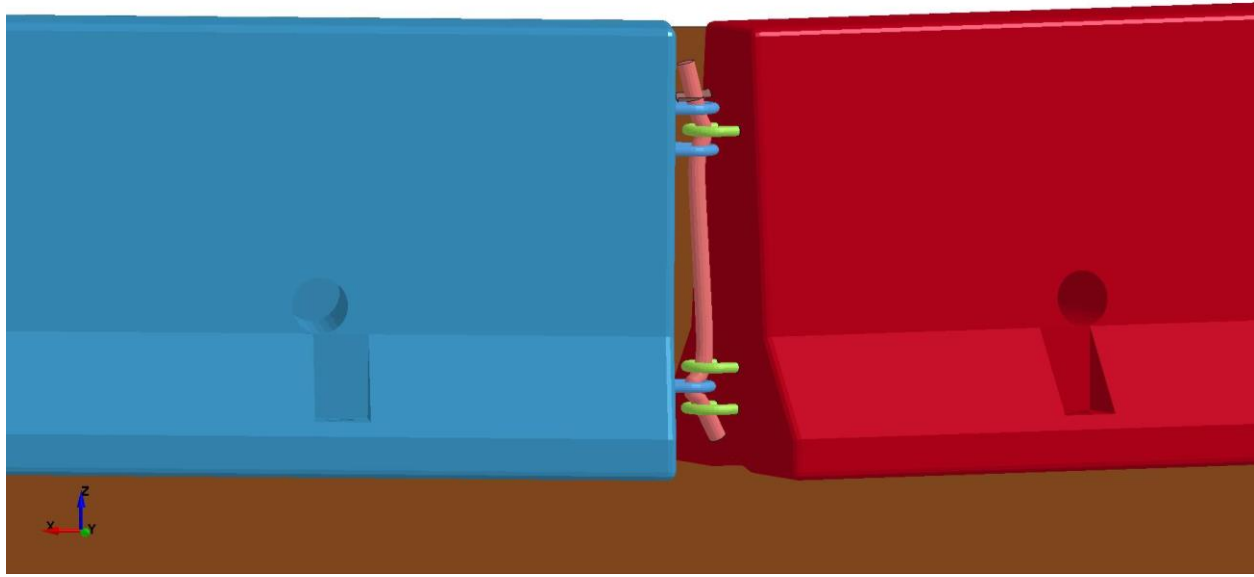
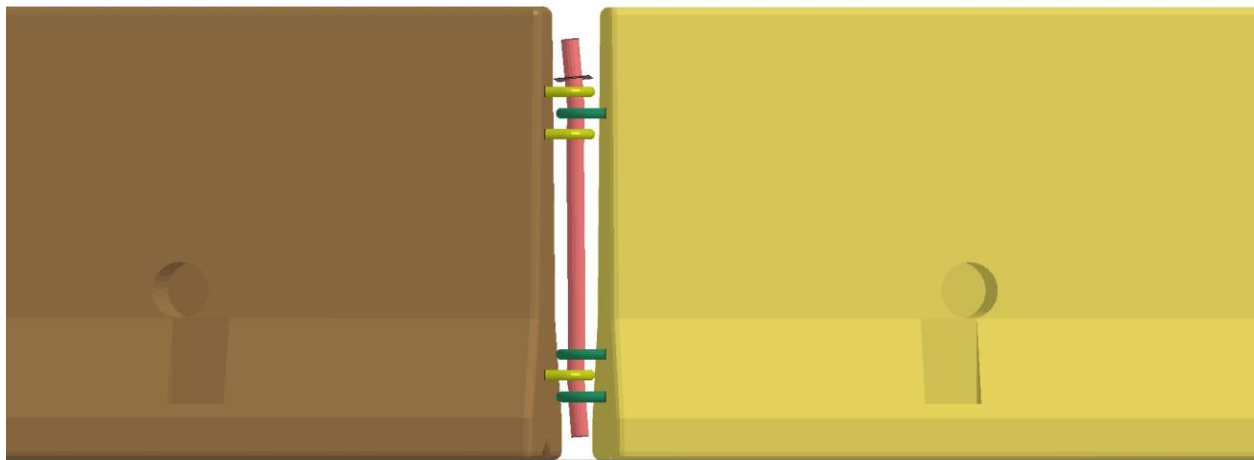


Figure 23. Beginning of LON Simulations, Maximum Longitudinal Displacement of Barrier No. 16



(a) Impact at Barrier No. 1

WI F-shape TCB - Free-Standing
Time = 1200



(b) Impact at Barrier No. 8 (Midspan)

Figure 24. Beginning of LON Connection Pin Deformation Comparison

5.2 End of Length of Need Simulations

The results from all of the simulations impacting the last eight barrier segments of the sixteen barrier, 200-ft (61-m) long F-shape PCB system were compared to evaluate a potential end of LON point. Sequential views comparing the behavior of the PCB system at all eight impact points are shown in Figures 25 through 32. Review of the simulations found that the performance of the F-shape PCB system changed significantly when impacted closer to the downstream end of the barrier system. Impacts on barrier nos. 9 through 14 resulted in vehicle redirection. This was largely due to the inertial resistance of the barriers being sufficient to supply the primary redirective forces necessary to prevent gating of the barrier. However, impact on barrier nos. 15 and 16 resulted in large deflections of the final barrier segment that represented more of a gating-type behavior for the end of the system. Gating of the system was also observed with respect to vehicle impact on barrier no. 14, but the 2270P vehicle was still effectively redirected in that impact prior to the large displacement of the end barrier segment. The time required for the vehicle to become parallel to the barrier during the impacts was similar for impacts on barrier nos. 9 through 15, but impact on barrier no. 16 yielded a delayed time to parallel due to the lack of downstream barriers and the gating of the end of the system. Occupant risk values were generally consistent for all of the impacts except barrier no. 16, which had much lower deceleration values due to the system gating and not redirecting the vehicle. Vehicle climb of the barrier was consistent through all the impacts. Vehicle stability for all of the impacts was acceptable, but vehicle roll and yaw tended to increase as the impact point moved downstream. Impacts on barrier nos. 12 through 15 displayed increased vehicle roll, while impacts on barrier nos. 15 and 16 yielded a significant increase in vehicle yaw. These increases in yaw and roll of the vehicle potentially indicated a concern for vehicle stability in these impacts on the downstream end of the system.

Barrier motions and deflections were also affected as the impact of the vehicle neared the downstream end of the system. Maximum lateral barrier deflections, shown in Figure 33, displayed only minor variations for impacts on barrier nos. 9 through 13 in the PCB system. Impacts on the last three barriers of the system showed much higher lateral deflections as the impact approached the end of the system. These lateral deflections were largely due to the gating behavior of the downstream end of the system noted previously. This was a cause for concern due to increased lateral deflections potentially affecting vehicle stability as well as requiring larger clear areas behind the barrier system.

The maximum longitudinal displacement of the end barriers of the PCB system was also collected during the simulations, as shown in Figures 34 and 35. Large displacements of the end barriers indicated that the barrier system was not potentially providing sufficient tension upstream and downstream of the impact point and that barrier performance may be degraded. Longitudinal displacement of barrier no. 16 on the downstream end was most affected as the vehicle impacts approached the downstream end. Displacement of this barrier tended to increase as the impact point moved downstream. These increases were less severe when impacting barrier nos. 9 through 12, but became larger when impacting the last four barriers of the system. Impact on barrier nos. 14 through 16 resulted in gating of the end of the barrier, which generated large lateral deflections of the end barrier but not large longitudinal displacement. Longitudinal displacement of barrier no. 1 was not as drastically affected, but the displacement of this barrier decreased as the impact point of the vehicle moved upstream.

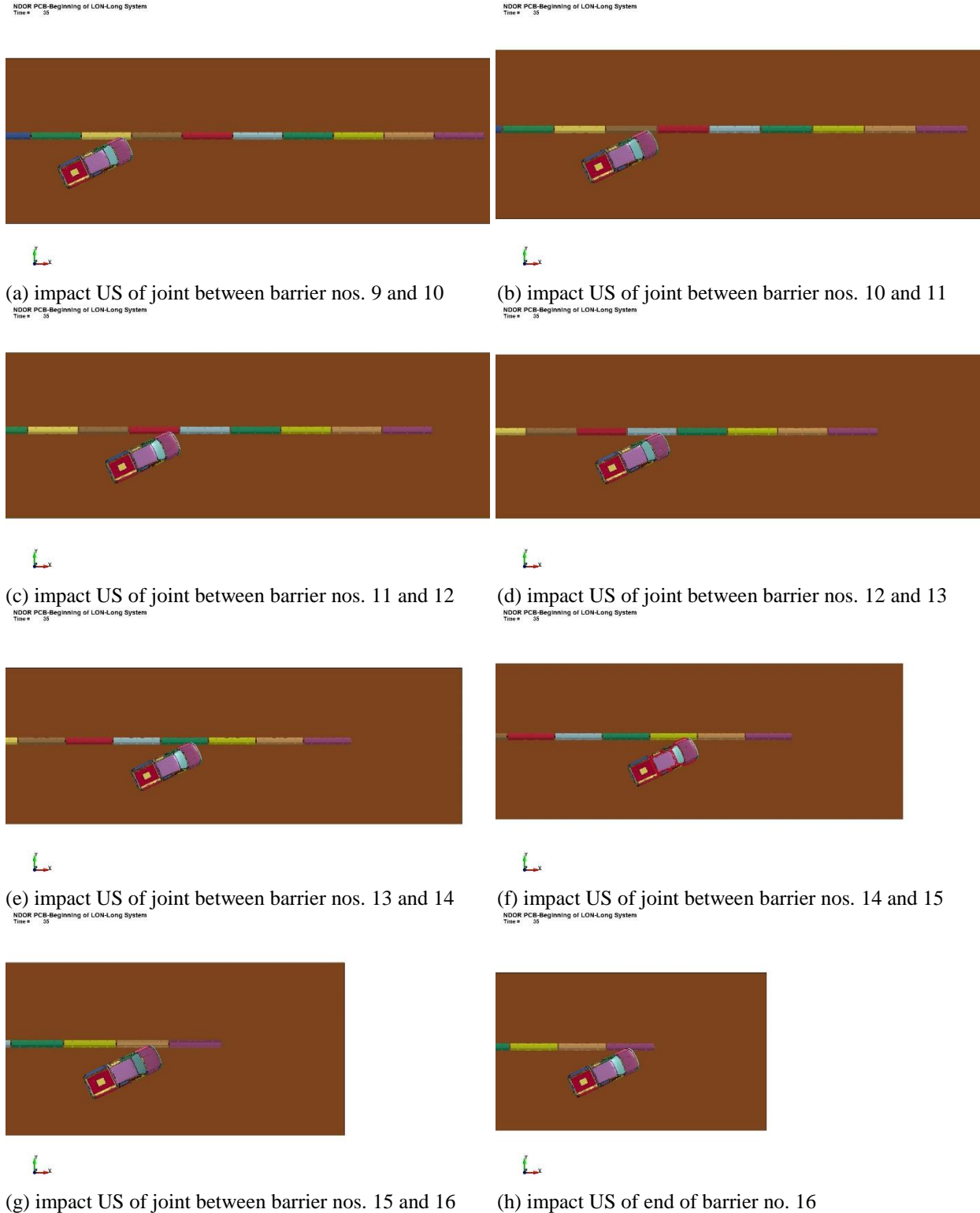


Figure 25. Simulation of End of LON for 16-Barrier F-Shape PCB System, Overhead View, $t=0.000$ sec

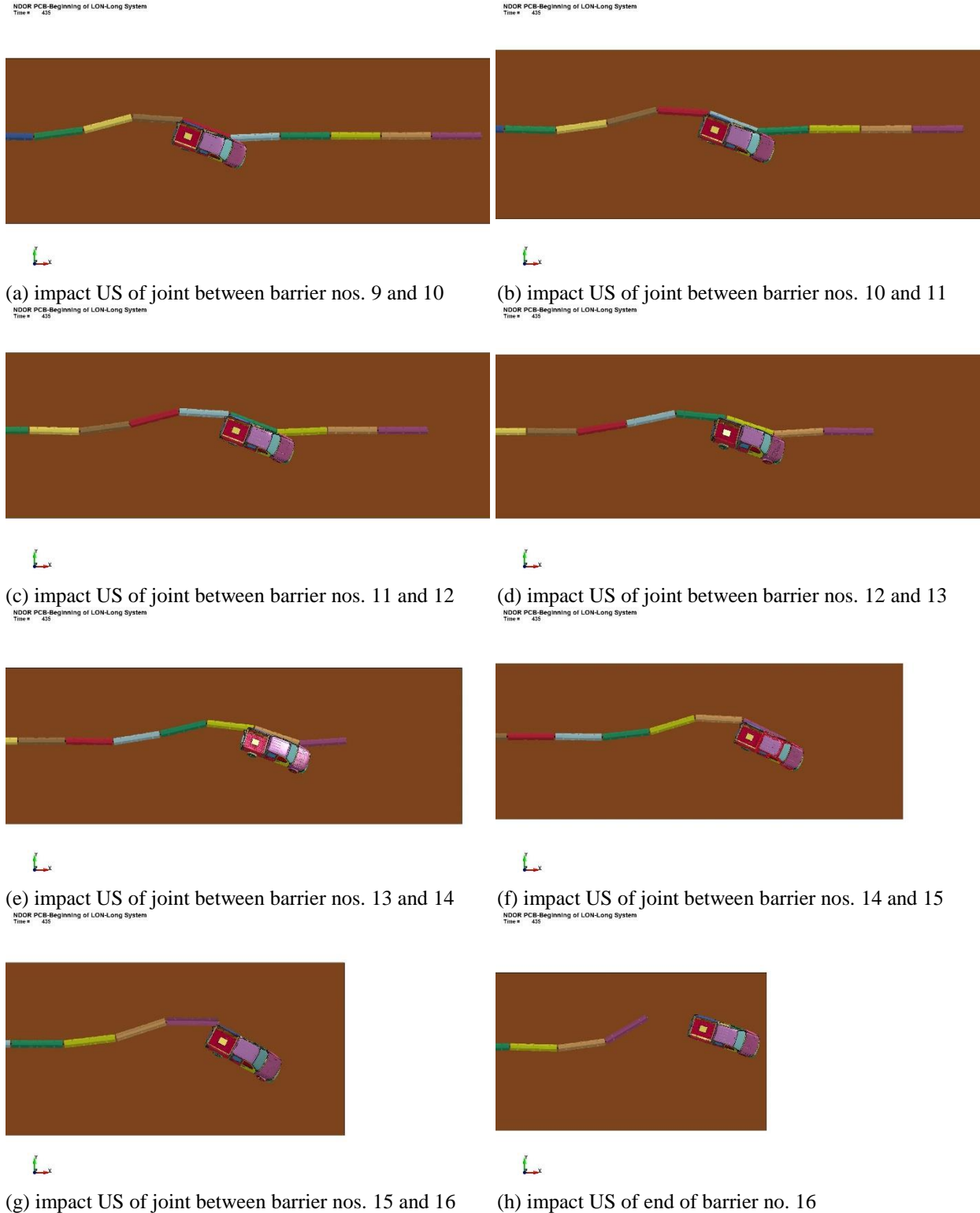


Figure 26. Simulation of End of LON for 16-Barrier F-Shape PCB System, Overhead View, $t=0.400$ sec

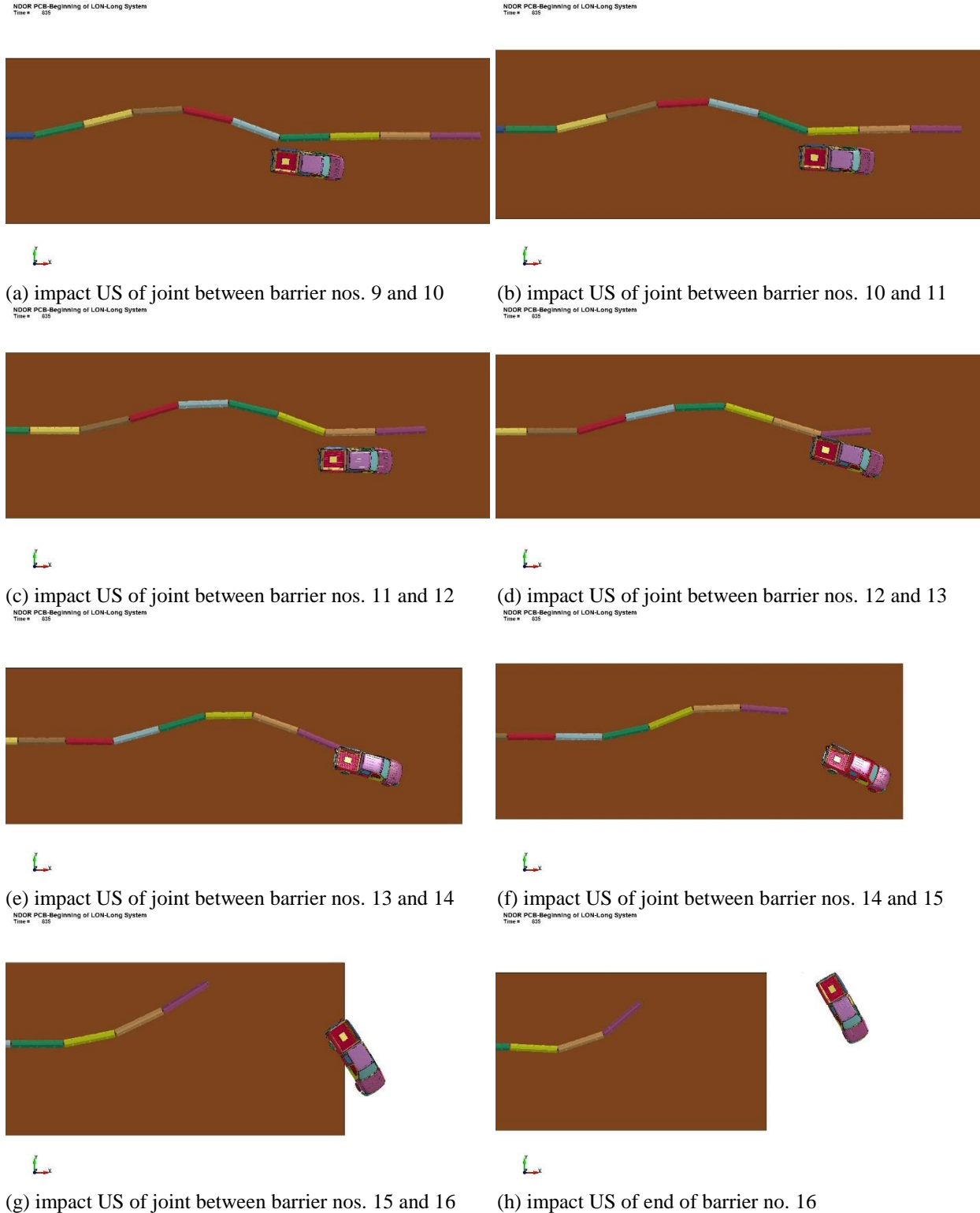


Figure 27. Simulation of End of LON for 16-Barrier F-Shape PCB System, Overhead View, $t=0.800$ sec

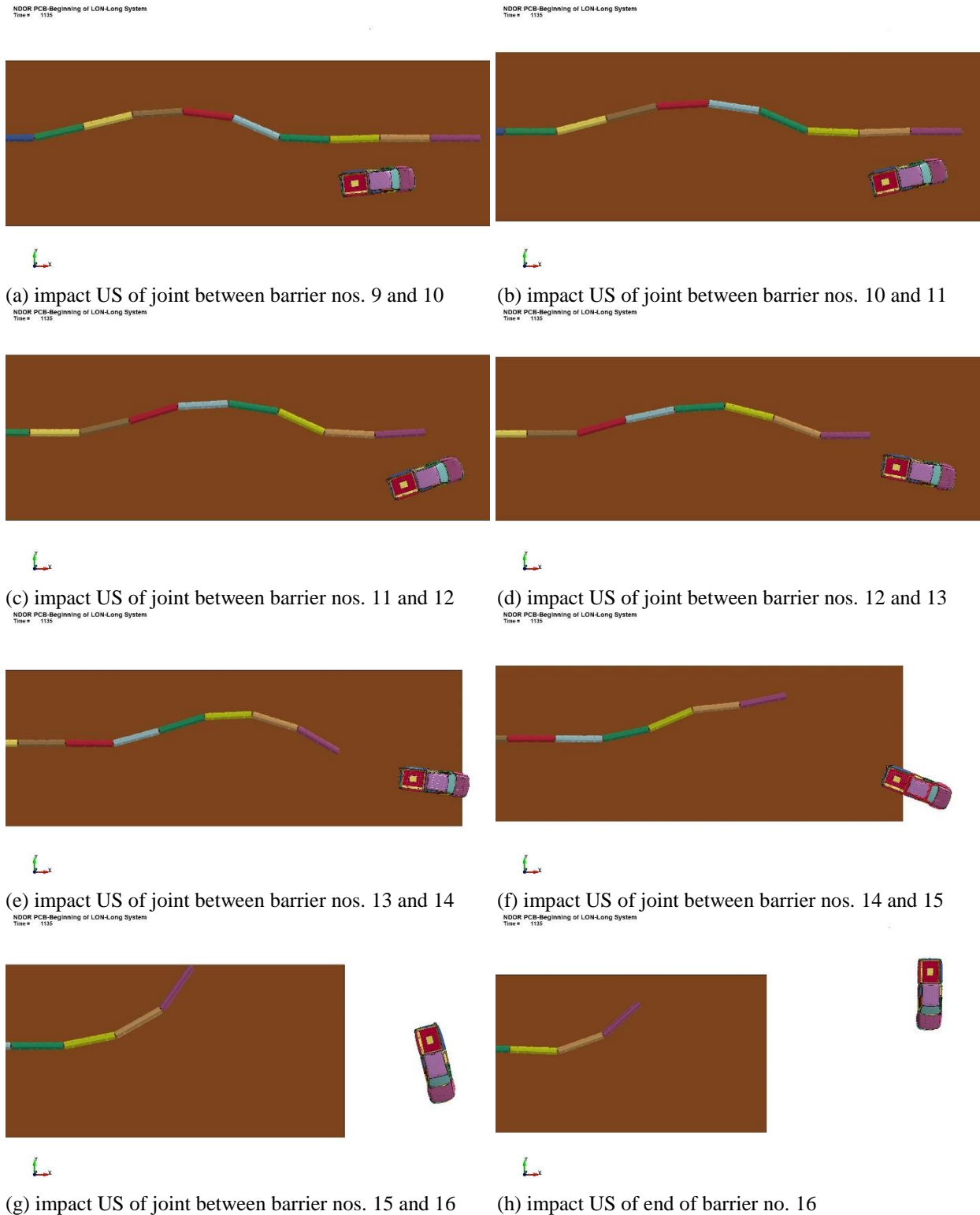


Figure 28. Simulation of End of LON for 16-Barrier F-Shape PCB System, Overhead View, $t=1.100$ sec

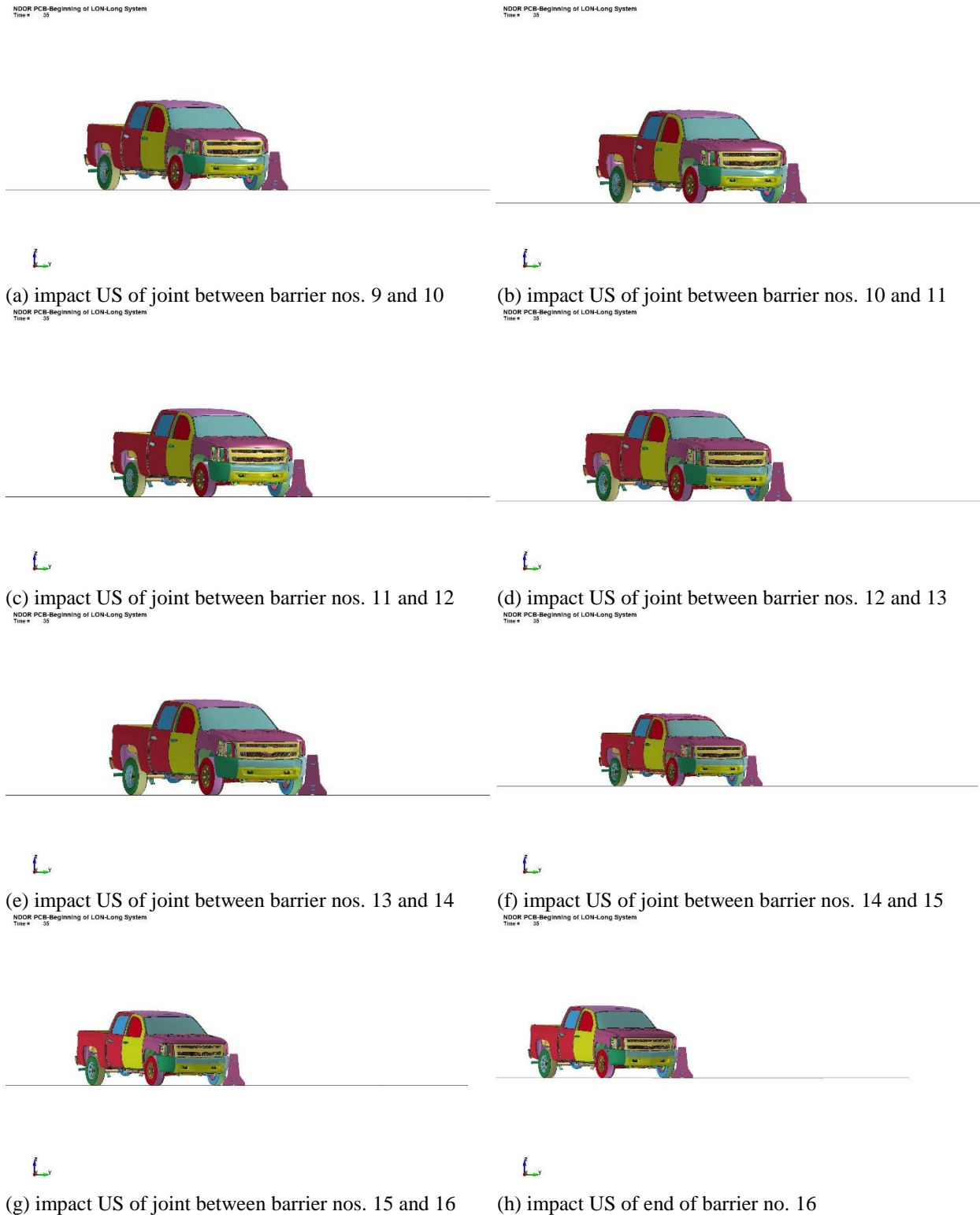


Figure 29. Simulation of End of LON for 16-Barrier F-Shape PCB System, Downstream View, $t=0.000$ sec

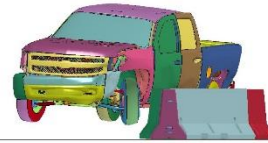
NDOR PCB-Beginning of LON-Long System
Time = 435



(a) impact US of joint between barrier nos. 9 and 10

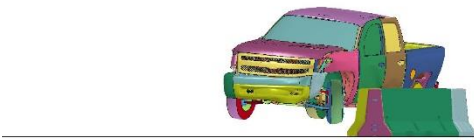
NDOR PCB-Beginning of LON-Long System
Time = 435

NDOR PCB-Beginning of LON-Long System
Time = 435



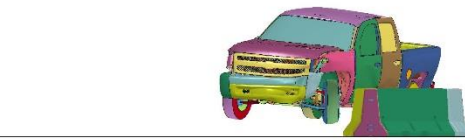
(b) impact US of joint between barrier nos. 10 and 11

NDOR PCB-Beginning of LON-Long System
Time = 435



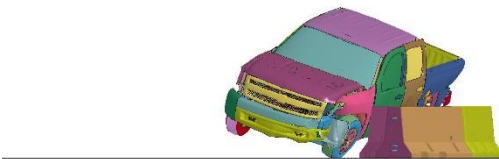
(c) impact US of joint between barrier nos. 11 and 12

NDOR PCB-Beginning of LON-Long System
Time = 435



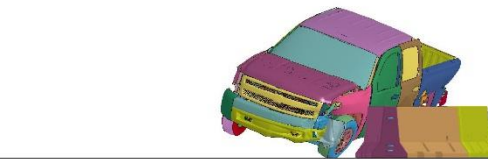
(d) impact US of joint between barrier nos. 12 and 13

NDOR PCB-Beginning of LON-Long System
Time = 435



(e) impact US of joint between barrier nos. 13 and 14

NDOR PCB-Beginning of LON-Long System
Time = 435



(f) impact US of joint between barrier nos. 14 and 15

NDOR PCB-Beginning of LON-Long System
Time = 435



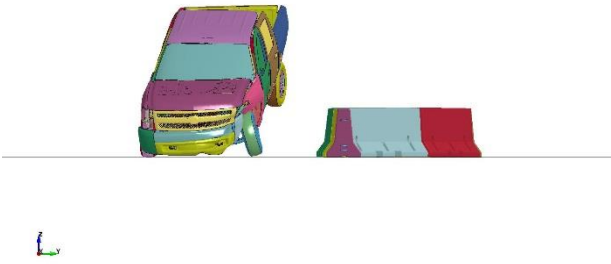
(g) impact US of joint between barrier nos. 15 and 16



(h) impact US of end of barrier no. 16

Figure 30. Simulation of End of LON for 16-Barrier F-Shape PCB System, Downstream View, $t=0.400$ sec

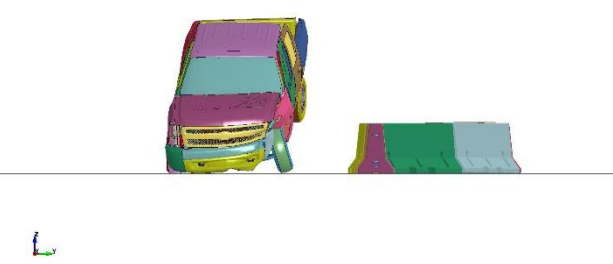
NDOR PCB-Beginning of LON-Long System
Time = 0.00



(a) impact US of joint between barrier nos. 9 and 10

NDOR PCB-Beginning of LON-Long System
Time = 0.00

NDOR PCB-Beginning of LON-Long System
Time = 0.00



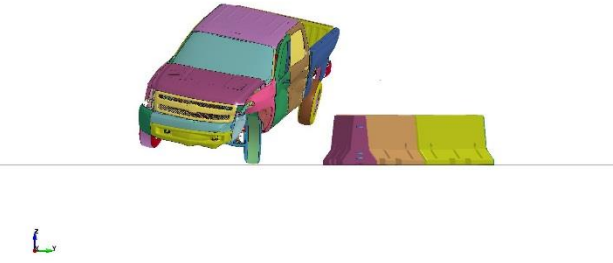
(b) impact US of joint between barrier nos. 10 and 11

NDOR PCB-Beginning of LON-Long System
Time = 0.00



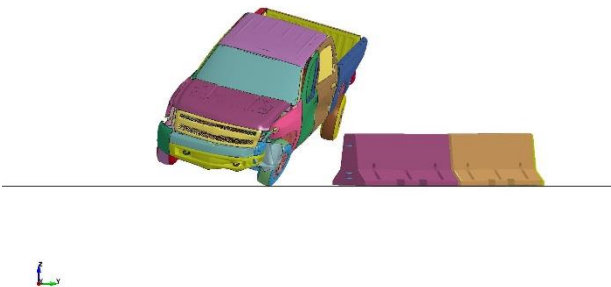
(c) impact US of joint between barrier nos. 11 and 12

NDOR PCB-Beginning of LON-Long System
Time = 0.00



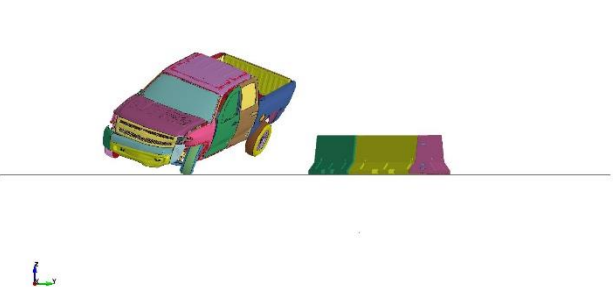
(d) impact US of joint between barrier nos. 12 and 13

NDOR PCB-Beginning of LON-Long System
Time = 0.00



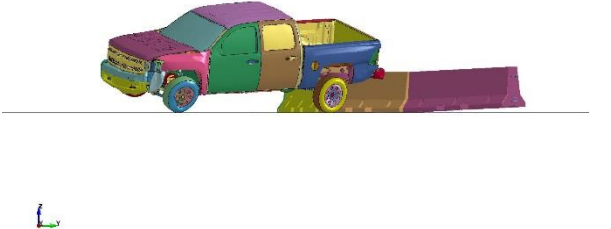
(e) impact US of joint between barrier nos. 13 and 14

NDOR PCB-Beginning of LON-Long System
Time = 0.00

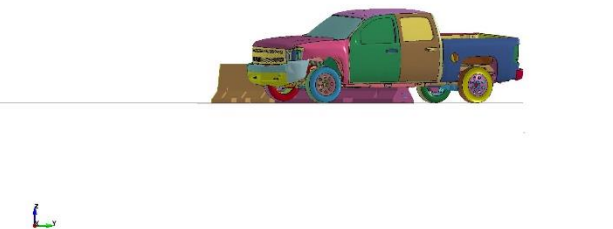


(f) impact US of joint between barrier nos. 14 and 15

NDOR PCB-Beginning of LON-Long System
Time = 0.00



(g) impact US of joint between barrier nos. 15 and 16



(h) impact US of end of barrier no. 16

Figure 31. Simulation of End of LON for 16-Barrier F-Shape PCB System, Downstream View, $t=0.800$ sec

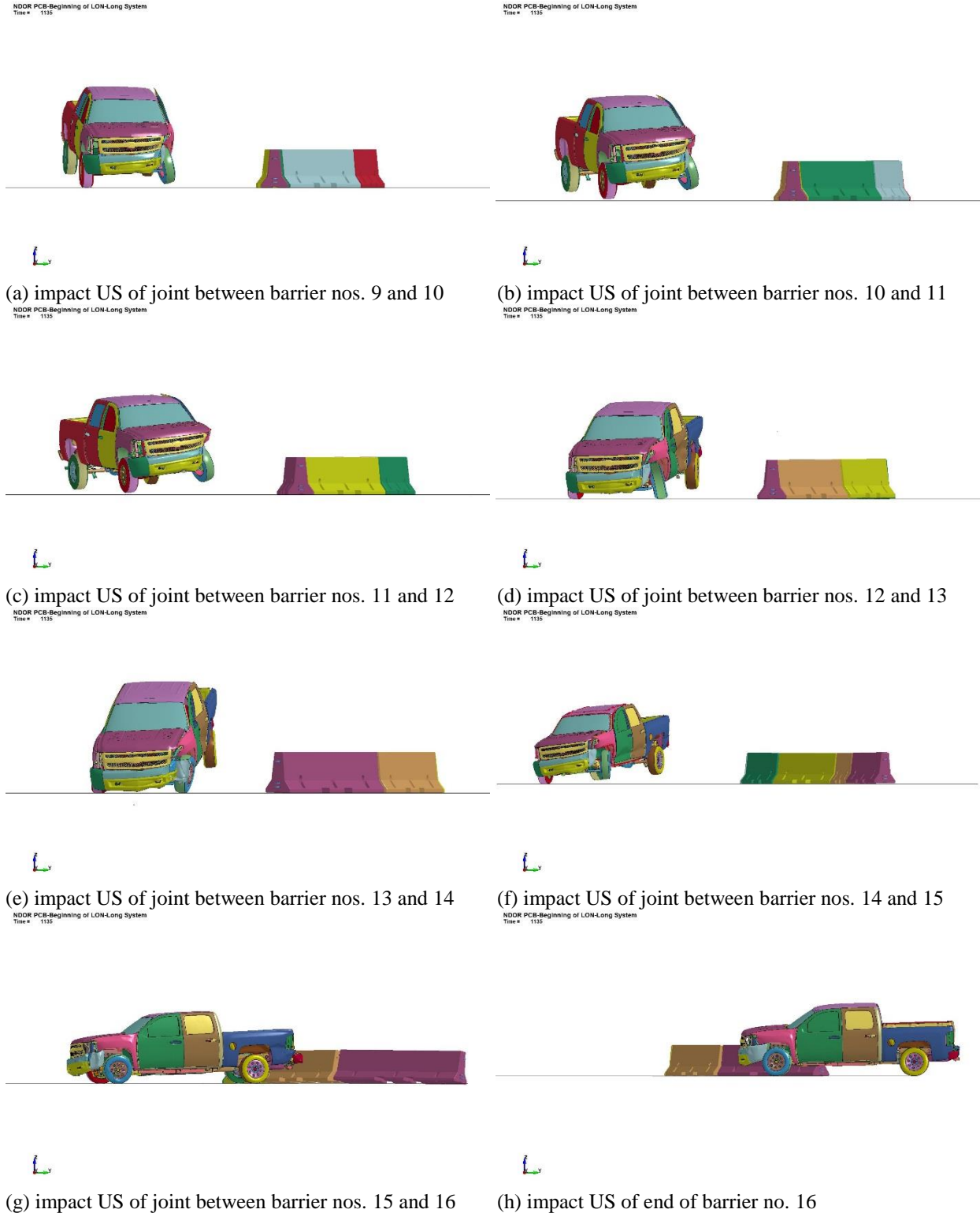


Figure 32. Simulation of End of LON for 16-Barrier F-Shape PCB System, Downstream View, $t=1.100$ sec

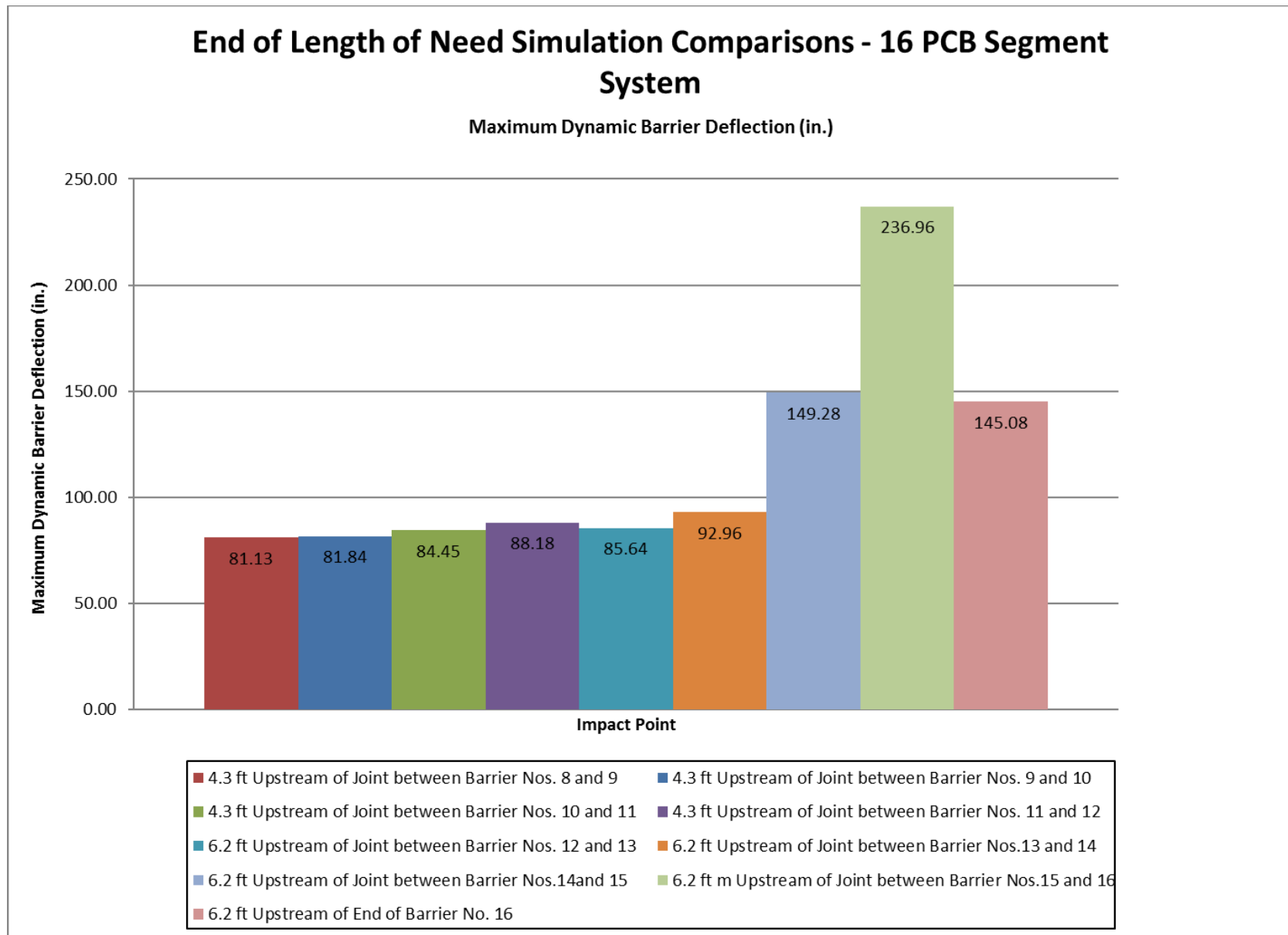


Figure 33. End of LON Simulations, Maximum Lateral Barrier Deflections

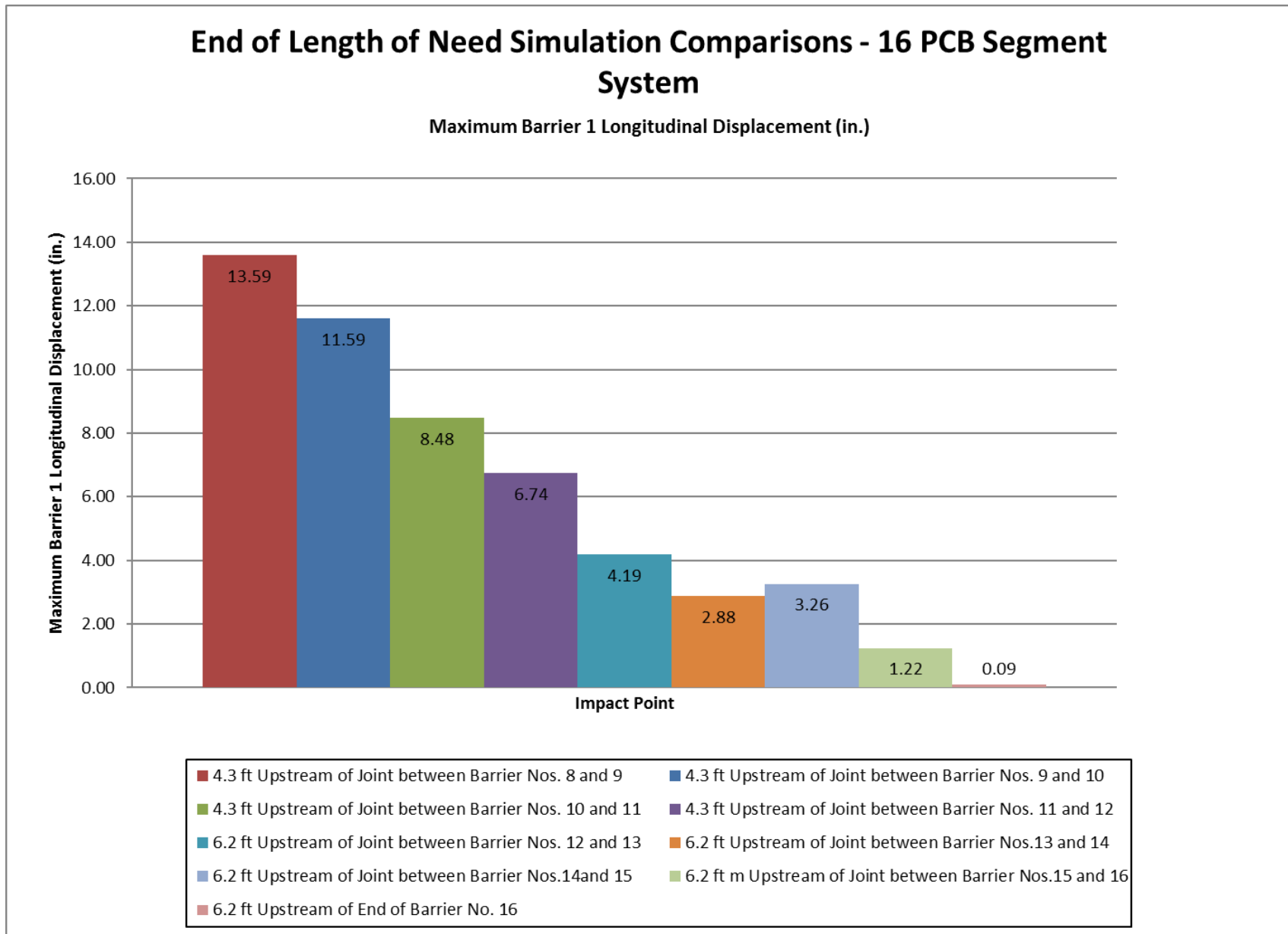


Figure 34. End of LON Simulations, Maximum Longitudinal Displacement of Barrier No. 1

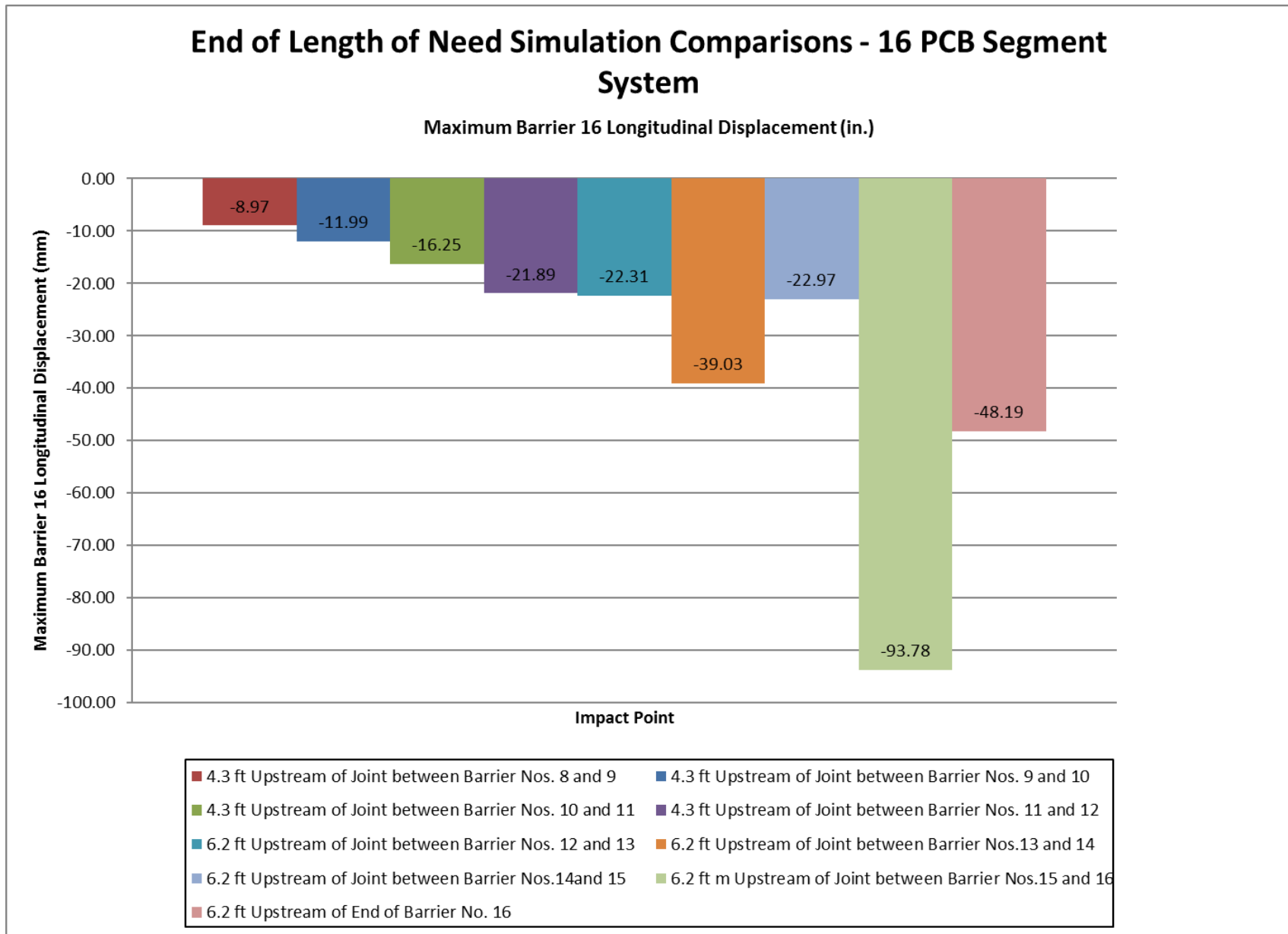


Figure 35. End of LON Simulations, Maximum Longitudinal Displacement of Barrier No. 16

Pocketing of the barrier ahead of the vehicle was not noted even with the increased barrier deflections. This was largely the result of the vehicle redirection occurring early in the impact event due to the inertial resistance of the barrier when barrier deflections were small.

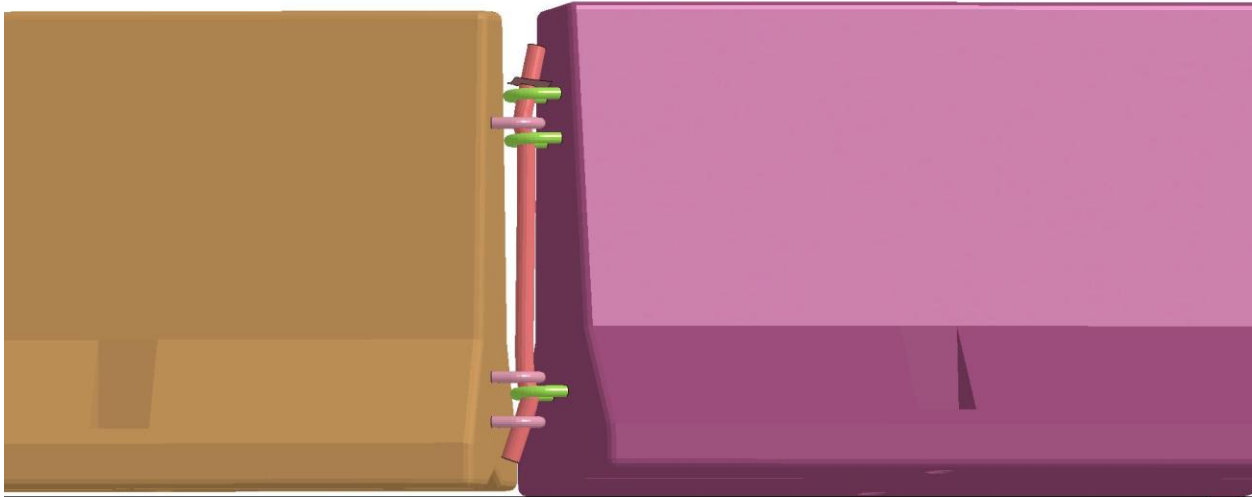
Finally, impacts near the downstream end of the system, particularly barrier nos. 14 and 15, produced high levels of deformation in the connection pin between the barrier segments. A comparison of the connecting pin deformation for the simulation of the baseline model impacted at the midspan and the impact of the vehicle on barrier no. 15 is shown in Figure 36. The connection pin in the simulation of the impact on barrier no. 2 showed a large degree of deformation in the regions where it was loaded by the barrier connection loops. This level of deformation was not observed in the simulation of the baseline model impacted at the midspan, nor was it observed in full-scale crash testing. Thus, the deformation of the pin indicated that the loading of the barrier joints was increasing for impacts near the end of the system.

5.3 Selection of Beginning and End of LON for 16 PCB Simulations

Review of the data from the simulations of the beginning and end of LON for the F-shape PCB system with sixteen barrier segments raised concerns regarding impacts at the far upstream and downstream ends of the system. On the upstream end of the PCB system, impacts on the first three barrier segments produced increased lateral barrier deflections and longitudinal barrier displacements. While all of the simulated impacts on the upstream end of the system produced stable vehicle redirection, there was concern that the high levels of barrier displacement would put the PCB system at the limits of its performance and may induce vehicle stability issues not captured by the model. Simulations near the upstream end of the system displayed increased vehicle roll that supported this concern. Additionally, excessively large deflections may cause operational issues related to clear zones behind the displaced barrier segments. Deformations of the PCB connection pins were also increased for impacts on the first three barriers of the PCB system, which would indicate increased loading of the barrier joint. Based on these concerns, it was recommended that a minimum of three barrier segments be used to define the beginning of LON of the PCB system without further analysis prior to investigation of reduced system lengths.

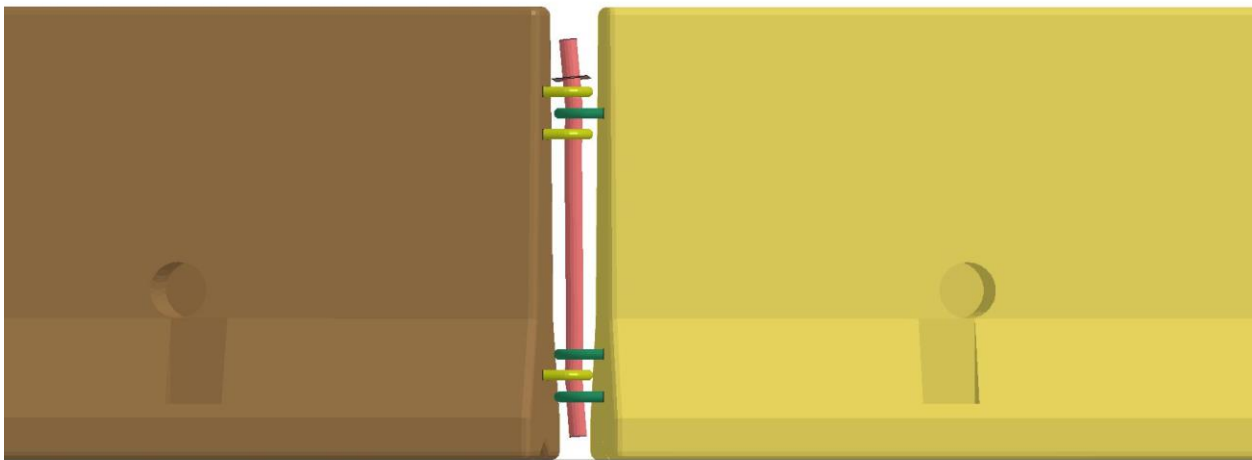
Similarly, simulation of impacts on the downstream end of the system demonstrated potential concerns when impacting the final three barriers of the PCB system. Impacts on barrier nos. 14 through 16 caused the end of the barrier to gate and display significantly higher deflections as compared to impacts farther upstream. Additionally, impacts on the final three barriers had a combination of increased vehicle yaw and roll motions, which raised potential concerns for vehicle stability. Pin deformations indicate potentially increased loading of the barrier joint were also observed when impacting barrier nos. 14 and 15. Based on these concerns and the improved performance of impacts farther upstream in the system, it was recommended that a minimum of three barrier segments be used to define the end of LON of the PCB system without further analysis prior to investigation of reduced system lengths.

NDOR PCB-Beginning of LON-Long System
Time = 1200



(a) Impact at Barrier No. 15

WI F-shape TCB - Free-Standing
Time = 1200



(b) Impact at Barrier No. 8 (Midspan)

Figure 36. End of LON Connection Pin Deformation Comparison

6 EVALUATION OF REDUCED SYSTEM LENGTHS

Once beginning and end of LON locations were selected for the sixteen-barrier F-shape PCB system, the researchers investigated of reduced system length. It was recognized that the overall performance of the barrier system, especially when impacted at the beginning and end of LON, could change if system lengths were minimized. Thus, simulation models were conducted on reduced length PCB systems to determine the potential for the reduced length system to continue to perform safely and to recommend a system length for full-scale crash testing and evaluation. Based on the previous recommendations for the sixteen-barrier system of a minimum of three barriers to define beginning of LON and three barriers to define the end of LON, the researchers selected a seven-barrier long system for investigation. This length would provide the recommended three barrier segments on each end of the system and a single barrier in the middle of the system to provide a finite redirective length.

6.1 Seven Barrier F-Shape PCB System Simulations

Two simulations were conducted on a seven-barrier long F-shape PCB system with the 2270P vehicle under the MASH impact conditions for test designation no. 3-11. One simulation was run impacting 4.3 ft (1.3 m) upstream of the joint between barrier nos. 3 and 4 to evaluate the beginning of LON for the reduced length system, while a second simulation was run impacting 4.3 ft (1.3 m) upstream of the joint between barrier nos. 4 and 5 to evaluate the end of LON for the reduced length system.

Simulation of the impact on the beginning of LON for the seven-barrier long system displayed acceptable results in terms of the barrier performance, as shown in Figures 37 and 38. The 2270P vehicle was safely and smoothly redirected with vehicle stability that compared well with the baseline model of the original sixteen-barrier long PCB system. Occupant risk values for the simulation were well below the MASH limits. As would be expected, lateral and longitudinal barrier displacements increased significantly as compared to an impact near the midspan of the standard 200-ft (61-m) system length used for full-scale crash testing. Peak lateral barrier deflections were found to be 95.3 in. (2,420 mm) at the downstream end of barrier no. 4, while the longitudinal displacement of the barriers on the upstream and downstream ends of the system were found to be 27.3 in. (693 mm) and 7.0 in. (178 mm), respectively. However, the peak lateral deflection was within 3 percent of the deflection of the standard length PCB system when impacted at the beginning of the LON.

It was noted that the reduced length and corresponding reduction in upstream and downstream tensile loads in the system altered the deflection of the PCB segments. Specifically, it was noted that a knee formed at the joint between barrier nos. 5 and 6 and impacted the rear, left-side door on the 2270P vehicle as the vehicle traversed the joint, as shown in Figure 39. The formation of a knee between the barrier segments that impacted the side of the vehicle was not observed in simulations of the full-length systems nor had it been noted in full-scale testing. The impact of the knee on the rear, left-side door caused only moderate damage and did not affect vehicle stability or occupant risk values. As such, this was not believed to pose a serious degradation of the barrier performance. However, it did indicate that the reduced length of the system affected barrier behavior.

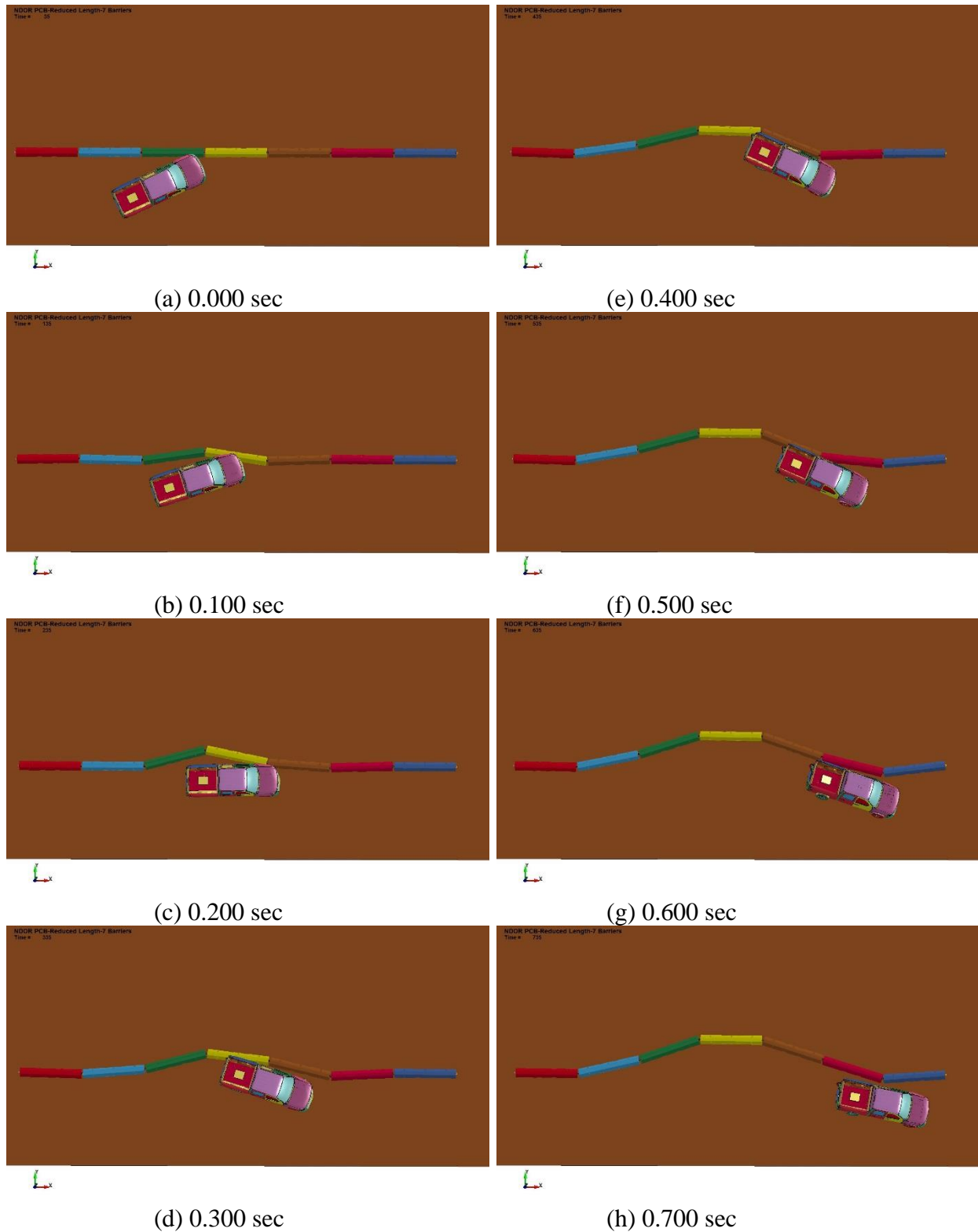


Figure 37. Simulation of Beginning of LON for 7-Barrier F-Shape PCB System, Overhead View

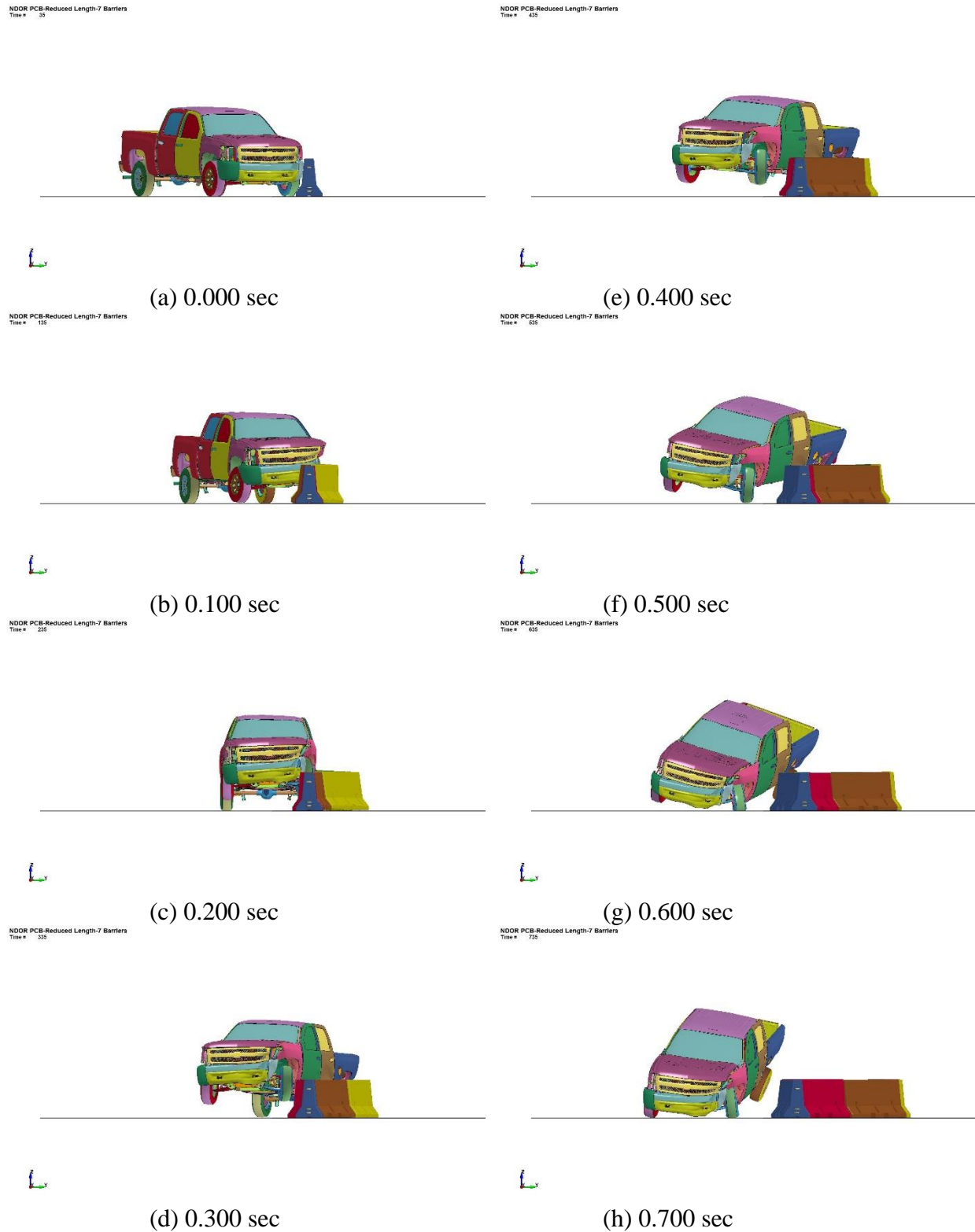


Figure 38. Simulation of Beginning of LON for 7-Barrier F-Shape PCB System, Downstream View

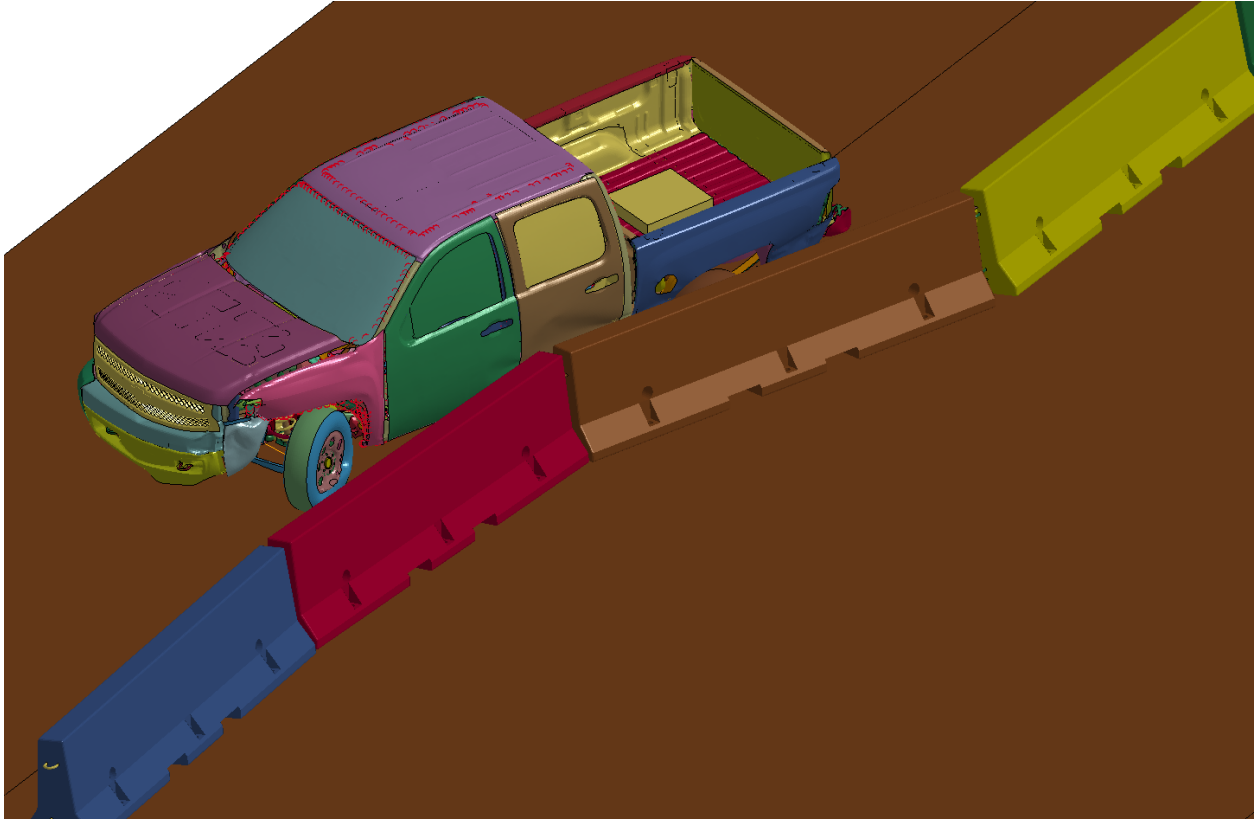


Figure 39. Simulation of Beginning of LON for 7-Barrier F-Shape PCB System, Barrier Knee Impact at Barrier Nos. 5 and 6 Joint

Simulation of the impact on the end of LON for the seven-barrier long system raised potential concerns regarding the use of the shorter system length. Sequential images of the seven-barrier F-shape PCB system impacted at the proposed end of LON are shown in Figures 40 and 41. The 2270P vehicle was redirected, and occupant risk values for the simulation were below the MASH limits. Peak lateral barrier deflections were 96.5 in. (2,451 mm) at the upstream end of barrier no. 6, while the longitudinal displacement of the barriers on the upstream and downstream ends of the system were found to be 17.2 in. (437 mm) and 23.2 in. (589 mm), respectively. Of more concern was the vehicle interaction with the barrier as it reached the end of the system. At .630 s after impact, the vehicle was proceeding past the final barrier in the PCB system when the final barrier in the system rotated into the left-side door, as shown in Figure 42. The motion of the PCB segments downstream of impact in the reduced-length system changed as compared to the full length system simulated previously due to the difference in longitudinal resistance provided on the upstream end of the system. This resulted in more pronounced rotation of the end barrier that caused the end of the barrier segment to impact the left-side door. Impact of the end of the barrier with the door in the simulation caused significant damage to the door and raised concerns with respect to occupant compartment safety, occupant risk concerns, and potential degradation of vehicle stability. Review of these results with the project sponsor verified these concerns, and it was desired to mitigate the potential for impact of the end barrier segment on the vehicle.

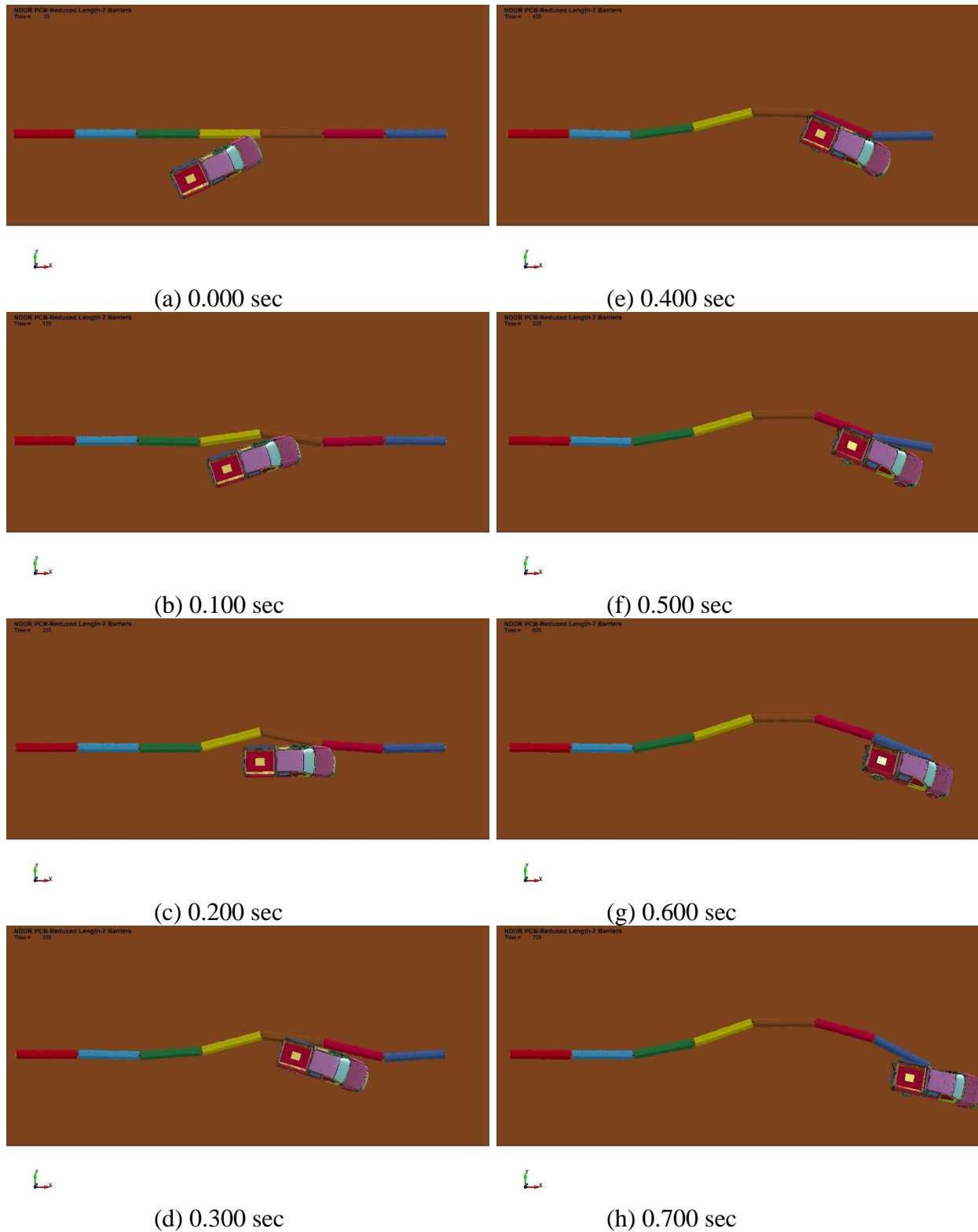


Figure 40. Simulation of End of LON for 7-Barrier F-Shape PCB System, Overhead View

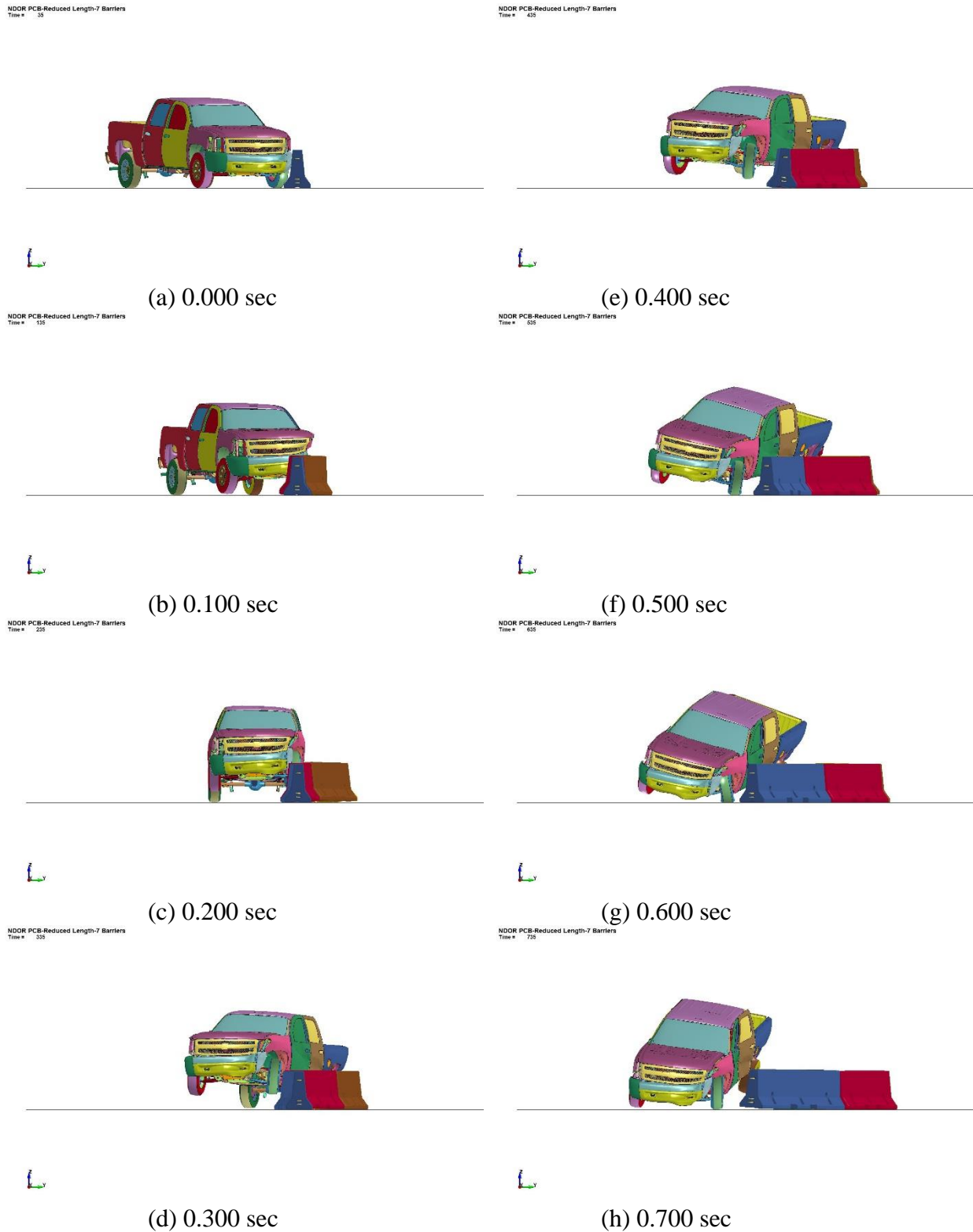


Figure 41. Simulation of End of LON for 7-Barrier F-Shape PCB System, Downstream View

NDOR PCB-Reduced Length-7 Barriers
Time = 655

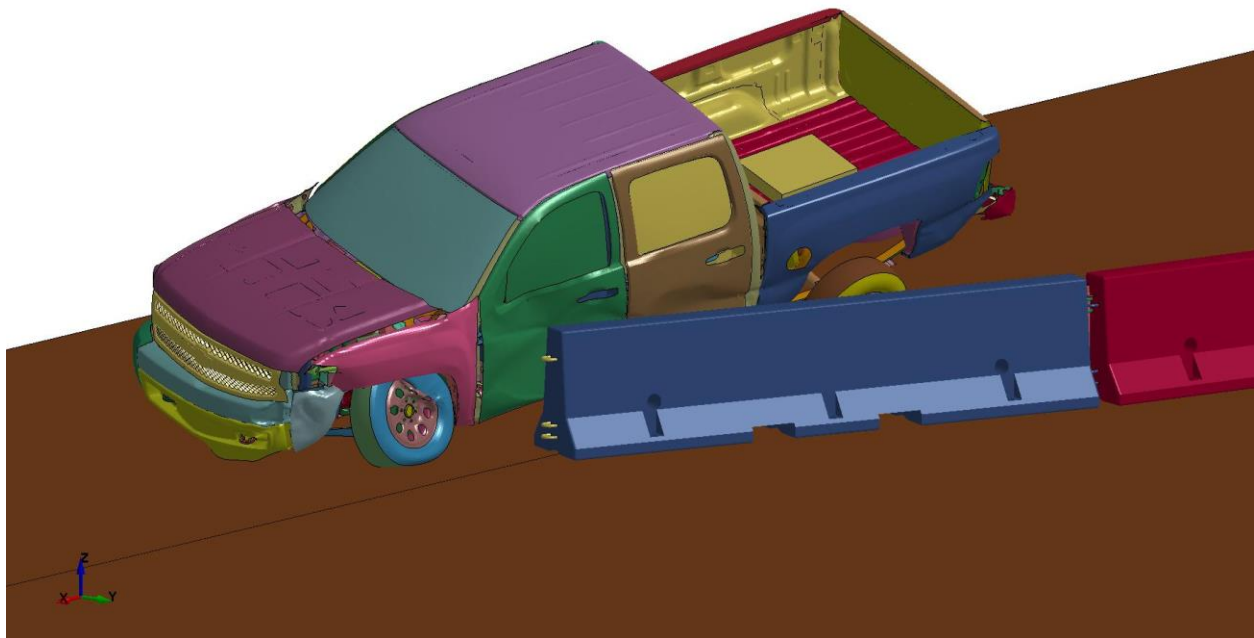


Figure 42. Simulation of End of LON for 7-Barrier F-Shape PCB System, Final Barrier Impact on Driver-Side Door

6.2 Eight-Barrier F-Shape PCB System Simulations

Based on the concerns with the door impact observed in the seven-barrier PCB system simulations, the researchers conducted additional simulation models on an eight-barrier long PCB system. In this system, three PCB segments were used for the beginning of LON, four PCB segments were used for the end of LON, and a single barrier segment was placed between the regions to provide a finite redirective length. It was believed that the use of an additional PCB segment in the end of LON region would mitigate the door impact observed in the seven PCB system simulation.

Two simulations were conducted on an eight-barrier long, F-shape PCB system with the 2270P vehicle under the MASH impact conditions for test designation no. 3-11. One simulation was run impacting 4.3 ft (1.3 m) upstream of the joint between barrier nos. 3 and 4 to evaluate the beginning of LON for the reduced length system, while a second simulation was run impacting 4.3 ft (1.3 m) upstream of the joint between barrier nos. 4 and 5 to evaluate the end of LON for the reduced length system.

Simulation of the impact on the beginning of LON for the eight-barrier long system displayed acceptable results in terms of the barrier performance, as shown in Figures 43 and 44. The 2270P vehicle was safely and smoothly redirected, and occupant risk values for the simulation were below the MASH limits. Peak lateral barrier deflections were 94.8 in. (2,408 mm) at the downstream end of barrier no. 4, while the longitudinal displacement of the barriers on the upstream and downstream ends of the system were found to be 28.7 in. (729 mm) and 2.9 in. (74 mm), respectively. The reduced length of the barrier system again allowed formation of a knee at the joint between barrier nos. 5 and 6 that impacted the side of the 2270P vehicle and produced similar damage as the previous simulation of the beginning of LON impact with a seven-barrier PCB system, as shown in Figure 45.

Simulation of the impact on the end of LON for the eight-barrier long system displayed improved performance as compared to the seven-barrier long system. Sequential images of the eight F-shape PCB system impacted at the proposed end of LON are shown in Figures 46 and 47. The 2270P vehicle was redirected, and occupant risk values for the simulation were below the MASH limits. Peak lateral barrier deflections were 90.0 in. (2,286 mm) at the downstream end of barrier no. 5, while the longitudinal displacement of the barriers on the upstream and downstream ends of the system were found to be 18.0 in. (458 mm) and 12.5 in. (318 mm), respectively. The use of an additional barrier on the end of the system mitigated the impact of the free-end of the final barrier segment with the side of the 2270P vehicle. However, it was noted that a knee formed at the joint between barrier nos. 6 and 7 and impacted the left side of the vehicle, as shown in Figure 48. The impact of the knee formed between these barrier segments posed less concern as the severity and damage associated with the vehicle contact with the knee appeared to be significantly less than the damage observed due to the rotation of the free end of the system into the door observed in the seven-barrier PCB system simulation.

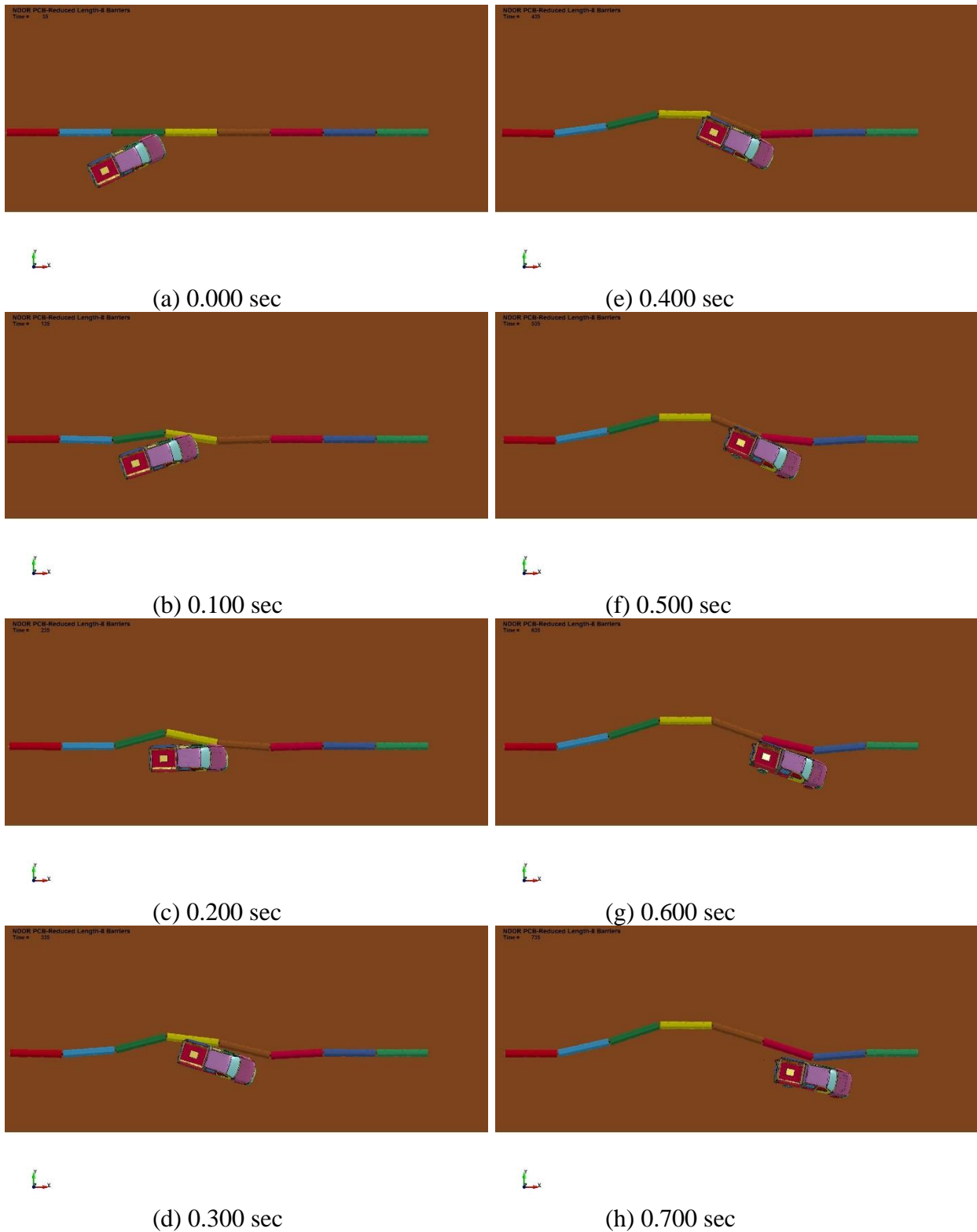


Figure 43. Simulation of Beginning of LON for 8-Barrier F-Shape PCB System, Overhead View

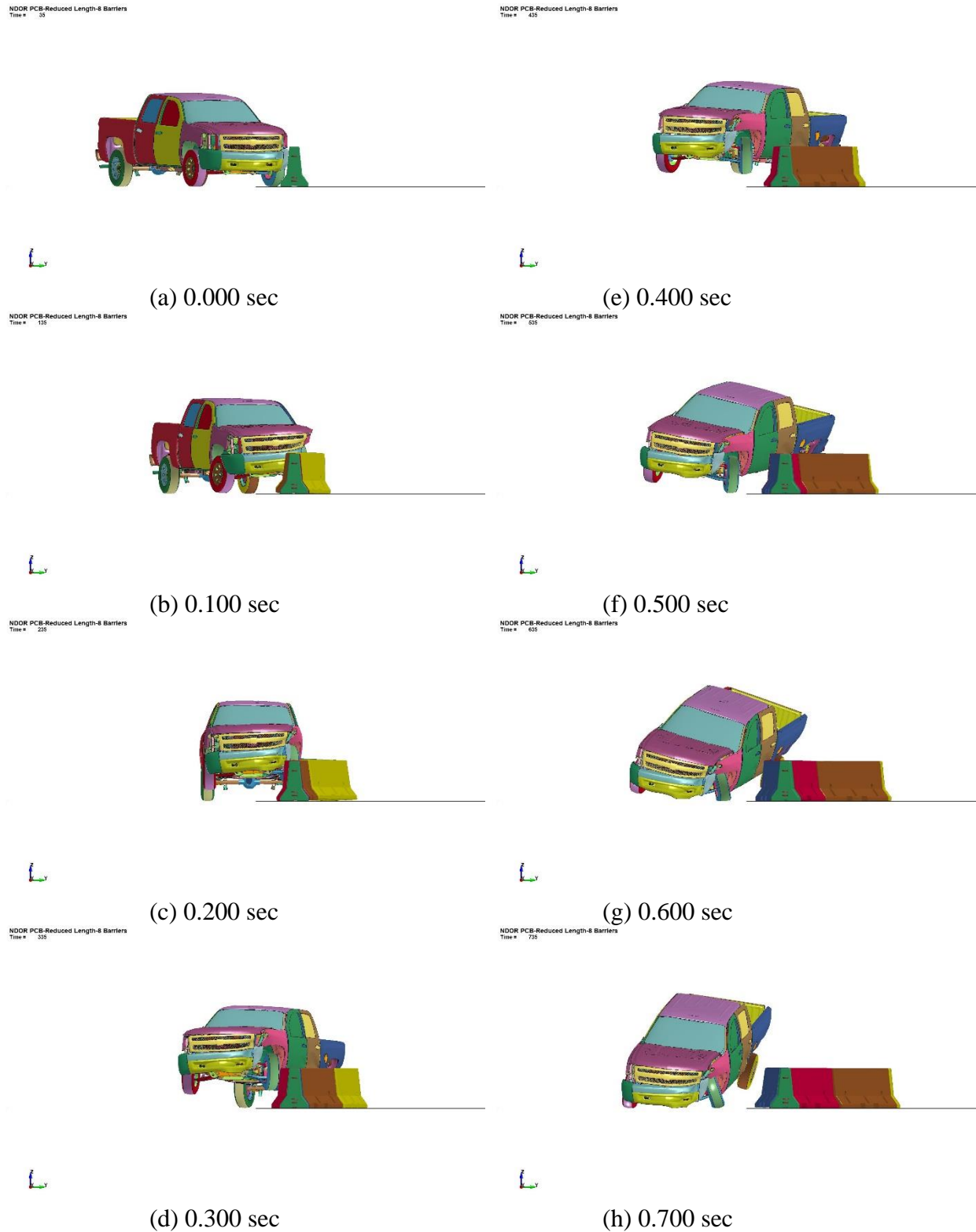


Figure 44. Simulation of Beginning of LON for 8-Barrier F-Shape PCB System, Downstream View

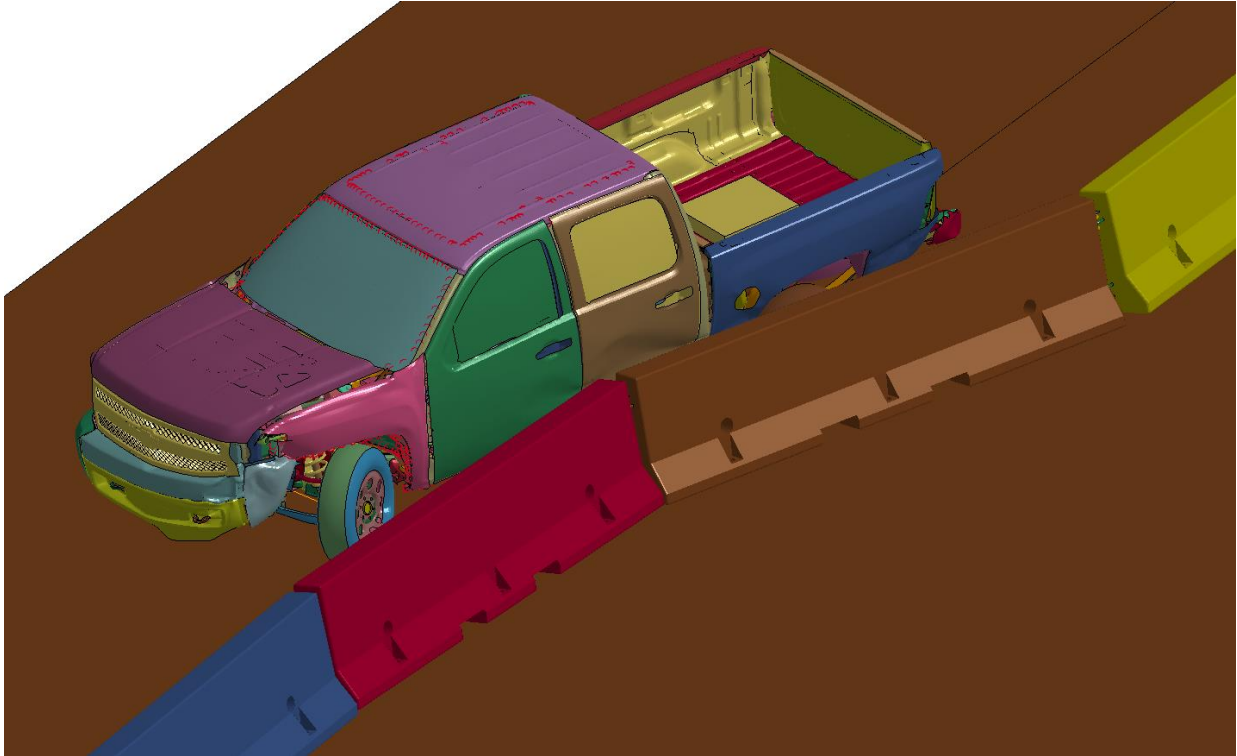


Figure 45. Simulation of Beginning of LON for 8-Barrier F-Shape PCB System, Barrier Knee Impact at Barrier Nos. 5 and 6 Joint

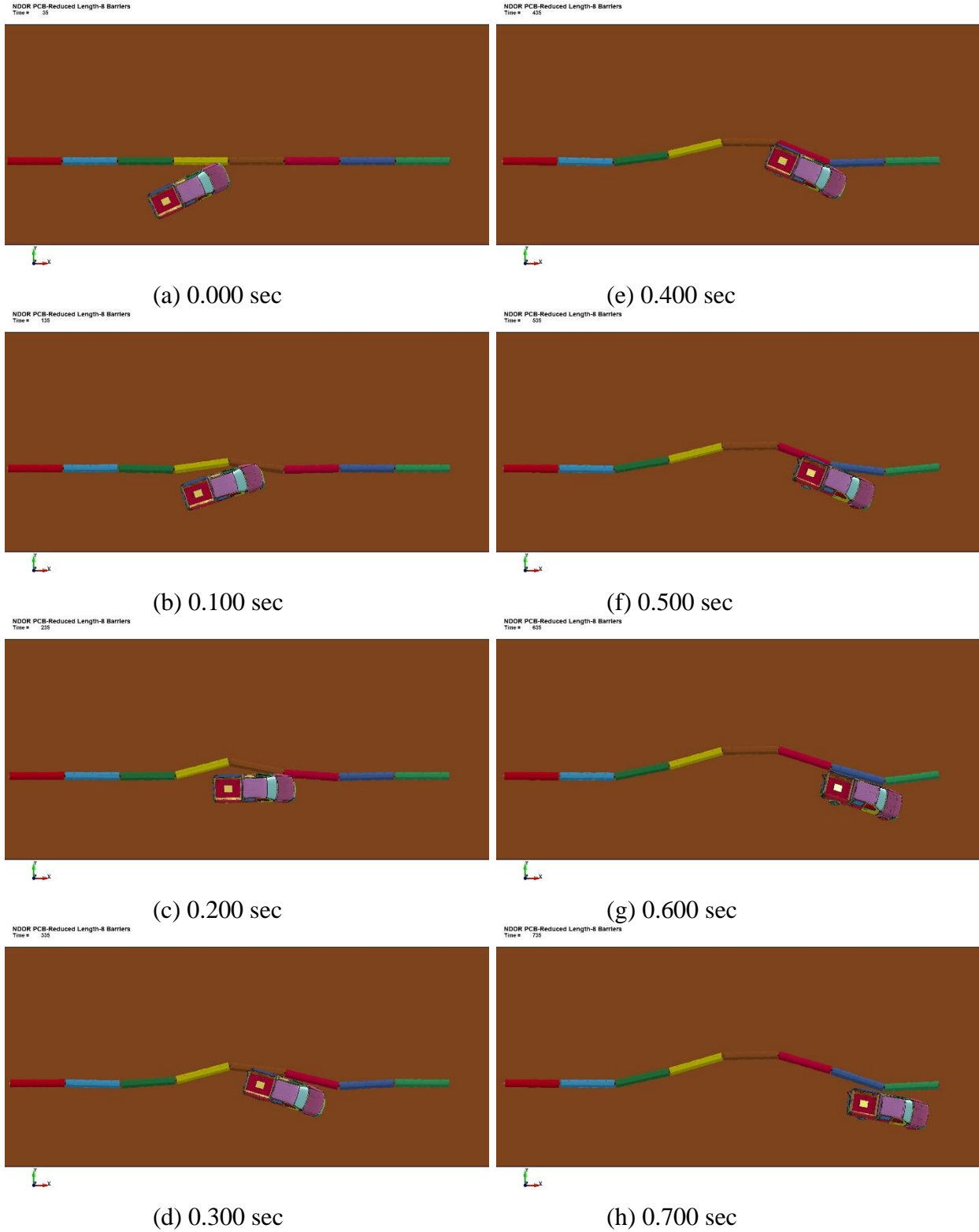


Figure 46. Simulation of End of LON for 8-Barrier F-Shape PCB System, Overhead View

NDOR PCB-Reduced Length-8 Barriers
Time = 0



(a) 0.000 sec

NDOR PCB-Reduced Length-8 Barriers
Time = 135



(b) 0.100 sec

NDOR PCB-Reduced Length-8 Barriers
Time = 235



(c) 0.200 sec

NDOR PCB-Reduced Length-8 Barriers
Time = 335



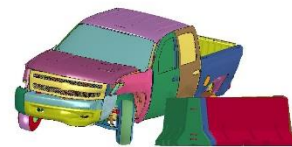
(d) 0.300 sec

NDOR PCB-Reduced Length-8 Barriers
Time = 435



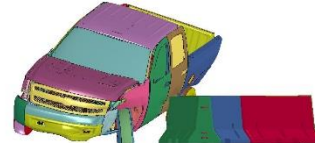
(e) 0.400 sec

NDOR PCB-Reduced Length-8 Barriers
Time = 535



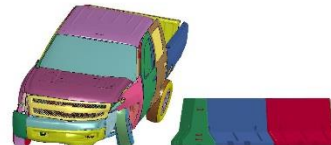
(f) 0.500 sec

NDOR PCB-Reduced Length-8 Barriers
Time = 635



(g) 0.600 sec

NDOR PCB-Reduced Length-8 Barriers
Time = 735



(h) 0.700 sec

Figure 47. Simulation of End of LON for 8-Barrier F-Shape PCB System, Downstream View

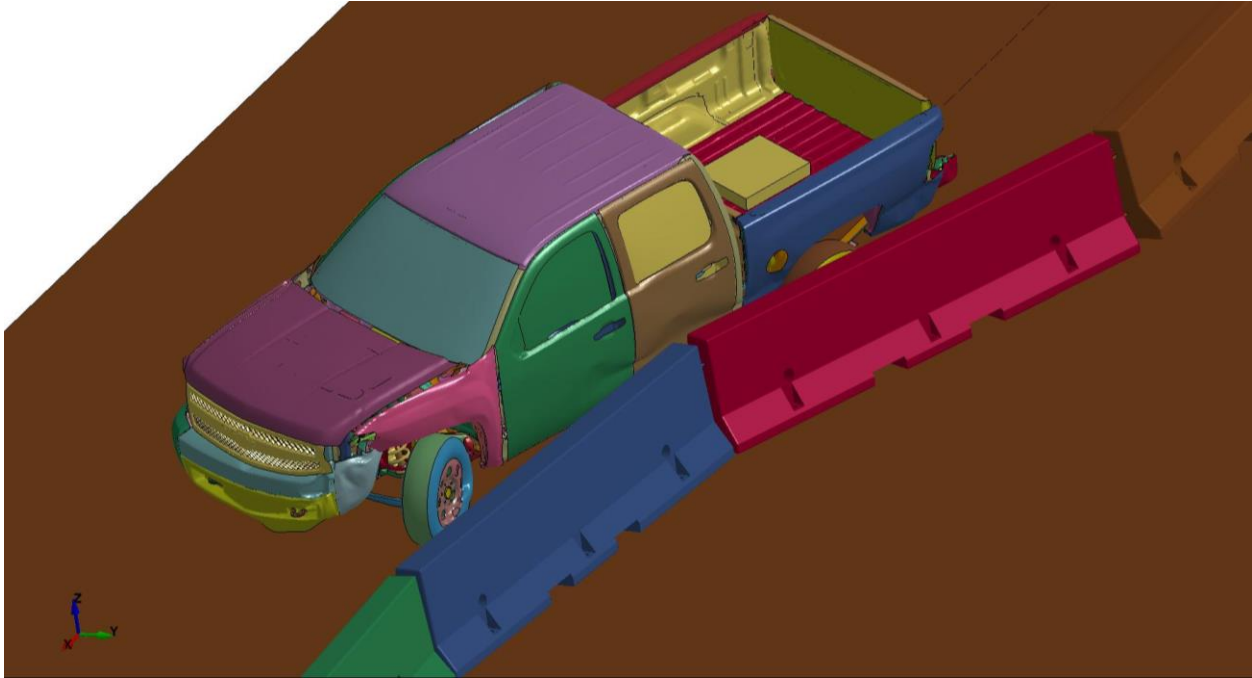


Figure 48. Simulation of End of LON for 8-Barrier F-Shape PCB System, Barrier Knee Impact at Barrier Nos. 6 and 7 Joint

6.3 Selection of System Length for Full-Scale Testing

The simulations of the reduced length F-shape PCB systems found that a seven-barrier long system was capable of redirecting the 2270P vehicle under the MASH TL-3 impact conditions, albeit with an increase in barrier deflections over those observed in midspan impacts with the standard sixteen-barrier long system evaluated previously in full-scale testing. However, impact near the end of LON of the seven barrier system showed a potential for the final barrier in the system to rotate and impact the left-side door, and raised concerns for the overall safety performance of the seven-barrier long system. To address this issue, an additional barrier was placed on the end of the system which increased the total system length to eight barriers. Simulation of the eight-barrier long PCB system demonstrated an improved response as the vehicle was safely redirected in both simulated impacts, and the rotation of the free end of the final barrier of the system was no longer able to impact the side of the vehicle. It was noted that a knee formed at the joint between barrier nos. 7 and 8 and still impacted the side of the vehicle. Similar knee formation and impact with the side of the vehicle was also observed in the beginning of LON impacts on both the seven and eight-barrier long systems. While the impact of the knee with the side of the 2270P vehicle caused moderate concern, the contact appeared to be less severe than the contact from the free barrier end in the seven-barrier long system. As such, it was decided to proceed with evaluation of an eight-barrier long F-shape PCB system under the MASH TL-3 criteria.

7 DESIGN DETAILS

The barrier system test installations were comprised of eight 12-ft 6-in. (3.81-m) long, rebar reinforced, F-shape portable concrete barriers. As the barrier system was identical for test nos. NELON-1 and NELON-2, only the design drawing depicting the targeted impact point is shown for NELON-2. The barrier system components for test nos. NELON-1 and NELON-2 are shown in Figures 51 through 55 and the barrier system layouts for test nos. NELON-1 and NELON-2 are shown in Figures 49 and 50, respectively. Photographs of the test installations are shown in Figures 56 and 57. Material specifications, mill certifications, and certificates of conformity for the system materials are shown in Appendix A.

The F-shape PCB segments were 12-ft 6-in. (3.81-m) long F-shape PCBs and constructed with a 5,000 psi (34.5 MPa) minimum compressive strength concrete. The barrier segments were 22½ in. (572 mm) wide at the base and 8 in. (203 mm) wide at the top. Each of the barrier segments were connected by 1¼-in. (32-mm) diameter A36 steel connection pins and connection pin plates placed between ¾-in. (19-mm) diameter, epoxy coated reinforcing bar loops extending from the end of the barrier sections. The connection loop bar material was A709 Grade 70 or A706 Grade 60 steel. All PCB segments were installed on the concrete tarmac at the MwRSF outdoor test facility.

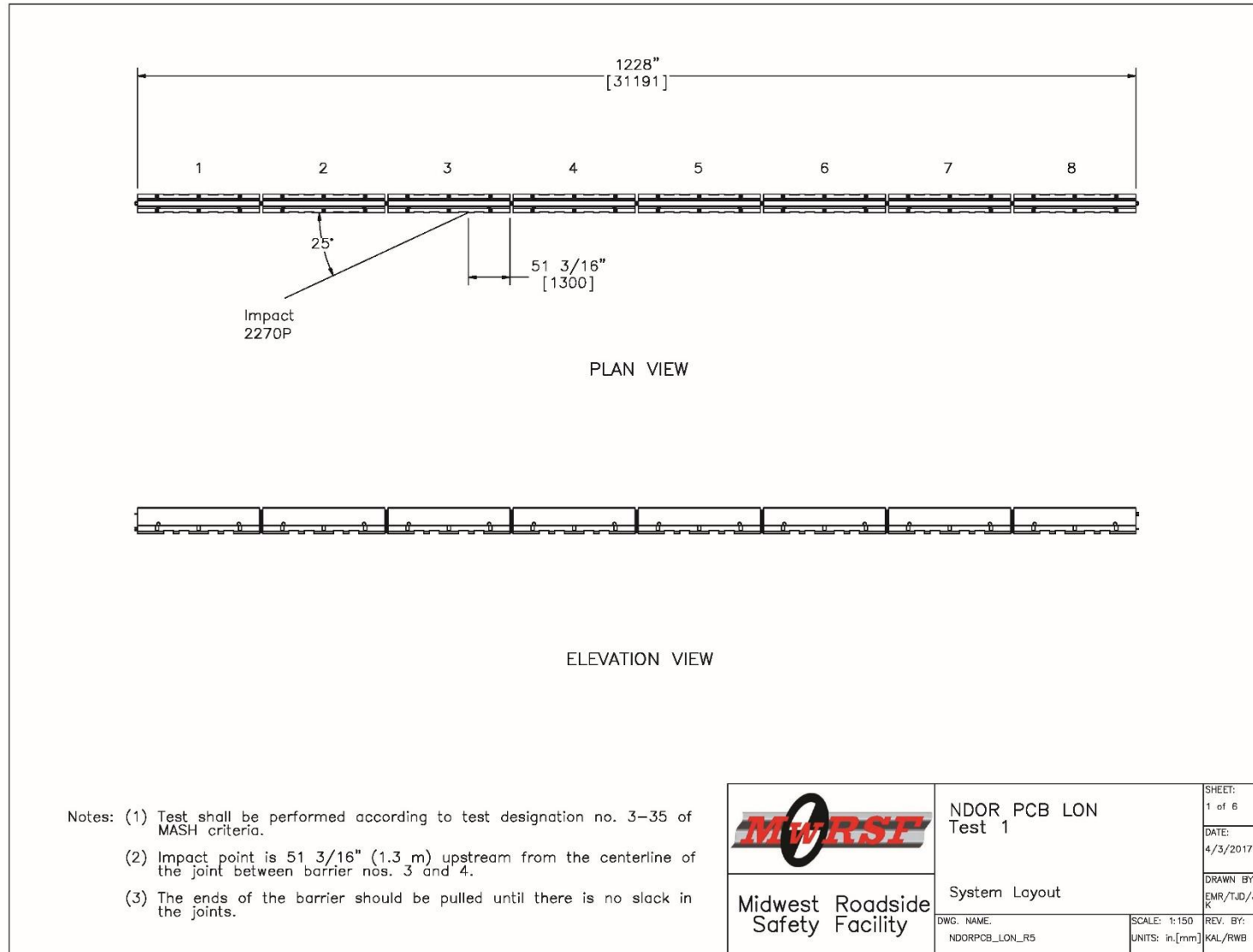


Figure 49. System Layout, Test No. NELON-1

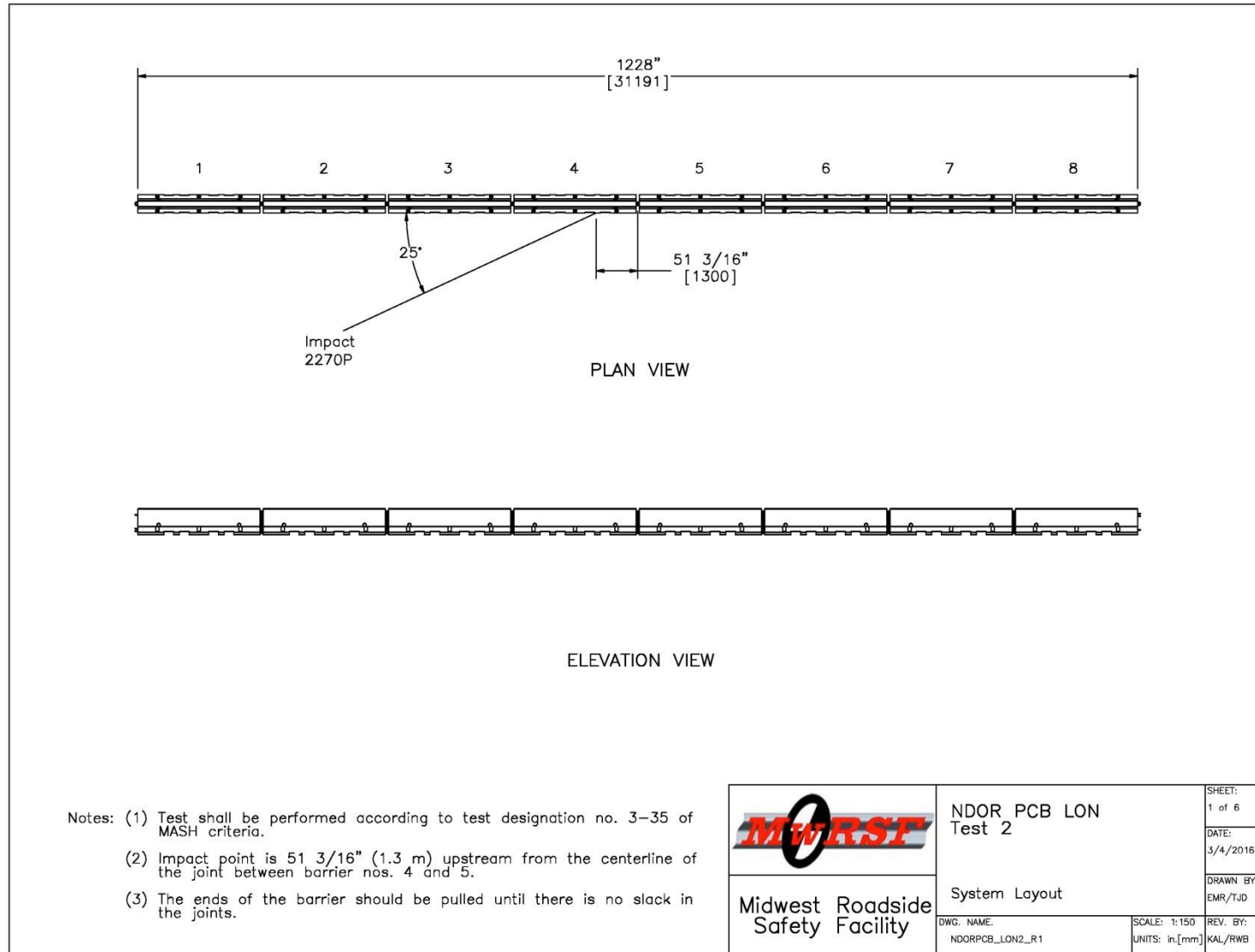


Figure 50. System Layout, Test No. NELON-2

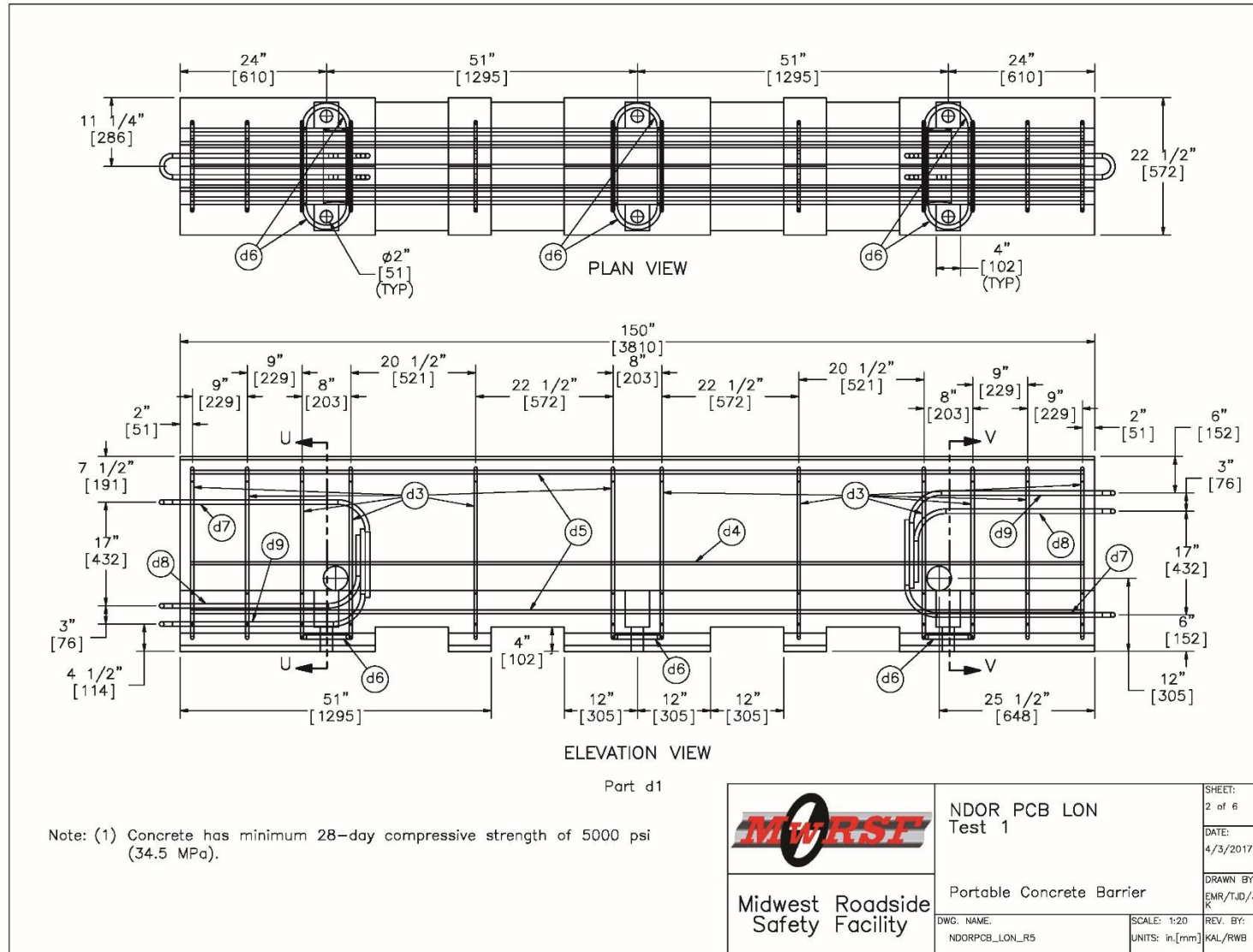


Figure 51. Portable Concrete Barrier, Test Nos. NELON-1 and NELON-2

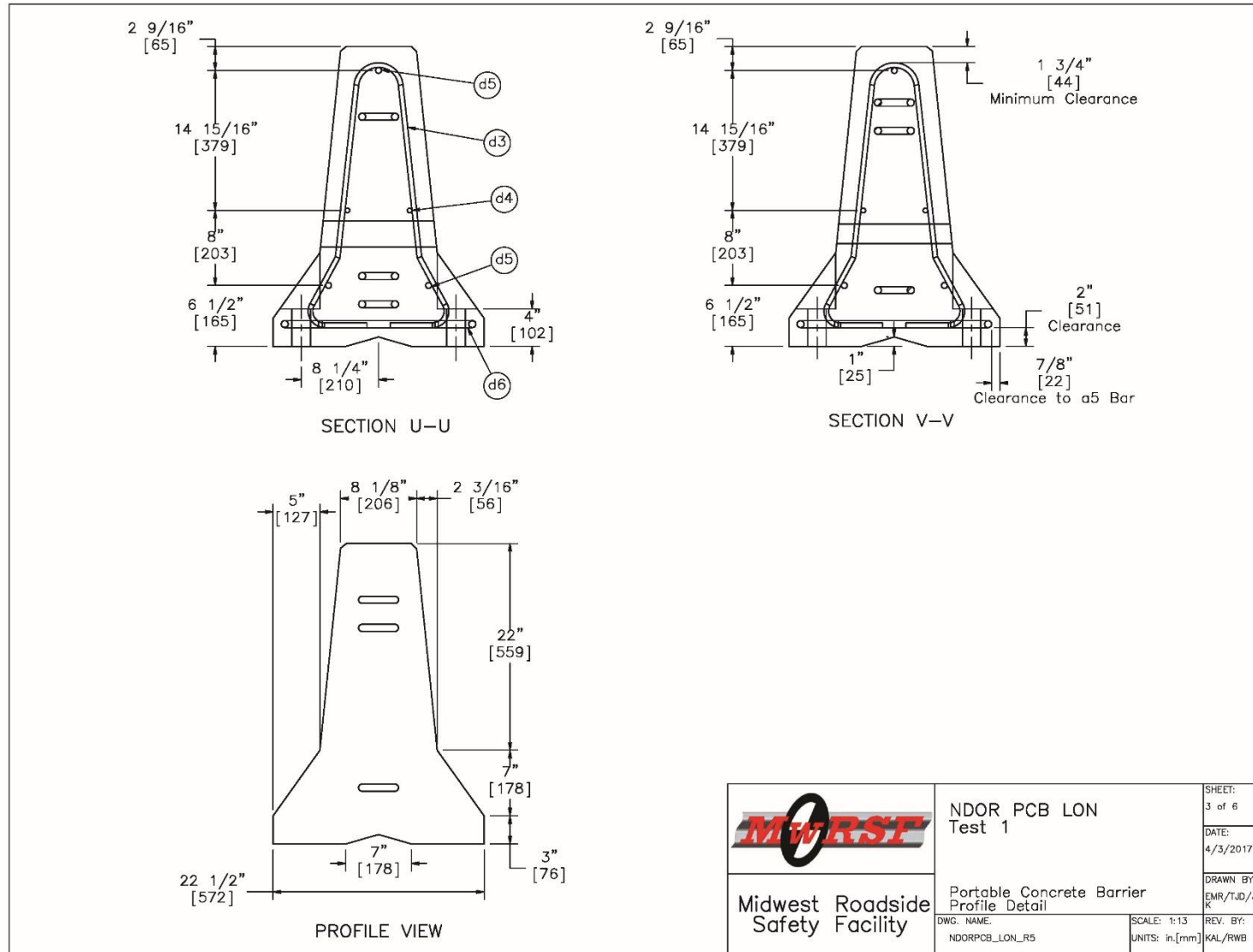


Figure 52. Portable Concrete Barrier Profile Detail, Test Nos. NELON-1 and NELON-2

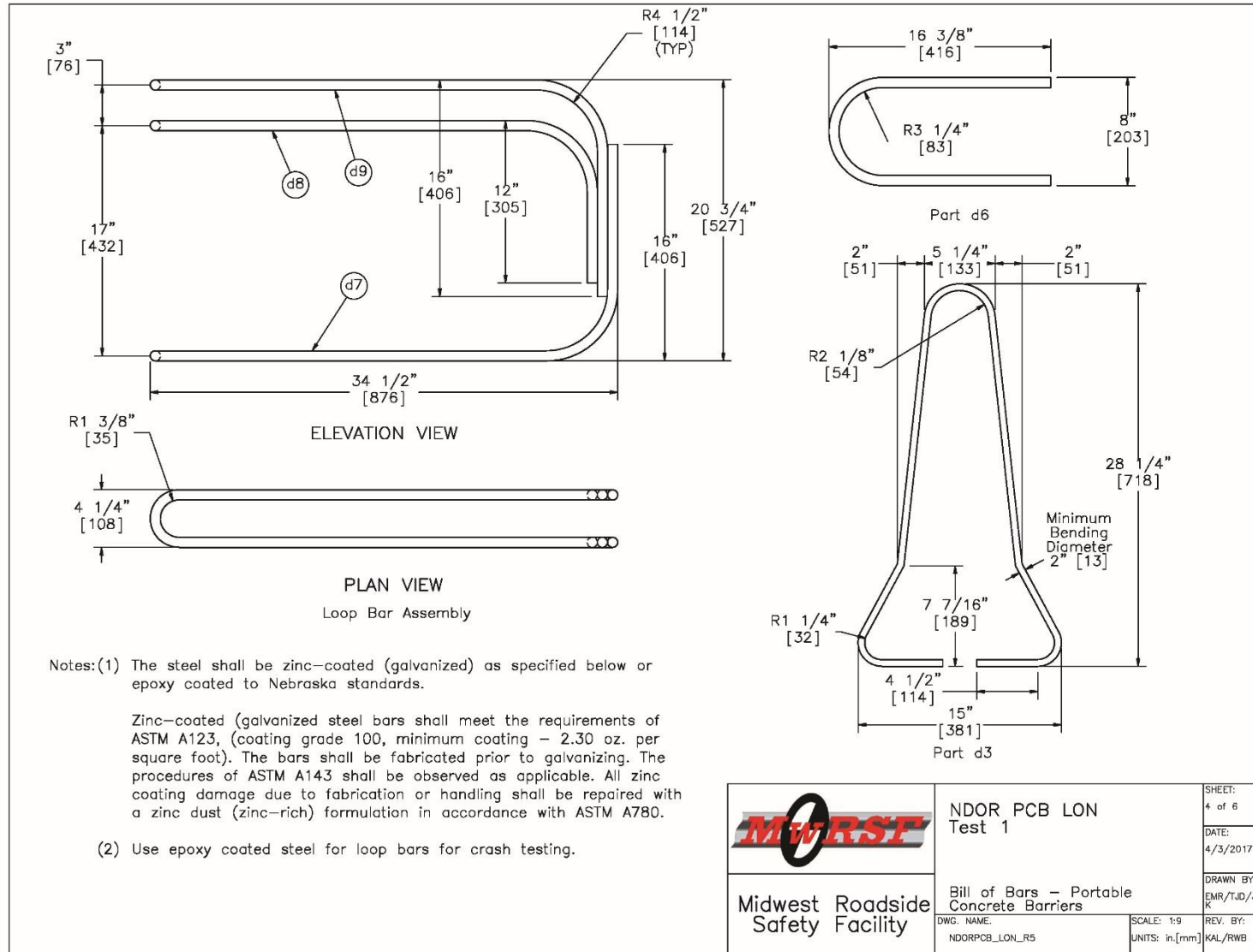


Figure 53. Bill of Bars – Portable Concrete Barriers, Test Nos. NELON-1 and NELON-2

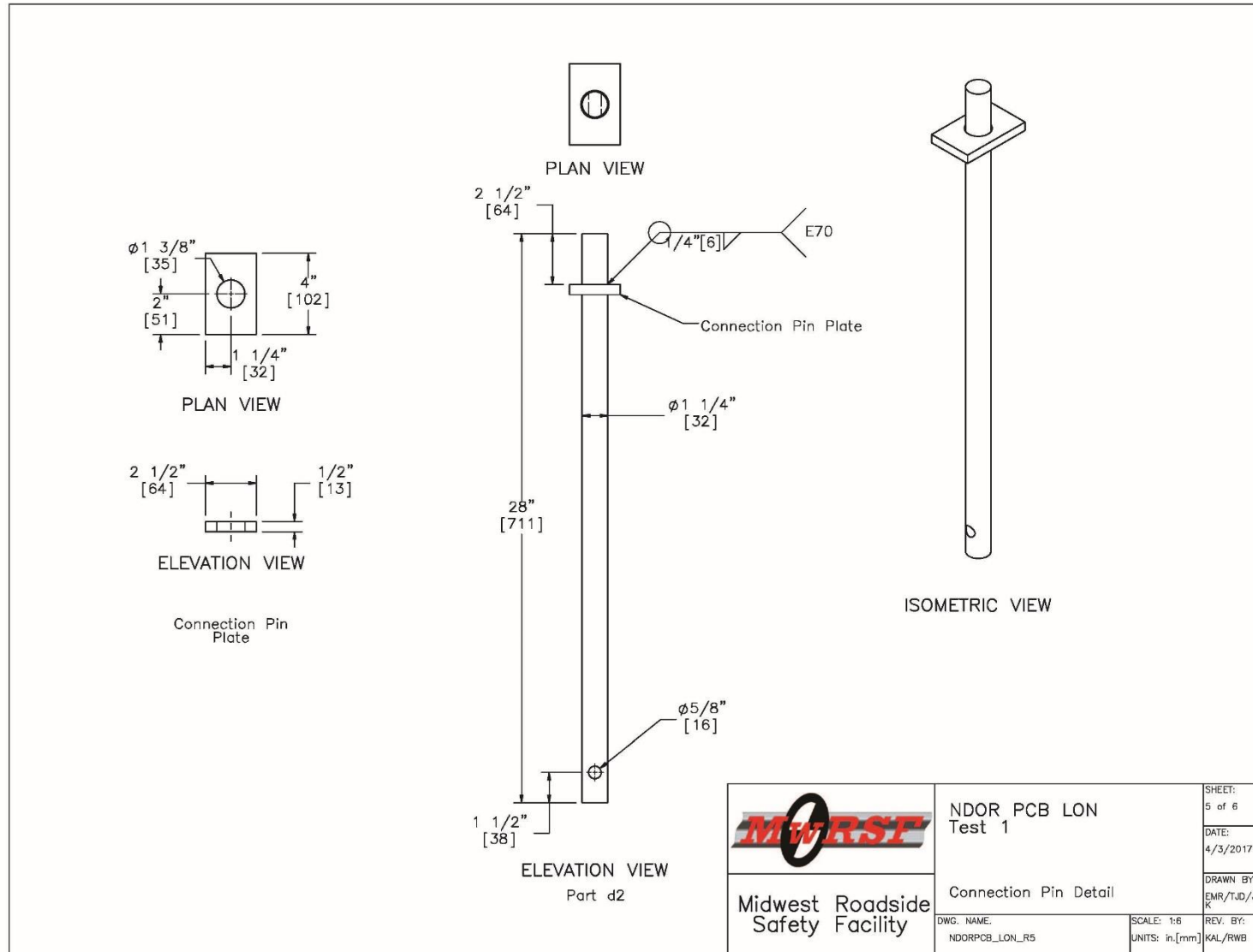


Figure 54. Connection Pin Detail, Test Nos. NELON-1 and NELON-2


Item No.	QTY.	Description	MaterialSpec	Hardware Guide
d1	8	NDOR Portable Concrete Barrier	min f'c=5000 psi [34.5 MPa]	SWC09
d2	7	1 1/4" [32] Dia., 28" [711] Long Connector Pin	ASTM A36	FMW02
d3	96	1/2" [13] Dia., 72" [1829] Long Form Bar	ASTM A615 Grade 60	—
d4	16	1/2" [13] Dia., 146" [3708] Long Longitudinal Bar	ASTM A615 Grade 60	—
d5	24	5/8" [16] Dia., 146" [3708] Long Longitudinal Bar	ASTM A615 Grade 60	—
d6	48	3/4" [19] Dia., 36" [914] Long Anchor Loop Bar	ASTM A615 Grade 60, Epoxy Coated or Galvanized	—
d7	16	3/4" [19] Dia., 102" [2591] Long Connection Loop Bar	ASTM A709 Grade 70 or A706 Grade 60, Epoxy Coated or Galvanized	—
d8	16	3/4" [19] Dia., 91" [2311] Long Connection Loop Bar	ASTM A709 Grade 70 or A706 Grade 60, Epoxy Coated or Galvanized	—
d9	16	3/4" [19] Dia., 101" [2565] Long Connection Loop Bar	ASTM A709 Grade 70 or A706 Grade 60, Epoxy Coated or Galvanized	—
<div> <div>  <div> Midwest Roadside Safety Facility </div> </div> <div> NDOR PCB LON Test 1 </div> <div> Bill of Materials </div> <div> DWG. NAME: NDORPCB_LON_R5 </div> <div> SCALE: None UNITS: in.[mm] </div> <div> SHEET: 6 of 6 DATE: 4/3/2017 DRAWN BY: EMR/TJD/JE K REV. BY: KAL/RWB </div> </div>				

Figure 55. Bill of Materials, Test Nos. NELON-1 and NELON-2



Figure 56. Test Installation Photographs, Test No. NELON-1



Figure 57. Test Installation Photographs, Test No. NELON-2

8 TEST REQUIREMENTS AND EVALUATION CRITERIA

8.1 Test Requirements

Terminals and redirective crash cushions, such as the free-standing, F-shape PCB system, must satisfy impact safety standards in order to be declared eligible for federal reimbursement by the Federal Highway Administration (FHWA) for use on the National Highway System (NHS). For new hardware, these safety standards consist of the guidelines and procedures published in MASH [2]. According to the TL-3 safety performance criteria of MASH, terminals and redirective crash cushions must be subjected to nine full-scale vehicle crash tests. However, since this investigation did not involve a crash cushion or terminal and was solely focused on evaluating the beginning and end of the shortest length of need of the PCB system, only three full-scale vehicle crash tests were valid for evaluation of the system, as summarized in Table 2.

Table 2. MASH TL-3 Crash Test Conditions for Terminals and Crash Cushions

Test Article	Test Designation No.	Test Vehicle	Vehicle Weight, lb (kg)	Impact Conditions		Evaluation Criteria ¹
				Speed, mph (km/h)	Angle, deg.	
Terminals and Redirective Crash Cushions	3-34	1100C	2,425 (1,100)	62 (100)	25	A,D,F,H,I
	3-35	2270P	5,000 (2,270)	62 (100)	25	A,D,F,H,I
	3-37	2270P	5,000 (2,270)	62 (100)	25	A,D,F,H,I

¹ Evaluation criteria explained in Table 3.

The first test would consist of MASH test designation no. 3-35. This test involves an impact with a 2270P vehicle at a speed of 62 mph (100 km/h) and at an angle of 25 degrees on the beginning of the LON. This test would evaluate the effectiveness of the beginning of LON with a minimal system length. The second test would consist of a modified version of MASH test designation no. 3-37 with the intent of assessing the end of the LON for the PCB system rather than maximizing vehicle snag and instability on a terminal or crash cushion. This test involves an impact with a 2270P vehicle at a speed of 62 mph (100 km/h) and at an angle of 25 degrees on a critical impact point near the downstream end of the system. The system length and number of barrier segments on the beginning and end of the LON for both tests were based on the guidance determined during the simulation effort. The critical impact points were selected based on Table 2-6 of MASH and the beginning and end of LON. Thus, the impact point for test designation no. 3-35 would be 4.3 ft (1.3 m) upstream of the joint between the third and fourth barrier segments, while the impact point for test designation no. 3-37 would be 4.3 ft (1.3 m) upstream of the joint between the fourth and fifth barrier segments.

Test designation no. 3-34 with the 1100C vehicle would not be necessary based on comparison of barrier geometry with previous concrete barrier systems and the intended rationale for the test. With respect to previous testing, in test no. 7069-3, a rigid, F-shape bridge rail was

successfully impacted by a small car weighing 1,800 lb (816 kg) at 60.1 mph (96.7 km/h) and 21.4 degrees according to the American Association of State Highway and Transportation Officials (AASHTO) *Guide Specifications for Bridge Railings* [11-12]. In the same manner, test nos. CMB-5 through CMB-10, CMB-13, and 4798-1 showed that rigid New Jersey safety shape barriers struck by small cars meet safety performance standards [13-14]. In addition, in test no. 2214NJ-1, a New Jersey safety shape barrier was impacted by a passenger car weighing 2,579 lb (1,170 kg) at 60.8 mph (97.8 km/h) and 26.1 degrees according to the TL-3 standards set forth in MASH [15]. Furthermore, temporary New Jersey safety shape concrete median barriers have experienced only slight barrier deflections when impacted by small cars and behave similarly to rigid barriers, as seen in test no. 47 [16].

Additionally, test designation no. 3-34 is intended to evaluate the impact performance of terminals and crash cushions at the critical impact point where the behavior of the device changes from gating or capturing to redirection. Vehicle trajectory and occupant risk are the main concerns for this test. However, the PCB system evaluated herein does not use a fixed anchorage or other element to provide redirective forces at the beginning or end of LON, but rather relies on the inertia of the PCB segments and membrane tensile forces generated by the mass and corresponding friction of adjacent barrier segments. Additionally, the potential for gating or excessive deflection of the beginning or end of LON for the PCB system was expected due to the heavier 2270P vehicle rather than the lower weight 1100C vehicle. Thus, the critical impact point for the system as defined for test designation no. 3-34 would likely be upstream of the beginning of LON defined by the 2270P test. As the scope of this study did not extend into determining proper termination of the system outside of the LON, test designation no. 3-34 was believed to be unnecessary to evaluate the F-shape PCB minimum length of need and reduced system length.

It should be noted that the test matrix detailed herein represents the researchers' best engineering judgement with respect to the MASH safety requirements and their internal evaluation of critical tests necessary to evaluate the crashworthiness of the barrier system. However, the recent switch to new vehicle types as part of the implementation of the MASH criteria and the lack of experience and knowledge regarding the performance of the new vehicle types with certain types of hardware could result in unanticipated barrier performance. Thus, any tests within the evaluation matrix deemed non-critical may eventually need to be evaluated based on additional knowledge gained over time or revisions to the MASH criteria.

8.2 Evaluation Criteria

Evaluation criteria for full-scale vehicle crash testing are based on three appraisal areas: (1) structural adequacy; (2) occupant risk; and (3) vehicle trajectory after collision. Criteria for structural adequacy are intended to evaluate the ability of the portable concrete barrier to contain and redirect impacting vehicles. In addition, controlled lateral deflection of the test article is acceptable. Occupant risk evaluates the degree of hazard to occupants in the impacting vehicle. Post-impact vehicle trajectory is a measure of the potential of the vehicle to result in a secondary collision with other vehicles and/or fixed objects, thereby increasing the risk of injury to the occupants of the impacting vehicle and/or other vehicles. These evaluation criteria are summarized in Table 3 and defined in greater detail in MASH. The full-scale vehicle crash tests were conducted and reported in accordance with the procedures provided in MASH.

In addition to the standard occupant risk measures, the Post-Impact Head Deceleration (PHD), the Theoretical Head Impact Velocity (THIV), and the Acceleration Severity Index (ASI) were determined and reported on the test summary sheet. Additional discussion on PHD, THIV, and ASI is provided in MASH.

Table 3. MASH Evaluation Criteria for Terminals and Crash Cushions

Structural Adequacy	A. Test article should contain and redirect the vehicle or bring the vehicle to a controlled stop; the vehicle should not penetrate, underride, or override the installation although controlled lateral deflection of the test article is acceptable.									
Occupant Risk	D. Detached elements, fragments or other debris from the test article should not penetrate or show potential for penetrating the occupant compartment, or present an undue hazard to other traffic, pedestrians, or personnel in a work zone. Deformations of, or intrusions into, the occupant compartment should not exceed limits set forth in Section 5.3 and Appendix E of MASH.									
	F. The vehicle should remain upright during and after collision. The maximum roll and pitch angles are not to exceed 75 degrees.									
	H. Occupant Impact Velocity (OIV) (see Appendix A, Section A5.3 of MASH for calculation procedure) should satisfy the following limits: <table><tr><th colspan="3">Occupant Impact Velocity Limits</th></tr><tr><th>Component</th><th>Preferred</th><th>Maximum</th></tr><tr><td>Longitudinal and Lateral</td><td>30 ft/s (9.1 m/s)</td><td>40 ft/s (12.2 m/s)</td></tr></table>	Occupant Impact Velocity Limits			Component	Preferred	Maximum	Longitudinal and Lateral	30 ft/s (9.1 m/s)	40 ft/s (12.2 m/s)
	Occupant Impact Velocity Limits									
	Component	Preferred	Maximum							
	Longitudinal and Lateral	30 ft/s (9.1 m/s)	40 ft/s (12.2 m/s)							
I. The Occupant Ridedown Acceleration (ORA) (see Appendix A, Section A5.3 of MASH for calculation procedure) should satisfy the following limits: <table><tr><th colspan="3">Occupant Ridedown Acceleration Limits</th></tr><tr><th>Component</th><th>Preferred</th><th>Maximum</th></tr><tr><td>Longitudinal and Lateral</td><td>15.0 g's</td><td>20.49 g's</td></tr></table>	Occupant Ridedown Acceleration Limits			Component	Preferred	Maximum	Longitudinal and Lateral	15.0 g's	20.49 g's	
Occupant Ridedown Acceleration Limits										
Component	Preferred	Maximum								
Longitudinal and Lateral	15.0 g's	20.49 g's								

9 TEST CONDITIONS

9.1 Test Facility

The testing facility is located at the Lincoln Air Park on the northwest side of the Lincoln Municipal Airport and is approximately 5 miles (8.0 km) northwest of the University of Nebraska-Lincoln.

9.2 Vehicle Tow and Guidance System

A reverse-cable, tow system with a 1:2 mechanical advantage was used to propel the test vehicle. The distance traveled and the speed of the tow vehicle were one-half that of the test vehicle. The test vehicle was released from the tow cable before impact with the barrier system. A digital speedometer was used on the tow vehicle to increase the accuracy of the test vehicle's impact speed.

A vehicle guidance system that was developed by Hinch [17] was used to steer the test vehicle. A guide flag, attached to the right-front wheel and the guide cable, was sheared off before impact with the barrier system. The $\frac{3}{8}$ -in. (9.5-mm) diameter guide cable was tensioned to approximately 3,500 lb (15.6 kN) and supported both laterally and vertically every 100 ft (30.5 m) by hinged stanchions. The hinged stanchions stood upright while holding up the guide cable. As the vehicle was towed down the line, the guide flag struck and knocked each stanchion to the ground.

9.3 Test Vehicles

For test no. NELON-1, a 2008 Dodge Ram was used as the test vehicle. The curb, test inertial, and gross static vehicle weights were 4,833 lb (2,192 kg), 4,991 lb (2,264 kg), and 5,148 lb (2,335 kg), respectively. The test vehicle is shown in Figure 58, and vehicle dimensions are shown in Figure 59.

For test no. NELON-2, a 2008 Dodge Ram was also used as the test vehicle. The curb, test inertial, and gross static vehicle weights were 5,036 lb (2,284 kg), 5,005 lb (2,270 kg), and 5,161 lb (2,341 kg), respectively. The test vehicle is shown in Figure 60, and vehicle dimensions are shown in Figure 61.

The longitudinal component of the center of gravity (c.g.) was determined using the measured axle weights. The Suspension Method [18] was used to determine the vertical component of the c.g. for the pickup truck. This method is based on the principle that the c.g. of any freely suspended body is in the vertical plane through the point of suspension. The vehicle was suspended successively in three positions, and the respective planes containing the c.g. were established. The intersection of these planes pinpointed the final c.g. location for the test inertial condition. The location of the final c.g. is shown in Figures 59 and 61. Data used to calculate the location of the c.g. and ballast information is shown in Appendix B.



Figure 58. Test Vehicle, Test No. NELON-1

Date: <u>3/3/2016</u>	Test Number: <u>NELON-1</u>	Model: <u>Ram 1500 Quad</u>
Make: <u>Dodge</u>	Vehicle I.D.#: <u>1D7HA18K18J205205</u>	
Tire Size: <u>265/70R17</u>	Year: <u>2008</u>	Odometer: <u>171640</u>
Tire Inflation Pressure: <u>35</u>		

*(All Measurements Refer to Impacting Side)

Vehicle Geometry -- in. (mm)

a	<u>77 1/8 (1959)</u>	b	<u>75 (1905)</u>
c	<u>228 5/8 (5807)</u>	d	<u>46 3/4 (1187)</u>
e	<u>140 1/4 (3562)</u>	f	<u>41 5/8 (1057)</u>
g	<u>28 (713)</u>	h	<u>64 7/8 (1647)</u>
i	<u>14 1/4 (362)</u>	j	<u>29 1/8 (740)</u>
k	<u>20 1/4 (514)</u>	l	<u>28 5/8 (727)</u>
m	<u>67 5/8 (1718)</u>	n	<u>67 3/4 (1721)</u>
o	<u>44 7/8 (1140)</u>	p	<u>3 1/4 (83)</u>
q	<u>30 1/2 (775)</u>	r	<u>18 3/8 (467)</u>
s	<u>15 3/8 (391)</u>	t	<u>74 5/8 (1895)</u>

Wheel Center Height Front 14 5/8 (371)

Wheel Center Height Rear 14 3/4 (375)

Wheel Well Clearance (F) 34 1/2 (876)

Wheel Well Clearance (R) 37 5/8 (956)

Frame Height (F) 18 1/8 (460)

Frame Height (R) 24 7/8 (632)

Engine Type Gasoline

Engine Size 3.7 V6

Transmission Type: Automatic

Drive Type: RWD

Mass Distribution lb (kg)			
Gross Static	LF <u>1465 (665)</u>	RF <u>1312 (595)</u>	
	LR <u>1168 (530)</u>	RR <u>1203 (546)</u>	

Weights lb (kg)	Curb	Test Inertial	Gross Static
W-front	<u>2689 (1220)</u>	<u>2683 (1217)</u>	<u>2777 (1260)</u>
W-rear	<u>2144 (973)</u>	<u>2308 (1047)</u>	<u>2371 (1075)</u>
W-total	<u>4833 (2192)</u>	<u>4991 (2264)</u>	<u>5148 (2335)</u>

GVWR Ratings

Front	<u>3700</u>
Rear	<u>3900</u>
Total	<u>6700</u>

Dummy Data

Type: Hybrid II

Mass: 157 lb

Seat Position: Driver

Note any damage prior to test: None

Figure 59 Vehicle Dimensions, Test No. NELON-1



Figure 60. Test Vehicle, Test No. NELON-2

Date: <u>3/16/2016</u>	Test Number: <u>NELON-2</u>	Model: <u>Ram 1500</u>
Make: <u>Dodge</u>	Vehicle I.D.#: <u>1D7HA18N28S594876</u>	
Tire Size: <u>265/70R17</u>	Year: <u>2008</u>	Odometer: <u>189326</u>
Tire Inflation Pressure: <u>35</u>		

*(All Measurements Refer to Impacting Side)

Test Inertial C.M.

Vehicle Geometry -- in. (mm)

a	<u>78 1/8</u>	<u>(1984)</u>	b	<u>74 5/8</u>	<u>(1895)</u>
c	<u>227 1/4</u>	<u>(5772)</u>	d	<u>46 1/2</u>	<u>(1181)</u>
e	<u>140 3/8</u>	<u>(3566)</u>	f	<u>41 1/4</u>	<u>(1048)</u>
g	<u>28</u>	<u>(711)</u>	h	<u>61 4/8</u>	<u>(1561)</u>
i	<u>14 1/2</u>	<u>(368)</u>	j	<u>26 3/4</u>	<u>(679)</u>
k	<u>21 3/4</u>	<u>(552)</u>	l	<u>29 1/8</u>	<u>(740)</u>
m	<u>68 1/8</u>	<u>(1730)</u>	n	<u>67 5/8</u>	<u>(1718)</u>
o	<u>44 7/8</u>	<u>(1140)</u>	p	<u>3 1/2</u>	<u>(89)</u>
q	<u>30 1/4</u>	<u>(768)</u>	r	<u>18 1/2</u>	<u>(470)</u>
s	<u>15</u>	<u>(381)</u>	t	<u>74 1/4</u>	<u>(1886)</u>

Wheel Center Height Front	<u>14 3/4</u>	<u>(375)</u>
Wheel Center Height Rear	<u>15 1/8</u>	<u>(384)</u>
Wheel Well Clearance (F)	<u>34 5/8</u>	<u>(879)</u>
Wheel Well Clearance (R)	<u>37 7/8</u>	<u>(962)</u>
Frame Height (F)	<u>17 3/4</u>	<u>(451)</u>
Frame Height (R)	<u>25 1/4</u>	<u>(641)</u>
Engine Type	<u>Gas V8</u>	
Engine Size	<u>4.7 Liter</u>	
Transmission Type	<u>Automatic</u>	
Drive Type	<u>RWD</u>	

Mass Distribution lb (kg)			
Gross Static	LF	<u>1492</u>	<u>(677)</u>
	RF	<u>1416</u>	<u>(642)</u>
	LR	<u>1127</u>	<u>(511)</u>
	RR	<u>1126</u>	<u>(511)</u>

Weights lb (kg)	Curb	Test Inertial	Gross Static	
W-front	<u>2862</u>	<u>(1298)</u>	<u>2908</u>	<u>(1319)</u>
W-rear	<u>2174</u>	<u>(986)</u>	<u>2253</u>	<u>(1022)</u>
W-total	<u>5036</u>	<u>(2284)</u>	<u>5161</u>	<u>(2341)</u>

GVWR Ratings	Dummy Data
Front <u>3700</u>	Type: <u>Hybrid II</u>
Rear <u>3900</u>	Mass: <u>156 lb</u>
Total <u>6700</u>	Seat Position: <u>Driver</u>

Note any damage prior to test: none

Figure 61. Vehicle Dimensions, Test No. NELON-2

Square, black-and white-checked targets were placed on the vehicle for reference to be viewed from the high-speed digital video cameras and aid in the video analysis, as shown in Figures 62 and 63. Round, checked targets were placed on the c.g. on the left-side door, the right-side door, and the roof of the vehicle.

The front wheels of the test vehicle were aligned to vehicle standards except the toe-in value was adjusted to zero so that the vehicles would track properly along the guide cable. A 5B flash bulb was mounted under the vehicle's left-side windshield wiper and was fired by a pressure tape switch mounted at the impact corner of the bumper. The flash bulb was fired upon initial impact with the test article to create a visual indicator of the precise time of impact on the high-speed videos. A remote controlled brake system was installed in the test vehicle so the vehicle could be brought safely to a stop after the test.

9.4 Simulated Occupant

For test nos. NELON-1 and NELON-2, A Hybrid II 50th-Percentile, Adult Male Dummy, equipped with clothing and footwear, was placed in the left-front seat of the test vehicle with the seatbelt fastened. The dummy, which had a final weight of 156 lb (70 kg) for test no. NELON-1 and 157 lb (71 kg) for test no. NELON-2, was represented by model no. 572, serial no. 451, and was manufactured by Android Systems of Carson, California. As recommended by MASH, the dummy was not included in calculating the c.g. location.

9.5 Data Acquisition Systems

9.5.1 Accelerometers

Two environmental shock and vibration sensor/recorder systems were used to measure the accelerations in the longitudinal, lateral, and vertical directions. All of the accelerometers were mounted near the c.g. of the test vehicles. The electronic accelerometer data obtained in dynamic testing was filtered using the SAE Class 60 and the SAE Class 180 Butterworth filter conforming to the SAE J211/1 specifications [7].

The two systems, the SLICE-1 and SLICE-2 units, were modular data acquisition systems manufactured by Diversified Technical Systems, Inc. (DTS) of Seal Beach, California. The acceleration sensors were mounted inside the bodies of custom built SLICE 6DX event data recorders and recorded data at 10,000 Hz to the onboard microprocessor. Each SLICE 6DX was configured with 7 GB of non-volatile flash memory, a range of ± 500 g's, a sample rate of 10,000 Hz, and a 1,650 Hz (CFC 1000) anti-aliasing filter. The "SLICEWare" computer software program and a customized Microsoft Excel worksheet were used to analyze and plot the accelerometer data.

9.5.2 Rate Transducers

Two identical angle rate sensor systems mounted inside the bodies of the SLICE-1 and SLICE-2 event data recorders were used to measure the rates of rotation of the test vehicle. Each SLICE MICRO Triax ARS had a range of 1,500 degrees/sec in each of the three directions (roll, pitch, and yaw) and recorded data at 10,000 Hz to the onboard microprocessors. The raw data measurements were then downloaded, converted to the proper Euler angles for analysis, and

plotted. The “SLICEWare” computer software program and a customized Microsoft Excel worksheet were used to analyze and plot the angular rate sensor data.

9.5.3 Retroreflective Optic Speed Trap

The retroreflective optic speed trap was used to determine the speed of the vehicle before impact. Five retroreflective targets, spaced at approximately 18-in. (457-mm) intervals, were applied to the side of the vehicle. When the emitted beam of light was reflected by the targets and returned to the Emitter/Receiver, a signal was sent to the data acquisition computer, recording at 10,000 Hz, as well as the external LED box activating the LED flashes. The speed was then calculated using the spacing between the retroreflective targets and the time between the signals. LED lights and high-speed digital video analysis are only used as a backup in the event that vehicle speeds cannot be determined from the electronic data.

9.5.4 Digital Photography

Five AOS high-speed digital video cameras, eight GoPro digital video cameras, and two JVC digital video cameras were utilized to film test nos. NELON-1 and NELON-2. Camera details, camera operating speeds, lens information, and schematics of the camera locations relative to the systems are shown in Figures 64 and 65.

The high-speed videos were analyzed using ImageExpress MotionPlus and RedLake MotionScope software programs. Actual camera speed and camera divergence factors were considered in the analysis of the high-speed videos. A Nikon D3200 digital still camera was also used to document pre- and post-test conditions for all tests.

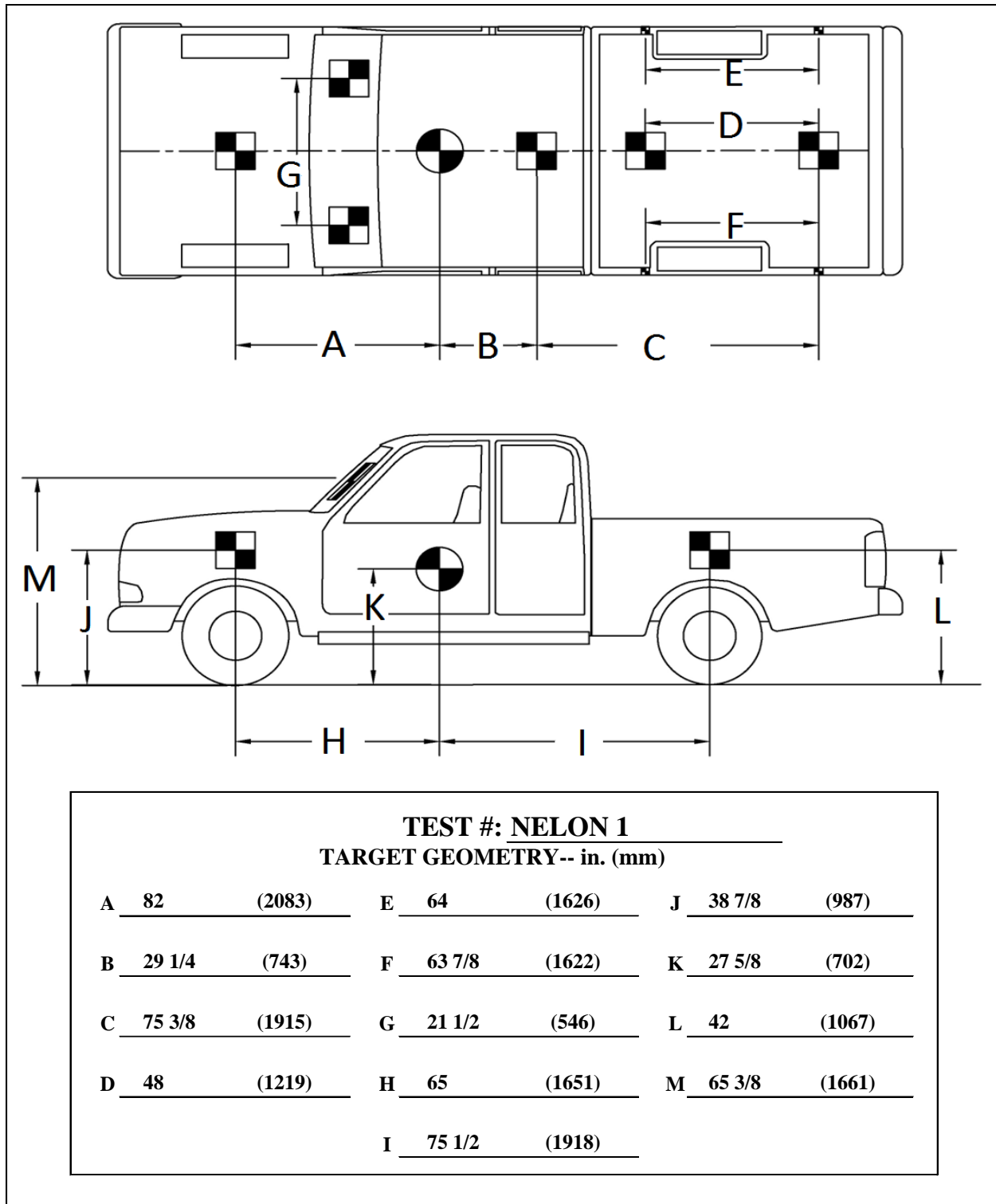


Figure 62. Target Geometry, Test No. NELON-1

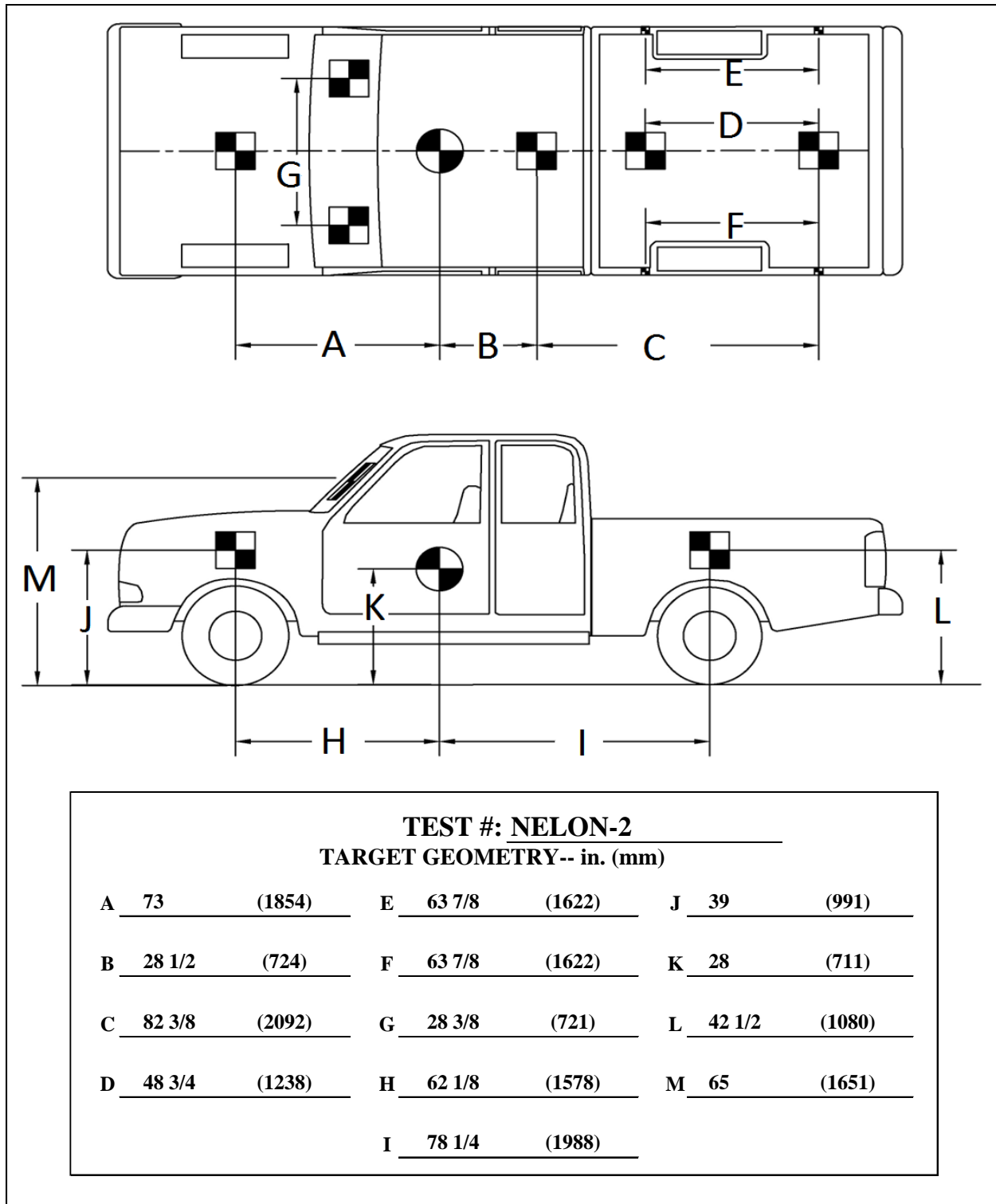
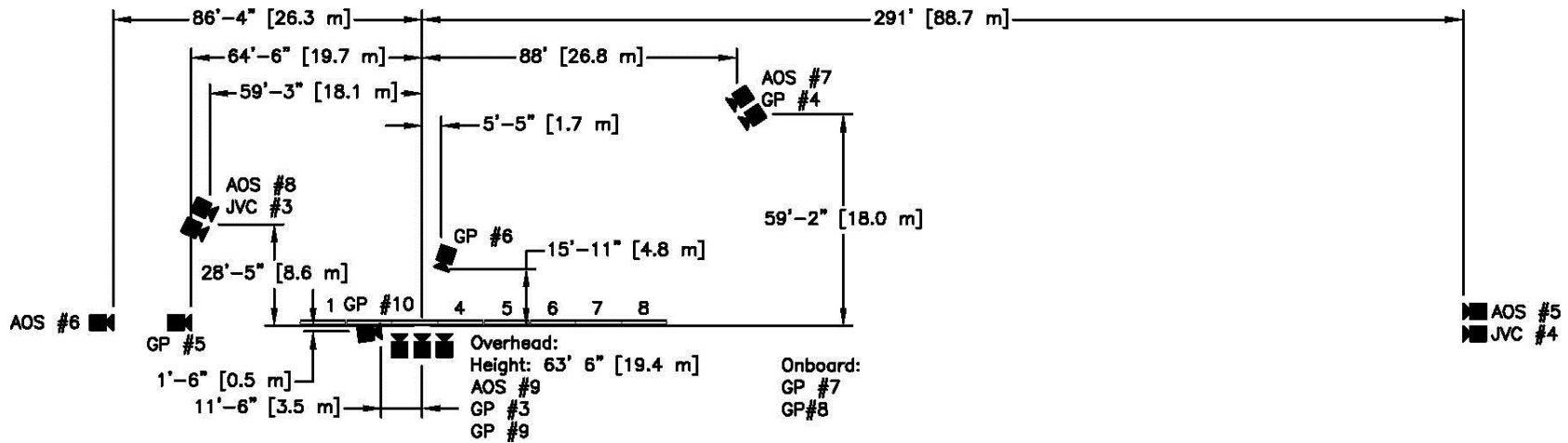


Figure 63. Target Geometry, Test No. NELON-2



No.	Type	Operating Speed (frames/sec)	Lens	Lens Setting
AOS-5	AOS X-PRI Gigabit	500	Vivitar 135 mm Fixed	-
AOS-6	AOS X-PRI Gigabit	500	Fujinon 50 mm	-
AOS-7	AOS X-PRI Gigabit	500	Sigma 28-70 DG	50
AOS-8	AOS S-VIT 1531	500	Sigma 28-70	35
AOS-9	AOS TRI-VIT 2236	500	Kowa 12 mm Fixed	-
GP-3	GoPro Hero 3+	120		
GP-4	GoPro Hero 3+	120		
GP-5	GoPro Hero 3+	120		
GP-6	GoPro Hero 3+	120		
GP-7	GoPro Hero 4	120		
GP-8	GoPro Hero 4	120		
GP-9	GoPro Hero 4	120		
GP-10	GoPro Hero 4	120		
JVC-3	JVC – GZ-MG27u (Everio)	29.97		
JVC-4	JVC – GZ-MG27u (Everio)	29.97		

Figure 64. Camera Locations, Speeds, and Lens Settings, Test No. NELON-1

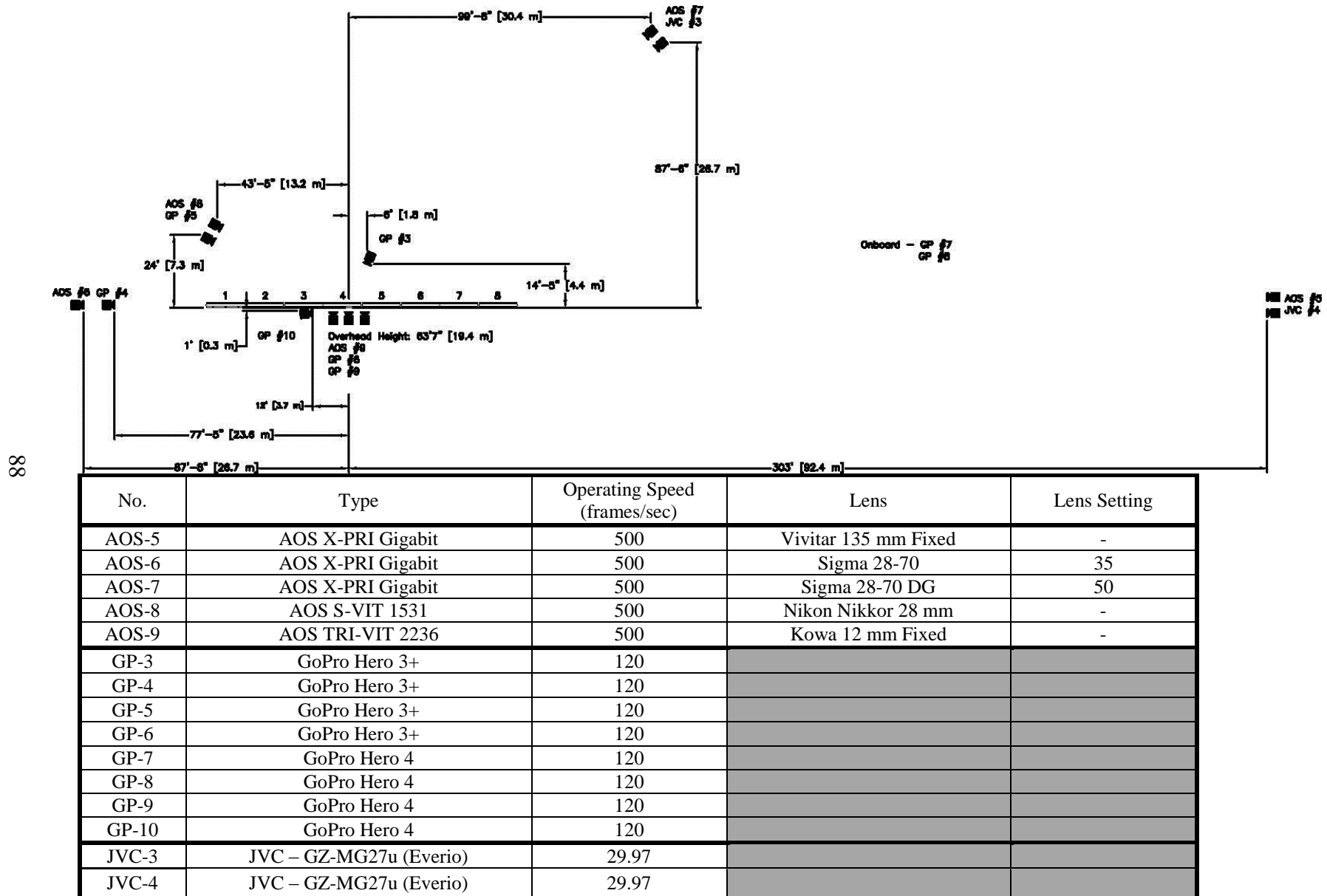


Figure 65. Camera Locations, Speeds, and Lens Settings, Test No. NELON-2

10 FULL-SCALE CRASH TEST NO. NELON-1

10.1 Weather Conditions

Test no. NELON-1 was conducted on March 3, 2016 at approximately 1:30 p.m. The weather conditions as per the National Oceanic and Atmospheric Administration (station 14939/LNK) were reported and are shown in Table 4.

Table 4. Weather Conditions, Test No. NELON-1

Temperature	46° F
Humidity	52 %
Wind Speed	15 mph
Wind Direction	0° from True North
Sky Conditions	Cloudy
Visibility	10 Statute Miles
Pavement Surface	Dry
Previous 3-Day Precipitation	0 in.
Previous 7-Day Precipitation	0 in.

10.2 Test Description

The 4,991-lb (2,264-kg) pickup truck impacted the portable concrete barrier system at a speed of 62.1 mph (100.0 km/h) and at an angle of 24.8 degrees. A summary of the test results and sequential photographs are shown in Figure 66. Additional sequential photographs are shown in Figures 67 and 68. Documentary photographs of the crash test are shown in Figures 69 and 70.

Initial vehicle impact was to occur $51\frac{3}{16}$ in. (1,300 mm) upstream from the centerline of the joint between barrier nos. 3 and 4, as shown in Figure 71. The impact point was selected based on LS-DYNA simulation of the beginning of the LON for the reduced length PCB system and MASH guidance for the critical impact point on PCB systems. The actual point of impact was $48\frac{11}{16}$ in. (1,237 mm) upstream from the centerline of the joint between barrier nos. 3 and 4. A sequential description of the impact events is contained in Table 5. Following the initial impact, the 2270P vehicle was captured and safely redirected by the barrier system. The vehicle came to rest 191 ft – 9 in (58.4 m) downstream of the initial impact point and 9 ft – 8 in. (2.9 m) in front of the front face of the barrier system. The vehicle trajectory and final position are shown in Figures 66 and 72, respectively.

Table 5. Sequential Description of Impact Events, Test No. NELON-1

TIME (sec)	EVENT
0.000	Vehicle's left-front bumper contacted barrier no. 3.
0.002	Vehicle's left-front bumper deformed, and vehicle's left-front tire contacted barrier no. 3.

0.008	Vehicle's left headlight deformed.
0.010	Vehicle's left quarter panel deformed.
0.016	Vehicle's left-front tire lost contact with ground, and downstream end of barrier no. 3 deflected backward.
0.022	Vehicle's left-front door flexed away from frame at upper rear corner.
0.024	Vehicle's grille and engine hood deformed.
0.028	Upstream end of barrier no. 4 deflected backward.
0.038	Downstream end of barrier no. 4 deflected forward.
0.042	Vehicle pitched upward.
0.044	Vehicle's left-rear door flexed away from frame at upper rear corner, and vehicle yawed away from barrier.
0.048	Upstream end of barrier no. 5 deflected forward.
0.054	Vehicle rolled toward barrier system, and vehicle's left headlight shattered and disengaged from vehicle.
0.056	Downstream end of barrier no. 5 deflected backward.
0.058	Airbags deployed.
0.062	Barrier no. 5 deflected upstream.
0.064	Barrier no. 3 deflected downstream.
0.066	Barrier no. 3 rotated counterclockwise.
0.068	Barrier no. 2 deflected downstream.
0.072	Barrier no. 6 rotated clockwise.
0.074	Vehicle's right-front tire became airborne.
0.078	Downstream end of barrier no. 2 deflected forward.
0.084	Barrier no. 1 deflected downstream.
0.118	Barrier no. 6 deflected upstream.
0.120	Barrier no. 7 deflected downstream.
0.134	Upstream end of barrier no. 3 deflected backward.
0.144	Upstream end of barrier no. 6 deflected forward.
0.164	Upstream end of barrier no. 2 deflected forward.
0.194	Vehicle was parallel to system at a speed of 50.3 mph (80.9 km/h).
0.200	Vehicle's right-rear tire became airborne.
0.202	Downstream end of barrier no. 6 deflected backward.
0.204	Downstream end of barrier no. 1 deflected forward.
0.232	Upstream end of barrier no. 7 deflected backward.
0.272	Vehicle's left-rear quarter panel contacted barrier no. 4 and deformed, and vehicle's left taillight contacted barrier no. 4 and deformed.
0.278	Left taillight disengaged from vehicle.

0.298	Vehicle pitched downward.
0.312	Barrier no. 4 deflected downstream.
0.378	Vehicle's left-front tire regained contact with ground.
0.424	Vehicle's left-front door impacted knee formed by joint between barrier nos. 5 and 6.
0.454	Vehicle's left-rear door impacted knee formed by joint between barrier nos. 5 and 6.
0.542	Vehicle lost contact with the system at a speed of 44.8 mph (72 km/h) and a 12.3 degree angle.
0.550	Vehicle's left rear tire was airborne.
0.692	Vehicle pitched upward.
0.768	Vehicle rolled away from barrier.
1.066	Vehicle's right-front tire regained contact with ground.
1.180	Vehicle's right-rear tire regained contact with ground.
1.230	Vehicle's left-rear tire regained contact with ground.
3.154	Vehicle came to rest 191 ft – 9 in. (58.4 m) downstream and 9 ft – 8 in. (2.9 m) laterally in front of the barrier system.

10.3 Barrier Damage

Damage to the barrier system was moderate, as shown in Figures 73 through 79. Barrier system damage consisted of contact marks on the front face of the concrete barriers, spalling and gouging of the concrete, and concrete cracking and fracture. The length of vehicle contact along the barrier system was approximately 29 ft - 3 in. (8.9 m), which spanned from 14 in. (356 mm) upstream of the targeted impact point to the downstream edge of barrier no. 5.

A 5½-in. (140-mm) wide x ½-in. (13-mm) thick piece of concrete disengaged from the downstream end toe on the back side of barrier no. 1. A 7½-in. (191-mm) wide x 2-in. (51-mm) thick piece of concrete disengaged from the upstream toe corner on the back side of barrier no. 2. Contact marks began 14 in. (356 mm) upstream from the targeted impact point near the groundline and extended the length of barrier no. 3. Barrier no. 3 had gouging that started 2½ in. (64 mm) downstream from the targeted impact point and 13 in. (330 mm) from the groundline and extended 6 in. (152 mm) upward and 16 in. (406 mm) downstream. A 4-in. (102-mm) wide x 10½-in. (267-mm) tall concrete piece disengaged from the downstream corner of the front side of barrier no. 3, beginning 19½ in. (495 mm) from the ground. A 6¼-in. (159-mm) wide x 6¼-in. (159-mm) tall piece disengaged from the downstream corner of the toe on the front side of barrier no. 3. A crack began 15 in. (381 mm) upstream of the impact point and extended around both faces of barrier no. 3.

Cracking was found on the upstream end of barrier no. 4 that started 21 in. (533 mm) from the ground and extended 10¾ in. (273 mm) upward and onto the barrier's front face and ended 5 in. (127 mm) downstream. A 1-in. (25-mm) wide gouge started 12 in. (305 mm) from the ground and extended 18½ in. (470 mm) upward on the corner of the upstream end and continued onto the front face of barrier no. 4. A 6-in. wide x 7-in. tall x 3½-in. deep (152-mm x 178-mm x 89-mm)

piece of concrete disengaged from the upstream corner of the front side on the toe of barrier no. 4. Barrier no. 4 also had a crack on the front face 36 in. (914 mm) downstream from the upstream end that extended to the back side of the barrier. On the front face of barrier no. 4, a 47½-in. (1,207-mm) long x 10-in. tall (254-mm) piece of concrete disengaged 26 in. (660 mm) from the upstream end at the groundline. Concrete that measured 18 in. x 10 in. x 5 in. (457 mm x 254 mm x 127 mm) disengaged from the bottom of the toe on the back face of barrier no. 4 starting at 52½ in. (1,334 mm) downstream from the upstream end of the barrier.

Barrier no. 5 damage included cracking, gouging, spalling, and contact marks. Multiple cracks were found on the upstream face with one beginning 2 in. (51 mm) from the front face and the other beginning 4 in. (102 mm) from the front face. Both cracks extended from the top of the barrier to the connection loop on the side of the barrier. Cracking was also present starting 12 in. (305 mm) downstream from the center extending vertically around both sides and the top of the barrier. Gouges on the upstream front corner of the barrier began at the top of the barrier and extended 8 in. (203 mm) downward. A 6-in. wide x 6-in. tall x 2-in. deep (152-mm x 152-mm x 51-mm) concrete piece disengaged from the front upstream toe corner of barrier no. 5. A 7 in.-wide x 7-in. tall x 2-in. deep (178-mm x 178-mm x 51-mm) concrete piece disengaged from the downstream front corner at the top of barrier no. 5. Contact marks were found 2 in. (51 mm) from the top of the barrier and began 6 in. (152 mm) upstream from the center and extended to the downstream end.

The damage on barrier nos. 6 and 7 was limited to spalling and gouging. A gouge started at the top of barrier no. 6 and extended 10 in. (254 mm) down on the front-upstream corner. A 6-in. wide x 7 in.-tall x 2 in.-deep (152-mm x 178-mm x 51-mm) piece of concrete at the upstream-back corner at the bottom disengaged from barrier no. 6. A 3½-in. wide x 5½-in. tall x 1-in. deep (89-mm x 140-mm x 25-mm) piece of concrete disengaged from the downstream back corner at the bottom of barrier no. 6. Barrier no. 7 had two pieces disengage from the barrier. A 12-in. wide x 7-in. tall x 1½-in. deep (305-mm x 178-mm x 38-mm) piece of concrete disengaged 40 in. (1,016 mm) downstream from the center of barrier no. 7. A 13-in. wide x 6-in. tall x 1½-in. deep (330-mm x 152-mm x 38-mm) piece of concrete disengaged from the upstream-back corner at the bottom of barrier no. 7.

Multiple connection pins within the PCB system experienced deformations during the impact. The connection pins between barrier nos. 3 and 4, as well as between barrier nos. 4 and 5 bent slightly near the location of the lower connection loops.

The permanent set of the barrier system was 128 in. (3,251 mm), as measured in the field. The longitudinal barrier displacement of the barriers on the upstream and downstream ends of the barrier system were found to be 47½ in. (1,207 mm) and 4 in. (102 mm), respectively, as measured in the field. The maximum lateral dynamic barrier deflection was 128.3 in. (3,259 mm), as determined from high-speed digital video analysis. The working width of the system was found to be 150.8 in. (3,830 mm), also determined from high-speed digital video analysis.

10.4 Vehicle Damage

The damage to the vehicle was moderate, as shown in Figures 80 through 82. The maximum occupant compartment deformations are listed in Table 6 along with the deformation limits established in MASH for various areas of the occupant compartment. Note that none of the

established MASH deformation limits were violated. Complete occupant compartment and vehicle deformations and the corresponding locations are provided in Appendix C.

Table 6. Maximum Occupant Compartment Deformations by Location

LOCATION	MAXIMUM DEFORMATION in. (mm)	MASH ALLOWABLE DEFORMATION in. (mm)
Wheel Well & Toe Pan	1½ (38)	≤ 9 (229)
Floor Pan & Transmission Tunnel	½ (13)	≤ 12 (305)
Side Front Panel (in Front of A-Pillar)	⅝ (16)	≤ 12 (305)
Side Door (Above Seat)	½ (13)	≤ 9 (229)
Side Door (Below Seat)	½ (13)	≤ 12 (305)
Roof	½ (13)	≤ 4 (102)
Windshield	½ (13)	≤ 3 (76)

The majority of damage was concentrated on the left-front corner and left side of the vehicle where the impact occurred. The left side of the front bumper was crushed inward and back 16 in. (406 mm). The left headlight housing assembly disengaged. The grille was fractured around the left-side headlight assembly and had a 1-in. (25-mm) long crack in the center. The front bumper had a 1-in. (25-mm) crease on the bottom edge 3 in. (76 mm) left of center. The left-front fender was pushed upward and inward in front of the left-front wheel. The left-front tire disengaged from its bead and was deflated with significant tearing on the sidewall. The left-front rim was deformed significantly with a 16-in. (406-mm) long dent on the bottom of the rim. Denting and scraping were observed on the entire left side of the vehicle with the most significant being a 62-in. long x 30-in. tall x 4-in. deep (1,575-mm x 762-mm x 102-mm) dent beginning at the rear of the left-front door and extending rearward to the left-rear wheel well. The left-rear door was dented and was ajar approximately 1½ in. (38 mm) at the top of the door, but the door remained latched. There was a 1½-in. (38-mm) long buckle on the C-pillar at the top of the bed. The left-rear wheel assembly disengaged from the vehicle at the axle shaft. The tire was found deflated, and a 9-in. (229-mm) long buckle was present on the outside of the wheel. The left-rear brake line was sheared off and leaked brake fluid. The left taillight disengaged from the vehicle. A 3-in. (76-mm) gap was found between the front edge of the right-front fender and the corner of the hood. A ⅛-in. (3-mm) gap was found between the top of the right-rear quarter panel and the top of the tailgate. Both airbags deployed.

10.5 Occupant Risk

The calculated occupant impact velocities (OIVs) and maximum 0.010-sec average occupant ridedown accelerations (ORAs) in both the longitudinal and lateral directions are shown in Table 7. Note that the OIVs and ORAs were within suggested limits, as provided in MASH. The calculated THIV, PHD, and ASI values are also shown in Table 7. The results of the occupant risk analysis, as determined from the accelerometer data, are summarized in Figure 66. The

recorded data from the accelerometers and the rate transducers are shown graphically in Appendix D.

Table 7. Summary of OIV, ORA, THIV, PHD, and ASI Values, Test No. NELON-1

Evaluation Criteria		Transducer		MASH Limits
		SLICE-1	SLICE-2 (Primary)	
OIV ft/s (m/s)	Longitudinal	-14.57 (-4.44)	-13.75 (-4.19)	±40 (12.2)
	Lateral	15.68 (4.78)	16.93 (5.16)	±40 (12.2)
ORA g's	Longitudinal	-6.63	-6.92	±20.49
	Lateral	16.76	15.20	±20.49
MAX. ANGULAR DISPL. deg.	Roll	-30.56	-26.93	±75
	Pitch	-12.96	-15.00	±75
	Yaw	53.51	52.23	not required
THIV ft/s (m/s)		20.0 (6.08)	20.7 (6.32)	not required
PHD g's		16.84	15.23	not required
ASI		1.12	1.10	not required

10.6 Discussion

The analysis of the test results for test no. NELON-1 showed that the beginning of the LON for the free-standing, F-shape PCB system adequately contained and redirected the 2270P vehicle with controlled lateral displacements of the barrier. There were no detached elements nor fragments which showed potential for penetrating the occupant compartment nor presented undue hazard to other traffic. Deformations of, or intrusions into, the occupant compartment that could have caused serious injury did not occur. The test vehicle did not penetrate nor ride over the barrier and remained upright during and after the collision. Vehicle roll, pitch, and yaw angular displacements, as shown in Appendix D, were deemed acceptable, because they did not adversely influence occupant risk nor cause rollover. After impact, the vehicle exited the barrier at an angle of 12.3 degrees and its trajectory did not violate the bounds of the exit box. Therefore, test no. NELON-1 was determined to be acceptable according to the MASH safety performance criteria for test designation no. 3-35.

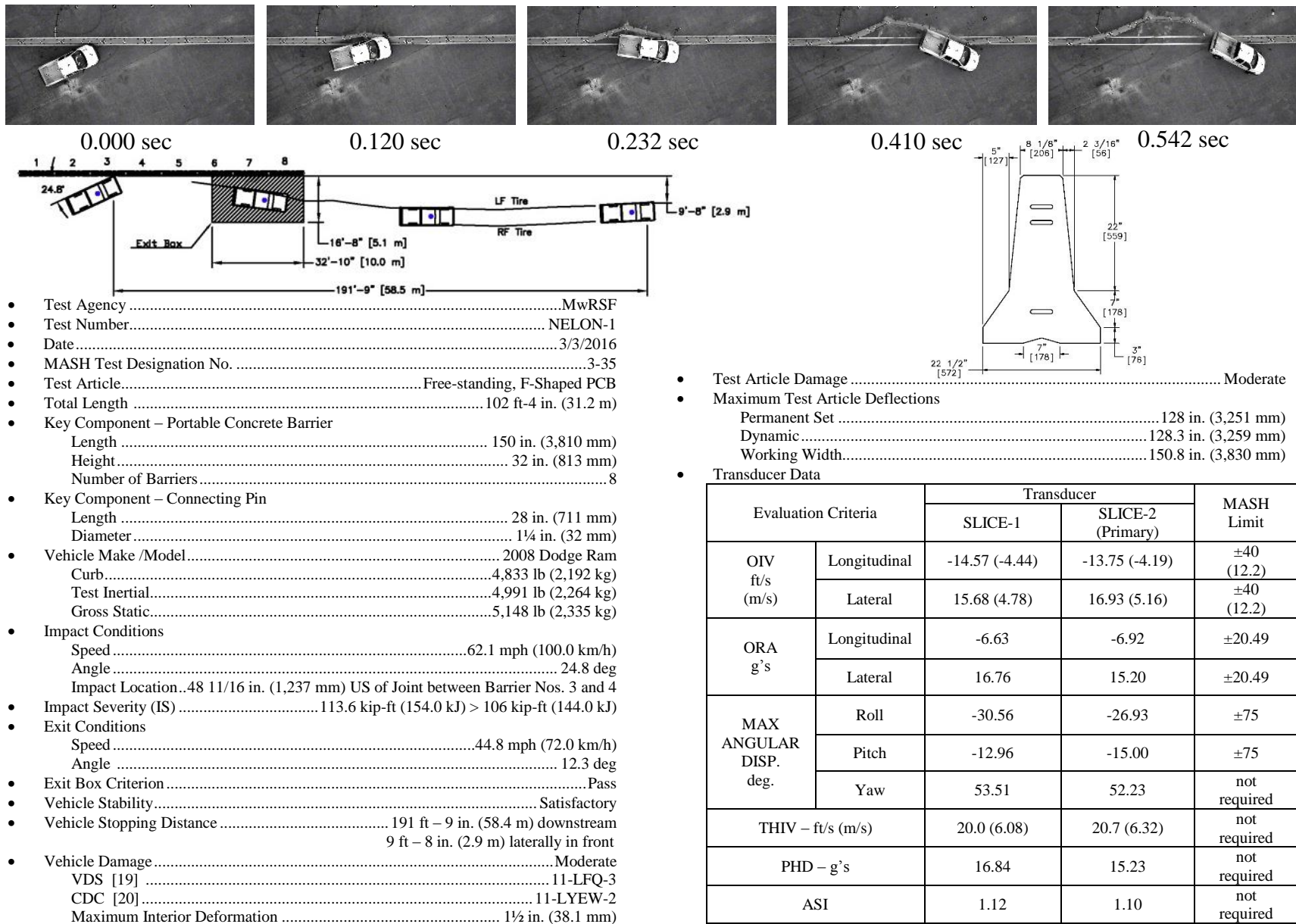


Figure 66. Summary of Test Results and Sequential Photographs, Test No. NELON-1



0.000 sec



0.058 sec



0.200 sec



0.378 sec



0.550 sec



1.834 sec



0.000 sec



0.058 sec



0.278 sec



0.692 sec



1.180 sec



1.604 sec

Figure 67. Additional Sequential Photographs, Test No. NELON-1



0.000 sec



0.016 sec



0.044 sec



0.078 sec



0.272 sec



0.542 sec



0.000 sec



0.038 sec



0.064 sec



0.370 sec



1.282 sec



1.866 sec

Figure 68. Additional Sequential Photographs, Test No. NELON-1



Figure 69. Documentary Photographs, Test No. NELON-1



Figure 70. Documentary Photographs, Test No. NELON-1

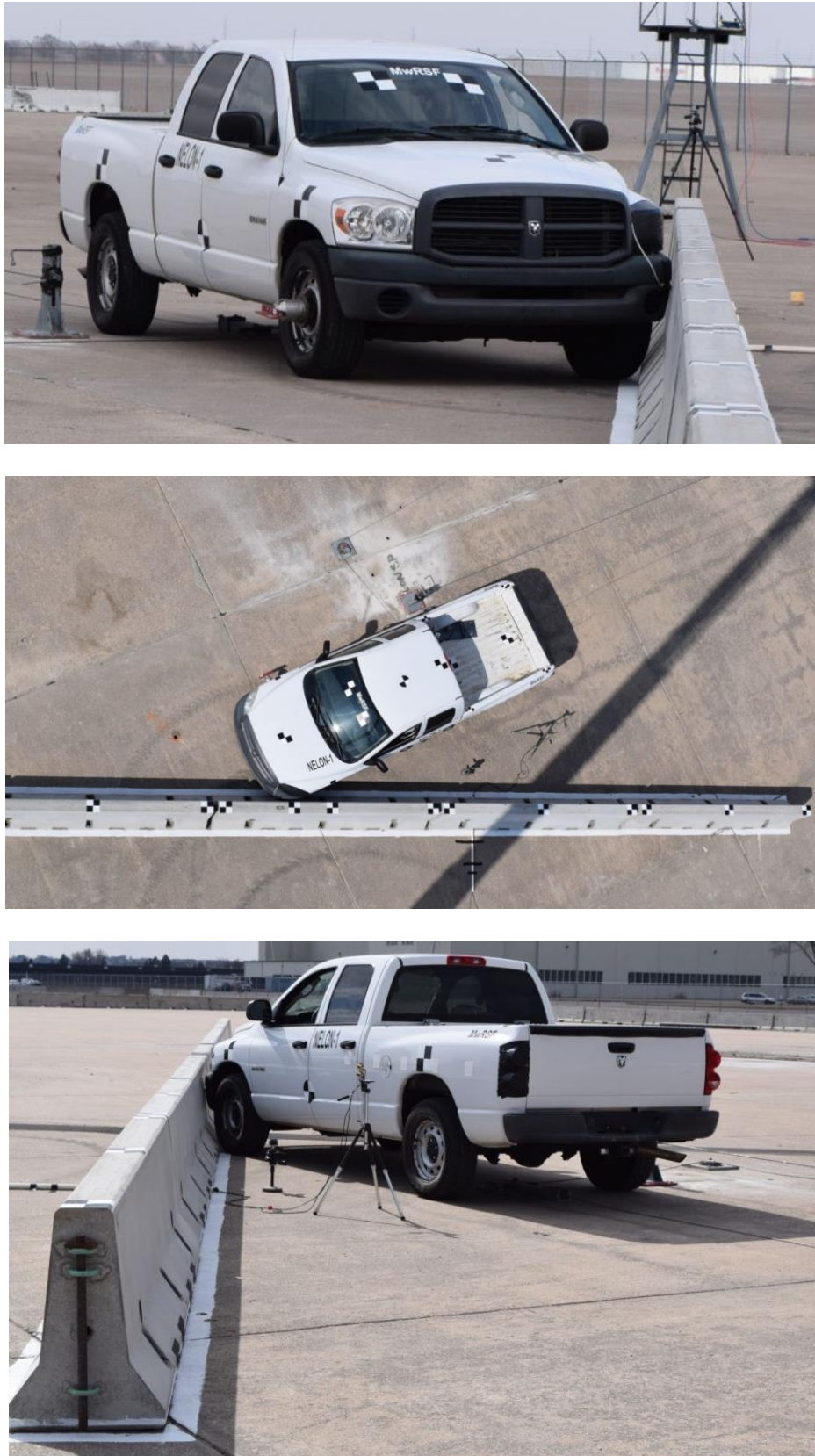


Figure 71. Impact Location, Test No. NELON-1



Figure 72. Vehicle Final Position and Trajectory Marks, Test No. NELON-1



Figure 73. System Deflection and Damage, Test No. NELON-1



Figure 74. Barrier Nos. 1 and 2 Damage, Test No. NELON-1



Figure 75. Barrier No. 3 Damage, Test No. NELON-1



Figure 76. Barrier No. 4 Damage, Test No. NELON-1



Figure 77. Barrier No. 5 Damage, Test No. NELON-1



Figure 78. Barrier No. 6 Damage, Test No. NELON-1



Figure 79. Barrier Nos. 7 and 8 Damage, Test No. NELON-1



Figure 80. Vehicle Damage, Test No. NELON-1

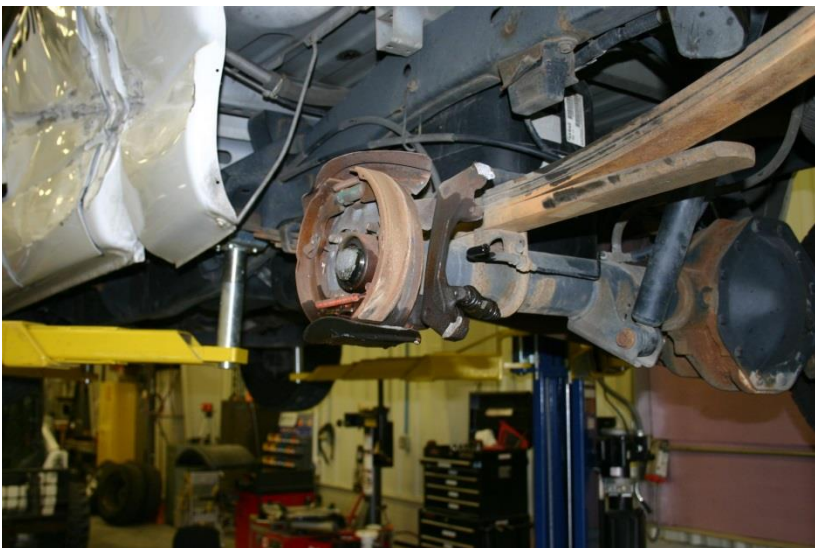


Figure 81. Vehicle Damage, Test No. NELON-1



Figure 82. Occupant Compartment Damage, Test No. NELON-1

11 FULL-SCALE CRASH TEST NO. NELON-2

11.1 Weather Conditions

Test no. NELON-2 was conducted on March 16, 2016 at approximately 1:00 p.m. The weather conditions as per the National Oceanic and Atmospheric Administration (station 14939/LNK) were reported and are shown in Table 8.

Table 8. Weather Conditions, Test No. NELON-2

Temperature	59° F
Humidity	27 %
Wind Speed	18 mph
Wind Direction	290° from True North
Sky Conditions	Sunny
Visibility	10 Statute Miles
Pavement Surface	Dry
Previous 3-Day Precipitation	0.51 in.
Previous 7-Day Precipitation	0.58 in.

11.2 Test Description

The 5,005-lb (2,270-kg) pickup truck impacted the portable concrete barrier system at a speed of 63.0 mph (101.4 km/h) and at an angle of 24.5 degrees. A summary of the test results and sequential photographs are shown in Figure 84. Additional sequential photographs are shown in Figures 85 and 86. Documentary photographs of the crash test are shown in Figures 87 and 88.

Initial vehicle impact was to occur 51³/₁₆ in. (1,300 mm) upstream from the centerline of the joint between barrier nos. 4 and 5, as shown in Figure 89. The impact point was selected based on LS-DYNA simulation of the end of the LON for the reduced length PCB system and MASH guidance for the critical impact point on PCB systems. The actual point of impact was 63 in. (1,600 mm) upstream from the downstream edge of barrier no. 4. A sequential description of the impact events is contained in Table 9. During the impact, the 2270P vehicle was captured and redirected, however, the left-front door unlatched and opened when the vehicle rolled onto its left side before rolling back and exiting the system. The vehicle came to rest 165 ft – 10 in (50.5 m) downstream of the initial impact point and 28 ft – 11 in. (8.8 m) in front of the front face of the barrier system. The vehicle trajectory and final position are shown in Figures 84 and 90, respectively.

Table 9. Sequential Description of Impact Events, Test No. NELON-2

TIME (sec)	EVENT
0.000	Vehicle's left-front bumper contacted downstream end of barrier no. 4.
0.002	Vehicle's front bumper deformed.

0.006	Vehicle's left headlight deformed, and vehicle's left fender contacted barrier no. 4.
0.008	Vehicle's left fender deformed.
0.020	Downstream end of barrier no. 4 deflected backward.
0.024	Vehicle's engine hood deformed.
0.026	Vehicle's grille deformed, and vehicle's left-front door flexed away from frame at upper rear corner.
0.036	Upstream end of barrier no. 5 deflected backward.
0.046	Vehicle's airbags deployed.
0.052	Vehicle yawed away from barrier system, vehicle rolled toward barrier system, and vehicle's left-rear door flexed away from frame at upper rear corner.
0.056	Upstream end of barrier no. 6 deflected forward.
0.090	Barrier no. 5 cracked at center.
0.092	Vehicle's right-front tire became airborne, and downstream end of barrier no. 3 deflected backward.
0.102	Vehicle pitched upward.
0.118	Barrier no. 3 deflected downstream, and barrier no. 2 deflected downstream.
0.120	Barrier no. 1 deflected downstream.
0.132	Upstream end of barrier no. 6 deflected backward.
0.142	Vehicle's left headlight detached.
0.172	Vehicle's right-rear tire became airborne.
0.182	Upstream end of barrier no. 7 deflected forward.
0.194	Vehicle was parallel to system at a speed of 51.2 mph (82.3 km/h).
0.264	Vehicle's left quarter panel contacted barrier no. 5 and deformed.
0.268	Vehicle's left taillight deformed.
0.272	Vehicle's left-front tire contacted ground.
0.280	Vehicle pitched downward, and vehicle's rear bumper deformed.
0.282	Upstream end of barrier no. 8 deflected backward, and barrier no. 2 deflected forward.
0.302	Vehicle's left taillight detached.
0.346	Upstream end of barrier no. 7 cracked.
0.376	Upstream end of barrier no. 8 deflected forward.
0.390	Vehicle's left-front door contacted downstream knee formed at joint between barrier nos. 6 and 7.
0.404	Downstream end of barrier no. 6 cracked.
0.420	Downstream end of barrier no. 6 spalled.
0.438	Vehicle's left-rear door contacted downstream knee formed at joint between barrier nos. 6 and 7.

0.448	Vehicle's left side mirror contacted barrier system.
0.454	Upstream end of barrier no. 7 deflected backward.
0.524	Vehicle's left-front door opened.
0.528	Vehicle lost contact with system at a speed of 39.4 mph (63.4 km/h) and an angle of 10.4 degrees.
0.602	Vehicle's tailgate deformed.
0.724	Downstream end of barrier no. 2 deflected backward.
0.762	Upstream end of barrier no. 8 deflected backward.
0.858	Vehicle's open left-front door contacted ground.
1.336	PCB system deflection came to a stop.
1.544	Vehicle's left-rear tire contacted ground.
1.602	Vehicle's left quarter panel contacted ground.
1.636	Vehicle's rear bumper contacted ground.
1.692	Vehicle rolled away from barrier system.
2.160	Vehicle's left quarter panel contacted ground.
2.866	Vehicle's right-front tire regained contact with ground.
2.886	Vehicle's right-rear tire regained contact with ground.
3.208	Vehicle came to rest 165 ft – 10 in. (50.5 m) downstream and 28 ft – 11 in. (8.8 m) laterally in front of barrier system.

11.3 Barrier Damage

Damage to the barrier system was moderate, as shown in Figures 91 through 96. Barrier system damage consisted of contact marks on the front face of the concrete barriers, spalling and gouging of the concrete, and concrete cracking and fracture. The length of vehicle contact along the barrier system was approximately 30 ft – 2 in. (9.2 m), which spanned from 18 in. (457 mm) downstream from the center target of barrier no. 4 to 9 in. (229 mm) downstream from the upstream edge of barrier no. 7.

A 1-in. wide x 3-in. tall x ¼-in. deep (25-mm x 76-mm x 6-mm) concrete portion disengaged from barrier no. 2 at the downstream corner on the back face of the toe at the groundline. A 4-in. wide x 2¼-in. tall x ¼-in. deep (102-mm x 57-mm x 6-mm) piece of concrete disengaged from the upstream corner of the back face of barrier no. 3 on the bottom of the toe. Gouges started 17 in. (432 mm) from the groundline and 24 in. (610 mm) downstream from the center target on barrier no. 4 and extended a total length of 21¼ in. (540 mm). A 4-in. wide x 15¼-in. tall x 2½-in. deep (102-mm x 387-mm x 64-mm) concrete piece located at the downstream edge 15½ in. (394 mm) above the groundline disengaged from barrier no. 4. A 1½-in. wide x 8¾-in. tall x 1½-in. deep (38-mm x 222-mm x 38-mm) piece of concrete disengaged from the downstream corner of the front face on the bottom of the toe of barrier no. 4.

A 7-in. (178-mm) long crack was found on the upstream side of barrier no. 5 that started 2 in. (51 mm) from the front face and 2½ in. (64 mm) from the top of the barrier. On the upstream

edge of barrier no. 5, a 2¾-in. wide x 15-in. tall x ⅛-in. deep (70-mm x 381-mm x 3-mm) portion of concrete disengaged 2½ in. (64 mm) from the ground on the front face. Two concrete portions disengaged from the front face of the toe at the bottom of barrier no. 5; the first was located at the upstream edge and was 8 in. wide x 8½ in. tall x 3 in. deep (203 mm x 216 mm x 76 mm) and the second began 39½ in. (1,003 mm) downstream from the upstream edge and extended 51½ in. (1,308 mm) downstream. A 17¼-in. wide x 11-in. tall x 4½-in. deep (438-mm x 279-mm x 114-mm) piece of concrete disengaged from the toe on the back face of barrier no. 5 beginning 52½ in. (1,334 mm) from the upstream edge. A crack was located 61½ in. (1,562 mm) downstream of the upstream edge of barrier no. 5 and extended across both faces of the barrier. Another large crack was located 31¼ in. (794 mm) downstream from the center target and extended vertically across the back face and the width of barrier no. 5 at the top. Cracking was found 14 in. (356 mm) downstream from the center target that extended across both faces of barrier no. 5.

Gouges started at the top of barrier no. 6 and extended 16 in. (406 mm) downward with a maximum width of 2¾ in. (70 mm) on the front face at the upstream edge. A 12½-in. wide x 8¼-in. tall x 4-in. deep (318-mm x 210-mm x 102-mm) concrete portion disengaged from the bottom of the toe on the upstream side of barrier no. 6. A 22½-in. wide x 7-in. tall x 2-in. deep (572-mm x 178-mm x 51-mm) concrete portion that began 52 in. (1,321 mm) downstream from the center of the barrier at the bottom of the toe disengaged from the downstream edge of the back face. A 4-in. wide x 13-in. tall x 3½-in. deep (102-mm x 330-mm x 89-mm) portion of concrete disengaged from barrier no. 6 on the downstream edge of the front face.

A 2½-in. wide x 9½-in. tall x ½-in. deep (64-mm x 241-mm x 13-mm) concrete portion disengaged from the upstream edge on the front face of barrier no. 7 at 24 in. (610 mm) from the ground. A 6-in. wide x 8-in. tall x 2-in. deep (152-mm x 203-mm x 51-mm) concrete piece disengaged from the upstream edge on the back face at the bottom of the toe. A 5¼-in. wide x 5½-in. tall x 2-in. deep (133-mm x 140-mm x 51-mm) concrete portion disengaged from the downstream edge on the back face at the bottom of the toe. A 9½-in. wide x 7½-in. tall x 2-in. deep (241-mm x 191-mm x 51-mm) concrete portion disengaged from the upstream edge on the back face of the toe at the bottom of barrier no. 8.

Multiple connection pins between the PCBs were deformed during the impact. The connecting pin between barrier nos. 4 and 5 had a slight bend at the location of the lower connection loops. The connecting pin between barrier nos. 5 and 6 had a slight bend at the location of the upper connection loops.

The permanent set of the barrier system was 126 in. (3,200 mm), as measured in the field. The longitudinal displacement of the barriers on the upstream and downstream ends of the system were found to be 28½ in. (724 mm) and 22⅞ in. (581 mm), respectively, as measured in the field. The maximum lateral dynamic barrier deflection was 127.8 in. (3,246 mm), as determined from high-speed digital video analysis. The working width of the system was found to be 150.3 in. (3,818 mm), also determined from high-speed digital video analysis.

11.4 Vehicle Damage

The damage to the vehicle was moderate, as shown in Figures 97 and 98. The maximum occupant compartment deformations are listed in Table 10 along with the deformation limits established in MASH for various areas of the occupant compartment. Note that none of the

established MASH deformation limits were violated. Complete occupant compartment and vehicle deformations and the corresponding locations are provided in Appendix C.

Table 10. Maximum Occupant Compartment Deformations by Location

LOCATION	MAXIMUM DEFORMATION in. (mm)	MASH ALLOWABLE DEFORMATION in. (mm)
Wheel Well & Toe Pan	$\frac{3}{8}$ (9)	≤ 9 (229)
Floor Pan & Transmission Tunnel	$\frac{1}{8}$ (3)	≤ 12 (305)
Side Front Panel (in Front of A-Pillar)	0 (0)	≤ 12 (305)
Side Door (Above Seat)	2 (51)	≤ 9 (229)
Side Door (Below Seat)	1 $\frac{1}{4}$ (32)	≤ 12 (305)
Roof	$\frac{1}{2}$ (13)	≤ 4 (102)
Windshield	$\frac{1}{2}$ (13)	≤ 3 (76)

The majority of damage was concentrated on the left-front corner and the left side of the vehicle where the impact occurred. There was a 5-in. long x 1-in. tall x $\frac{3}{4}$ -in. deep (127-mm x 25-mm x 19-mm) buckle on the radiator core support below the radiator. There was also a 10-in. (254-mm) long scrape on the radiator core support behind the left headlight housing. Buckling occurred on the left side of the front bumper that was 13 $\frac{3}{8}$ in. long x 8 in. tall x 3 $\frac{1}{2}$ in. deep (340 mm x 203 mm x 89 mm). The front bumper had a kink on the bottom at the centerline and scraping on the left side. The left headlight assembly disengaged from the vehicle. The left-front fender was pushed upward and inward in front of the left-front wheel. The left-front steel wheel was deformed significantly with a 15-in. long x 7 $\frac{1}{2}$ -in. wide (381-mm x 191-mm) buckle on the hubcap. The left-front tire was deflated and had 4 $\frac{1}{8}$ in. long x 2 $\frac{7}{8}$ in. wide (105 mm x 73 mm) and 8 $\frac{1}{2}$ in. long x 3 $\frac{1}{8}$ in. wide (216 mm x 79 mm) tears in the sidewall. The right-front tire bead disengaged from the wheel and was deflated and there was a 3 $\frac{1}{2}$ -in. (89-mm) long kink on the wheel. Scraping measuring 1 $\frac{1}{2}$ in. (38 mm) long was found on the bottom of both lower control arms as well as indications that the bump stops on both control arms came into contact with the frame of the vehicle. The left side motor mount was fractured on the engine side of the mount. The front grille disengaged from the vehicle and was located on the ground approximately 10 feet (3 m) downstream from the front of the final position of the vehicle. A 4-in. long x 1 $\frac{1}{4}$ -in. tall (102-mm x 32-mm) tear was found in the sheet metal at the midspan of the left-front door. A 9-in. long x 2 $\frac{1}{4}$ -in. wide by $\frac{1}{8}$ -in. deep (229-mm x 57-mm x 3-mm) gouge was found in the middle of the left-front door. The rear of the left-front door was ajar 2 in. (51 mm) and the top of the left-rear door was ajar 2 $\frac{3}{4}$ in. (70 mm). A 1-in. (25-mm) deep dent on the lower portion of the front of the left-rear door was 9 $\frac{1}{2}$ in. long x 8 in. tall (241 mm x 203 mm). A large buckle in the middle of the front of the left-rear door was 11 in. long x 3 $\frac{1}{4}$ in. wide (279 mm x 83 mm). Denting, scraping, and gouging were observed on the entire left side of the vehicle with the most significant being a 105-in. (2,667-mm) long gouge that began at the front of the left-front door and extended rearward to the left-rear wheel well. The left-rear wheel assembly had cracking and a 13 $\frac{3}{4}$ -in. long x 7 $\frac{1}{4}$ -in. tall (349-mm x 184-mm) buckle on the hubcap as well as scrape marks on the steel wheel. A gouge on the quarter panel began above the left-rear wheel and extended 52 $\frac{1}{2}$ in. (1,334 mm) to the rear

of the vehicle. A dent on the left-rear quarter panel above the fuel door measured 6½ in. long x 8½ in. tall x ⅛ in. deep (165 mm x 216 mm x 3 mm). The left taillight of the vehicle disengaged and there was scraping around the taillight housing. The left side of the rear bumper was scraped and had a 2-in. long x 2¼-in. wide (51-mm x 57-mm) kink. The tailgate disengaged from its hinges but remained attached to its support cables. Both airbags deployed.

In test no. NELON-2, an onboard GoPro camera view indicated significant deformation of the left side B-pillar due to impact with the knee formed at the joint between barrier nos. 6 and 7. Due to this deformation, attempts were made to measure and report the displacement of the B-pillar. B-pillar deformation measurements for test no. NELON-2 consisted of both physical measurements of the maximum B-pillar deformation and film analysis measurements utilizing the GoPro cameras mounted inside of the vehicle. The measurements were reviewed and only the physical measurements were deemed appropriate for the final report:

1. Three different film analysis attempts were made and all three yielded different data. There were concerns that the motion of the camera, the alignment of the camera, and lens correction issues influenced the results. As such, these were not deemed appropriate for reporting purposes.
2. The permanent set deformations taken by the field staff were measured at two locations on the B-pillar. These measurements were taken by measuring the distance from one side of the vehicle to the other on an undamaged Dodge Ram and then measuring the same distance on the test vehicle. The difference was the measured lateral permanent set deflection of the B-pillar. The values obtained are shown in Table 11.

Table 11. B-Pillar Deformation, Test No. NELON-2

B-Pillar Measurement Location in. (mm)	Undamaged Vehicle Measurement in. (mm)	NELON-2 Vehicle Measurement in. (mm)	Lateral Permanent Set B-Pillar Deformation in. (mm)
Lower B-Pillar, 6¼ (159) above floorpan	64⅞ (1,648)	61¼ (1,556)	3⅝ (92)
Mid B-Pillar, 16½ (419) above floorpan	64¾ (1,645)	60 (1,524)	4¾ (121)



Figure 83. B-Pillar Deformation, Test No. NELON-2

11.5 Occupant Risk

The calculated occupant impact velocities (OIVs) and maximum 0.010-sec average occupant ridedown accelerations (ORAs) in both the longitudinal and lateral directions are shown in Table 12. Note that the OIVs and ORAs were within suggested limits, as provided in MASH. The calculated THIV, PHD, and ASI values are also shown in Table 12. The results of the occupant risk analysis, as determined from the accelerometer data, are summarized in Figure 84. The recorded data from the accelerometers and the rate transducers are shown graphically in Appendix E.

Table 12. Summary of OIV, ORA, THIV, PHD, and ASI Values, Test No. NELON-2

Evaluation Criteria		Transducer		MASH Limits
		SLICE-1	SLICE-2 (Primary)	
OIV ft/s (m/s)	Longitudinal	-12.86 (-3.92)	-11.94 (-3.64)	±40 (12.2)
	Lateral	15.49 (4.72)	17.59 (5.36)	±40 (12.2)
ORA g's	Longitudinal	-5.73	-6.45	±20.49
	Lateral	13.48	11.02	±20.49
MAX. ANGULAR DISPL. deg.	Roll	-86.06	-82.28	±75
	Pitch	-20.30	-20.17	±75
	Yaw	49.78	48.29	not required
THIV ft/s (m/s)		18.7 (5.71)	21.5 (6.55)	not required
PHD g's		13.74	11.39	not required
ASI		1.01	1.11	not required

11.6 Discussion

The analysis of the test results for test no. NELON-2 showed that the end of LON for the reduced length, free-standing, F-shape PCB system adequately contained and redirected the 2270P vehicle with controlled lateral displacements of the barrier. There were no detached elements nor fragments which showed potential for penetrating the occupant compartment nor presented undue hazard to other traffic. Deformations of, or intrusions into, the occupant compartment that could have caused serious injury did not occur. However, the left-front door of the vehicle became unlatched and opened during the impact. The cause for the door latch release was not determined. Examination of the door latch did not reveal damage or fracture that would have caused the latch to disengage, but motion of the dummy limbs or the impact of the door into the barrier may have potentially activated the latch mechanism. While this behavior is not specifically outlined as violating the safety requirements in MASH, there was potential concern that the opening of the door exposed the vehicle occupant. The test vehicle did not penetrate nor ride over the barrier and remained upright during and after the collision. Vehicle pitch and yaw angular displacements, shown in Appendix E, were deemed acceptable because they did not adversely influence occupant risk, however, vehicle roll did exceed the occupant risk safety criteria of 75 degrees established in MASH. After impact, the vehicle exited the barrier at an angle of 10.4 degrees, and its trajectory did not violate the bounds of the exit box. Therefore, due to the excessive roll of the vehicle, test no. NELON-2 was determined to be unacceptable according to the MASH safety performance criteria for test designation no. 3-37.

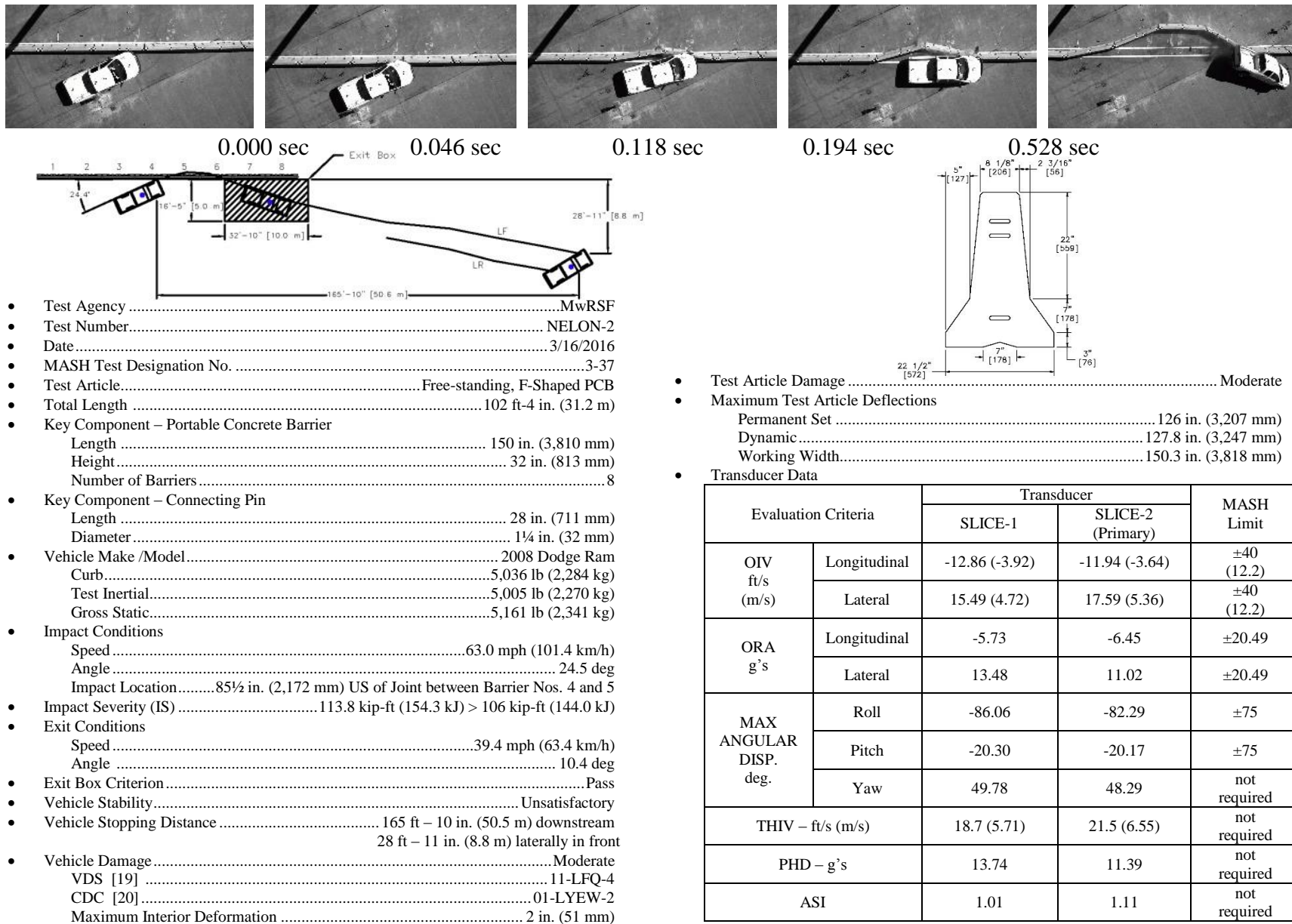


Figure 84. Summary of Test Results and Sequential Photographs, Test No. NELON-2



0.000 sec



0.046 sec



0.102 sec



0.282 sec



0.528 sec



0.858 sec



0.000 sec



0.052 sec



0.102 sec



0.194 sec



0.282 sec



0.724 sec

Figure 85. Additional Sequential Photographs, Test No. NELON-2



0.000 sec



0.046 sec



0.102 sec



0.194 sec



0.302 sec



0.438 sec



0.000 sec



0.046 sec



0.090 sec



0.194 sec



0.528 sec



1.726 sec

Figure 86. Additional Sequential Photographs, Test No. NELON-2



Figure 87. Documentary Photographs, Test No. NELON-



Figure 88. Documentary Photographs, Test No. NELON-2



Figure 89. Impact Location, Test No. NELON-2



Figure 90. Vehicle Final Position and Trajectory Marks, Test No. NELON-2



Figure 91. System Deflection and Damage, Test No. NELON-2



Figure 92. Barrier Nos. 1 through 3 Damage, Test No. NELON-2



Figure 93. Barrier No. 4 Damage, Test No. NELON-2



Figure 94. Barrier No. 5 Damage, Test No. NELON-2



Figure 95. Barrier No. 6 Damage, Test No. NELON-2



Figure 96. Barrier Nos. 7 and 8 Damage, Test No. NELON-2



Figure 97. Vehicle Damage, Test No. NELON-2



Figure 98. Vehicle Damage, Test No. NELON-2



Figure 99. Occupant Compartment Damage, Test No. NELON-2

12 DISCUSSION OF FULL-SCALE TEST RESULTS

The researchers reviewed the results of full-scale crash test nos. NELON-1 and NELON-2 to assess the performance of the reduced-length F-shape PCB system when impacted at the beginning and end of LON. In test no. NELON-1, the 2270P vehicle impacted the beginning of LON on the eight-barrier long F-shape PCB system and was safely redirected. This correlated well with the behavior predicted by the LS-DYNA simulation models, including the impact from the knee that formed at the joint between barrier nos. 5 and 6 into the side of the vehicle and the corresponding damage to the front and rear doors. The maximum dynamic barrier deflection for test no. NELON-1 was 128.3 in. (3,259 mm), which was a 35 percent increase over the dynamic deflection predicted by the LS-DYNA computer simulation prior to the test. The increase in barrier deflection was more than anticipated, but did not cause issues with respect to the safe redirection of the vehicle.

It was theorized that the increased deflection was likely due to a combination of factors. First, simplifications in the PCB model may have reduced barrier deflections. The PCB model uses non-deformable, rigid elements for the PCB body and the connection loop rebar. The rigid element body of the barrier does not allow for fracture of the barrier toes or other barrier damage that would allow increased joint rotations and increased barrier motions. The inability to fracture the barrier toes may have had a significant effect as the loss of the barrier toes allows the barriers to deflect more prior to the corners of the barriers locking up and transmitting tension to adjacent barrier segments. This could have significantly increased the deflections, as observed in the full-scale testing. Similarly, the use of rigid connection loops may make the PCB connection stiffer and further reduce deflections. Differences between the simulated and actual vehicles used in the analysis may have also contributed to the difference in deflection.

Test no. NELON-2 initially performed similarly to test no. NELON-1 as the vehicle was captured and redirected. Peak lateral barrier deflections were similar to NELON-1 and were again larger than those predicted by the LS-DYNA simulation. However, test no. NELON-2 was deemed unacceptable according to the MASH safety requirements due to vehicle roll that exceeded 75 degrees after it exited the barrier system. Review of the test suggested potential factors that may have contributed to the vehicle rollover. First, the increased barrier deflections observed in test no. NELON-2 due to reduced system length and impact at the downstream LON point may have adversely affected the vehicle trajectory. Comparison of the barrier deflections and vehicle trajectories from test nos. NELON-1, NELON-2, and 2214TB-2 are shown in Figures 100 through 103. Review of these three tests showed that the reduced length system tests displayed higher deflections of barrier segments near the impact of the vehicle and less gradual deflection of adjacent barrier segments as compared to the full-length PCB system. These differences were likely due to both the reduced upstream and downstream tensile forces developed by shorter systems, as evidenced by the increased longitudinal displacement of the ends of the system, and increased barrier damage, as noted previously. The increased deflection of the reduced length systems clearly affected vehicle trajectory. Test nos. NELON-1 and NELON-2 exhibited higher exit angles of 12.3 degrees and 10.4 degrees, respectively, as compared to 7.9 degrees for test no. 2214TB-2. Similarly, comparison of vehicle roll angles during the first 0.500 sec of the vehicle redirection exhibited significantly higher roll for the reduced length systems, as shown in Figure 104. Thus, it was believed that the effect of reduced system length on the PCB deflections contributed to vehicle instability.

A second factor that potentially contributed to the vehicle instability observed in test no. NELON-2 was the impact from a knee formed at the joint between barrier segment nos. 6 and 7. The knee extended forward laterally from the original barrier line and impacted the left-front door of the 2270P vehicle at approximately 0.390 sec after initial impact. The impact of the knee into the door may have further increased vehicle instability.

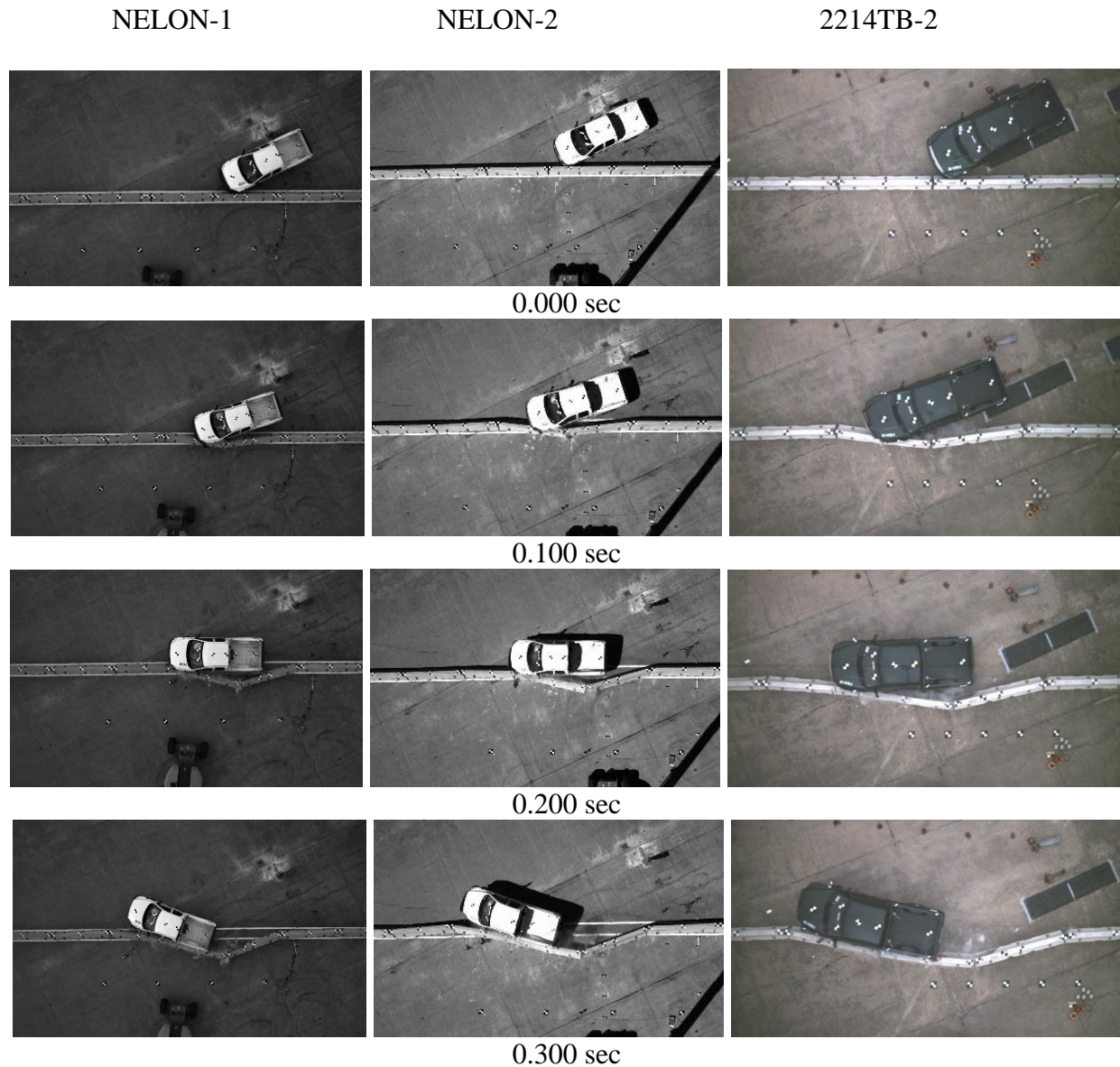


Figure 100. PCB System Comparison, Overhead View

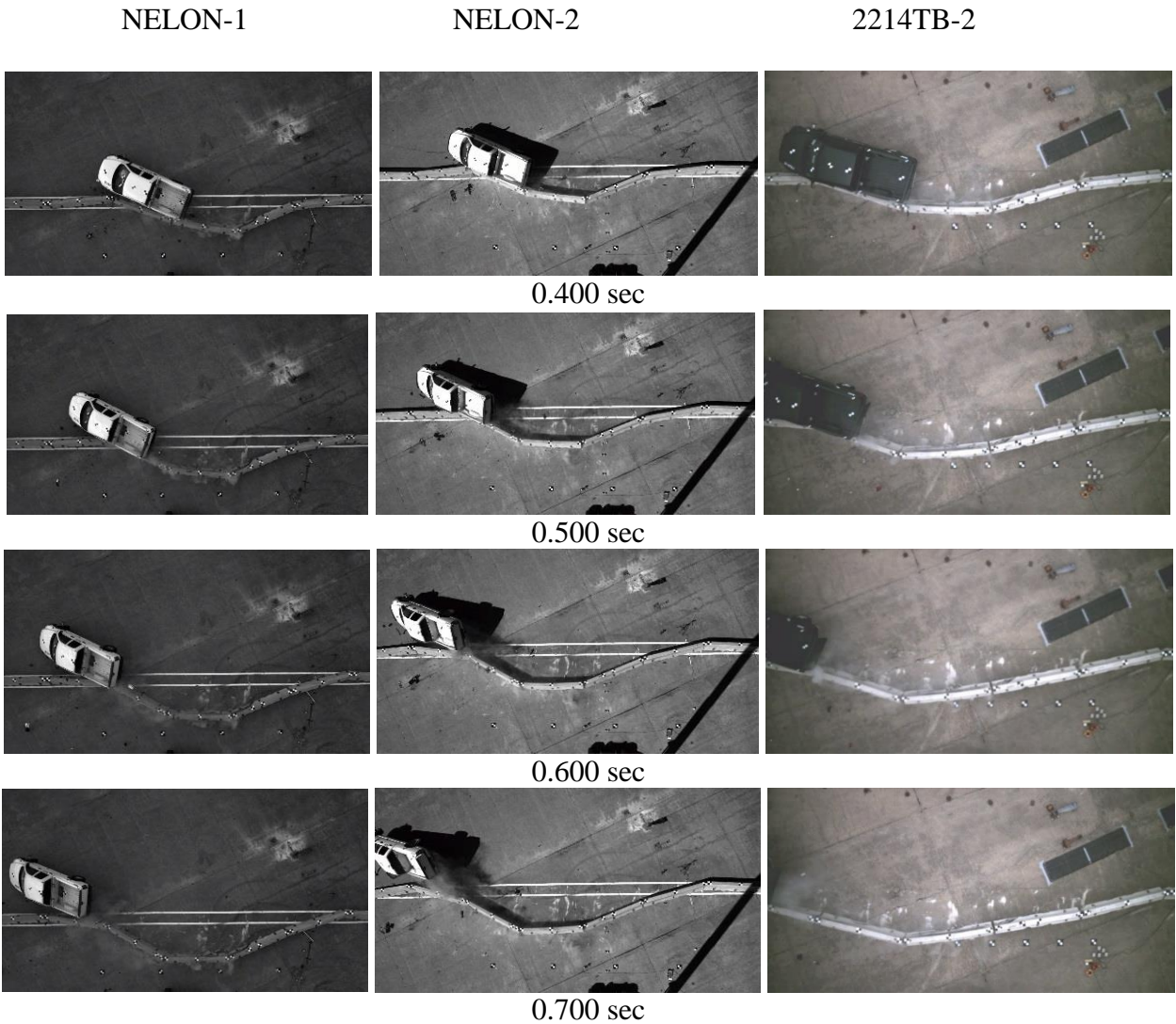


Figure 101. PCB System Comparison, Overhead View

NELON-1

NELON-2

2214TB-2



0.000 sec



0.100 sec



0.200 sec



0.300 sec

Figure 102. PCB System Comparison, Downstream View

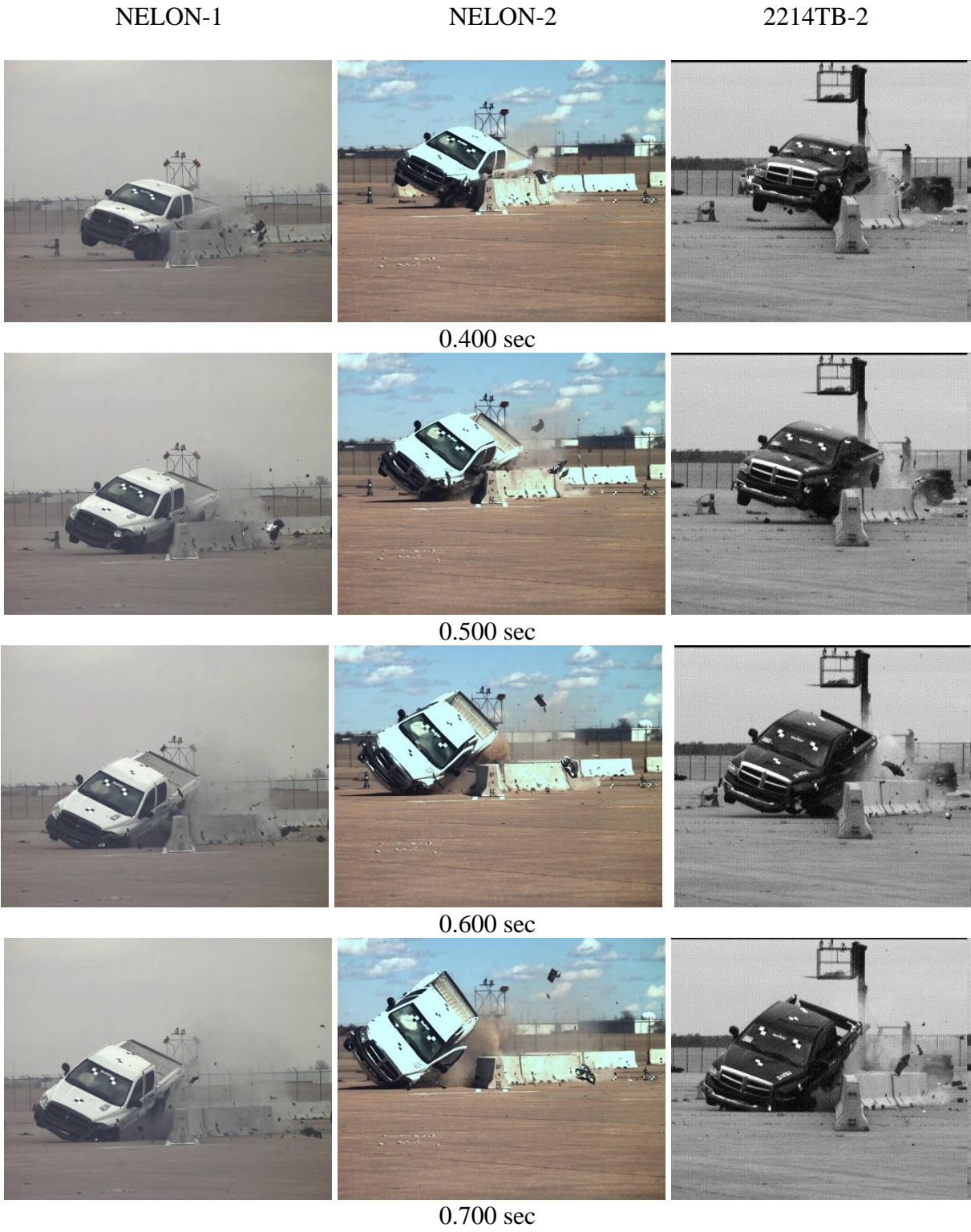


Figure 103. PCB System Comparison, Downstream View

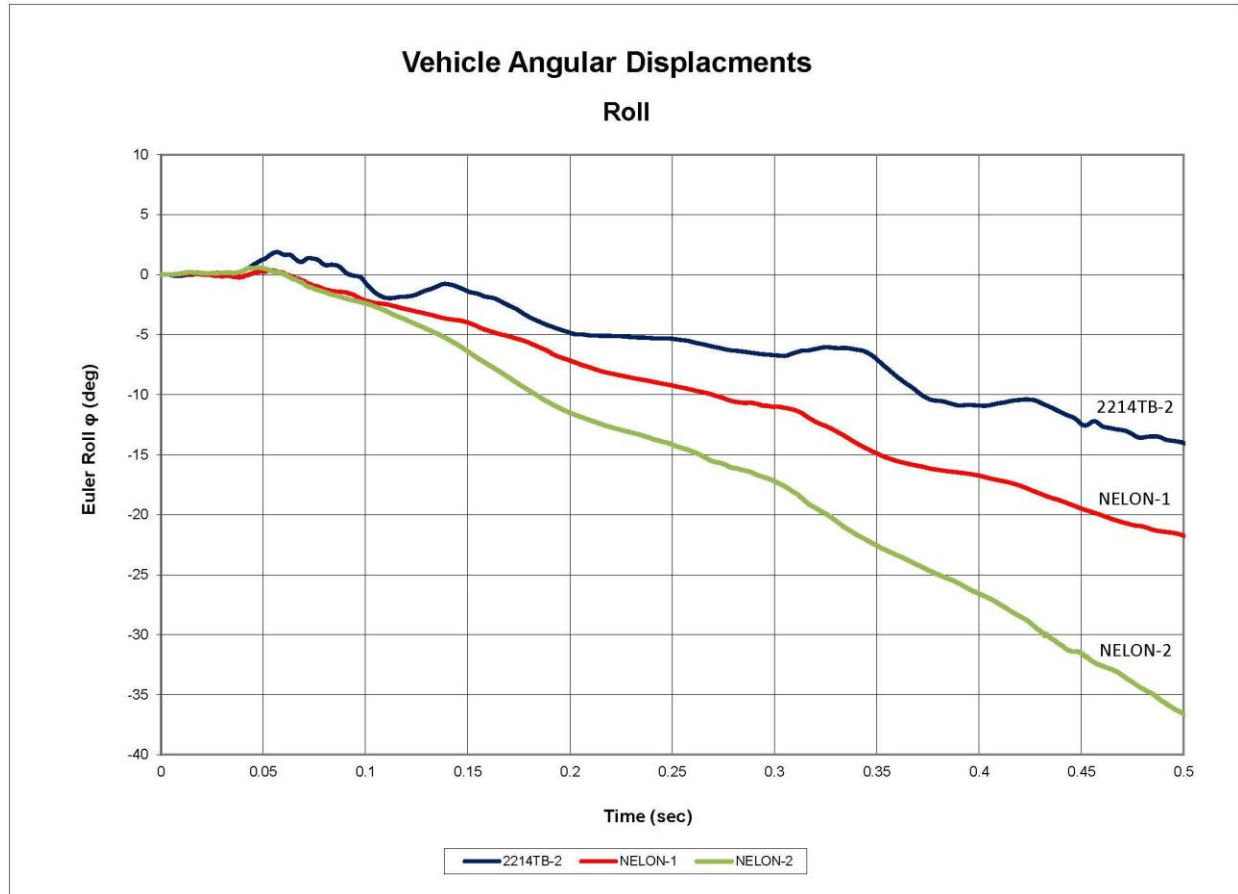


Figure 104. Vehicle Roll Angle Comparison for PCB Testing

While the results from test nos. NELON-1 and NELON-2 found that an eight-barrier long PCB system was not adequate to safely redirect vehicles under MASH TL-3 criteria, it was believed that a nine-barrier long system would be sufficient for safe barrier performance. A nine barrier system would be comprised of three PCB segments before the beginning of LON, one a barrier segment for a finite redirective length, and five barrier segments following the end of the LON, as shown in Figure 105. Test no. NELON-1 demonstrated that three barrier segments prior to the beginning of LON was sufficient for an eight-barrier long PCB system. The addition of a fifth barrier segment to the downstream end of the system provides the same number of downstream barriers for an impact at the end of LON as were utilized in NELON-1. An impact on the end of length of need for a nine-barrier long system would be expected to perform similarly to test no. NELON-1. Thus, it is recommended that the minimum system length for the free-standing, F-shape PCB system be set at nine barrier segments.

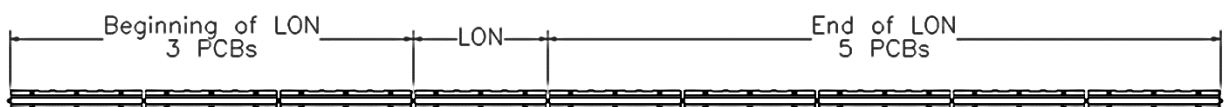


Figure 105. Nine Barrier Segment Reduced Length PCB System

13 ANALYSIS OF BARRIER DEFLECTIONS

A final component of the research study was an investigation of the PCB system's lateral deflections when used with intermediate system lengths. With the potential for system lengths less than the standard sixteen-barrier long PCB system, it was desired to estimate potential barrier deflections for systems between nine and sixteen barriers long at the midspan and beginning and end of LON for the system.

13.1 Simulation Calibration with Full-Scale Crash Test

Although additional crash tests could be conducted to determine the deflection of the reduced length PCB systems, the cost would be extremely high. Instead, LS-DYNA computer simulation of the reduced length systems was used to estimate the deflection of the barrier segments. LS-DYNA was used to model the behavior of the barrier system when subjected to full-scale crash testing. After the model was calibrated to accurately predict barrier deflections for the high-energy crash test conditions, the impact conditions were revised and the barrier deflections were estimated for the lower energy crash.

In order to calibrate the simulation model of the reduced length PCB system, a simulation model of test no. NELON-1 was created and simulated under the test impact conditions. Initial simulations of test no. NELON-1 demonstrated significantly lower deflections than the full-scale test. The discrepancy between the physical test and the model was largely attributed to the concrete damage and fracture observed in the test which was not reproduced in the rigid PCB model.

The researchers discussed applying a LS-DYNA concrete material model in order to capture the concrete damage seen in the physical test. However, this was rejected because of the researchers' limited confidence in the ability of the concrete material model to capture the damage in the full-scale test and a lack of previous experience applying the material model to the simulation of PCB segments. As such, a significant amount of additional component level simulation and modeling would have been required to accurately model a PCB segment using the concrete material model. Additionally, the concrete damage that contributed to the deflections in test no. NELON-1 was distributed through several barrier segments. Thus, capturing the damage would require modeling of fully-reinforced PCB segments with the concrete material model at a fine enough mesh size to capture the barrier segment damage. It was believed that this would be very computationally expensive. Based on these considerations the PCB system deflection was modeled without the concrete material model.

As a compromise, the simulation model of test no. NELON-1 was modified to reduce the barrier to ground friction level until the simulation model reproduced the dynamic barrier deflections observed in the full-scale test. While this was not the optimal solution, it provided a conservative baseline with which to create simulations using the reduced impact conditions. It was believed that the reduction in barrier friction would produce conservative estimates of the deflection of the barrier system. The concrete damage in the simulation model, for which the reduced friction was acting as a surrogate, would not be as large of a factor for impacts involving larger system lengths, as those systems tend to display less barrier damage. Thus, the reduction in friction would likely generate larger estimated deflections than explicit modeling of concrete damage and provide a conservative result.

A simulation model of the reduced deflection PCB system tested in test no. NELON-1 was simulated using a reduced barrier-to-ground friction coefficient of 0.27. The results from this model estimated a dynamic lateral barrier deflection of 126.9 in. (3,223 mm). This value correlated well with the 128.3 in. (3,259 mm) dynamic lateral barrier deflection from test no. NELON-1. Comparison of sequential images from the simulation and crash test also demonstrated good correlation, as shown in Figures 106 through 109. Thus, the model with a reduced friction coefficient was used to simulate deflections for the intermediate system lengths.

NELON-1

LS-DYNA Simulation

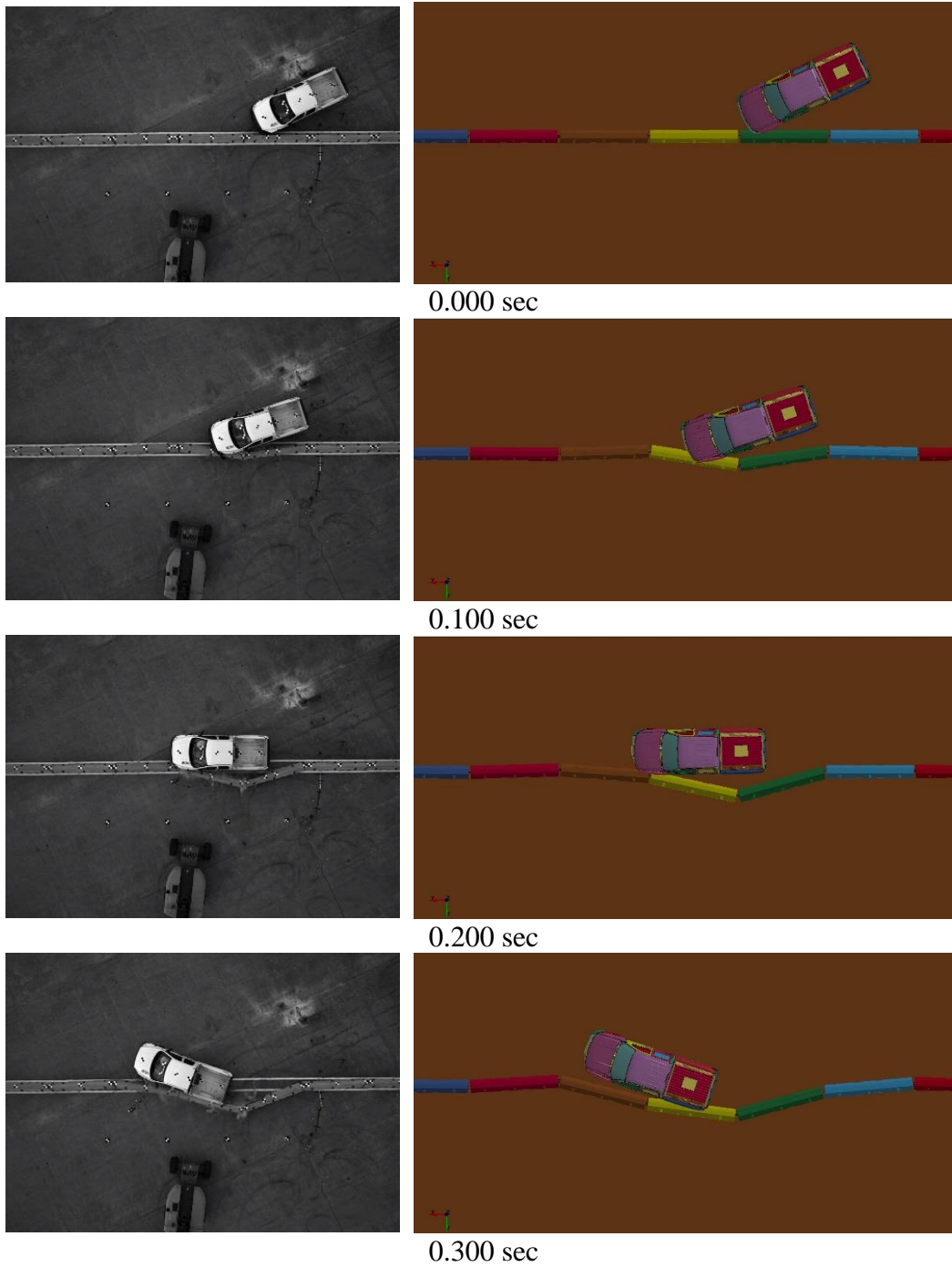


Figure 106. Test No. NELON-1 vs. LS-DYNA Simulation, Overhead View

NELON-1

LS-DYNA Simulation

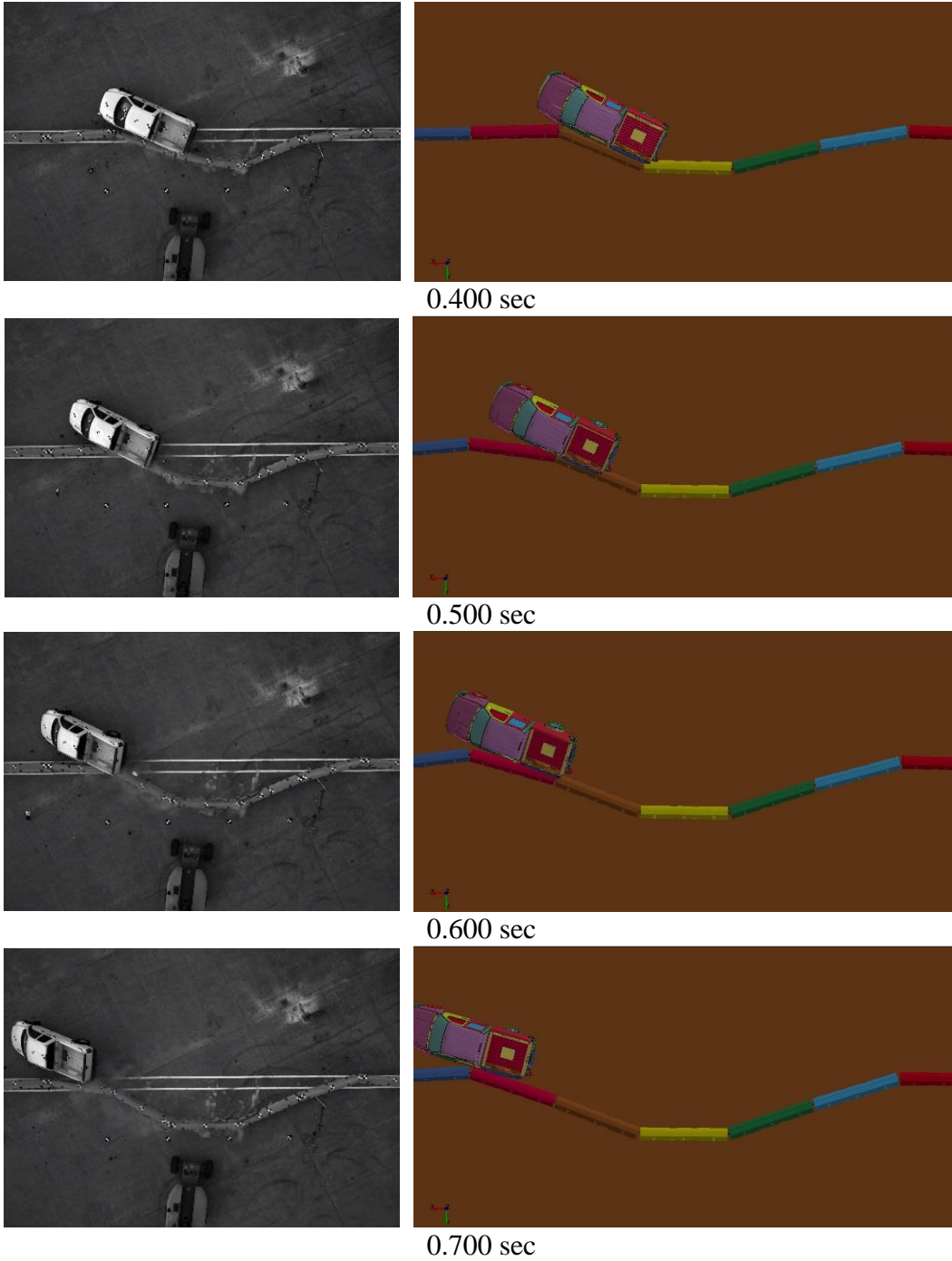


Figure 107. Test No. NELON-1 vs. LS-DYNA Simulation, Overhead View

NELON-1

LS-DYNA Simulation



0.000 sec



0.100 sec



0.200 sec



0.300 sec

Figure 108. Test No. NELON-1 vs. LS-DYNA Simulation, Downstream View

NELON-1

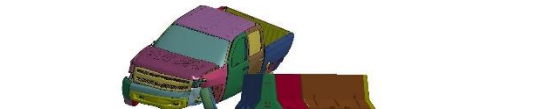
LS-DYNA Simulation



0.400 sec



0.500 sec



0.600 sec



0.700 sec

Figure 109. Test No. NELON-1 vs. LS-DYNA Simulation, Downstream View

13.2 TL-3 PCB Deflections for Intermediate System Lengths

In order to estimate the lateral barrier deflections for intermediate system lengths, a series of simulations were conducted on the F-shape PCB system with varying lengths at the beginning of LON, the midspan of the system, and the end of LON. System lengths of 9, 10, 12, 14, and 16 barriers were simulated. Note that no midspan simulation was conducted for the nine-barrier long system as this location would have been outside of the LON of the barrier. As noted previously, a reduced barrier-to-ground friction coefficient of 0.27 was used for the simulations to better correlate with the full-scale testing conducted near the ends of the system. While simulating the barriers with the reduced friction value may overestimate barrier deflections, it was believed that a conservative approach was warranted when estimating potential system deflections. The simulation model of the midspan impact on the sixteen barrier F-shape PCB system used the original barrier-to-ground friction coefficient of 0.40, as this model had previously been validated against test no. 2214TB-2. All simulations were conducted using the MASH TL-3 impact conditions of 62 mph (100 km/h) and an angle of 25 degrees with the 2270P vehicle model.

The lateral barrier deflection results from the simulations of intermediate systems lengths are shown in Figure 110. Lateral barrier deflections were plotted versus the number of barriers in the system for the beginning of LON, end of LON, and midspan impacts. The beginning of LON impacts demonstrated the highest lateral deflections as the impact was closer to the end of the system than the other conditions. The lateral barrier deflection values for the beginning of LON impacts ranged from 125.5 in. (3,188 mm) to 131.6 in. (3,343 mm) and tended to increase slightly as the number of barriers in the system increased. The lateral deflections did not vary significantly due to the proximity of the impact to the free end of the system having a greater effect than the length of the system. Similarly, barrier deflections did not decrease as system length increased, as would typically be expected, because the increased system length provided more anchorage at the downstream end of the system and created increased loading and deflection of the upstream end of the barriers.

Lateral barrier deflections for impacts at the end of LON displayed similar behavior. The lateral barrier deflection values for the end of LON impacts ranged from 111.7 in. (2,837 mm) to 121.9 in. (3,096 mm) and tended to increase slightly as the number of barriers in the system increased. Deflection magnitude decreased as compared to the beginning of LON impacts due to the impact being two barrier segments farther from the free end of the system. However, a similar trend toward an increase in barrier deflections with increased barrier system length was noted.

Finally, midspan impacts on intermediate length F-shape PCB systems demonstrated the lowest lateral barrier deflections. The lateral barrier deflection values for the midspan impacts ranged from 114.6 in. (2,911 mm) for a 10-barrier long system to 81.1 in. (2,060 mm) for a 16-barrier long system. For the midspan impacts, lateral barrier deflection tended to decrease as system length increased.

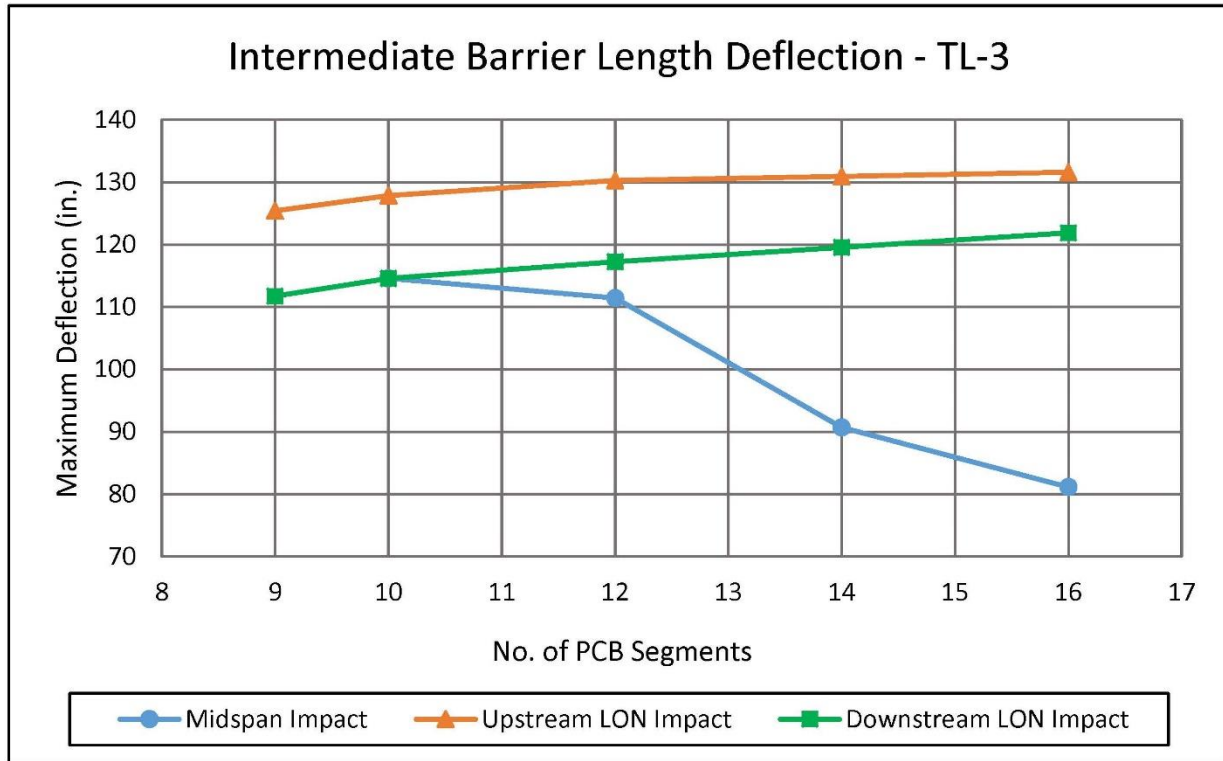


Figure 110. Lateral Barrier Deflections for Intermediate PCB System Lengths, MASH TL-3

13.3 85th Percentile Impact Severity PCB Deflections for Intermediate System Lengths

Previous research at MwRSF investigated PCB deflection limits for less critical PCB installations [21]. This research argued that when temporary concrete barriers are used on the edge of a bridge, the risk of the entire line of barriers falling off the deck requires that deflection limits be selected to preclude such behavior in almost all impact scenarios. Hence, it was recommended that at the edge of a bridge deck, design deflection limits should be selected to contain more than 95 percent of all crashes. In all other barrier applications, the consequences of a barrier exceeding the design deflection criteria are not severe. In these situations, a more modest deflection limit criterion based on an 85th percentile impact severity was deemed more appropriate. The sponsor of this research effort requested that a similar analysis be performed on the low-deflection PCB system developed herein in order to provide deflection limits for less critical installations.

A number of research studies have shown that the impact severity (IS), as defined below, is a good indicator of the degree of loading and the lateral deflections of longitudinal barriers [22-24].

$$\frac{1}{2} m(v \sin \theta)^2$$

where:

m = mass of impacting vehicle
v = velocity of impacting vehicle
θ = angle of impact.

IS incorporates the effect of the mass of the impacting vehicle to provide a good measure of the severity of impact and the magnitude of the resulting barrier deflections. In order to determine appropriate IS values for this study, data was taken from the results of the NCHRP 22-17 project [25]. NCHRP 22-17 was used to generate the impact conditions for MASH and represented the most applicable data set to draw from. While the NCHRP 22-17 data was biased toward severe and fatal crashes, it was believed that the dataset would provide a conservative basis for the analysis that correlated with the impact conditions specified in MASH.

Figure 111 shows the IS distribution for freeways from NCHRP 22-17. As shown in Figure 111, the 95th percentile IS value was 127.6 kip-ft (173.0 kJ). It was reasonable to utilize the deflections measured during full-scale crash testing no. 2214TB-2 when selecting barrier deflection limits for use near the edge of a bridge deck or drop-off or other critical installations. However, the 85th percentile IS value, which is more appropriate for all other applications of temporary concrete barriers, was 78.3 kip-ft (106.2 kJ). An IS value of 78.3 kip-ft (106.2 kJ) would correspond to an impact velocity of 51.2 mph (82.4 km/h) for a 5,000-lb (2,268-kg) pickup truck impacting the barrier at an angle of 25 degrees. Barrier deflections under this impact condition would be less than those observed under the MASH TL-3 criteria.

Thus, a second series of computer simulations were conducted on the F-shape PCB system to estimate lateral dynamic barrier deflections for the 85th percentile IS value. Simulations were conducted on the F-shape PCB system with 9, 10, 12, 14, and 16 barriers and at the beginning of LON, the midspan of the system, and the end of LON. Note that no midspan simulation was conducted for the nine-barrier long system as this location would have been outside of the LON of the barrier. As noted previously, a reduced barrier-to-ground friction coefficient of 0.27 was used for the simulations to better correlate with the full-scale testing conducted near the ends of the system. The simulation model of the midspan impact on the sixteen barrier F-shape PCB system used the original barrier-to-ground friction coefficient of 0.40, as this model had previously been validated against test no. 2214TB-2. All simulations were conducted using the 85th percentile IS impact conditions of 51.2 mph (82.4 km/h) and an angle of 25 degrees with the 2270P vehicle model.

The lateral barrier deflections from the simulations of intermediate systems lengths using 85th percentile IS impact conditions are shown in Figure 112. Lateral barrier deflections were plotted versus the number of barriers in the system for the beginning of LON, end of LON, and midspan impacts. The beginning of LON impacts demonstrated the highest lateral deflections as the impact was closer to the end of the system than the other conditions. The lateral barrier deflection values for the beginning of LON impacts ranged from 86.9 in. (2,207 mm) to 96.8 in. (2,459 mm) and tended to increase slightly as the number of barriers in the system increased. The lateral deflections did not vary significantly due to the proximity of the impact to the free end of the system having a greater effect than the system length. Similarly, barrier deflections did not decrease as system length increased, as would typically be expected, because the increased system length provides more anchorage of the downstream end of the system and created increased loading and deflection of the upstream end of the barriers.

Distribution of IS Values at Road Departure

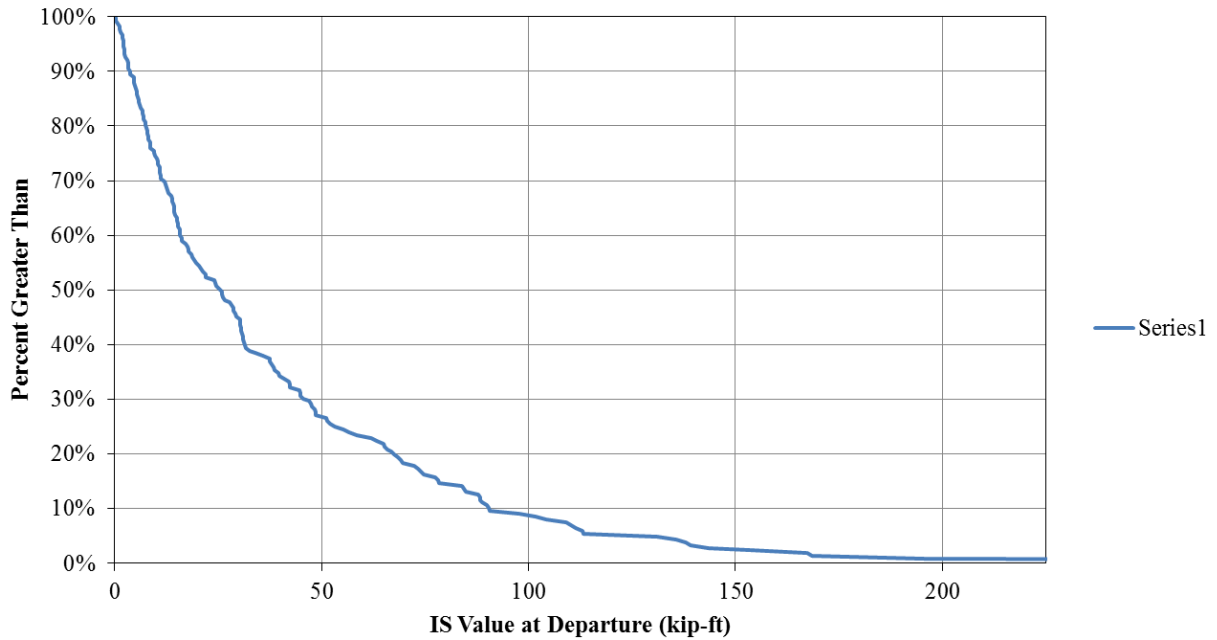


Figure 111. NCHRP 22-17 IS Distribution for Freeways

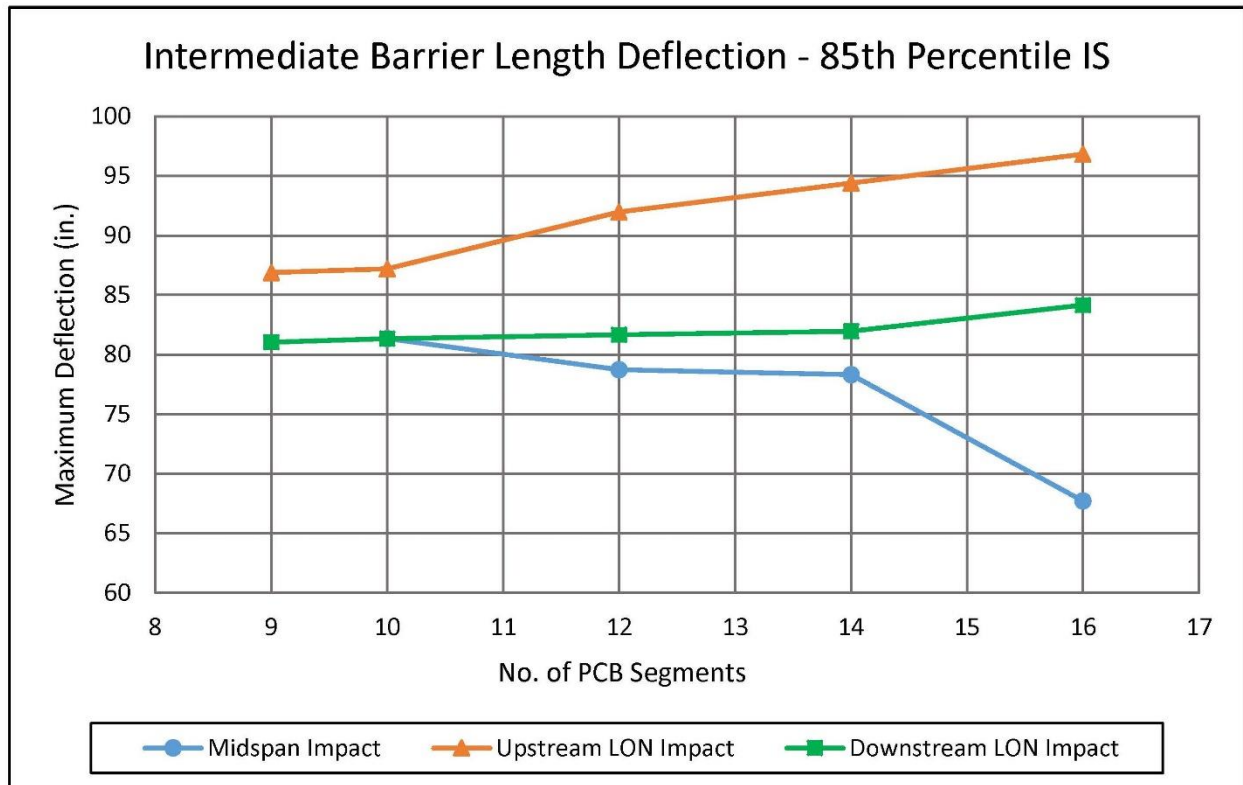


Figure 112. Lateral Barrier Deflections for Intermediate PCB System Lengths, 85th Percentile IS

Lateral barrier deflections for impacts at the end of LON displayed similar behavior. The lateral barrier deflection values for the end of LON impacts ranged from 81.0 in. (2,057 mm) to 84.2 in. (2,139 mm) and tended to increase slightly as the number of barriers in the system increased. The deflection magnitude decreased as compared to the beginning of LON impacts due to the impact being two barrier segments farther from the free end of the system. However, a similar trend toward an increase in barrier deflections with increased barrier system length was noted.

Finally, midspan impacts on intermediate length F-shape PCB systems demonstrated the lowest lateral barrier deflections, which ranged from 81.3 in. (2,065 mm) for a 10-barrier long system to 67.7 in. (1,720 mm) for a 16-barrier long system. For the midspan impacts, lateral barrier deflection tended to decrease as system length increased.

13.4 Discussion

Determination of guidance for lateral barrier deflections for varying system lengths under TL-3 and 85th percentile IS impact conditions was dependent on several factors:

1. The estimated lateral barrier deflections taken from the simulation models
2. The MASH TL-3 full-scale crash test deflections of the F-shape PCB
3. The effect of the location along the length of the barrier

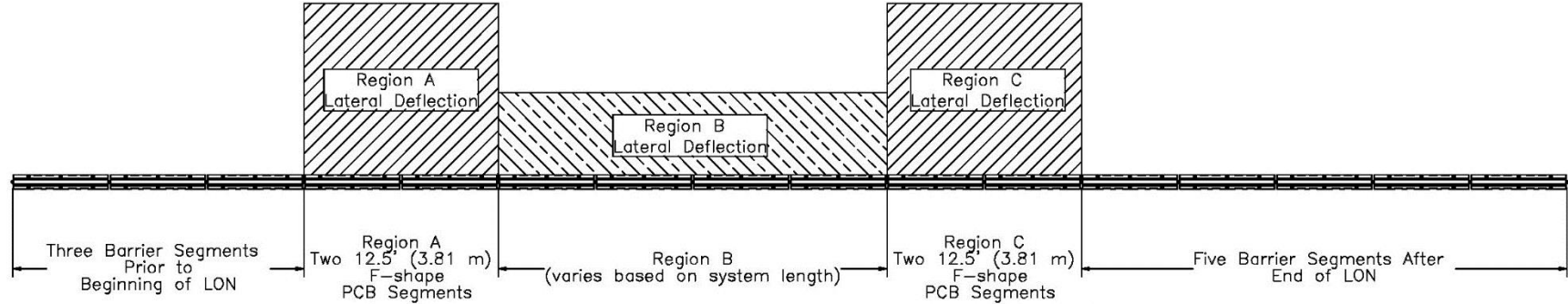
The estimated lateral barrier deflections observed in the simulation models of intermediate system lengths were discussed in detail in the previous sections. The available full-scale crash test data consisted primarily of test no. 2214TB-2. In this test, a 2270P vehicle impacted the F-shape PCB used in this study and exhibited a dynamic deflection of 79.6 in. (2,021 mm) when impacting near the middle of a 16-barrier test system with an overall length of 200 ft (61 m). Test nos. NELON-1 and NELON-2 were not directly considered for the deflection guidance as they were conducted on eight-barrier long systems, which was below the recommended minimum system length. However, it was noted that the lateral barrier deflections for test nos. NELON-1 and NELON-2 of 128.3 in. (3,259 mm) and 127.8 in. (3,247 mm), respectively, were significantly higher than the values for an impact near the midspan of a longer system.

The third factor that was taken into consideration was the impact location along the barrier length. The initial simulations used to locate potential beginning and end of LON locations on a barrier system with sixteen F-shape PCBs indicated that lateral and longitudinal barrier deflections increased for impacts along several barrier segments adjacent to the beginning and end of LON locations. Thus, similar behavior would be expected for barrier systems with varying lengths. Review of the simulations for the beginning of LON showed that the combination of lateral and longitudinal barrier deflections began to increase significantly when the barrier was impacted upstream of barrier segment no. 5 or two barrier segments downstream of the beginning of LON. This would suggest that barrier deflections in the region between the beginning of LON and two barriers downstream of the beginning of LON would be similar and greater than impacts closer to the midspan of the system. Similarly, review of simulated impacts near the end of LON found that the combination of lateral and longitudinal barrier deflections appeared to increase more significantly downstream of barrier segment no. 10 or two barrier segments upstream of the end of LON.

In order to provide guidance for deflections for varying PCB system lengths, it was proposed to divide the barrier system into three separate deflection regions, as shown in Figures 113 and 114. Region A was defined as the beginning of LON following the end of the third barrier in the system to two barriers downstream of the beginning of LON. Region C was defined as the end of LON to two barriers upstream of the end of LON. Regions A and C were expected to have increased barrier deflections associated with their proximity to the beginning and end of LON. Region B was defined as a region comprised of the remaining middle section of the barrier system that would have deflections that corresponded with impacts at the midspan of the PCB system length.

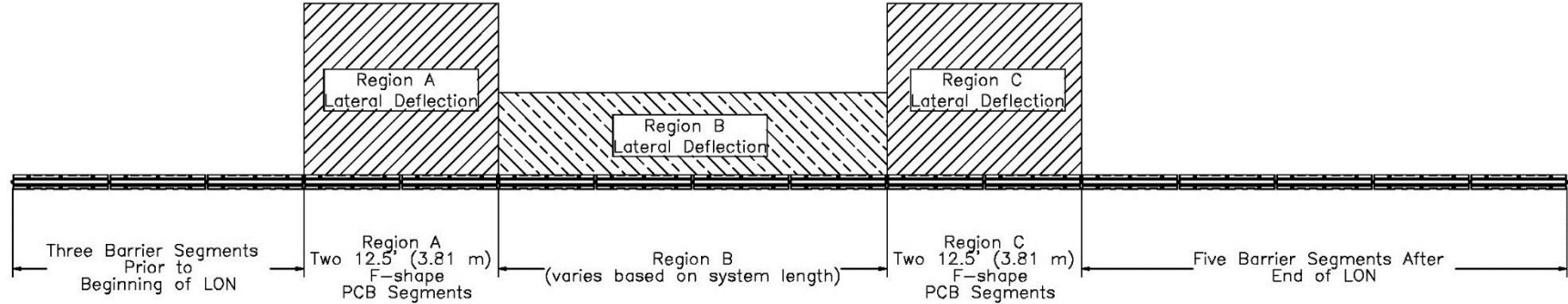
Deflection guidance for each region based on PCB system length is provided in Figures 113 and 114. Figure 113 displays the barrier deflection guidance for MASH TL-3 impact conditions and Figure 114 displays the barrier deflection guidance for the 85th percentile IS impact condition. For simplicity and ease of implementation, the lateral barrier deflections in regions A and C were assumed to be the same. The magnitude of the lateral deflection was selected in a conservative manner due to the use of computer simulation to determine the values. Thus, the deflection for regions A and C were selected as the maximum lateral deflection predicted by the simulations over the range of system lengths for both the beginning or end of the LON point. The deflection of region B was based on the simulated lateral deflections for a midspan impact on the various system lengths. Note that for system lengths of 12 barriers or less, region B does not exist and the deflection values for regions A and C are used throughout the LON. System lengths greater than or equal to 16 barrier segments are assumed to have similar lateral deflections in all regions. Also, deflection guidance was not provided for the areas outside of the beginning and end of the LON point as the performance of the PCB system in these areas is unknown.

It is recommended that installations in non-critical locations use the estimated lateral deflection values for the 85th percentile IS impact provided in Figure 114 until further full-scale crash testing at reduced IS values or in-service evaluation of system damage for lower severity impacts indicate that lower deflection estimates are more appropriate. For critical installations adjacent to drop-offs or bridge deck edges, the MASH TL-3 system deflections provided in Figure 113 should be applied.



PCB System Length (No. of Barrier Segments)	MASH TL-3 Estimated Lateral Barrier Deflection in. (mm)		
	Region A	Region B	Region C
9	132 (3,353)	-	132 (3,353)
10	132 (3,353)	-	132 (3,353)
12	132 (3,353)	-	132 (3,353)
14	132 (3,353)	91 (2,311)	132 (3,353)
≥ 16	132 (3,353)	80 (2,032)	132 (3,353)

Figure 113. F-Shape PCB Lateral Deflection Guidance, MASH TL-3



PCB System Length (No. of Barrier Segments)	85 th Percentile IS Estimated Lateral Barrier Deflection in. (mm)		
	Region A	Region B	Region C
9	97 (2,464)	-	97 (2,464)
10	97 (2,464)	-	97 (2,464)
12	97 (2,464)	-	97 (2,464)
14	97 (2,464)	78 (1,981)	97 (2,464)
≥ 16	97 (2,464)	68 (1,727)	97 (2,464)

Figure 114. F-Shape PCB Lateral Deflection Guidance, 85th Percentile IS

14 SUMMARY, CONCLUSIONS, AND RECOMMENDATIONS

This study consisted of analysis, full-scale crash testing, and evaluation of the LON for a minimum length, free-standing, F-shaped PCB system. LS-DYNA computer simulation was the primary tool used to analyze the PCB system. A baseline model of the F-shape PCB system was developed and verified, and impacts along the entire length of the PCB system were simulated to determine potential beginning and end of LON points for the barrier at its standard length. The simulation results found that three barriers on the upstream end of the system were sufficient to define beginning of LON and three barriers on the downstream end of the system were sufficient to define end of LON.

A second series of LS-DYNA simulations were conducted on reduced length PCB systems to evaluate if the selected beginning and end of LON points remained viable for shorter systems. Simulation of a seven barrier segment PCB system suggested that vehicle redirection with the reduced length was possible, but concerns about the impacts at the end of LON of the system arose due to rotation of the final barrier segment into the doors of the impacting vehicle. Simulation of an eight-barrier long F-shape PCB system with one additional barrier segment added downstream of the end of LON mitigated the rotation of the end of the PCB segment into the side of the vehicle, but impact of a knee between two barrier segments on the door was noted.

In order to further evaluate the selected beginning and end of LON and the reduced system length, full-scale crash testing was performed on an eight-barrier long F-shape system. Two full scale crash tests were performed according to the TL-3 safety performance criteria defined in MASH, test designation no. 3-35 and a modified version of test designation no. 3-37. Test no. NELON-1 evaluated the effectiveness of the beginning of LON for a system with a minimal length and test no. NELON-2 assessed the end of LON for a system with a minimal length.

Test no. NELON-1 consisted of a 4,991-lb (2,264-kg) pickup truck impacting the PCB at a speed of 62.1 mph (100.0 km/h) and at an angle of 24.8 degrees, resulting in an impact severity of 113.6 kip-ft (154.0 kJ). The vehicle was successfully contained and smoothly redirected with moderate damage to the barrier and the vehicle. All vehicle decelerations fell within the recommended safety limits established in MASH. Thus, test no. NELON-1 passed the safety criteria of MASH test designation no. 3-35.

Test no. NELON-2 consisted of a 5,005-lb (2,270-kg) pickup truck impacting the PCB at a speed of 63.0 mph (101.4 km/h) and at an angle of 24.5 degrees, resulting in an impact severity of 113.8 kip-ft (154.3 kJ). The vehicle was successfully contained and redirected with moderate damage to the barrier and the vehicle. All vehicle decelerations fell within the recommended safety limits, however, the vehicle's maximum roll exceeded the 75 degree limit established in MASH. Thus, test no. NELON-2 did not pass the safety requirements for MASH test designation no. 3-37. A summary of the safety performance evaluation for both tests is provided in Table 13, and a comparison of test results is provided in Table 14.

Review of the results from both crash tests suggested that reduced length and impacts near the beginning and end of LON of the PCB system affected the performance of the barrier. Barrier deflections increased significantly and the vehicle stability was reduced. However, the successful result from test no. NELON-1 led to the recommendation that a nine-barrier long PCB system could meet the MASH TL-3 safety requirements. Thus, a minimum system length of nine barriers

was recommended with three barriers upstream of the beginning of LON and five barriers downstream of the end of LON. It should be noted that the recommended minimum length of nine barriers would pertain to a roadside PCB installation with potential impacts restricted to oncoming traffic. If the PCB installation is adjacent to narrow, opposing two lane traffic or was a median installation where the potential for impacts in opposing directions on the PCB system exist, a minimum of five barriers is required on each end of LON of the system to account for impacts in both directions of travel. This would set the minimum system length at eleven barriers for these types of installations.

The final task undertaken in this research was evaluation of the estimated lateral displacements of the reduced length F-shape PCB system under both MASH TL-3 and 85th percentile IS impact conditions. Previous research at MwRSF suggested that it was feasible to use deflection limits for PCB systems in non-critical areas based on the estimated deflection of the PCB system when impacted at the 85th percentile IS value, as determined from accident data. Computer simulation analysis was performed on the F-shape PCB with lengths ranging from 9 to 16 PCBs and estimated lateral barrier deflections were provided for the barrier system for both MASH TL-3 and the 85th percentile IS based on PCB system length. The recommended lateral barrier deflections varied relative to the location of the impact along the LON of the barrier system. The MASH TL-3 barrier deflection guidance was recommended for critical PCB installations, while the 85th percentile IS barrier deflection guidance was recommended for general PCB use in non-critical areas.

Determination of the beginning and end of LON and minimum system length for the F-shape PCB required to meet MASH TL-3 provides users with the option to use shorter PCB installations than have been previously recommended. Shorter length PCB systems have installation advantages in terms of flexibility and the reduction of the number of impacts. Additionally, longer installations can define the beginning and end of LON using three and five barrier segments, respectively, rather than the eight barriers previously recommended.

Table 13. Summary of Safety Performance Evaluation Results, Test Nos. NELON-1 and NELON-2

Evaluation Factors	Evaluation Criteria	Test No. NELON-1	Test No. NELON-2		
Structural Adequacy	A. Test article should contain and redirect the vehicle or bring the vehicle to a controlled stop; the vehicle should not penetrate, underide, or override the installation although controlled lateral deflection of the test article is acceptable.	S	S		
Occupant Risk	D. Detached elements, fragments or other debris from the test article should not penetrate or show potential for penetrating the occupant compartment, or present an undue hazard to other traffic, pedestrians, or personnel in a work zone. Deformations of, or intrusions into, the occupant compartment should not exceed limits set forth in Section 5.3 and Appendix E of MASH.	S	S		
	F. The vehicle should remain upright during and after collision. The maximum roll and pitch angles are not to exceed 75 degrees.	S	U		
	H. Occupant Impact Velocity (OIV) (see Appendix A, Section A5.3 of MASH for calculation procedure) should satisfy the following limits:	S	S		
	Occupant Impact Velocity Limits				
	Component			Preferred	Maximum
	Longitudinal and Lateral			30 ft/s (9.1 m/s)	40 ft/s (12.2 m/s)
	I. The Occupant Ridedown Acceleration (ORA) (see Appendix A, Section A5.3 of MASH for calculation procedure) should satisfy the following limits:	S	S		
Occupant Ridedown Acceleration Limits					
Component	Preferred			Maximum	
Longitudinal and Lateral	15.0 g's			20.49 g's	
MASH Test Designation		3-35	3-37 (modified)		
Final Evaluation (Pass or Fail)		Pass	Fail		

S – Satisfactory U – Unsatisfactory NA - Not Applicable

Table 14. Comparison of Test Results, Test Nos. NELON-1 and NELON-2

Test No.		NELON-1		NELON-2	
MASH Test Designation		3-35		3-37 (modified)	
Vehicle Weight lb (kg)		4,991 (2,264)		5,005 (2,270)	
Impact Severity kip-ft (kJ)		113.6 (154.0)		113.8 (154.3)	
Contact Length ft (m)		29 ft - 3 in. (8.9)		30 ft. - 2 in. (9.2)	
ORA g's	Lateral	-6.63	-6.92	-5.73	-6.45
	Longitudinal	16.76	15.20	13.48	11.01
OIV ft/s (m/s)	Lateral	-14.57 (-4.44)	-13.73 (-4.18)	-12.86 (-3.92)	-11.94 (-3.64)
	Longitudinal	15.68 (4.78)	16.92 (5.16)	15.49 (4.72)	17.59 (5.36)
Exit Time (sec)		.526		.528	
Exit Velocity mph (km/h)		44.8 (72.0)		39.4 (63.4)	
Exit angle (degrees)		12.3		10.4	
Permanent Set in. (mm)		128 (3,251)		126 (3,207)	
Dynamic Deflection in. (mm)		128.3 (3,259)		127.8 (3,247)	
Working Width in. (mm)		150.8 (3,831)		150.3 (3,818)	
Final Evaluation		Pass		Fail	

14.1 Recommendations

Several recommendations should be made regarding the research described herein. First, while the use of a nine-barrier long F-shape PCB system was deemed acceptable under MASH TL-3, end users should be cognizant of the increased lateral barrier deflections for these shorter installations and should account for correspondingly increased clear areas behind the PCBs to account for these deflections. Similarly, PCB installations should account for larger clear areas behind the PCBs near the ends of the barrier length to account for increased deflection observed with vehicle impacts near the ends of the system.

It may be desired to use the research developed herein to establish minimum system lengths and beginning and end of LON guidance for other PCB systems. However, the behavior of any PCB system can be significantly affected by differences in barrier segment length, barrier reinforcement and structural capacity, barrier shape, and the connection design. Due to the potential effect of these differences on barrier performance and the fact that the tests evaluated herein were near the limits of the barrier performance, the reduced system lengths and LON definitions developed are not recommended for use with other PCB systems without further research and evaluation.

Finally, the research effort has indicated that system lengths may be reduced significantly as compared to current guidance. The current research indicates that three and five barriers will be sufficient to define the beginning and end of LON, respectively, and safely redirect vehicles impacting between both points. This would shorten PCB installations approximately 44 percent as compared to current guidance. However, impacts between the beginning and end of LON and the ends of the system have not been evaluated. Computer simulations have indicated that vehicle impacts outside the LON may produce large barrier deflections, vehicle instability, increased barrier loading, and other hazards. Thus, research is needed to further investigate the potential hazards associated with impacts outside the proposed LON and to develop methods to safely terminate the PCB system in order to make effective use of reduced system lengths. Potential methods could include anchored system ends, flared barrier system ends, and/or shielded system ends. There is also the potential to evaluate critical impacts outside of the LON and determine if the system is crashworthy in areas beyond the LON that are outside the scope of the current study.

15 REFERENCES

1. Ross, H.E., Sicking, D.L., Zimmer, R.A., and Michie, J.D., *Recommended Procedures for the Safety Performance Evaluation of Highway Features*, National Cooperative Highway Research Program (NCHRP) Report 350, Transportation Research Board, Washington, D.C., 1993.
2. *Manual for Assessing Safety Hardware (MASH)*, American Association of State Highway and Transportation Officials (AASHTO), Washington, D.C., 2009.
3. Faller, R.K., Rohde, J.R., Rosson, B.T., Smith, R.P., and Addink, K.H., *Development of a TL-3 F-Shape Temporary Concrete Median Barrier*, Final Report to the Midwest States Regional Pooled Fund Research Program, Report No. TRP-03-64-96, Midwest Roadside Safety Facility, University of Nebraska-Lincoln, Lincoln, Nebraska, December 1996.
4. Polivka, K.A., Faller, R.K., Sicking, D.L., Rohde, J.R., Bielenberg, B.W., Reid, J.D., and Coon, B.A., *Performance Evaluation of the Free-Standing Temporary Barrier – Update to NCHRP 350 Test No. 3-11 with 28" C.G. Height (2214TB-2)*, Final Report to the National Cooperative Highway Research Program (NCHRP), Report No. TRP-03-174-06, Midwest Roadside Safety Facility, University of Nebraska-Lincoln, Lincoln, Nebraska, October 2006.
5. R. P. Bligh, N. M. Sheikh, W. L. Menges, and R. R. Haug. *Development of Low-Deflection Precast Concrete Barrier*. Report No. 0-4162-3. Texas Transportation Institute, College Station, TX, January 2005.
6. Bielenberg, R.W., Quinn, T.E., Faller, R.K., Sicking, D.L., and Reid, J.D., *Development of a Retrofit, Low-Deflection, Temporary Concrete Barrier System*, Final Report to the Wisconsin Department of Transportation, Report No. TRP 03-295-14, Midwest Roadside Safety Facility, University of Nebraska-Lincoln, Lincoln, Nebraska, March 31, 2014.
7. Society of Automotive Engineers (SAE), *Instrumentation for Impact Test – Part 1 – Electronic Instrumentation*, SAE J211/1 MAR95, New York City, NY, July, 2007.
8. Mongiardini, M., Ray, M.H., Plaxico, C.A., Anghileri, M., *Procedures for Verification and Validation of Computer Simulations Used for Roadside Safety Applications*, Final Report to the National Cooperative Highway Research Program (NCHRP), NCHRP Report No. W179, Project No. 22-24, Worcester Polytechnic Institute, March 2010.
9. Bielenberg, B.W., Faller, R.K., Rohde, J.R., Reid, J.D., Sicking, D.L., and Holloway, J.C., *Development of Tie-Down and Transition Systems for Temporary Concrete Barrier on Asphalt Road Surfaces*, Final Report to the Midwest States Regional Pooled Regional Pooled Fund Program, Report No. TRP 03-180-06, Midwest Roadside Safety Facility, University of Nebraska-Lincoln, Lincoln, Nebraska, February 23, 2007.

10. Gutierrez, D.A., Bielenberg, R.W., Faller, R.K., Reid, J.D., and Lechtenberg, K.A., *Development of a Mash TL-3 Transition Between Guardrail and Portable Concrete Barriers*, Final Report to the Nebraska Department of Roads, Report No. TRP-03-300-14, Midwest Roadside Safety Facility, University of Nebraska-Lincoln, Lincoln, Nebraska, June 26, 2014.
11. Buth, C. E., Hirsch, T. J., and McDevitt, C. F., *Performance Level 2 Bridge Railings*, Transportation Research Record No. 1258, Transportation Research Board, National Research Council, Washington, D.C., 1990.
12. *Guide Specifications for Bridge Railings*, American Association of State Highway and Transportation Officials (AASHTO), Washington, D.C., 1989.
13. Bronstad, M. E., Calcote, L. R., and Kimball Jr, C. E., *Concrete Median Barrier Research-Vol.2 Research Report*, Report No. FHWA-RD-77-4, Submitted to the Office of Research and Development, Federal Highway Administration, Performed by Southwest Research Institute, San Antonio, TX, March 1976.
14. Buth, C. E., Campise, W. L., Griffin III, L. I., Love, M. L., and Sicking, D. L., *Performance Limits of Longitudinal Barrier Systems-Volume I: Summary Report*, FHWA/RD-86/153, Final Report to the Federal Highway Administration, Office of Safety and Traffic Operations R&D, Performed by Texas Transportation Institute, Texas A&M University, College Station, TX, May 1986.
15. Polivka, K.A., Faller, R.K., Sicking, D.L., Rohde, J.R., Bielenberg, B.W., Reid, J.D., and Coon, B.A., *Performance Evaluation of the Permanent New Jersey Safety Shape Barrier – Update to NCHRP 350 Test No. 3-10 (2214NJ-1)*, Final Report to the National Cooperative Highway Research Program, Report No. TRP-03-117-06, Midwest Roadside Safety Facility, University of Nebraska-Lincoln, Lincoln, Nebraska, October 13, 2006.
16. Fortuniewicz, J. S., Bryden, J. E., and Phillips, R. G., *Crash Tests of Portable Concrete Median Barrier for Maintenance Zones*, Report No. FHWA/NY/RR-82/102, Final Report to the Office of Research, Development, and Technology, Federal Highway Administration, Performed by the Engineering Research and Development Bureau, New York State Department of Transportation, December 1982.
17. Hinch, J., Yang, T.L., and Owings, R., *Guidance Systems for Vehicle Testing*, ENSCO, Inc., Springfield, Virginia, 1986.
18. *Center of Gravity Test Code - SAE J874 March 1981*, SAE Handbook Vol. 4, Society of Automotive Engineers, Inc., Warrendale, Pennsylvania, 1986.
19. *Vehicle Damage Scale for Traffic Investigators*, Second Edition, Technical Bulletin No. 1, Traffic Accident Data (TAD) Project, National Safety Council, Chicago, Illinois, 1971.
20. *Collision Deformation Classification – Recommended Practice J224 March 1980*, Handbook Volume 4, Society of Automotive Engineers (SAE), Warrendale, Pennsylvania, 1985.

21. Sicking, D.L., Reid, J.D., and Polivka, K.A., *Deflection Limits for Temporary Concrete Barriers*, Revised Final Report to the Midwest States Regional Pooled Fund Program, Report No. TRP-03-113-03, Midwest Roadside Safety Facility, University of Nebraska-Lincoln, Lincoln, Nebraska, June 18, 2003.
22. Bronstad, M.E., and Michie, J.D., *Multiple Service-Level Highway Bridge Railing Selection Procedures*, National Cooperative Highway Research Program (NCHRP) Report No. 239, Transportation Research Board, Washington, D.C., November 1981.
23. Sicking, D.L., *Guidelines for Positive Barrier Use in Construction Zones*, Transportation Research Record No. 1035, Transportation Research Board, National Research Council, Washington D.C., 1985.
24. Mak, K.K., and Sicking, D.L., *Evaluation of Performance Level Selection Criteria for Bridge Railings*, Final Report, NCHRP Project 22-8, Texas Transportation Institute, Texas A&M University, September 1993.
25. Mak, K.M., Sicking, D.L., Benicio, F.D., and Coon, B.A., NCHRP Report 665 – *Identification of Vehicular Impact Conditions Associated with Serious Run-Off-Road Crashes*, Final Report to the National Cooperative Highway Research Program (NCHRP) NCHRP Report No. 665, Project No. 17-22, University of Nebraska, 2010.

16 APPENDICES


Appendix A. Material Specifications

Table 15. Bill of Materials, Test Nos. NELON-1 and NELON-2

Item No.	QTY.	Description	Material Spec	Hardware Guide	Reference
d1	8	Portable Concrete Barrier	min f'c=5000 psi [34.5 MPa]	-	See Test Report, NDOR LON Barriers R#16-0198, page 11
d2	7	1 1/4" [32] Dia., 28" [711] Long Connector Pin	ASTM A36	FMW02	H#737194
d3	96	1/2" [13] Dia., 72" [1829] Long Form Bar	ASTM A615 Grade 60	-	H#581898
d4	16	1/2" [13] Dia., 146" [3708] Long Longitudinal Bar	ASTM A615 Grade 60	-	H#62133981/02
d5	24	5/8" [16] Dia., 146" [3708] Long Longitudinal Bar	ASTM A615 Grade 60	-	H#58022182/02
d6	48	3/4" [19] Dia., 36" [914] Long Anchor Loop Bar	ASTM A615 Grade 60, Epoxy Coated or Galvanized	-	H#57147246/02
d7	16	3/4" [19] Dia., 102" [2591] Long Connection Loop Bar	ASTM A709 Grade 70 or A706 Grade 60, Epoxy Coated or Galvanized	-	H#KN15101113
d8	16	3/4" [19] Dia., 91" [2311] Long Connection Loop Bar	ASTM A709 Grade 70 or A706 Grade 60, Epoxy Coated or Galvanized	-	H#KN15101113
d9	16	3/4" [19] Dia., 101" [2565] Long Connection Loop Bar	ASTM A709 Grade 70 or A706 Grade 60, Epoxy Coated or Galvanized	-	H#KN15101113

dA bars Longitudinal

Page 1/1

 GERDAU US-ML-ST PAUL 1678 RED ROCK ROAD SAINT PAUL, MN 55119 USA	CERTIFIED MATERIAL TEST REPORT		CUSTOMER SHIP TO NEBCO INC STEEL DIVISION HAVELOCK, NE 68529 USA	CUSTOMER BILL TO CONCRETE INDUSTRIES INC LINCOLN, NE 68529-0529 USA	GRADE 60 (420)	SHAPE / SIZE Rebar / #4 (13MM)
	SALES ORDER 1017302/000010	CUSTOMER MATERIAL N°	LENGTH 60'00"	WEIGHT 33,186 LB	HEAT / BATCH 62133981/02	
	CUSTOMER PURCHASE ORDER NUMBER 107053		BILL OF LADING 1332-0000018591	DATE 07/03/2014	SPECIFICATION / DATE or REVISION 1-ASTM A615/A615M-09	

CHEMICAL COMPOSITION											
C %	Mn %	P %	S %	Si %	Cu %	Ni %	Cr %	Mo %	Sn %	V %	Nb %
0.41	1.09	0.020	0.031	0.23	0.35	0.08	0.14	0.016	0.015	0.004	0.002

MECHANICAL PROPERTIES		YS	UTS	UTS	G/L	G/L
PSI		MPa	PSI	MPa	Inch	mm
69500		479	104500	720	8.000	203.2

MECHANICAL PROPERTIES		Bend Test
Elong. %		
15.60		OK

GEOMETRIC CHARACTERISTICS			
% Light	Def Hgt. Inch	Def Gap Inch	Def Space Inch
-2.00	0.034	0.117	0.336

COMMENTS / NOTES

Material 100% melted and rolled in the USA. Manufacturing processes for this steel, which may include scrap melted in an electric arc furnace and hot rolling, has been performed at Gerdau St. Paul Mill, 1678 Red Rock Rd., St. Paul, Minnesota, USA. All products produced from strand cast billets. Silicon killed (deoxidized) steel. No weld repairment performed. Steel not exposed to mercury or any liquid alloy which is liquid at ambient temperatures during processing or while in Gerdau St. Paul Mill's possession. Any modification to this certification as provided by Gerdau - St. Paul Mill without the expressed written consent of Gerdau St. Paul Mill negates the validity of this test report. This report shall not be reproduced except in full, without the expressed written consent of Gerdau St. Paul Mill. Gerdau St. Paul Mill is not responsible for the inability of this material to meet specific applications.

Roll batch 62133981/02 roll did 2/17/2014

The above figures are certified chemical and physical test records as contained in the permanent records of company. This material, including the billets, was melted and manufactured in the USA. CMTR complies with EN 10204 3.1.

Maskar

BHASKAR YALAMANCHILI
QUALITY DIRECTOR

Mz

ALEA BRANDENBURG
QUALITY ASSURANCE MGR.

Figure A-1. ½-in. (13-mm) Dia., 146-in. (3,708-mm) Long Longitudinal Steel Bars, Test Nos. NELON-1 and NELON-2



ROCKY MOUNTAIN STEEL
A DIVISION OF EVRAZ INC. NA

2100 S. Freeway
Pueblo, CO 81004 USA

MATERIAL TEST REPORT

Date Printed: 02-OCT-15

d3 bars Vert form bent

Date Shipped: 02-OCT-15

Product: DEF #4 (1/2")

Specification: ASTM A-706/A-615

FWIP: 52825704

Customer: CONCRETE INDUSTRIES INC

Cust. PO: 115501

Heat Number	CHEMICAL ANALYSIS (In Weight %, uncertainty of measurement 0.005%)														(Heat cast 08/27/15)		
	C	Mn	P	S	Si	Cu	Ni	Cr	Mo	Al	V	B	Co	Se	N	Ti	
581898	0.27	1.25	0.009	0.017	0.27	0.23	0.08	0.11	0.017	0.003	0.038	0.0003	0.000	0.010	0.0103	0.001	

Carbon Equivalent = 0.495

Heat Number	Sample No.	MECHANICAL PROPERTIES						(Tensile test date 09/11/15)		Bend	Wt/Wt
		Yield (Psi)	Ultimate (Psi)	Elongation (%)	Reduction (%)						
581898	01	68691	94670	16.0						OK	0.666
		(MPa)	652.7								
581898	02	67769	93410	14.3						OK	0.664
		(MPa)	644.0								

All melting and manufacturing processes of the material subject to this test certificate occurred in the United States of America.

ERMS also certifies this material to be free from Mercury contamination.

This material has been produced, tested and conforms to the requirements of the applicable specifications. We hereby certify that the above test results represent those contained in the records of the Company.

Methods used: ASTM A370, A510, A615, A706.

Material test report shall not be reproduced except in full, without approval of the company.

Valores Varick

Valores Varick
General Supervisor of Quality

FROM: EVRAZ SHIPPING WEST

10/02/2015 14:48 #165 P.002/002

Figure A-2. 1/2-in. (13-mm) Dia., 72-in. (1,828-mm) Long Form Bar, Test Nos. NELON-1 and NELON-2

Date: 11-3-15

Preheat Temperature Line 1: 463 - 475

Gel Time Line 1 : 11 Seconds

Holidays Line 1 : 14.00

Boxes used: 11

3/4 144

Axalta 7-2719 - Powder Lot # H1508042359

Epoxy Coated in accordance with ASTM A 775 / A 775M - 07b

7b 8.652 w, t Shift

Preheat Temperature Line 2: 463-475°

Gel Time Line 2: 10 Seconds

Holidays Line 2: 145

Shift : Day (☒) Night (☐)[illegible]

Certified By : _____

Plant Operator Daniel Parra

Jose Siguina

Figure A-4. 3/4-in. (19-mm) Dia. Connection Loop Bar, Test Nos. NELON-1 and NELON-2



		CERTIFIED MATERIAL TEST REPORT				Page 1/1																											
US-ML-MIDLOTHIAN 300 WARD ROAD MIDLOTHIAN, TX 76065 USA		CUSTOMER SHIP TO NEBCO INC STEEL DIVISION HAVELOCK, NE 68529 USA		CUSTOMER BILL TO CONCRETE INDUSTRIES INC LINCOLN, NE 68529-0529 USA		GRADE 60 (420)	SHAPE / SIZE Rebar / #5 (16MM)																										
		SALES ORDER 2295588/000010		CUSTOMER MATERIAL N°		LENGTH 60'00"	WEIGHT 144,192 LB	HEAT / BATCH 58022182/02																									
CUSTOMER PURCHASE ORDER NUMBER 112911		BILL OF LADING 1327-0000158963		DATE 06/10/2015		SPECIFICATION / DATE or REVISION ASTM A615/A615M-14																											
CHEMICAL COMPOSITION <table border="1"> <thead> <tr> <th>C</th> <th>Mn</th> <th>P</th> <th>S</th> <th>Si</th> <th>Cu</th> <th>Ni</th> <th>Cr</th> <th>Mo</th> <th>Sb</th> <th>V</th> <th>Nb</th> <th>Al</th> </tr> </thead> <tbody> <tr> <td>0.43</td> <td>0.83</td> <td>0.013</td> <td>0.031</td> <td>0.25</td> <td>0.27</td> <td>0.13</td> <td>0.17</td> <td>0.025</td> <td>0.006</td> <td>0.018</td> <td>0.000</td> <td>0.005</td> </tr> </tbody> </table>								C	Mn	P	S	Si	Cu	Ni	Cr	Mo	Sb	V	Nb	Al	0.43	0.83	0.013	0.031	0.25	0.27	0.13	0.17	0.025	0.006	0.018	0.000	0.005
C	Mn	P	S	Si	Cu	Ni	Cr	Mo	Sb	V	Nb	Al																					
0.43	0.83	0.013	0.031	0.25	0.27	0.13	0.17	0.025	0.006	0.018	0.000	0.005																					
CHEMICAL COMPOSITION CEq _{A706} 0.59																																	
MECHANICAL PROPERTIES <table border="1"> <thead> <tr> <th>YS PSI</th> <th>YS MPa</th> <th>UTS PSI</th> <th>UTS MPa</th> <th>G/L inch</th> <th>G/L mm</th> </tr> </thead> <tbody> <tr> <td>70072</td> <td>483</td> <td>101603</td> <td>701</td> <td>8.000</td> <td>200.0</td> </tr> </tbody> </table>								YS PSI	YS MPa	UTS PSI	UTS MPa	G/L inch	G/L mm	70072	483	101603	701	8.000	200.0														
YS PSI	YS MPa	UTS PSI	UTS MPa	G/L inch	G/L mm																												
70072	483	101603	701	8.000	200.0																												
MECHANICAL PROPERTIES Elong. % 16.60																																	
Bend Test OK																																	
COMMENTS / NOTES																																	
<div style="display: flex; justify-content: space-between; align-items: flex-end;"> <div> <p>The above figures are certified chemical and physical test records as contained in the permanent records of company. We certify that these data are correct and in compliance with specified requirements. This material, including the billets, was melted and manufactured in the USA. CMTR complies with EN 10204 3.1.</p> <p><i>Bhaskar</i> BHASKAR YALAMANCHILI QUALITY DIRECTOR</p> </div> <div> <p><i>Tom Harrington</i> TOM HARRINGTON QUALITY ASSURANCE MGR.</p> </div> </div>																																	

Figure A-5. 5/8-in. (16-mm) Dia. Longitudinal Bar, Test Nos. NELON-1 and NELON-2



GERDAU

US-ML-KNOXVILLE
1919 TENNESSEE AVENUE N. W.
KNOXVILLE, TN 37921
USA

CERTIFIED MATERIAL TEST REPORT

Page 1/1

CUSTOMER SHIP TO NEBCO INC STEEL DIVISION HAVELOCK, NE 68529 USA		CUSTOMER BILL TO CONCRETE INDUSTRIES INC LINCOLN, NE 68529-0529 USA		GRADE 60 (420) TMX	SHAPE / SIZE Rebar / #6 (19MM)	
SALES ORDER 1879247/000010		CUSTOMER MATERIAL N°		LENGTH 60'00"	WEIGHT 28,116 LB	HEAT / BATCH 57147246/02
SPECIFICATION / DATE of REVISION ASTM A615/A615M-14						

CUSTOMER PURCHASE ORDER NUMBER 111200	BILL OF LADING 1326-0000030911	DATE 02/16/2015
--	-----------------------------------	--------------------

CHEMICAL COMPOSITION											
C %	Mn %	P %	S %	Si %	Cu %	Ni %	Cr %	Mo %	Sn %	V %	CEq _{A706} %
0.33	0.61	0.012	0.045	0.21	0.27	0.10	0.09	0.015	0.003	0.002	0.45

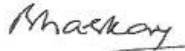
MECHANICAL PROPERTIES		YS		UTS		UTS		G/L		G/L	
PSI		MPa		PSI		MPa		Inch		mm	
80570		556		98760		681		8.000		200.0	

MECHANICAL PROPERTIES		Bend Test	
Elong. %		OK	
14.00			


GEOMETRIC CHARACTERISTICS			
%Light	Def Hgt Inch	Def Clap Inch	Def Space Inch
3.93	0.054	0.105	0.474

COMMENTS / NOTES
 This grade meets the requirements for the following grades:

The above figures are certified chemical and physical test records as contained in the permanent records of company. We certify that these data are correct and in compliance with specified requirements. This material, including the billets, was melted and manufactured in the USA. CMTR complies with EN 10204 3.1.



BHASKAR YALAMANCHILI
QUALITY DIRECTOR



LISA CHURNETSKI
QUALITY ASSURANCE MGR.

Figure A-6. 3/4-in. (19-mm) Dia. Anchor Loop Bar, Test Nos. NELON-1 and NELON-2

GENERAL TESTING LABORATORIES

TELEPHONE (402)434-1891
FAX (402)434-2161

P.O. BOX 29529
LINCOLN, NEBRASKA 68529

March 9, 2016

Dave Borchers
Concrete Industries, Inc.
6300 Cornhusker Hwy.
Lincoln, NE 68507

Dear Dave,

Below are the strength values to date for the UNL Barrier Curbs produced at Concrete Industries.

Cast Date	Release	7 Day	28 Day
11/6/2015	5717	6685	8012
11/9/2015	4102	6956	8265
11/10/2015	4478	8115	9492
11/11/2015	3642	7417	8765
11/12/2015	4666	7888	8887

General Testing Lab,



Rod Leber, Manager

Figure A-7. Concrete Strength Values, Test Nos. NELON-1 and NELON-2

06/13/2006 From: NORFOLK IRON & METAL CO. To: CONCRETE INDUSTRIES INC
PO # :59101 Inv # :01410860

06/08/2006 From: NORFOLK IRON & METAL CO. To: NORFOLK IRON & METAL
Inv # :04009576

BL#-0238492 P.O.-04009324

Date: 5/01/06

Nucor Corporation

Heat Number: 737194

Nucor Steel Division
Post Office Box 309 Norfolk, Nebraska 68702 Phone (402) 644-0200
Mill Certification



Chemical Testing
Certificate: 0780-01
Expires: 11/30/06

Chemical Analysis

Test conform to ASTM A29, ASTM E415 and ASTM E1019-resulphurized grades
Spec: A36 ASTM A36-01 Size: 1 1/4 Rounds
ASME SA-36 E98 1.2500

C	.17	P	.02	Mo	.03
Mn	.72	Cu	.26	V	.001
Si	.19	Cr	.13	Nb	.001
S	.02	Ni	.10		

Physical Properties

	Imperial			Metric		
Yield	48,126	46,440	psi	332	320	MPA
Tensile	68,999	69,609	psi	476	480	MPA
% Elongation	26	24	% in 8"	26	24	% in 203.3 mm

Strand Cast

Reduction Ratio: 36:1

NORFOLK IRON & METAL CO
1701 E. SOUTH AVE
EMPORIA, KS 66801


Jim Hill Division Metallurgist

All Manufacturing processes, including melting have been performed in the U.S.A. Mercury, in any form, has not been used in the production or testing of this material. Welding or weld repair was not performed on this material. This material conforms to the specifications described on this document and may not be reproduced except in full, without written approval of Nucor Corporation. This product is NAFTA certified under Paragraph "B" of the NAFTA rules of origin.
FORM: 10F002 HT3000R

Figure A-8. 1 1/4-in. (32-mm) Dia., 28-in. (71-mm) Long Connector Pin, Test Nos. NELON-1 and NELON-2

Appendix B. Vehicle Center of Gravity Determination

Test: NELON-1

Vehicle:

Dodge Ram 1500 Quad

Vehicle CG Determination

VEHICLE	Equipment	Weight (lb.)	Vertical CG (in.)	Vertical M (lb-in.)
+	Unbalasted Truck (Curb)	4833	28.25628	136562.63
+	Hub	19	14.3125	271.9375
+	Brake activation cylinder & frame	7	29	203
+	Pneumatic tank (Nitrogen)	27	25.875	698.625
+	Strobe/Brake Battery	5	25.5	127.5
+	Brake Reciever/Wires	5	52	260
+	CG Plate including DAS	42	29.5	1239
-	Battery	-41	43	-1763
-	Oil	-5	18.5	-92.5
-	Interior	-77	27	-2079
-	Fuel	-154	19	-2926
-	Coolant	-10	36	-360
-	Washer fluid	-5	38	-190
+	Water Ballast	227	19	4313
+	Onboard Battery	14	24.5	343
	Steel Ballast	100	33.25	3325
Note: (+) is added equipment to vehicle, (-) is removed equipment from vehicle				139933.19

Estimated Total Weight (lb.) 4987
 Vertical CG Location (in.) 28.05959

Wheel Base (in.) 140.25

Center of Gravity	2270P MASH Targets	Test Inertial	Difference
Test Inertial Weight (lb.)	5000 ± 110	4991	-9.0
Longitudinal CG (in.)	63 ± 4	64.86	1.85614
Lateral CG (in.)	NA	0.020343	NA
Vertical CG (in.)	28 or greater	28.06	0.05959

Note: Long. CG is measured from front axle of test vehicle

Note: Lateral CG measured from centerline - positive to vehicle right (passenger) side

CURB WEIGHT (lb.)

	Left	Right
Front	1392	1297
Rear	1072	1072
FRONT	2689 lb.	
REAR	2144 lb.	
TOTAL	4833 lb.	

TEST INERTIAL WEIGHT (lb.)

	Left	Right
Front	1370	1313
Rear	1124	1184
FRONT	2683 lb.	
REAR	2308 lb.	
TOTAL	4991 lb.	

Figure B-1. Vehicle Mass Distribution, Test No. NELON-1

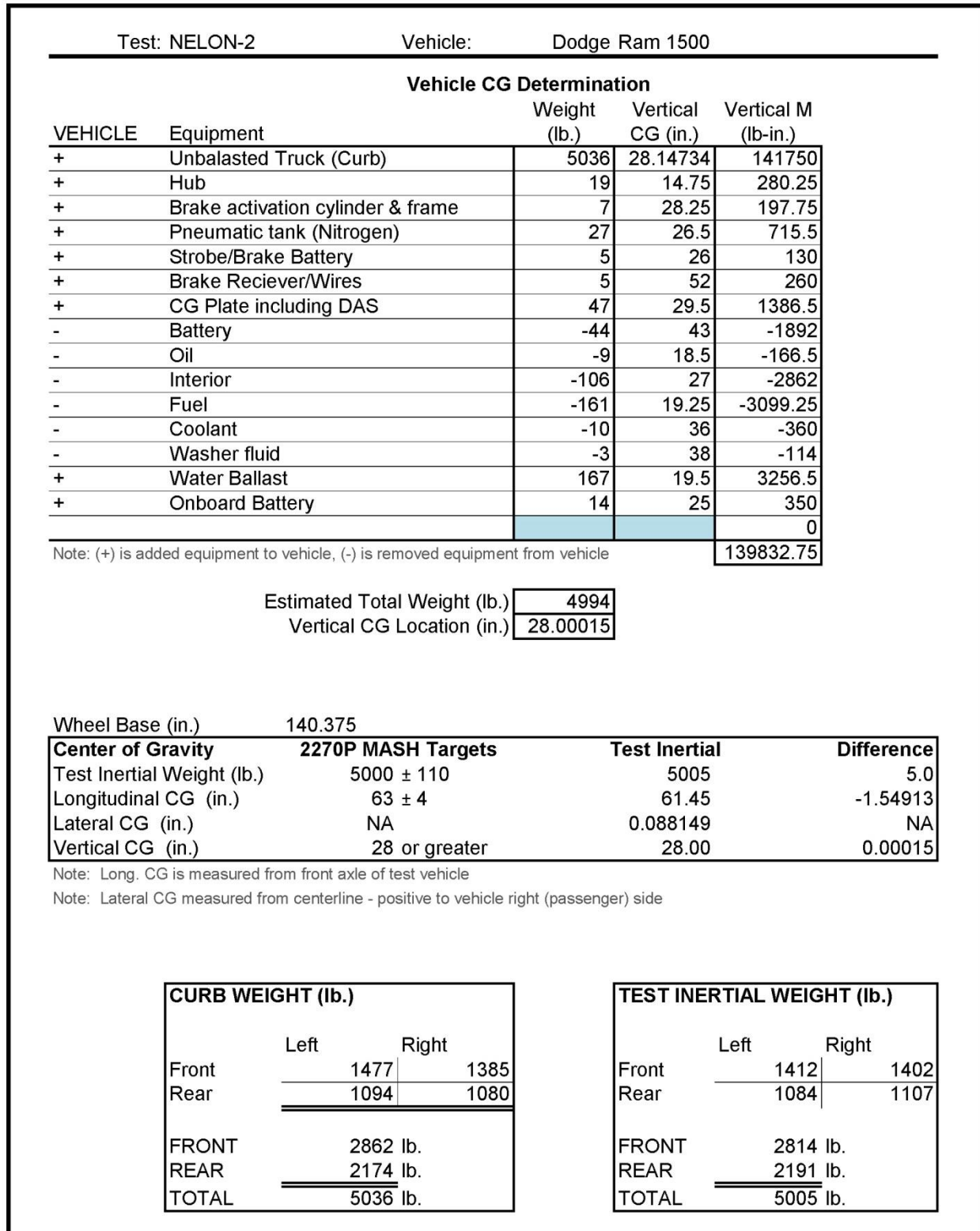


Figure B-2. Vehicle Mass Distribution, Test No. NELON-2

Appendix C. Vehicle Deformation Records

VEHICLE PRE/POST CRUSH
FLOORPAN - SET 1

TEST: NELON-1
VEHICLE: Dodge Ram 1500 Quad

POINT	X (in.)	Y (in.)	Z (in.)	X' (in.)	Y' (in.)	Z' (in.)	ΔX (in.)	ΔY (in.)	ΔZ (in.)
1	28.451	-29.537	3.763	27.903	-29.624	3.763	-0.548	-0.086	0.000
2	29.532	-26.222	2.297	28.518	-26.110	2.751	-1.013	0.112	0.454
3	30.647	-22.858	0.556	29.803	-22.690	0.755	-0.845	0.168	0.199
4	30.546	-18.233	-0.009	30.282	-18.393	-0.117	-0.264	-0.161	-0.108
5	26.466	-29.757	-0.180	26.067	-29.783	-0.294	-0.400	-0.026	-0.114
6	26.699	-25.845	-0.948	26.228	-25.902	-1.292	-0.471	-0.057	-0.344
7	26.372	-20.804	-1.548	26.068	-20.798	-1.743	-0.304	0.006	-0.195
8	26.288	-14.940	-2.205	26.122	-14.984	-2.410	-0.166	-0.044	-0.205
9	20.100	-28.969	-3.660	19.742	-28.932	-3.961	-0.358	0.037	-0.302
10	19.973	-25.114	-4.068	19.650	-25.151	-4.363	-0.323	-0.036	-0.295
11	20.087	-20.108	-4.515	19.735	-20.100	-4.800	-0.352	0.008	-0.285
12	20.071	-15.301	-5.094	19.798	-15.372	-5.340	-0.273	-0.071	-0.246
13	15.313	-29.029	-3.923	14.943	-28.915	-4.230	-0.369	0.114	-0.307
14	15.115	-24.489	-4.309	14.813	-24.651	-4.575	-0.302	-0.162	-0.266
15	14.777	-19.677	-4.789	14.485	-19.660	-5.020	-0.293	0.017	-0.231
16	14.880	-15.315	-5.276	14.530	-15.268	-5.532	-0.350	0.047	-0.255
17	10.424	-28.902	-3.575	10.162	-28.933	-3.837	-0.263	-0.031	-0.262
18	10.345	-24.504	-3.957	10.099	-24.586	-4.209	-0.246	-0.082	-0.252
19	10.457	-19.089	-4.536	10.223	-19.116	-4.771	-0.233	-0.027	-0.235
20	10.433	-14.591	-5.037	10.140	-14.638	-5.268	-0.294	-0.048	-0.231
21	6.072	-29.203	-3.596	5.784	-29.167	-3.819	-0.289	0.036	-0.223
22	5.922	-24.195	-4.050	5.693	-24.154	-4.294	-0.229	0.041	-0.244
23	6.111	-18.790	-4.666	5.874	-18.720	-4.905	-0.237	0.070	-0.239
24	6.289	-14.084	-5.184	6.008	-14.091	-5.416	-0.281	-0.007	-0.232
25	0.388	-27.834	0.323	0.153	-27.826	0.108	-0.235	0.008	-0.215
26	0.452	-22.814	-0.173	0.163	-22.729	-0.398	-0.289	0.085	-0.224
27	0.264	-17.403	-0.829	0.066	-17.349	-1.049	-0.197	0.055	-0.220
28	0.439	-13.366	-1.215	0.100	-13.318	-1.441	-0.339	0.048	-0.226

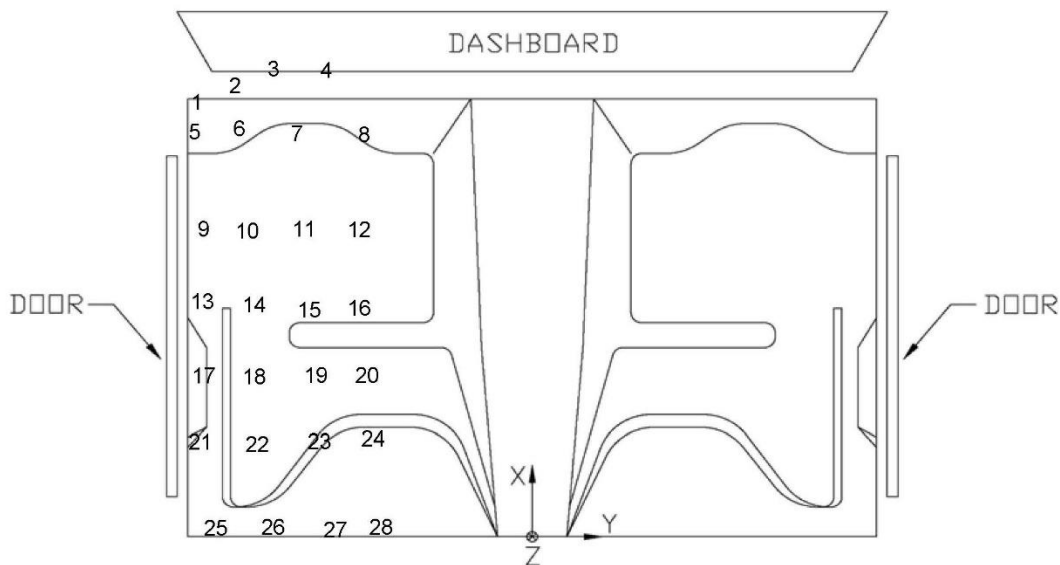


Figure C-1. Floor Pan Deformation Data - Set 1, Test No. NELON-1

VEHICLE PRE/POST CRUSH
FLOORPAN - SET 1

TEST: NELON-2
VEHICLE: Dodge Ram 1500

POINT	X (in.)	Y (in.)	Z (in.)	X' (in.)	Y' (in.)	Z' (in.)	ΔX (in.)	ΔY (in.)	ΔZ (in.)
1	29.988	-26.519	5.330	29.956	-26.523	5.228	-0.032	-0.004	-0.101
2	31.437	-22.653	3.346	31.555	-22.614	3.320	0.117	0.039	-0.026
3	32.492	-17.213	2.417	32.538	-17.150	2.084	0.046	0.063	-0.333
4	28.655	-10.962	3.719	28.897	-11.073	3.522	0.242	-0.111	-0.196
5	25.237	-27.458	-0.794	25.167	-27.261	-0.834	-0.069	0.198	-0.040
6	25.340	-23.380	-1.025	25.367	-23.125	-1.214	0.027	0.255	-0.189
7	25.374	-18.103	-1.567	25.391	-18.036	-1.682	0.017	0.068	-0.115
8	25.204	-12.251	-2.257	25.402	-12.099	-2.252	0.198	0.152	0.005
9	21.984	-27.423	-2.393	22.006	-27.199	-2.262	0.021	0.224	0.131
10	22.033	-23.695	-2.891	22.066	-23.751	-2.777	0.033	-0.056	0.114
11	22.108	-18.425	-3.330	22.204	-18.193	-3.331	0.096	0.232	-0.001
12	22.141	-12.955	-3.828	22.281	-12.993	-3.829	0.140	-0.038	0.000
13	18.352	-27.406	-3.694	18.473	-27.247	-3.761	0.121	0.159	-0.067
14	18.368	-23.694	-4.079	18.567	-23.481	-4.030	0.199	0.213	0.049
15	18.441	-18.541	-4.518	18.530	-18.352	-4.516	0.088	0.189	0.001
16	18.633	-13.291	-5.122	18.799	-13.211	-5.120	0.166	0.080	0.002
17	14.497	-27.341	-3.673	14.396	-26.904	-3.801	-0.101	0.437	-0.128
18	14.584	-23.793	-4.047	14.594	-23.701	-4.071	0.010	0.092	-0.024
19	14.831	-18.611	-4.560	14.885	-18.297	-4.584	0.054	0.314	-0.024
20	14.517	-13.812	-5.102	14.682	-13.731	-5.107	0.165	0.081	-0.005
21	8.837	-26.903	-3.661	8.716	-26.693	-3.771	-0.122	0.211	-0.110
22	8.922	-23.689	-4.002	8.820	-23.379	-4.092	-0.103	0.310	-0.090
23	8.854	-18.833	-4.525	8.941	-18.569	-4.551	0.087	0.264	-0.026
24	8.901	-14.103	-5.040	8.973	-13.978	-5.057	0.072	0.126	-0.018
25	-0.071	-26.707	0.258	-0.106	-26.347	0.152	-0.034	0.360	-0.105
26	-0.195	-22.638	-0.194	-0.129	-22.334	-0.233	0.066	0.305	-0.039
27	-0.267	-17.410	-0.763	-0.221	-17.274	-0.774	0.046	0.136	-0.011
28	-0.153	-13.294	-1.202	-0.100	-12.948	-1.220	0.053	0.346	-0.018

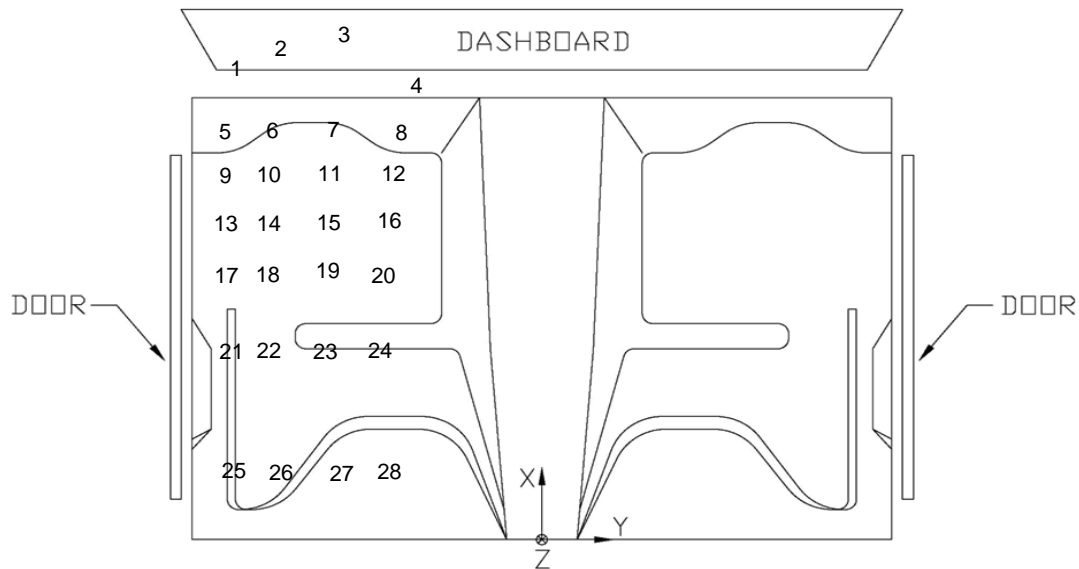


Figure C-2. Floor Pan Deformation Data - Set 1, Test No. NELON-2

VEHICLE PRE/POST CRUSH
FLOORPAN - SET 2

TEST: NELON-1
VEHICLE: Dodge Ram 1500 Quad

POINT	X (in.)	Y (in.)	Z (in.)	X' (in.)	Y' (in.)	Z' (in.)	ΔX (in.)	ΔY (in.)	ΔZ (in.)
1	53.734	-35.933	0.575	53.276	-36.446	1.387	-0.459	-0.513	0.812
2	54.816	-32.557	-0.364	53.900	-32.972	0.829	-0.916	-0.415	1.192
3	55.943	-28.859	-1.802	55.219	-29.318	-0.769	-0.724	-0.460	1.033
4	56.030	-24.203	-1.599	55.688	-24.834	-1.066	-0.343	-0.630	0.533
5	51.748	-35.566	-3.399	51.436	-36.166	-2.742	-0.312	-0.600	0.656
6	51.948	-31.654	-3.682	51.608	-32.174	-3.217	-0.340	-0.519	0.465
7	51.747	-26.446	-3.560	51.441	-27.099	-3.029	-0.306	-0.653	0.531
8	51.737	-20.671	-3.315	51.618	-21.353	-2.877	-0.119	-0.681	0.438
9	45.247	-34.420	-6.782	45.112	-34.695	-6.200	-0.135	-0.275	0.582
10	45.269	-30.511	-6.665	45.137	-31.107	-6.177	-0.132	-0.597	0.489
11	45.280	-25.316	-6.475	45.231	-25.967	-5.972	-0.049	-0.651	0.503
12	45.382	-20.627	-6.403	45.296	-21.205	-5.927	-0.086	-0.578	0.477
13	40.539	-34.200	-7.010	40.326	-34.749	-6.549	-0.213	-0.548	0.461
14	40.452	-29.931	-6.818	40.193	-30.345	-6.353	-0.260	-0.414	0.466
15	40.137	-24.977	-6.647	40.058	-25.444	-6.194	-0.079	-0.468	0.452
16	40.126	-20.466	-6.545	40.026	-21.045	-6.145	-0.100	-0.579	0.400
17	35.686	-34.005	-6.591	35.562	-34.757	-6.198	-0.124	-0.752	0.393
18	35.575	-29.982	-6.414	35.521	-30.380	-6.037	-0.054	-0.398	0.377
19	35.756	-24.301	-6.287	35.767	-24.824	-5.899	0.012	-0.522	0.388
20	35.710	-19.978	-6.211	35.656	-20.362	-5.850	-0.054	-0.385	0.360
21	31.431	-34.523	-6.659	31.096	-34.960	-6.266	-0.335	-0.438	0.393
22	31.292	-29.503	-6.474	31.114	-29.806	-6.128	-0.177	-0.303	0.346
23	31.464	-23.974	-6.381	31.402	-24.466	-6.044	-0.062	-0.492	0.337
24	31.626	-19.306	-6.287	31.522	-19.787	-5.945	-0.104	-0.481	0.342
25	25.587	-33.690	-2.589	25.492	-34.034	-2.287	-0.095	-0.344	0.302
26	25.746	-28.537	-2.429	25.639	-28.997	-2.140	-0.107	-0.460	0.289
27	25.569	-23.135	-2.377	25.586	-23.570	-2.090	0.017	-0.434	0.287
28	25.841	-18.988	-2.227	25.626	-19.523	-1.966	-0.215	-0.536	0.260

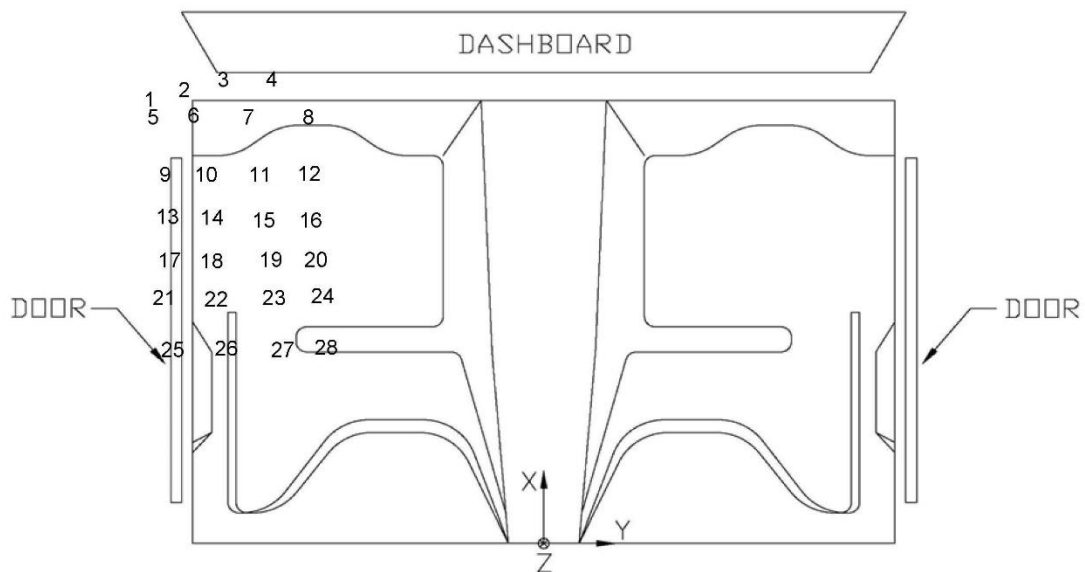


Figure C-3. Floor Pan Deformation Data - Set 2, Test No. NELON-1

VEHICLE PRE/POST CRUSH
FLOORPAN - SET 2

TEST: NELON-2
VEHICLE: Dodge Ram 1500

POINT	X (in.)	Y (in.)	Z (in.)	X' (in.)	Y' (in.)	Z' (in.)	ΔX (in.)	ΔY (in.)	ΔZ (in.)
1	54.566	-33.006	2.968	54.600	-32.819	3.008	0.034	0.187	0.040
2	56.040	-28.924	1.288	56.089	-28.863	1.499	0.048	0.061	0.211
3	57.101	-23.320	0.820	57.082	-23.318	0.830	-0.019	0.002	0.010
4	53.374	-17.347	2.979	53.500	-17.438	3.025	0.125	-0.091	0.046
5	49.756	-33.113	-3.123	49.736	-33.084	-3.116	-0.020	0.029	0.007
6	49.835	-28.998	-2.961	49.889	-29.011	-2.891	0.054	-0.014	0.070
7	49.883	-23.980	-2.957	49.851	-23.693	-2.913	-0.032	0.287	0.044
8	49.767	-18.046	-2.933	49.778	-17.767	-2.955	0.011	0.279	-0.022
9	46.406	-33.041	-4.532	46.352	-32.880	-4.460	-0.053	0.161	0.072
10	46.481	-29.184	-4.686	46.563	-29.064	-4.542	0.082	0.121	0.144
11	46.639	-23.914	-4.601	46.652	-23.743	-4.524	0.013	0.171	0.077
12	46.670	-18.370	-4.568	46.673	-18.294	-4.518	0.003	0.077	0.050
13	42.753	-32.871	-5.865	42.791	-32.611	-5.832	0.038	0.261	0.033
14	42.870	-29.235	-5.828	42.915	-29.046	-5.757	0.045	0.189	0.071
15	42.895	-23.957	-5.766	42.931	-23.891	-5.654	0.036	0.066	0.112
16	43.148	-18.630	-5.833	43.073	-18.513	-5.717	-0.075	0.117	0.116
17	38.866	-32.756	-5.715	39.001	-32.598	-5.769	0.135	0.157	-0.053
18	39.076	-29.264	-5.743	39.110	-29.209	-5.703	0.034	0.055	0.040
19	39.268	-24.023	-5.739	39.273	-23.891	-5.652	0.005	0.133	0.086
20	38.969	-19.165	-5.764	38.976	-19.016	-5.709	0.007	0.148	0.055
21	33.272	-32.326	-5.524	33.302	-32.225	-5.616	0.030	0.102	-0.091
22	33.259	-29.027	-5.556	33.355	-28.870	-5.594	0.096	0.156	-0.038
23	33.304	-24.152	-5.600	33.392	-24.138	-5.551	0.088	0.014	0.050
24	33.410	-19.367	-5.632	33.466	-19.276	-5.579	0.056	0.091	0.053
25	24.453	-32.408	-1.443	24.456	-32.376	-1.540	0.004	0.033	-0.097
26	24.333	-28.413	-1.491	24.319	-28.415	-1.518	-0.014	-0.002	-0.028
27	24.249	-23.106	-1.531	24.403	-23.110	-1.515	0.154	-0.003	0.017
28	24.445	-19.011	-1.533	24.504	-18.733	-1.514	0.059	0.278	0.019

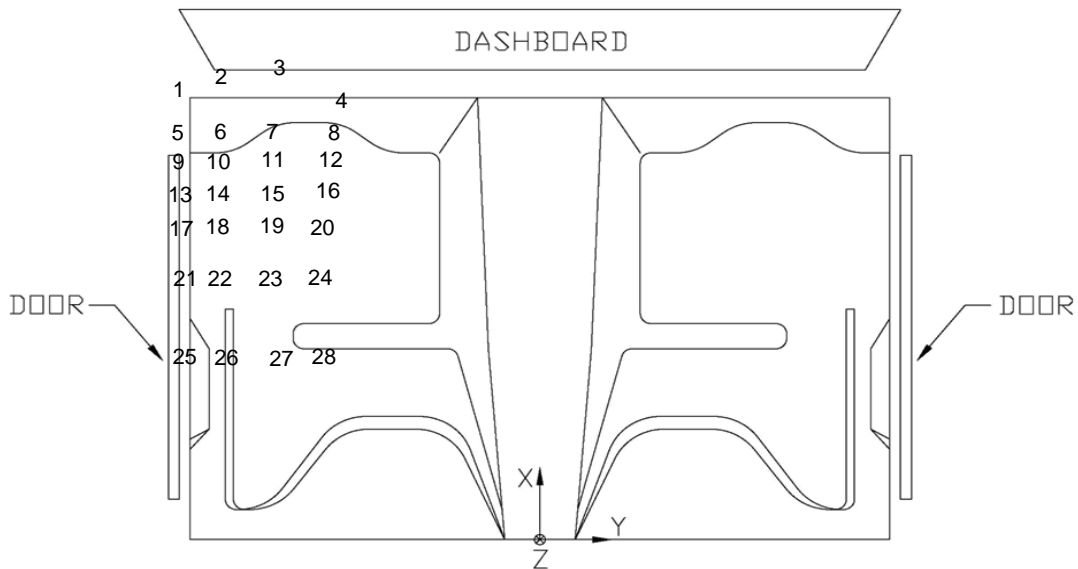


Figure C-4. Floor Pan Deformation Data - Set 2, Test No. NELON-2

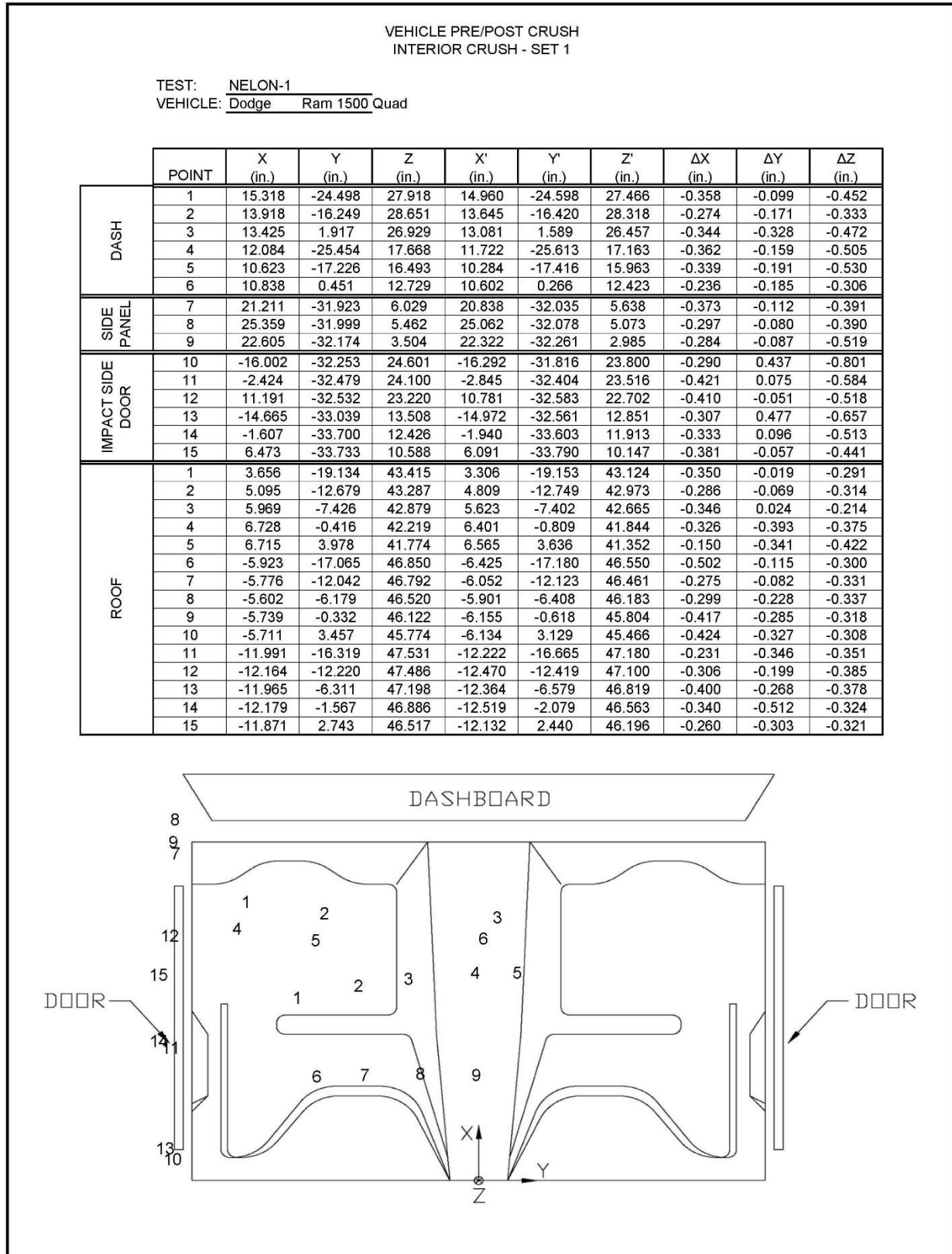


Figure C-5. Occupant Compartment Deformation Data - Set 1, Test No. NELON-1

VEHICLE PRE/POST CRUSH
INTERIOR CRUSH - SET 1

TEST: NELON-2
VEHICLE: Dodge Ram 1500

	POINT	X (in.)	Y (in.)	Z (in.)	X' (in.)	Y' (in.)	Z' (in.)	ΔX (in.)	ΔY (in.)	ΔZ (in.)
DASH	1	14.839	-22.275	29.322	15.111	-22.162	29.296	0.272	0.113	-0.025
	2	14.375	-9.603	28.314	14.460	-9.347	28.284	0.085	0.257	-0.030
	3	12.161	2.224	27.408	12.444	2.259	27.322	0.284	0.035	-0.087
	4	11.494	-24.019	16.827	11.576	-23.906	16.803	0.082	0.113	-0.025
	5	11.041	-11.482	15.576	11.434	-11.614	15.164	0.392	-0.133	-0.411
	6	9.595	0.988	13.955	9.892	1.200	13.770	0.297	0.212	-0.185
SIDE PANEL	7	20.885	-31.372	8.520	20.854	-31.280	8.326	-0.031	0.092	-0.194
	8	23.440	-31.521	8.133	23.526	-31.475	7.790	0.086	0.046	-0.343
	9	21.939	-31.747	5.995	21.974	-31.681	5.717	0.035	0.066	-0.278
IMPACT SIDE DOOR	10	-14.491	-33.180	21.338	-14.458	-31.172	21.238	0.033	2.008	-0.100
	11	-2.027	-33.056	21.277	-1.964	-31.743	21.098	0.062	1.314	-0.180
	12	9.096	-32.992	21.005	9.025	-32.281	20.797	-0.071	0.711	-0.208
	13	-13.646	-34.397	3.452	-13.815	-33.202	3.242	-0.168	1.196	-0.210
	14	2.452	-33.875	2.850	2.215	-33.069	2.738	-0.237	0.805	-0.112
	15	14.975	-34.422	2.274	14.689	-34.202	2.022	-0.286	0.220	-0.252
ROOF	1	2.492	-17.972	43.508	2.829	-17.760	43.485	0.337	0.212	-0.023
	2	3.702	-12.410	43.068	3.988	-11.728	43.394	0.286	0.682	0.326
	3	4.406	-6.557	42.778	4.800	-5.700	43.085	0.394	0.858	0.307
	4	4.808	-0.550	42.381	5.219	0.469	42.629	0.411	1.019	0.249
	5	5.007	3.771	41.939	5.462	4.744	42.117	0.455	0.973	0.178
	6	-5.546	-16.579	46.157	-5.264	-15.803	46.511	0.282	0.776	0.354
	7	-4.721	-12.065	45.928	-4.287	-11.048	46.348	0.435	1.017	0.420
	8	-3.772	-6.592	45.615	-3.507	-5.415	46.021	0.265	1.177	0.406
	9	-3.010	-0.495	45.144	-2.522	0.628	45.435	0.488	1.123	0.292
	10	-2.480	3.376	44.749	-2.109	4.658	44.974	0.371	1.282	0.225
	11	-11.354	-16.786	46.757	-10.961	-15.955	47.193	0.393	0.830	0.436
	12	-10.773	-12.001	46.615	-10.405	-10.980	47.079	0.368	1.021	0.464
	13	-10.120	-7.020	46.385	-9.766	-5.857	46.796	0.354	1.164	0.410
	14	-9.127	-0.988	45.990	-8.943	0.121	46.290	0.185	1.108	0.300
	15	-9.080	2.894	45.637	-8.744	4.076	45.900	0.336	1.181	0.264

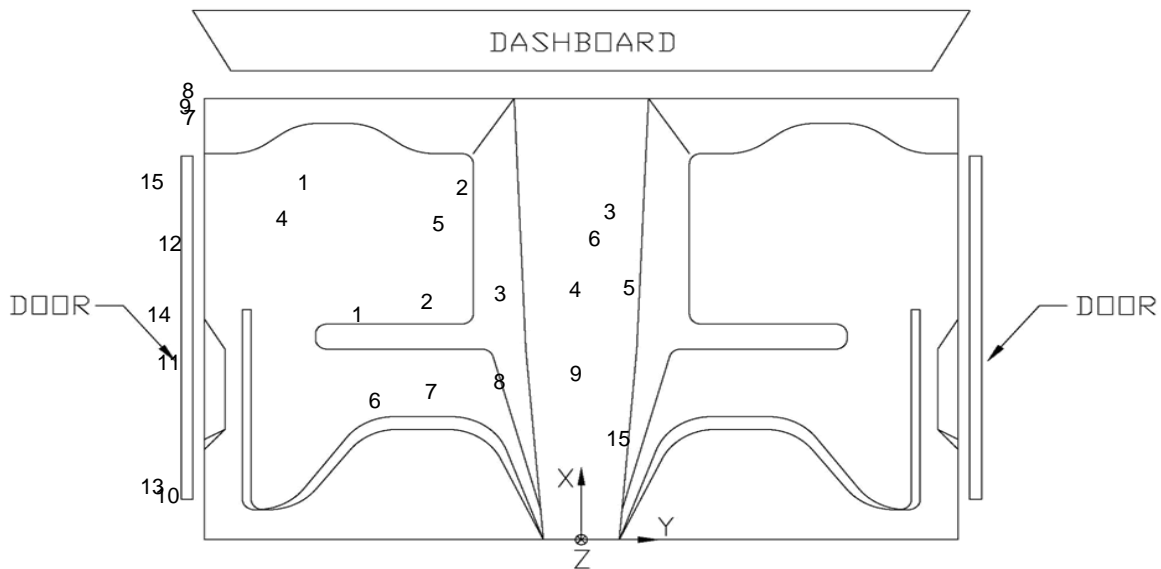


Figure C-6. Occupant Compartment Deformation Data - Set 1, Test No. NELON-2

VEHICLE PRE/POST CRUSH
INTERIOR CRUSH - SET 2

TEST: NELON-1
VEHICLE: Dodge Ram 1500 Quad

	POINT	X (in.)	Y (in.)	Z (in.)	X' (in.)	Y' (in.)	Z' (in.)	ΔX (in.)	ΔY (in.)	ΔZ (in.)
DASH	1	40.715	-33.893	25.207	40.162	-34.497	25.418	-0.553	-0.604	0.211
	2	39.341	-25.840	27.000	38.898	-26.432	27.256	-0.443	-0.592	0.256
	3	38.864	-7.672	27.609	38.539	-8.351	27.865	-0.326	-0.679	0.255
	4	37.409	-33.603	15.016	37.020	-34.214	15.267	-0.389	-0.611	0.252
	5	35.979	-25.249	14.872	35.648	-25.843	14.933	-0.331	-0.594	0.061
	6	36.293	-7.291	13.464	36.108	-7.774	13.611	-0.185	-0.483	0.148
SIDE PANEL	7	46.387	-38.525	2.576	46.195	-39.153	2.828	-0.192	-0.628	0.252
	8	50.652	-38.546	1.965	50.340	-39.167	2.129	-0.313	-0.621	0.164
	9	47.913	-38.450	-0.098	47.656	-39.055	0.122	-0.257	-0.605	0.220
IMPACT SIDE DOOR	10	9.235	-41.098	20.803	8.842	-41.152	20.824	-0.393	-0.053	0.021
	11	22.853	-41.327	20.388	22.320	-41.732	20.468	-0.533	-0.406	0.080
	12	36.576	-41.306	19.446	35.996	-41.837	19.699	-0.580	-0.530	0.253
	13	10.646	-40.447	9.726	10.301	-40.468	9.759	-0.345	-0.020	0.033
	14	23.491	-41.016	8.485	23.308	-41.417	8.755	-0.183	-0.401	0.269
	15	31.765	-40.848	6.812	31.335	-41.418	7.027	-0.430	-0.570	0.215
ROOF	1	29.080	-30.643	41.255	28.580	-31.266	41.310	-0.500	-0.623	0.055
	2	30.695	-24.059	41.921	29.949	-24.826	42.095	-0.746	-0.767	0.173
	3	31.468	-18.789	42.291	30.784	-19.539	42.495	-0.685	-0.750	0.204
	4	32.360	-11.623	42.514	31.792	-12.564	42.685	-0.567	-0.941	0.171
	5	32.239	-7.310	42.691	31.824	-8.173	42.836	-0.415	-0.862	0.145
	6	19.544	-28.881	45.022	18.925	-29.453	45.031	-0.619	-0.573	0.008
	7	19.791	-23.839	45.619	19.061	-24.476	45.595	-0.730	-0.637	-0.024
	8	20.143	-17.895	46.091	19.375	-18.687	46.087	-0.769	-0.793	-0.004
	9	19.838	-12.010	46.477	19.274	-12.888	46.455	-0.564	-0.878	-0.022
	10	19.486	-8.371	46.662	19.223	-9.224	46.625	-0.263	-0.853	-0.037
	11	13.594	-28.243	45.799	12.726	-28.801	45.825	-0.868	-0.558	0.026
	12	13.470	-24.105	46.298	12.807	-24.595	46.281	-0.662	-0.490	-0.017
	13	13.772	-18.179	46.797	13.079	-18.712	46.764	-0.693	-0.533	-0.033
	14	13.446	-13.308	47.130	12.876	-14.072	47.132	-0.570	-0.764	0.002
	15	13.891	-9.110	47.271	13.223	-9.785	47.242	-0.668	-0.675	-0.029

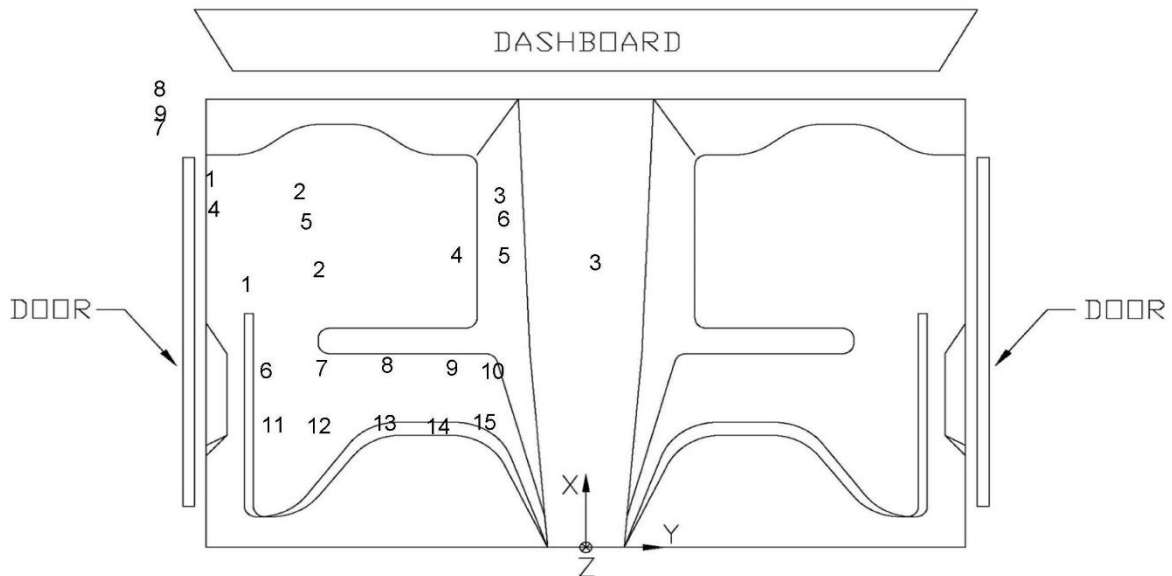


Figure C-7. Occupant Compartment Deformation Data - Set 2, Test No. NELON-1

VEHICLE PRE/POST CRUSH
INTERIOR CRUSH - SET 2

TEST: NELON-2
VEHICLE: Dodge Ram 1500

	POINT	X (in.)	Y (in.)	Z (in.)	X' (in.)	Y' (in.)	Z' (in.)	ΔX (in.)	ΔY (in.)	ΔZ (in.)
DASH	1	39.991	-31.020	27.576	39.905	-31.051	27.778	-0.087	-0.031	0.202
	2	39.604	-18.345	27.887	39.465	-18.300	27.965	-0.139	0.045	0.078
	3	37.469	-6.511	28.217	37.407	-6.514	28.273	-0.062	-0.003	0.056
	4	36.361	-31.609	14.932	36.421	-31.459	14.936	0.060	0.150	0.004
	5	36.106	-19.120	14.813	36.157	-19.178	14.779	0.051	-0.058	-0.034
	6	34.631	-6.380	14.648	34.604	-6.259	14.801	-0.027	0.122	0.153
SIDE PANEL	7	45.549	-38.025	5.833	45.575	-37.987	5.776	0.026	0.038	-0.056
	8	48.143	-38.151	5.345	48.117	-38.117	5.323	-0.026	0.033	-0.023
	9	46.516	-38.153	3.154	46.529	-38.107	3.163	0.014	0.047	0.009
IMPACT SIDE DOOR	10	10.353	-40.967	19.139	10.292	-39.300	19.098	-0.061	1.667	-0.041
	11	22.897	-40.901	18.697	22.874	-39.801	18.776	-0.023	1.100	0.079
	12	34.026	-40.899	18.123	33.929	-40.296	18.339	-0.097	0.603	0.216
	13	10.869	-40.328	1.169	10.718	-39.379	1.040	-0.151	0.950	-0.129
	14	26.919	-39.846	0.320	26.813	-39.181	0.330	-0.106	0.665	0.009
	15	39.518	-40.411	-0.835	39.409	-40.290	-0.797	-0.109	0.121	0.038
ROOF	1	27.965	-28.263	42.346	27.972	-28.186	42.413	0.006	0.077	0.068
	2	29.228	-22.183	42.816	29.129	-22.136	42.935	-0.099	0.046	0.119
	3	30.014	-16.214	43.121	29.901	-16.170	43.243	-0.113	0.044	0.122
	4	30.535	-10.099	43.270	30.493	-9.988	43.345	-0.042	0.111	0.075
	5	30.705	-5.698	43.243	30.476	-5.690	43.378	-0.229	0.007	0.134
	6	20.160	-26.702	45.564	19.978	-26.542	45.729	-0.182	0.160	0.165
	7	20.970	-21.893	45.956	20.812	-21.921	46.051	-0.158	-0.028	0.095
	8	21.939	-16.274	46.211	21.787	-16.339	46.258	-0.152	-0.065	0.047
	9	22.795	-9.998	46.284	22.589	-10.073	46.323	-0.207	-0.075	0.038
	10	23.190	-6.118	46.240	22.981	-6.209	46.278	-0.209	-0.091	0.038
	11	14.242	-26.924	46.302	14.225	-26.804	46.480	-0.017	0.120	0.177
	12	14.965	-21.987	46.742	14.847	-21.858	46.853	-0.117	0.130	0.111
	13	15.606	-16.807	47.031	15.588	-16.792	47.074	-0.018	0.014	0.043
	14	16.546	-10.787	47.147	16.375	-10.817	47.184	-0.171	-0.030	0.037
	15	16.729	-6.822	47.174	16.652	-6.692	47.195	-0.078	0.130	0.021

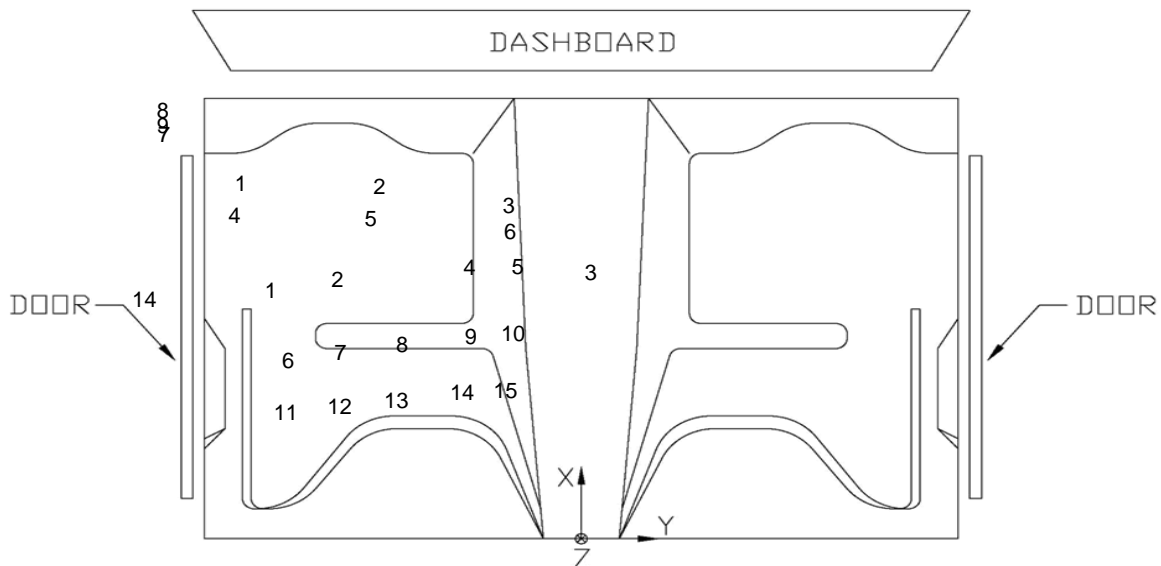


Figure C-8. Occupant Compartment Deformation Data - Set 2, Test No. NELON-2

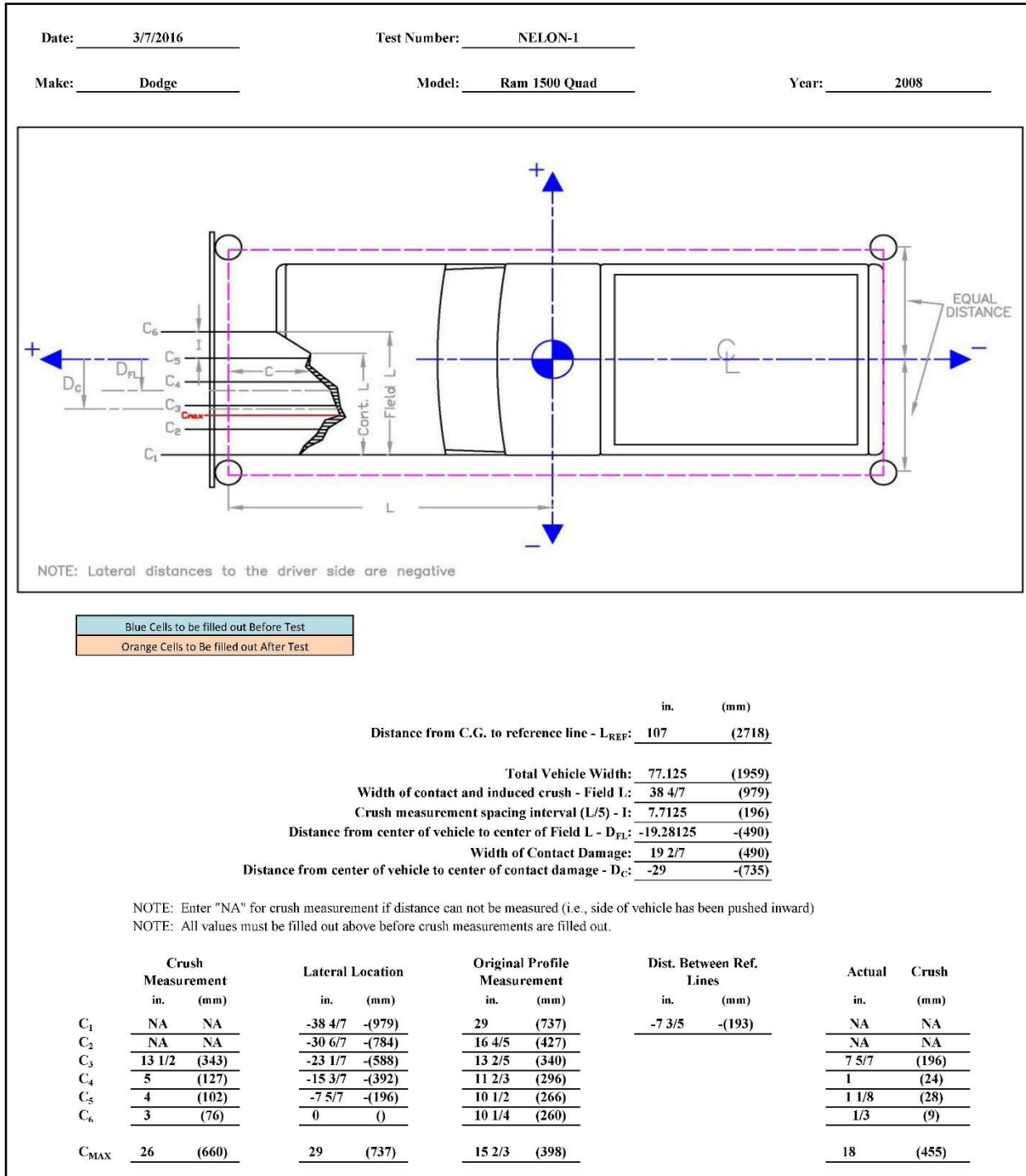


Figure C-9. Exterior Vehicle Crush (NASS) - Front, Test No. NELON-1

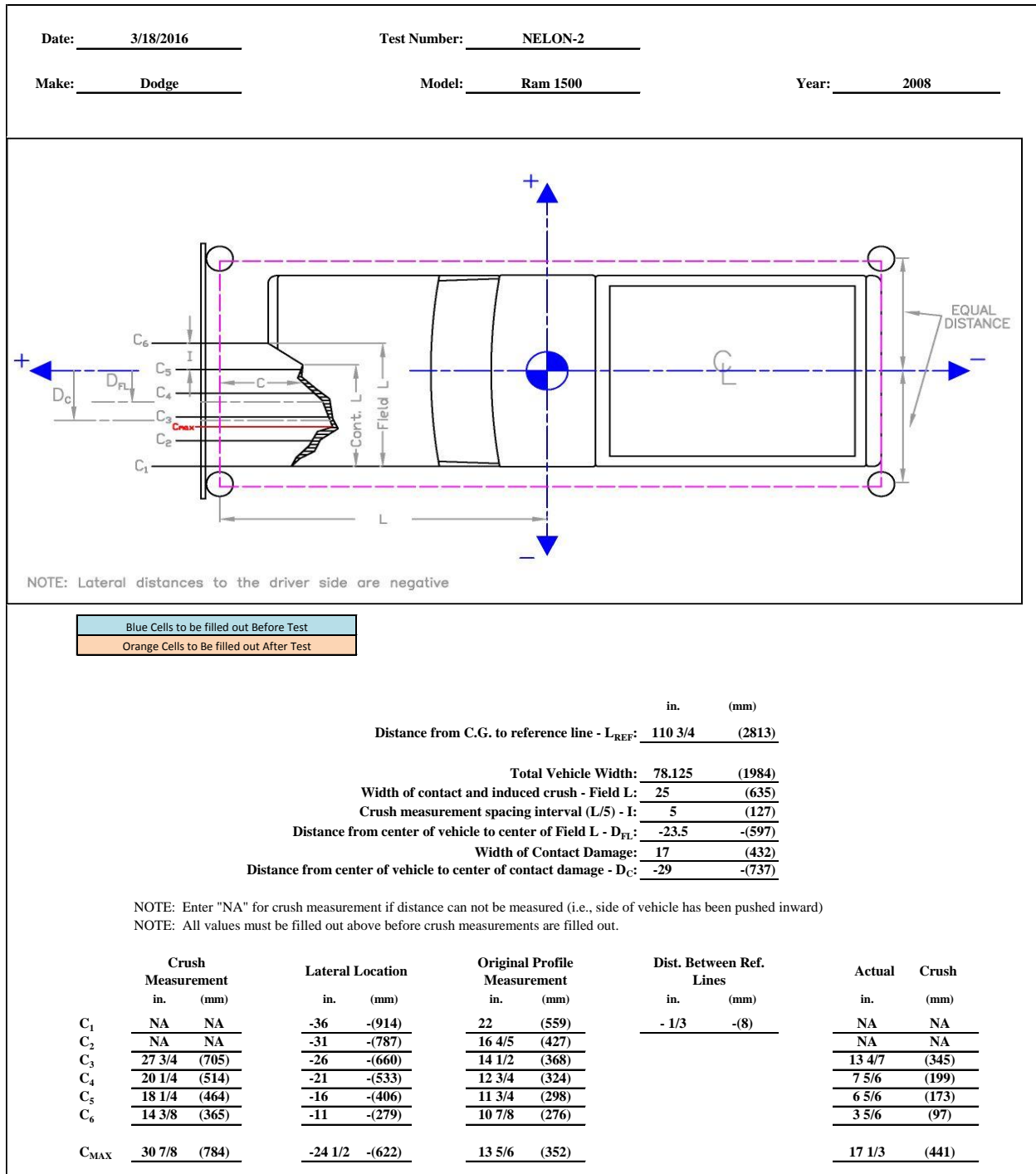
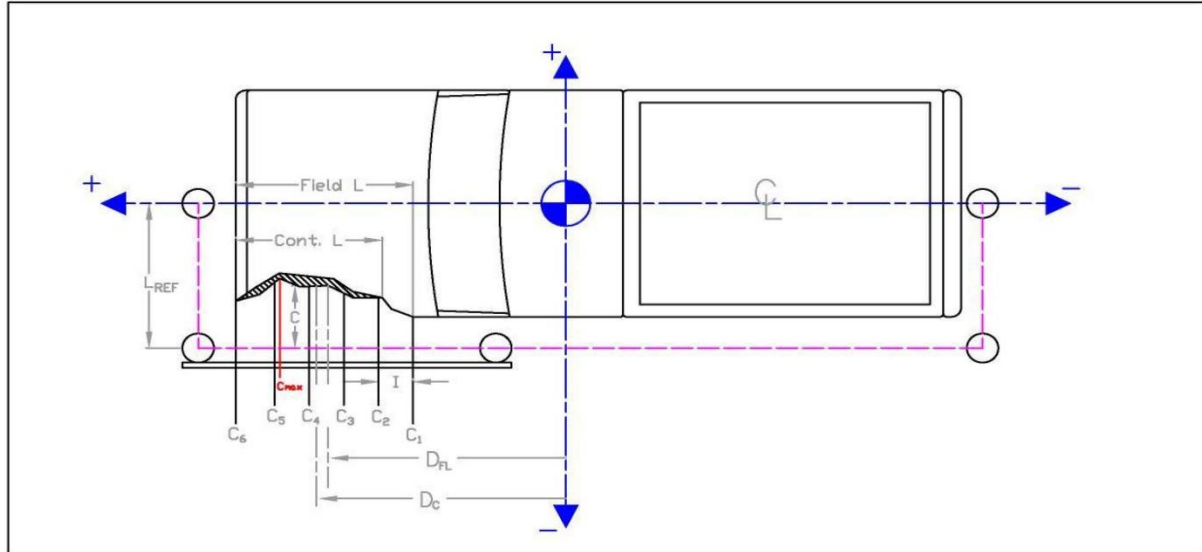


Figure C-10. Exterior Vehicle Crush (NASS) - Front, Test No. NELON-2

Date: 3/7/2016 Test Number: NELON-1
Make: Dodge Model: Ram 1500 Quad Year: 2008



Blue Cells to be filled out Before Test
Orange Cells to Be filled out After Test

Distance from centerline to reference line - L_{REF} : 47 in. (1194) mm
Total Vehicle Length: 228.625 (5807)
Width of contact and induced crush - Field L: 228 5/8 (5807)
Crush measurement spacing interval (L/5) - I: 45.725 (1161)
Distance from vehicle c.g. to center of Field L - D_{FL} : -7 5/6 -(199)
Width of Contact Damage: 228 5/8 (5807)
Distance from vehicle c.g. to center of contact damage - D_C : -7 5/6 -(199)

NOTE: Enter "NA" for crush measurement if distance can not be measured (i.e., front of vehicle has been pushed inward or tire has been removed)
NOTE: All values must be filled out above before crush measurements are filled out.

	Crush Measurement		Longitudinal Location		Original Profile Measurement		Dist. Between Ref. Lines		Actual Crush	
	in.	(mm)	in.	(mm)	in.	(mm)	in.	(mm)	in.	(mm)
C ₁	NA	NA	-122 1/7	-(3102)	37	(940)	-3	-(76)	NA	NA
C ₂	NA	NA	-76 3/7	-(1941)	10 1/2	(267)			NA	NA
C ₃	10 3/4	(273)	-30 2/3	-(780)	11 2/3	(297)			2	(52)
C ₄	6 1/4	(159)	15	(382)	11 1/4	(286)			-2	-(51)
C ₅	NA	NA	60 3/4	(1543)	10 1/2	(267)			NA	NA
C ₆	NA	NA	106 1/2	(2705)	37	(940)			NA	NA
C _{MAX}	20 1/2	(521)	84	(2134)	11 1/4	(286)			12 1/4	(311)

Figure C-11. Exterior Vehicle Crush (NASS) - Side, Test No. NELON-1

Date: <u>3/18/2016</u>	Test Number: <u>NELON-2</u>	
Make: <u>Dodge</u>	Model: <u>Ram 1500</u>	Year: <u>2008</u>

Blue Cells to be filled out Before Test
Orange Cells to be filled out After Test

	in.	(mm)
Distance from centerline to reference line - L_{REF} :	45	(1143)
Total Vehicle Length:	227.25	(5772)
Width of contact and induced crush - Field L:	227 1/4	(5772)
Crush measurement spacing interval (L/5) - I:	45.45	(1154)
Distance from vehicle c.g. to center of Field L - D_{FL} :	-11	-(277)
Width of Contact Damage:	227 1/4	(5772)
Distance from vehicle c.g. to center of contact damage - D_C :	-11	-(279)

NOTE: Enter "NA" for crush measurement if distance can not be measured (i.e., front of vehicle has been pushed inward or tire has been removed)

NOTE: All values must be filled out above before crush measurements are filled out.

	Crush Measurement		Longitudinal Location		Original Profile Measurement		Dist. Between Ref. Lines		Actual	Crush
	in.	(mm)	in.	(mm)	in.	(mm)	in.	(mm)		
C_1	NA	NA	-124 5/9	-(3164)	15 3/8	(391)	-5	-(127)	NA	NA
C_2	NA	NA	-79	-(2009)	10 1/2	(267)			NA	NA
C_3	7 1/2	(191)	-33 2/3	-(855)	11 4/7	(294)			1	(24)
C_4	5 1/2	(140)	11 4/5	(300)	11 1/4	(286)			- 3/4	-(19)
C_5	NA	NA	57 1/4	(1454)	10 1/2	(267)			NA	NA
C_6	NA	NA	102 5/7	(2609)	37	(940)			NA	NA
C_{MAX}	22	(559)	91 3/4	(2330)	14	(356)			13	(330)

S

Figure C-12. Exterior Vehicle Crush (NASS) - Side, Test No. NELON-2

Appendix D. Accelerometer and Rate Transducer Data Plots, Test No. NELON-1

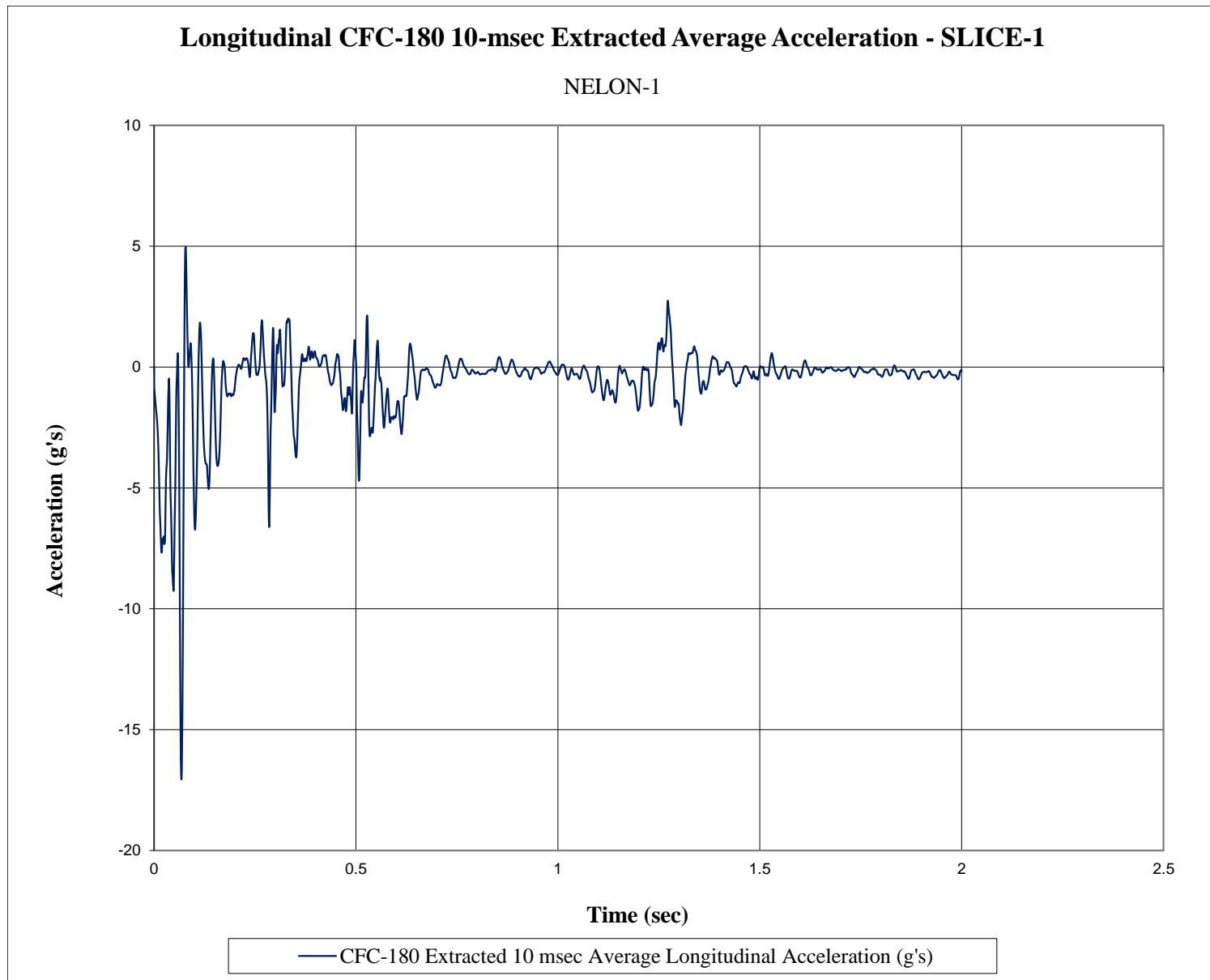


Figure D-1. 10-ms Average Longitudinal Deceleration (SLICE-1), Test No. NELON-1

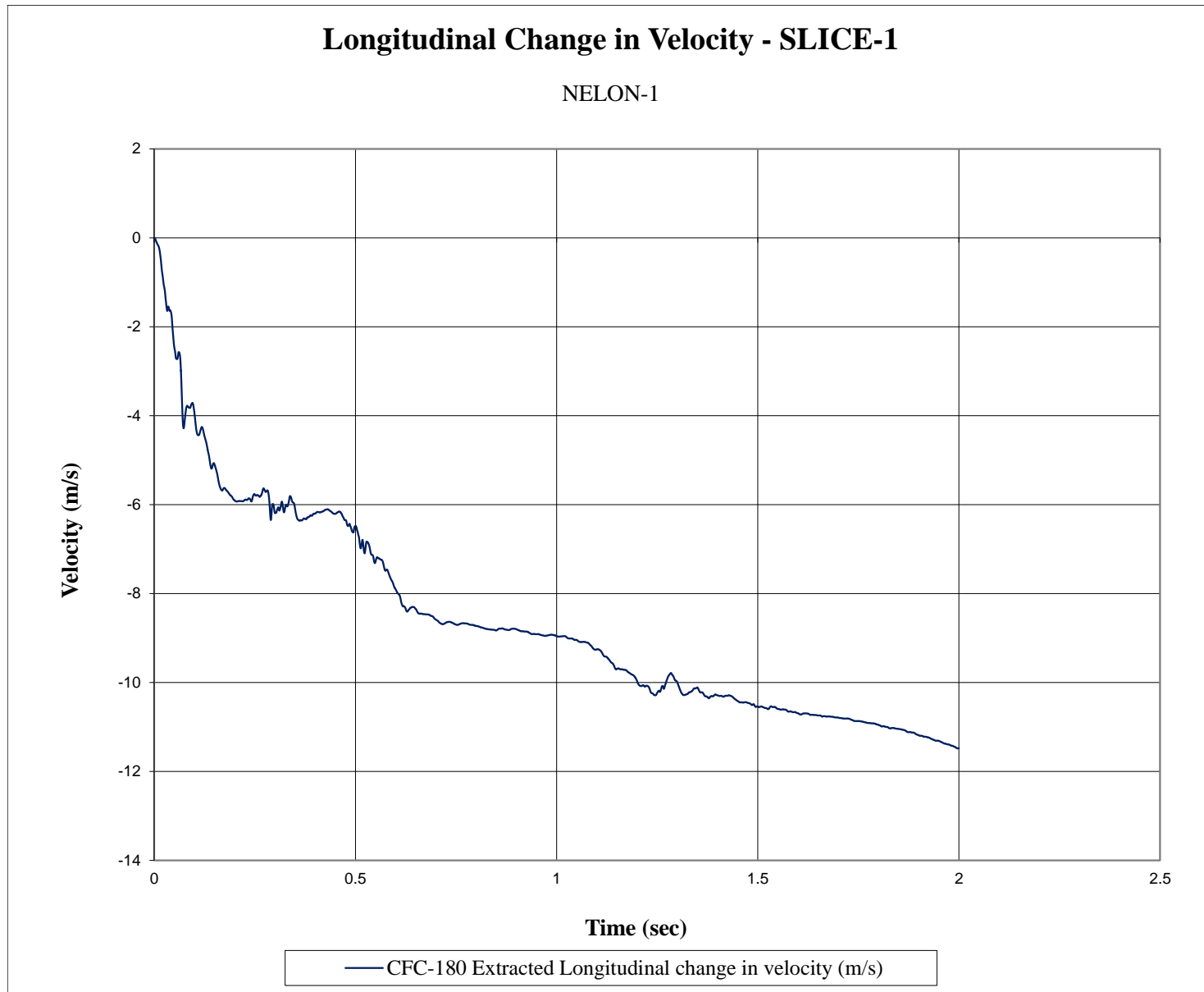


Figure D-2. Longitudinal Occupant Impact Velocity (SLICE-1), Test No. NELON-1

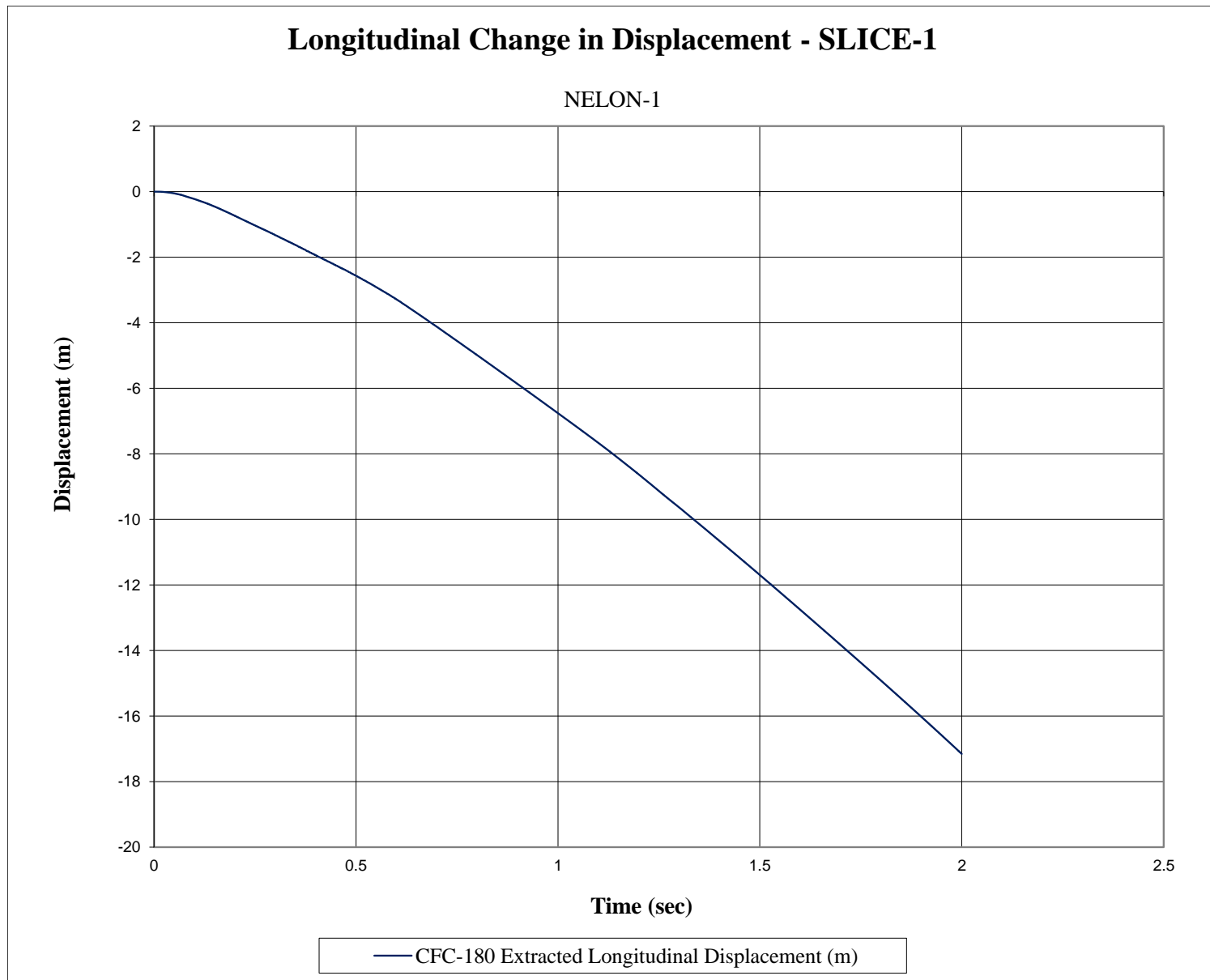


Figure D-3. Longitudinal Occupant Displacement (SLICE-1), Test No. NELON-1

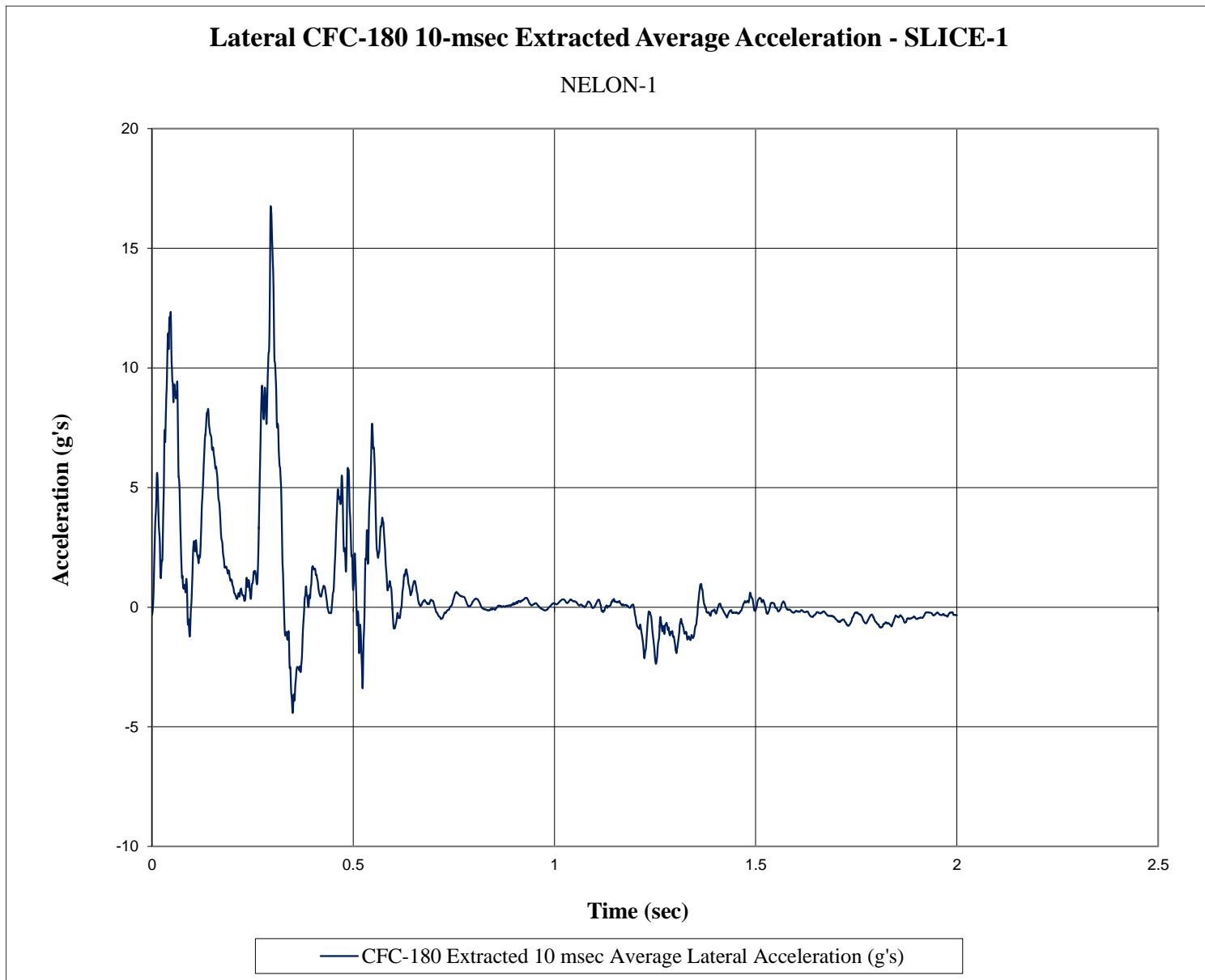


Figure D-4. 10-ms Average Lateral Deceleration (SLICE-1), Test No. NELON-1

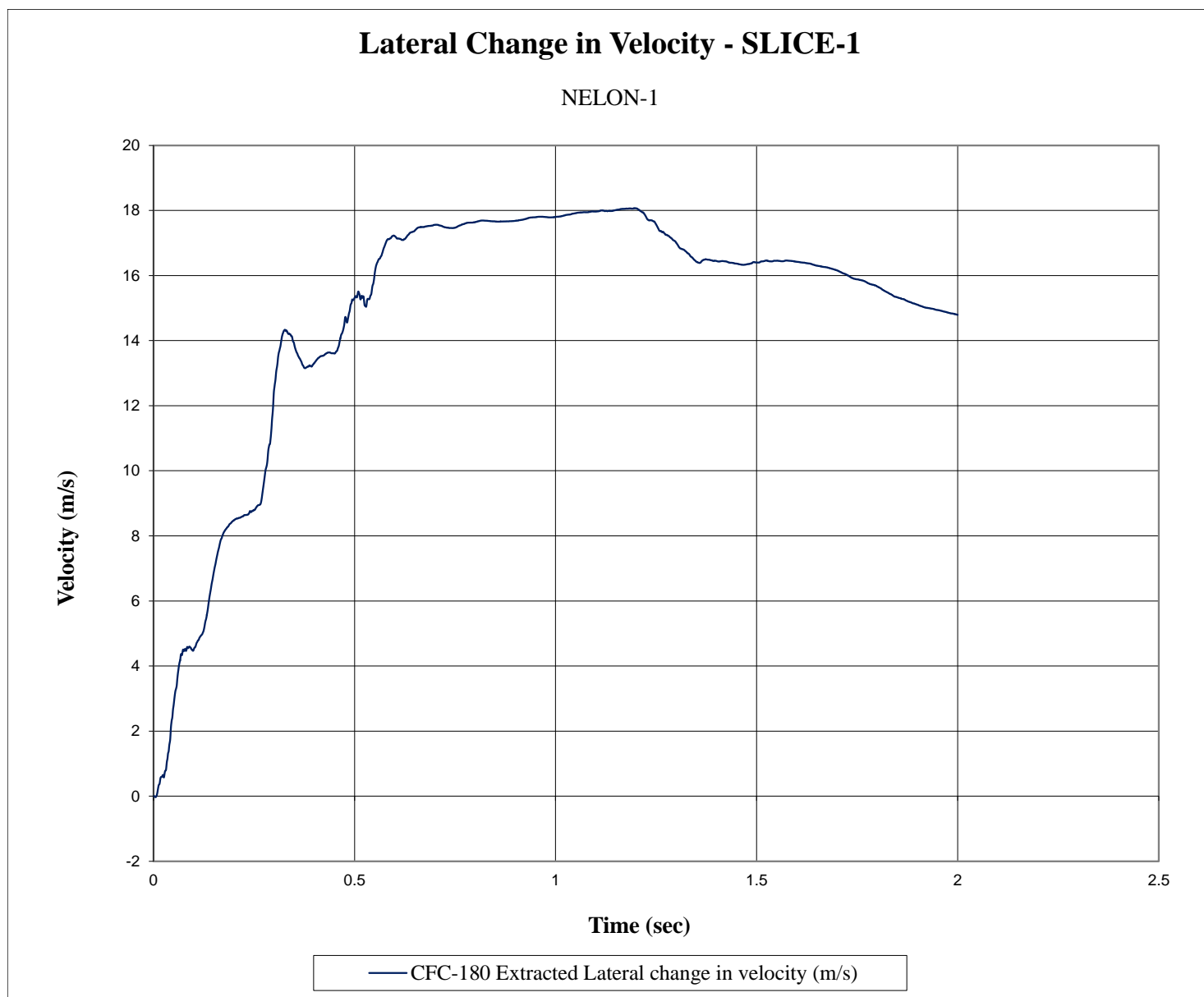


Figure D-5. Lateral Occupant Impact Velocity (SLICE-1), Test No. NELON-1

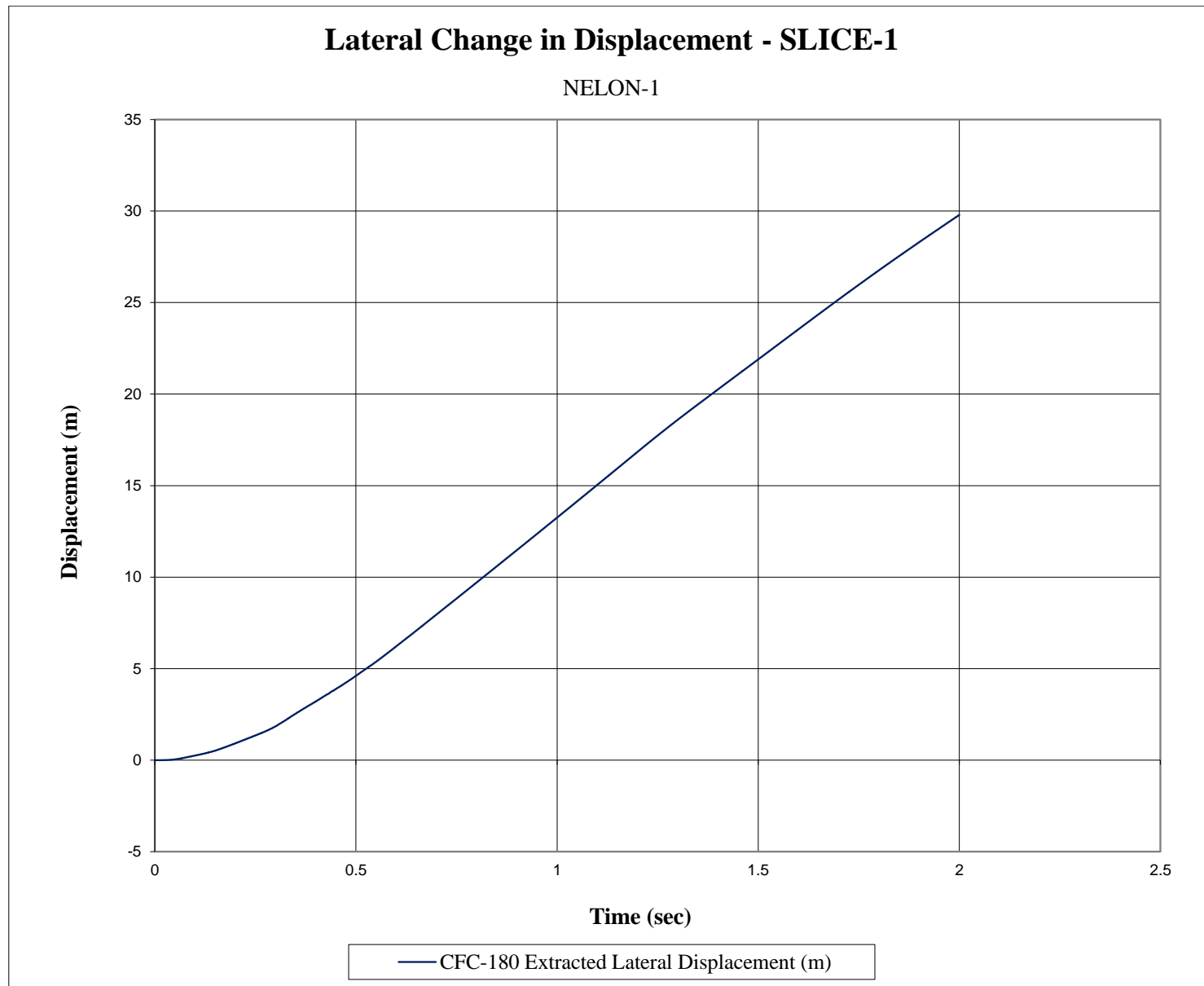


Figure D-6. Lateral Occupant Displacement (SLICE-1), Test No. NELON-1

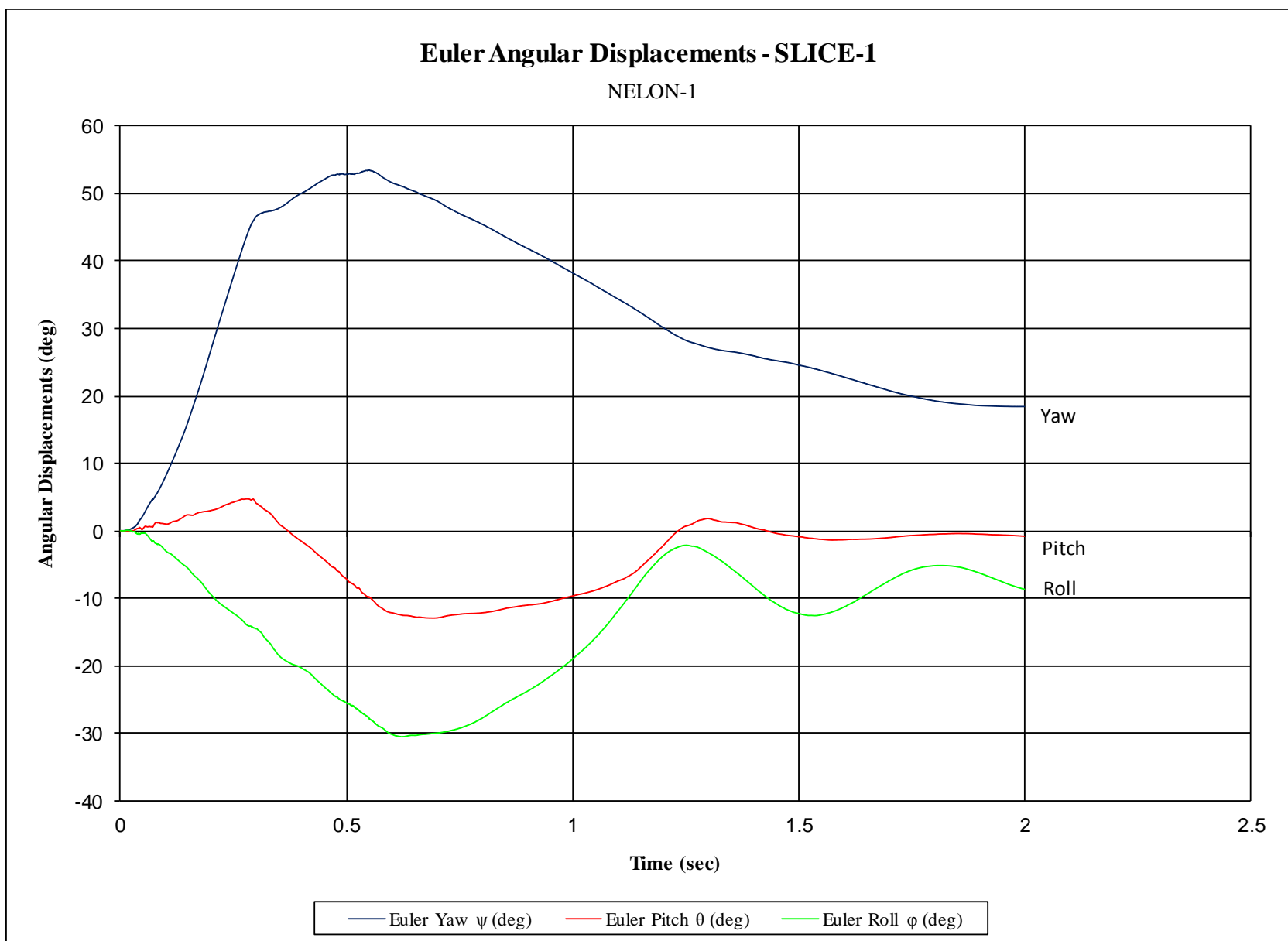


Figure D-7. Vehicle Angular Displacements (SLICE-1), Test No. NELON-1

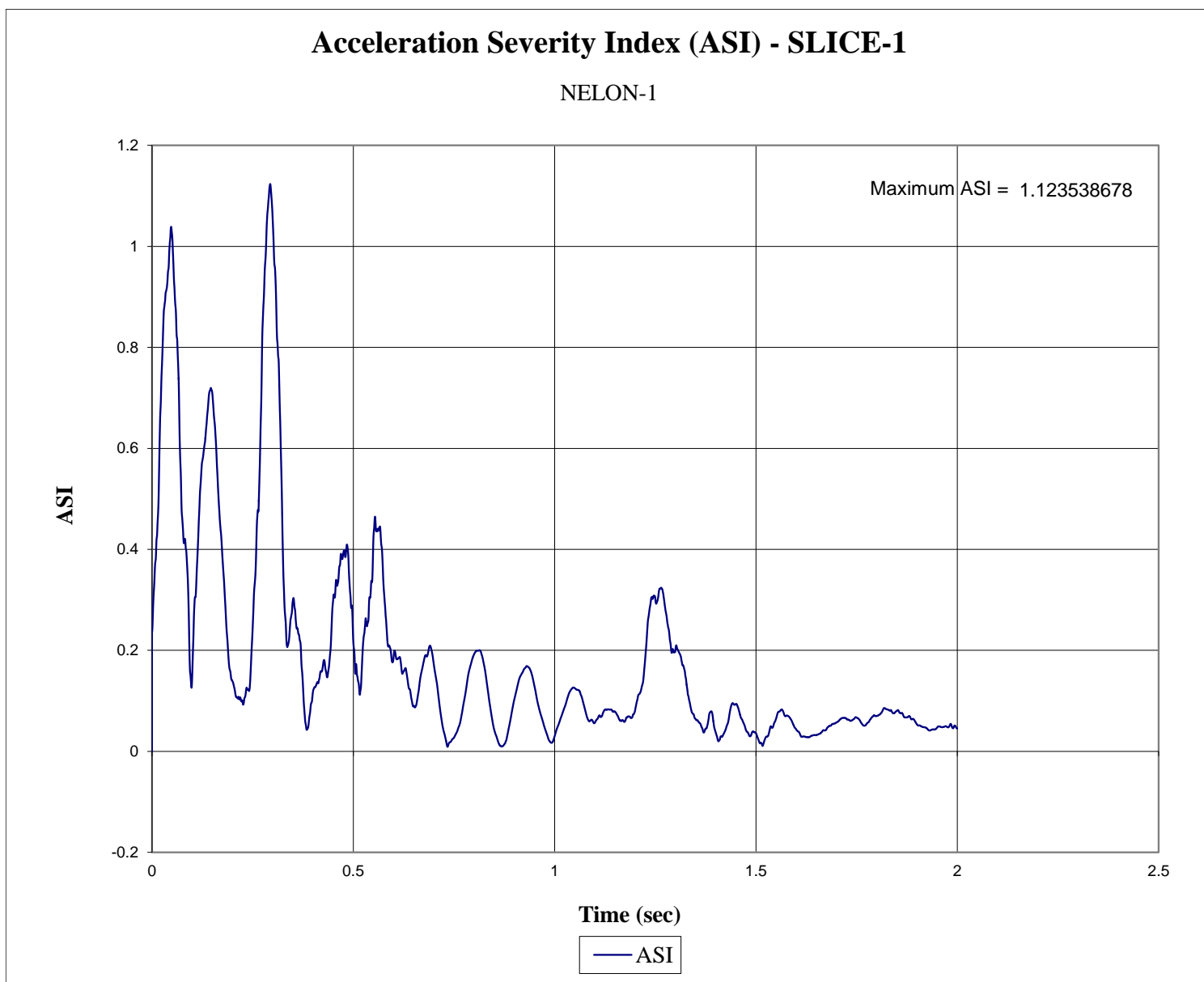


Figure D-8. Acceleration Severity Index (SLICE-1), Test No. NELON-1

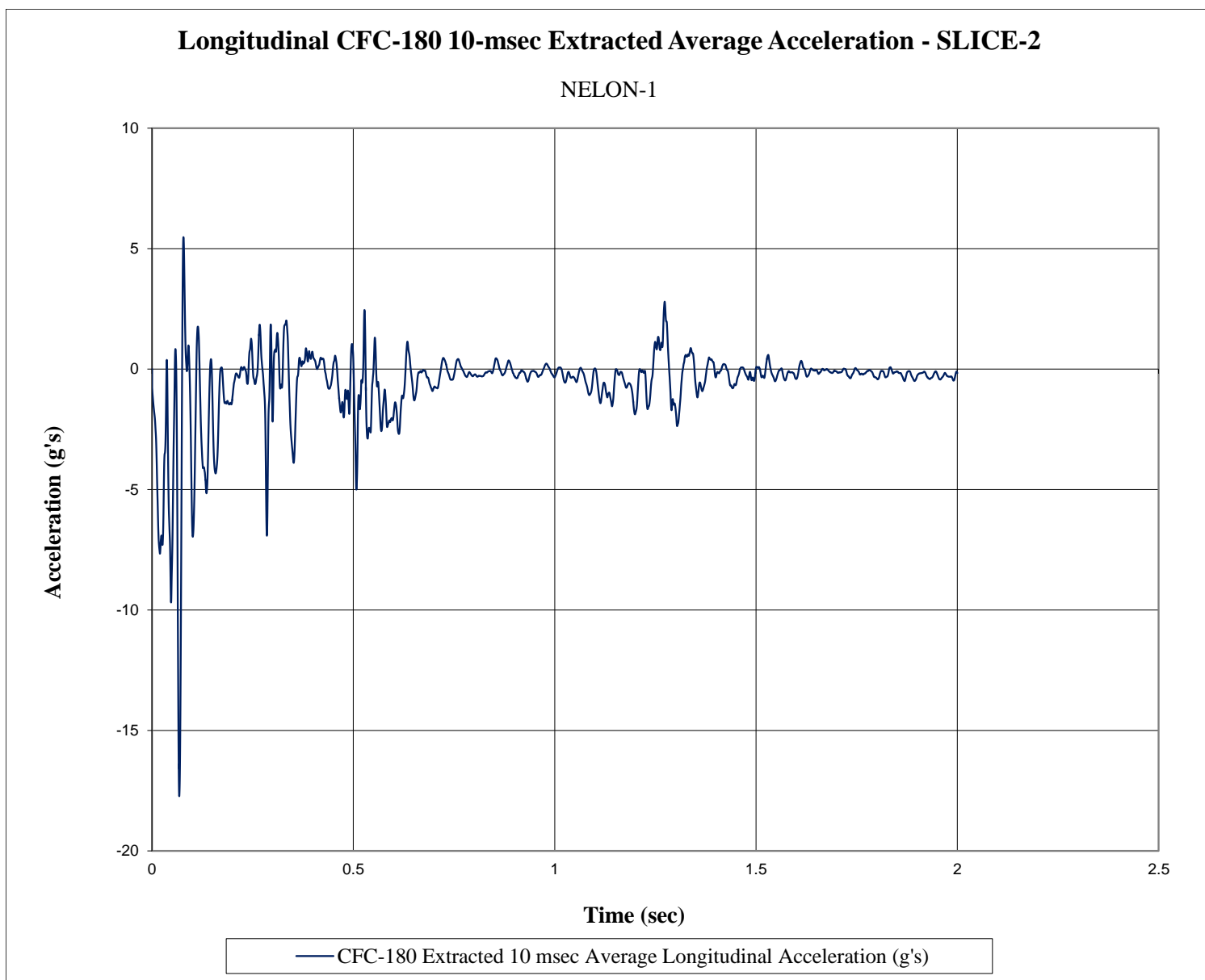


Figure D-9. 10-ms Average Longitudinal Deceleration (SLICE-2), Test No. NELON-1

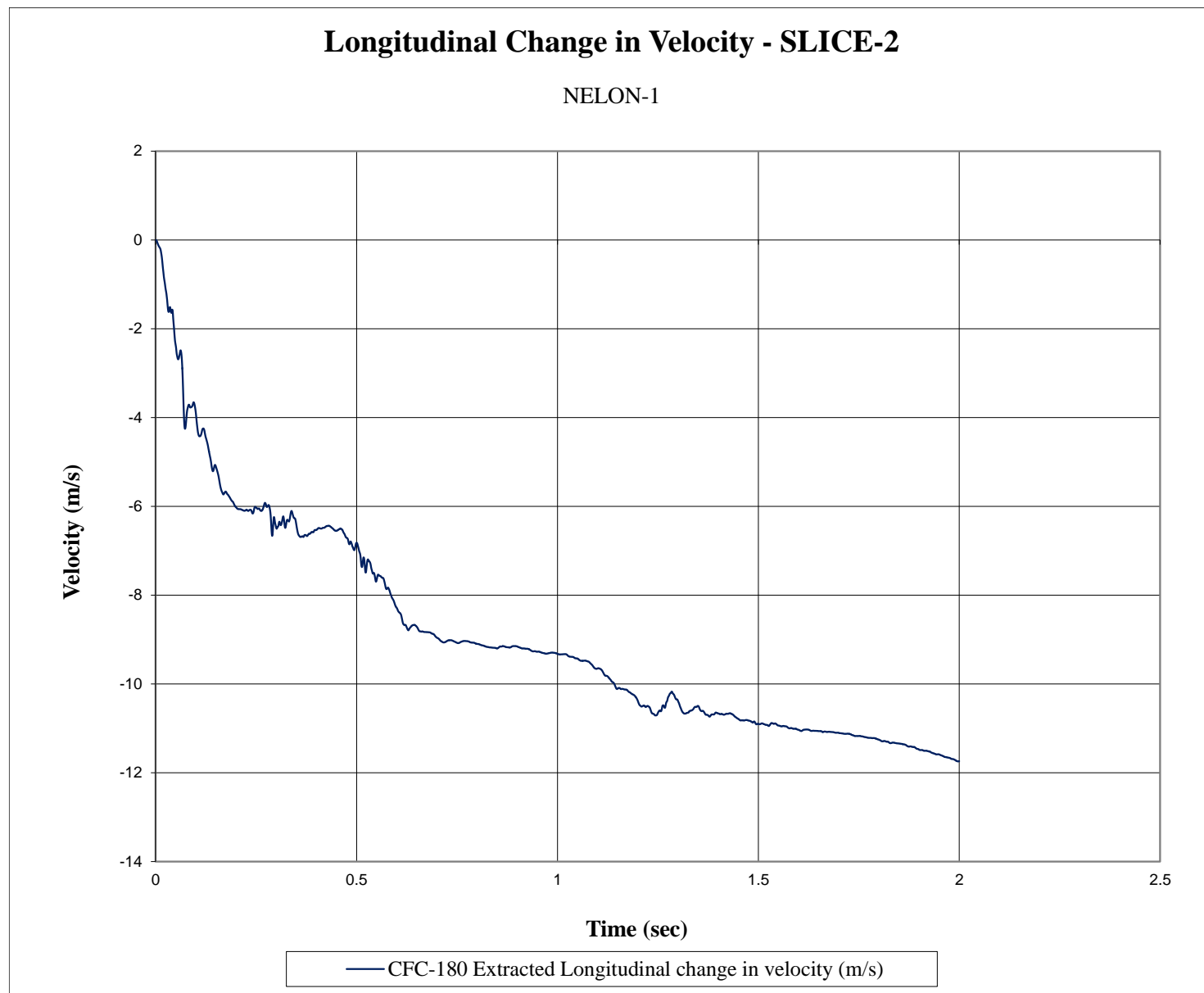


Figure D-10. Longitudinal Occupant Impact Velocity (SLICE-2), Test No. NELON-1

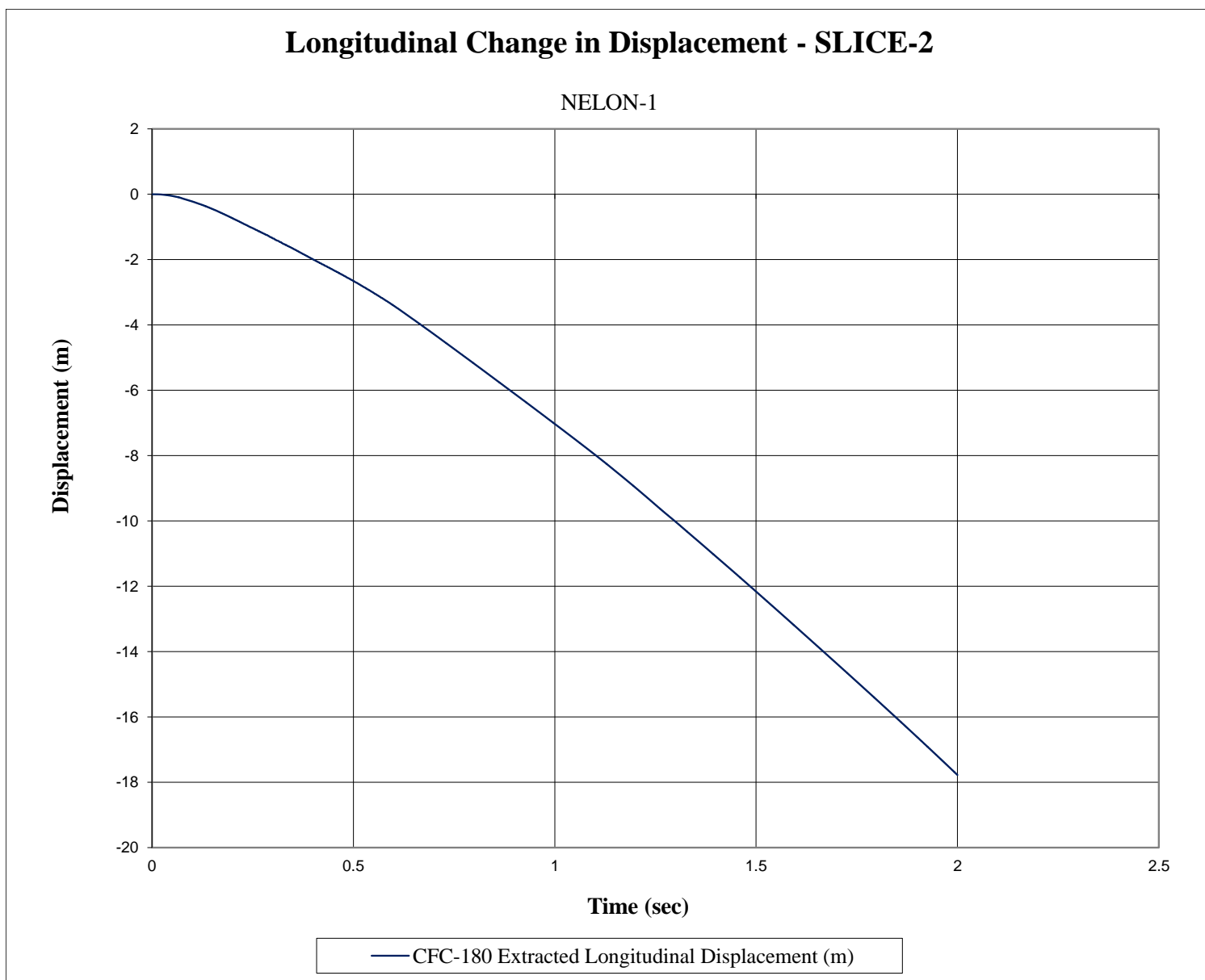


Figure D-11. Longitudinal Occupant Displacement (SLICE-2), Test No. NELON-1

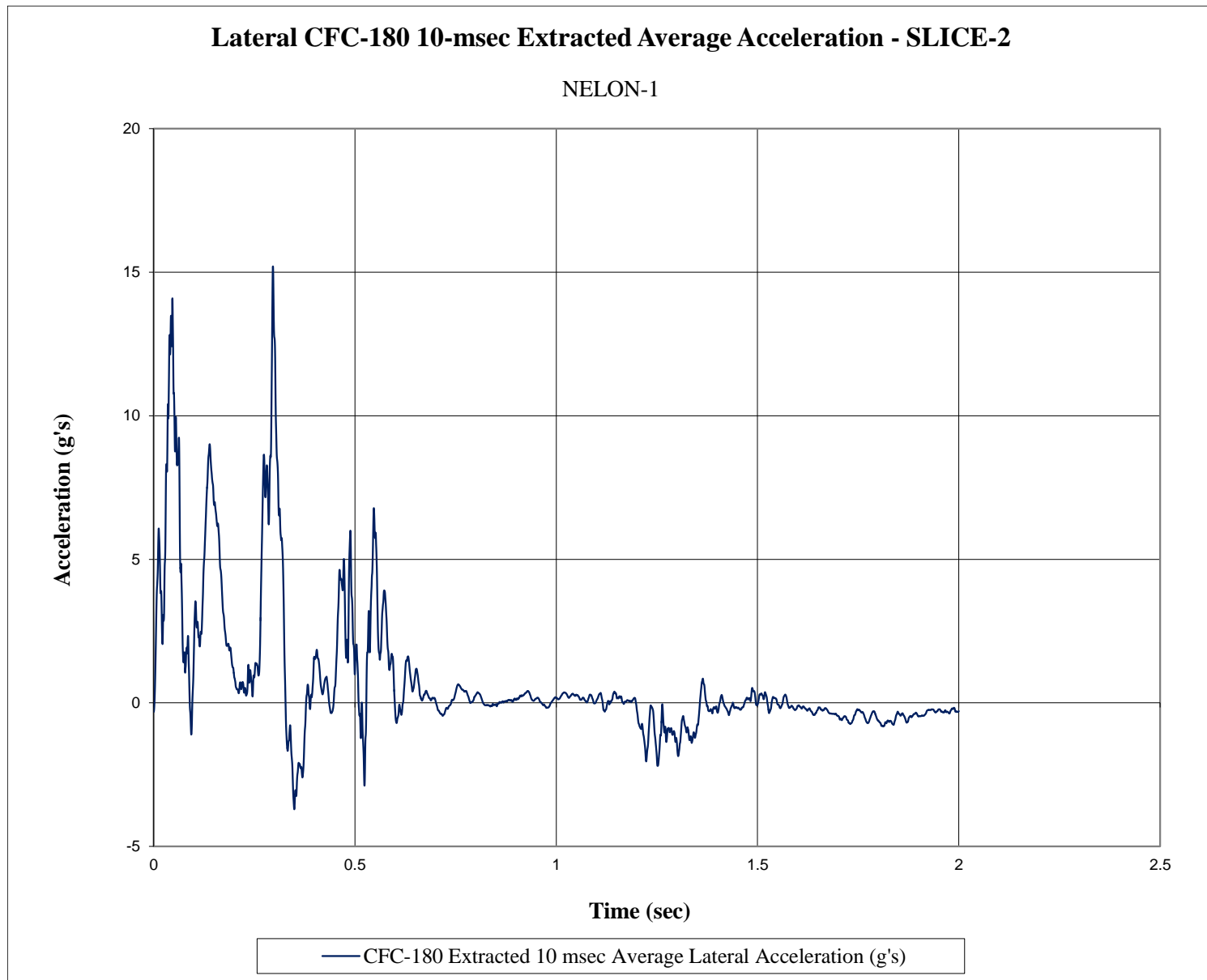


Figure D-12. 10-ms Average Lateral Deceleration (SLICE-2), Test No. NELON-1

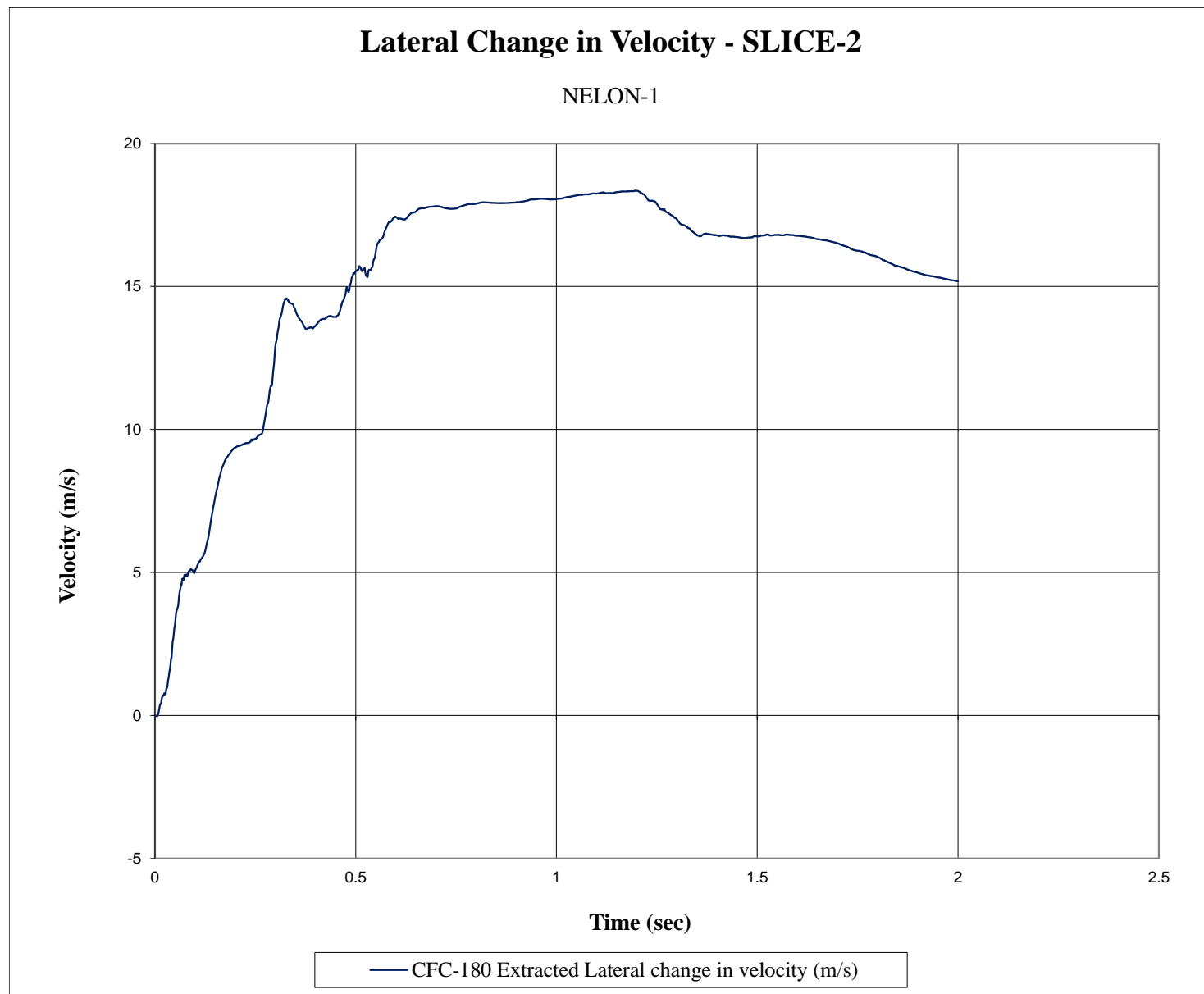


Figure D-13. Lateral Occupant Impact Velocity (SLICE-2), Test No. NELON-1

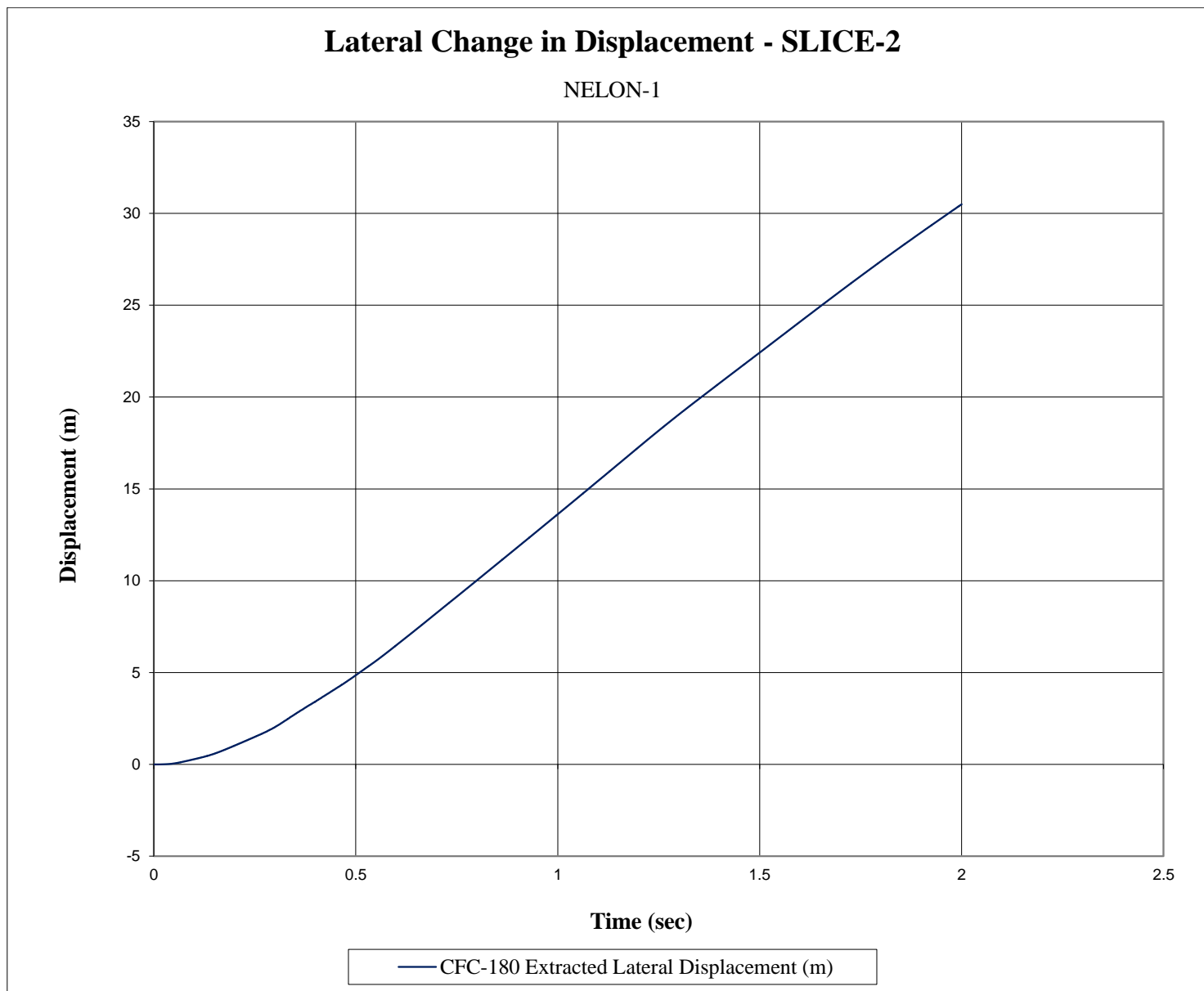


Figure D-14. Lateral Occupant Displacement (SLICE-2), Test No. NELON-1

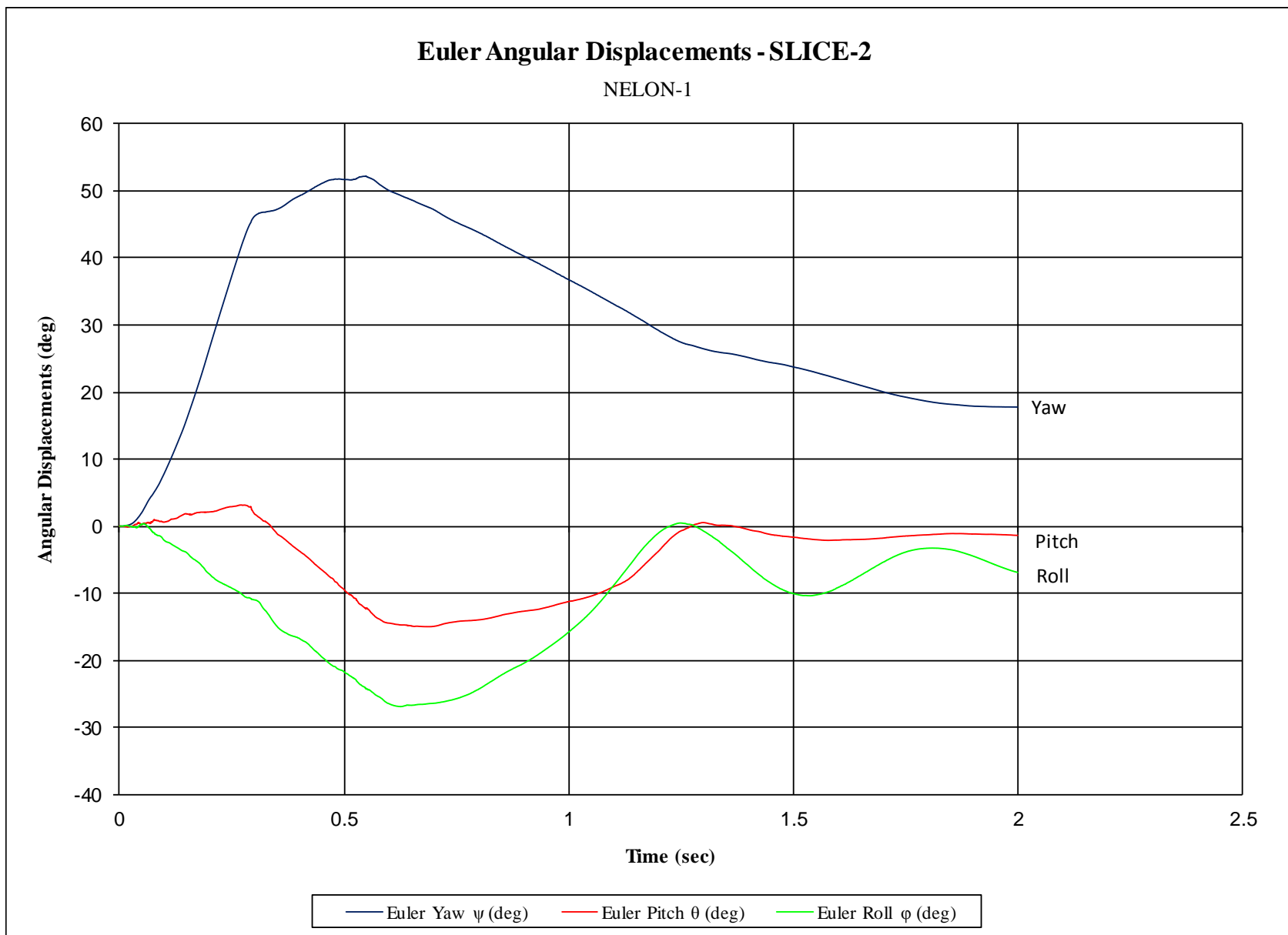


Figure D-15. Vehicle Angular Displacements (SLICE-2), Test No. NELON-1

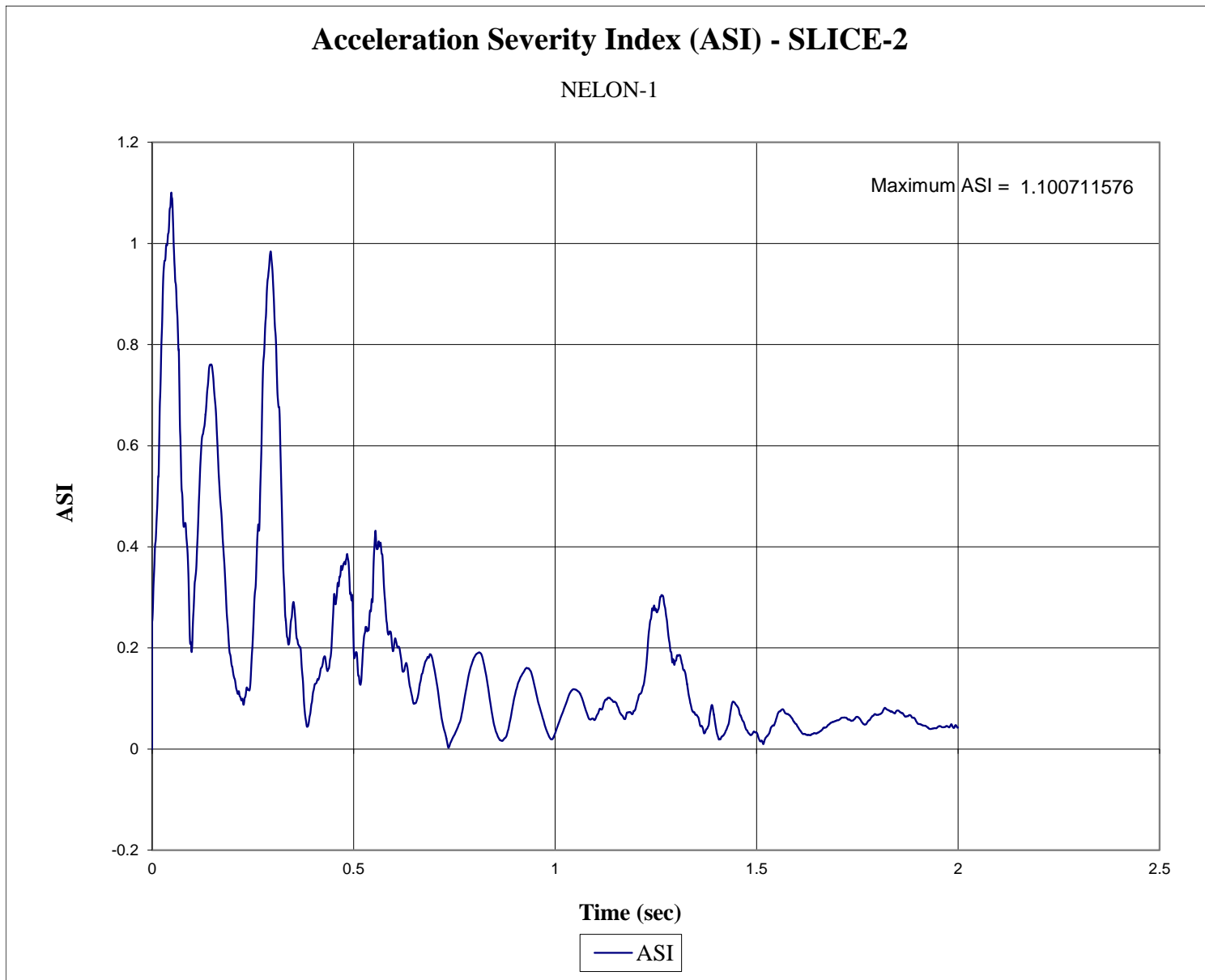


Figure D-16. Acceleration Severity Index (SLICE-2), Test No. NELON-1

Appendix E. Accelerometer and Rate Transducer Data Plots, Test No. NELON-2

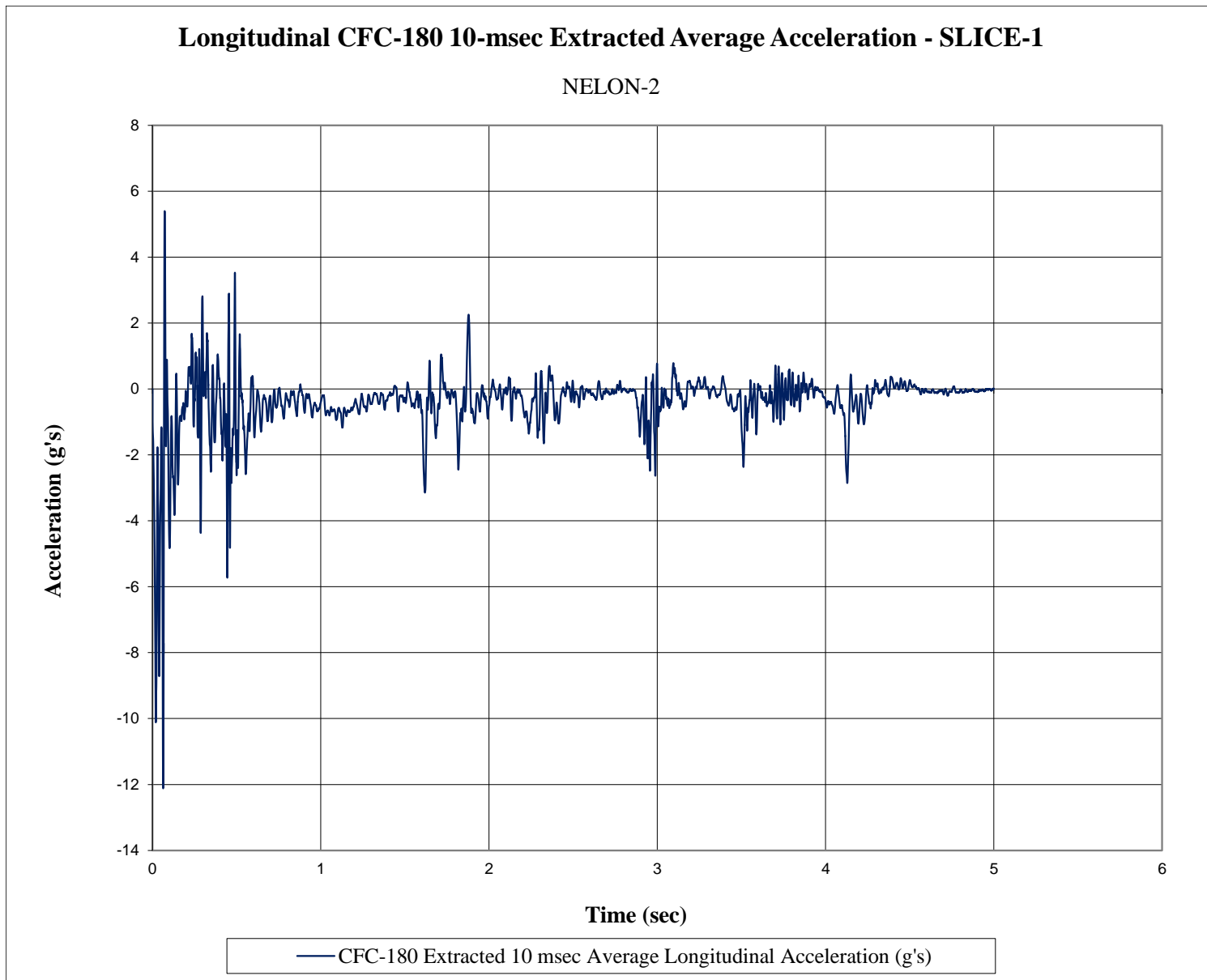


Figure E-1. 10-ms Average Longitudinal Deceleration (SLICE-1), Test No. NELON-2

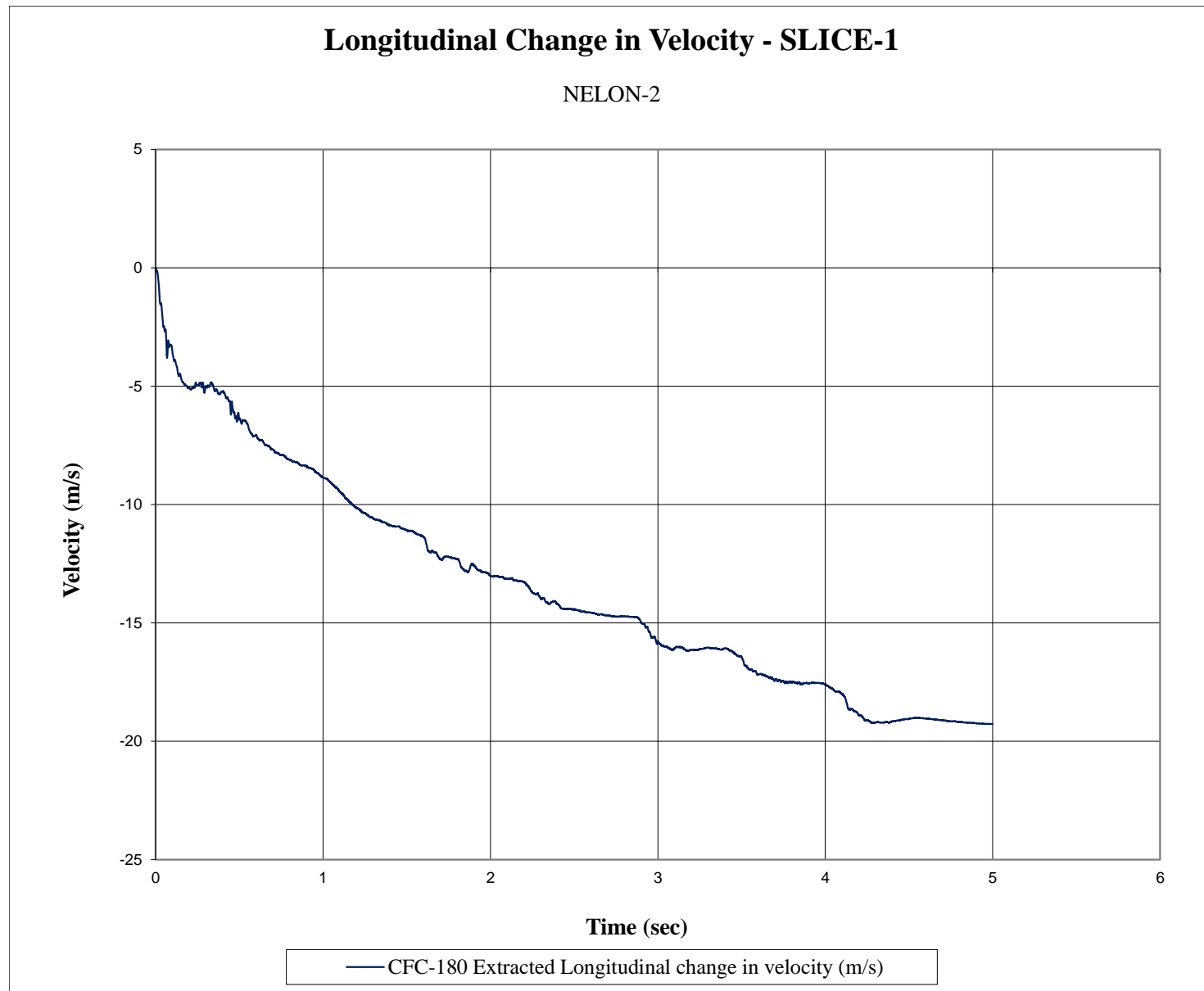


Figure E-2. Longitudinal Occupant Impact Velocity (SLICE-1), Test No. NELON-2

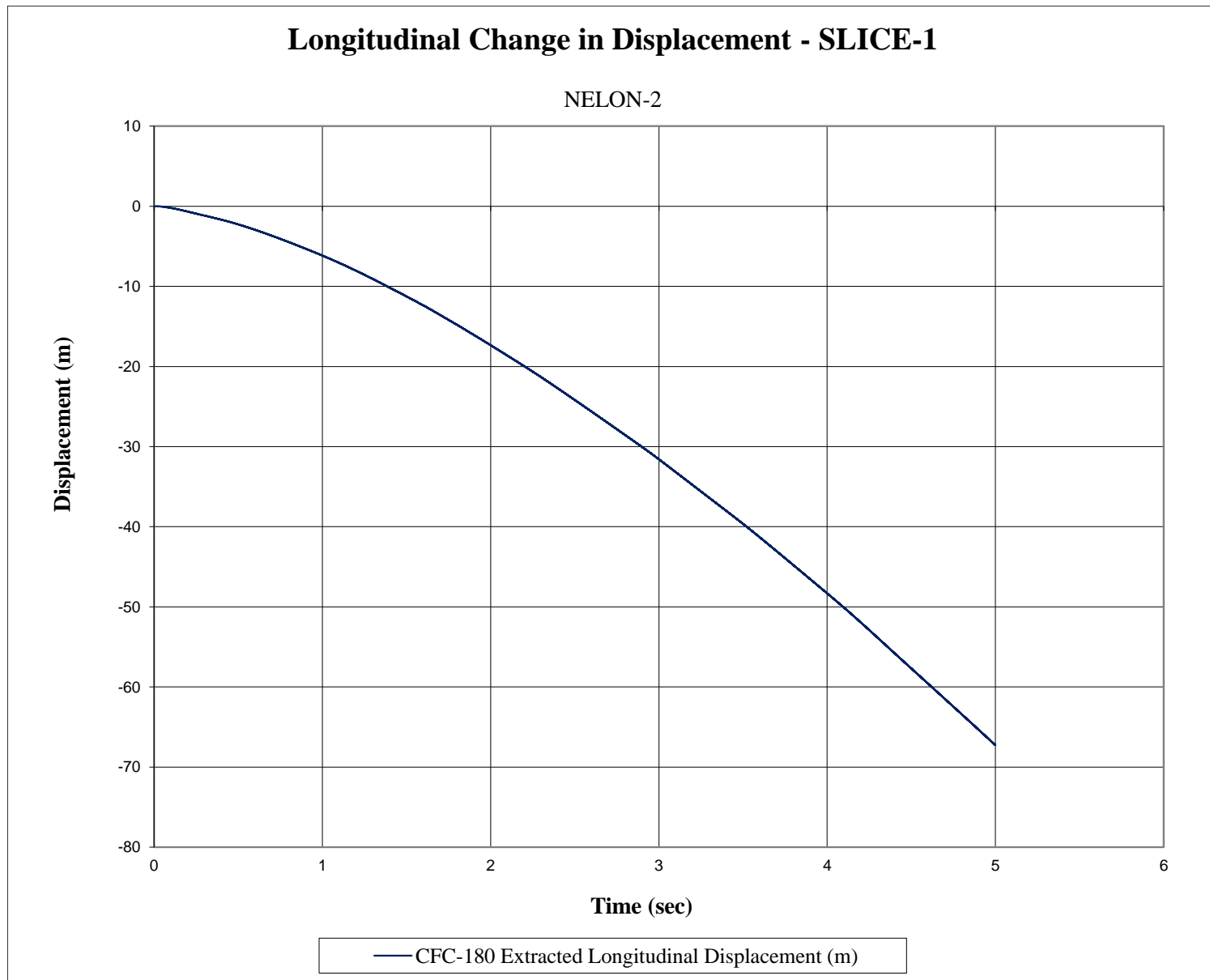


Figure E-3. Longitudinal Occupant Displacement (SLICE-1), Test No. NELON-2

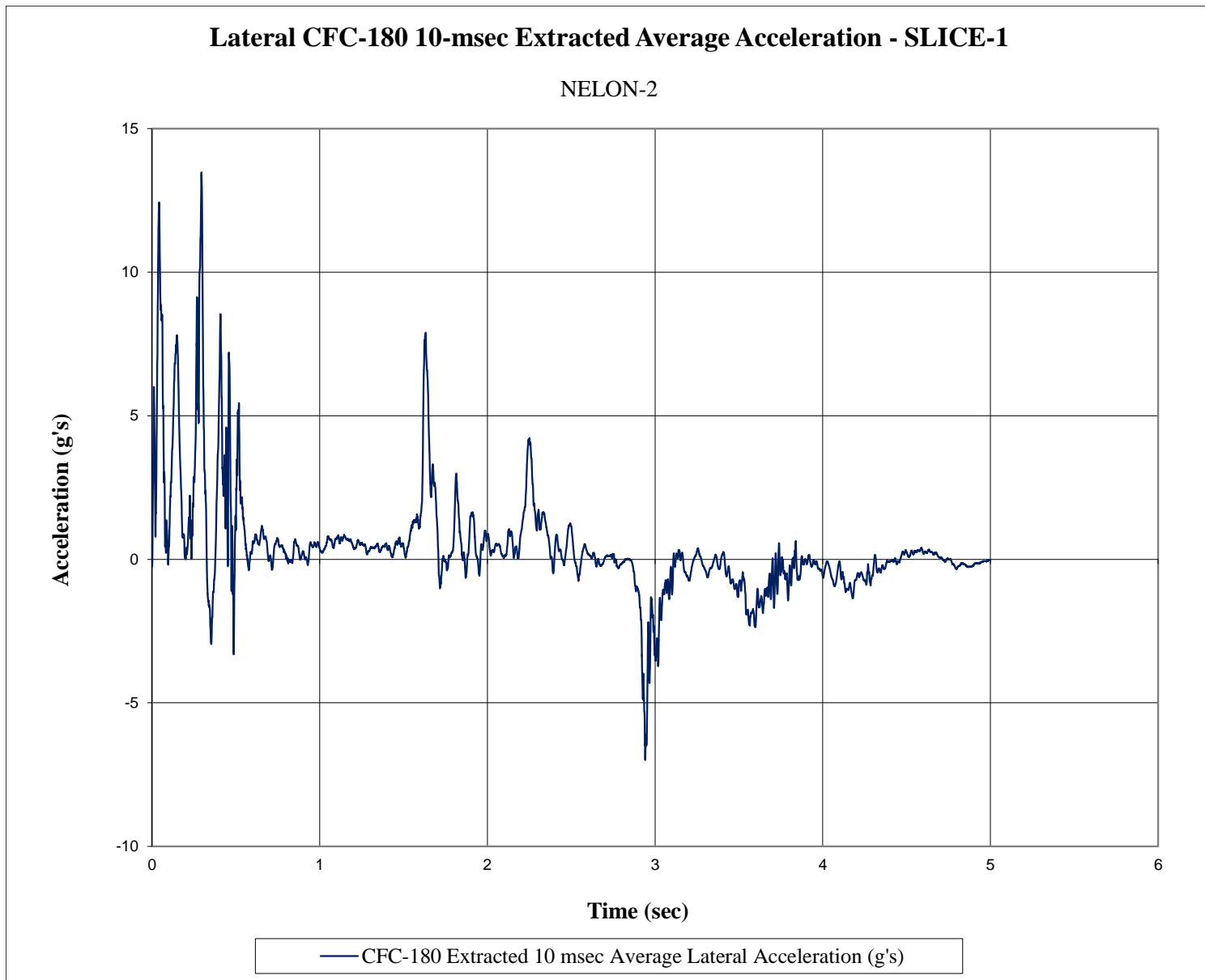


Figure E-4. 10-ms Average Lateral Deceleration (SLICE-1), Test No. NELON-2

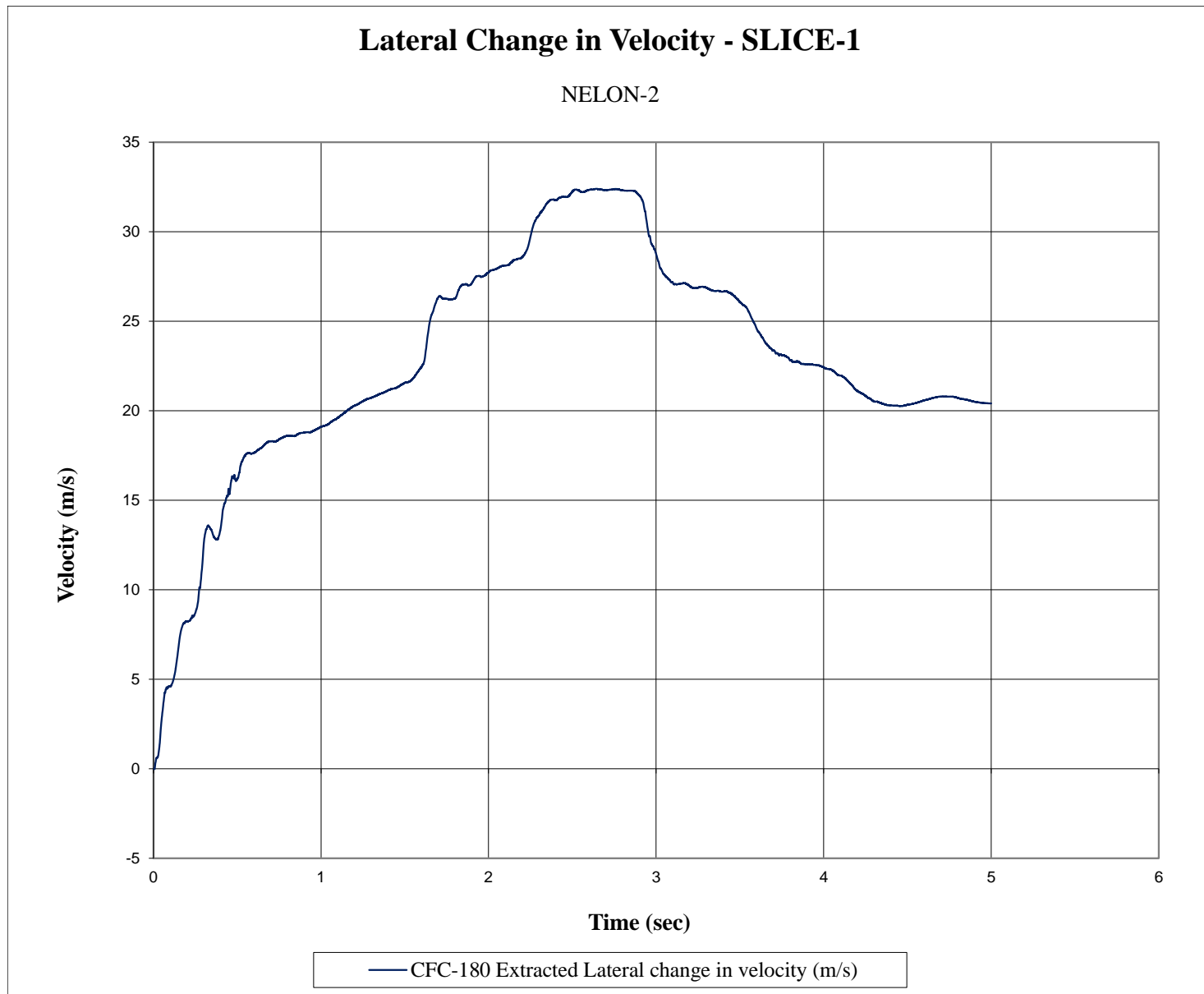


Figure E-5. Lateral Occupant Velocity (SLICE-1), Test No. NELON-2

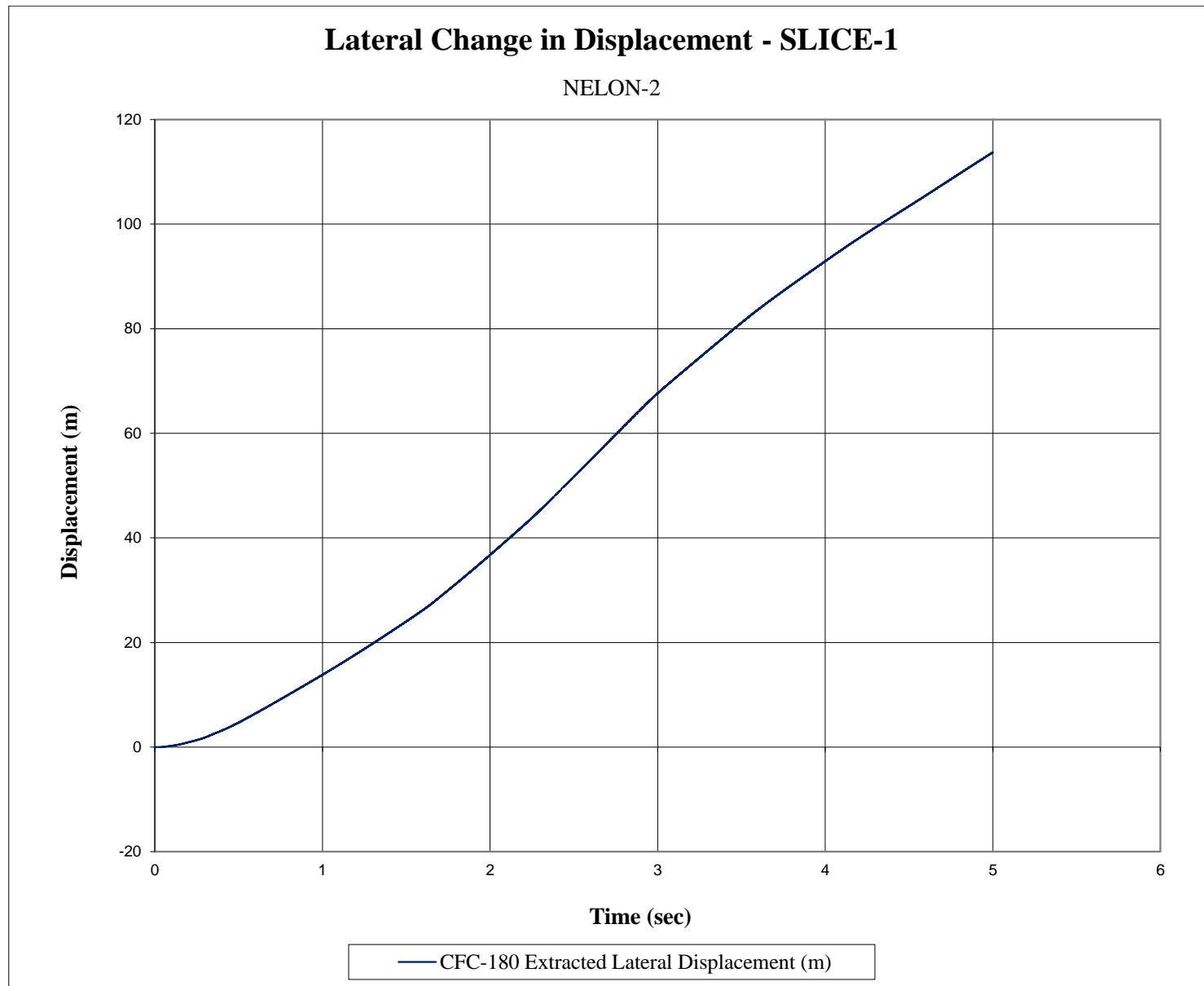


Figure E-6. Lateral Occupant Displacement (SLICE-1), Test No. NELON-2

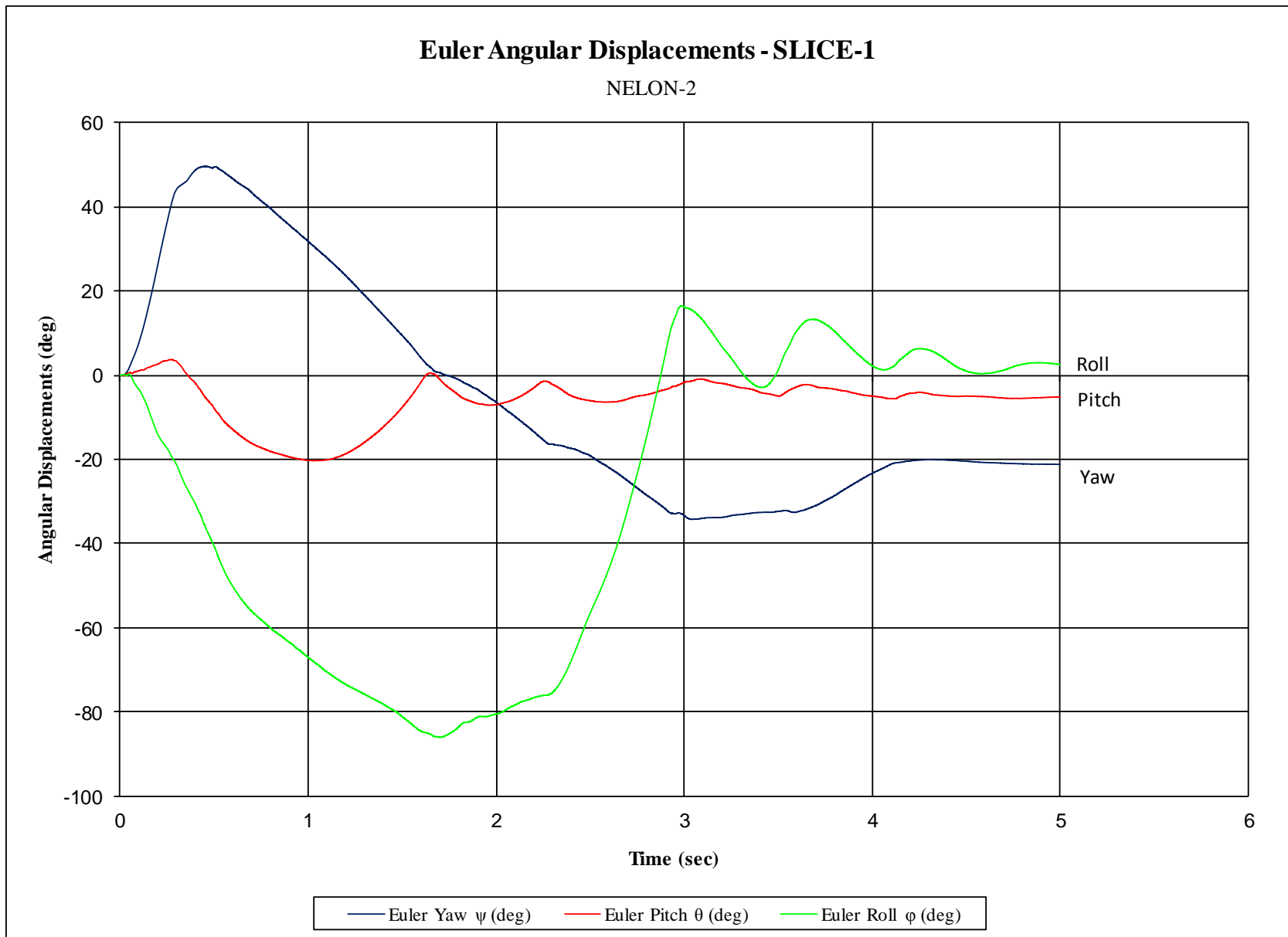


Figure E-7. Vehicle Angular Displacements (SLICE-1), Test No. NELON-2

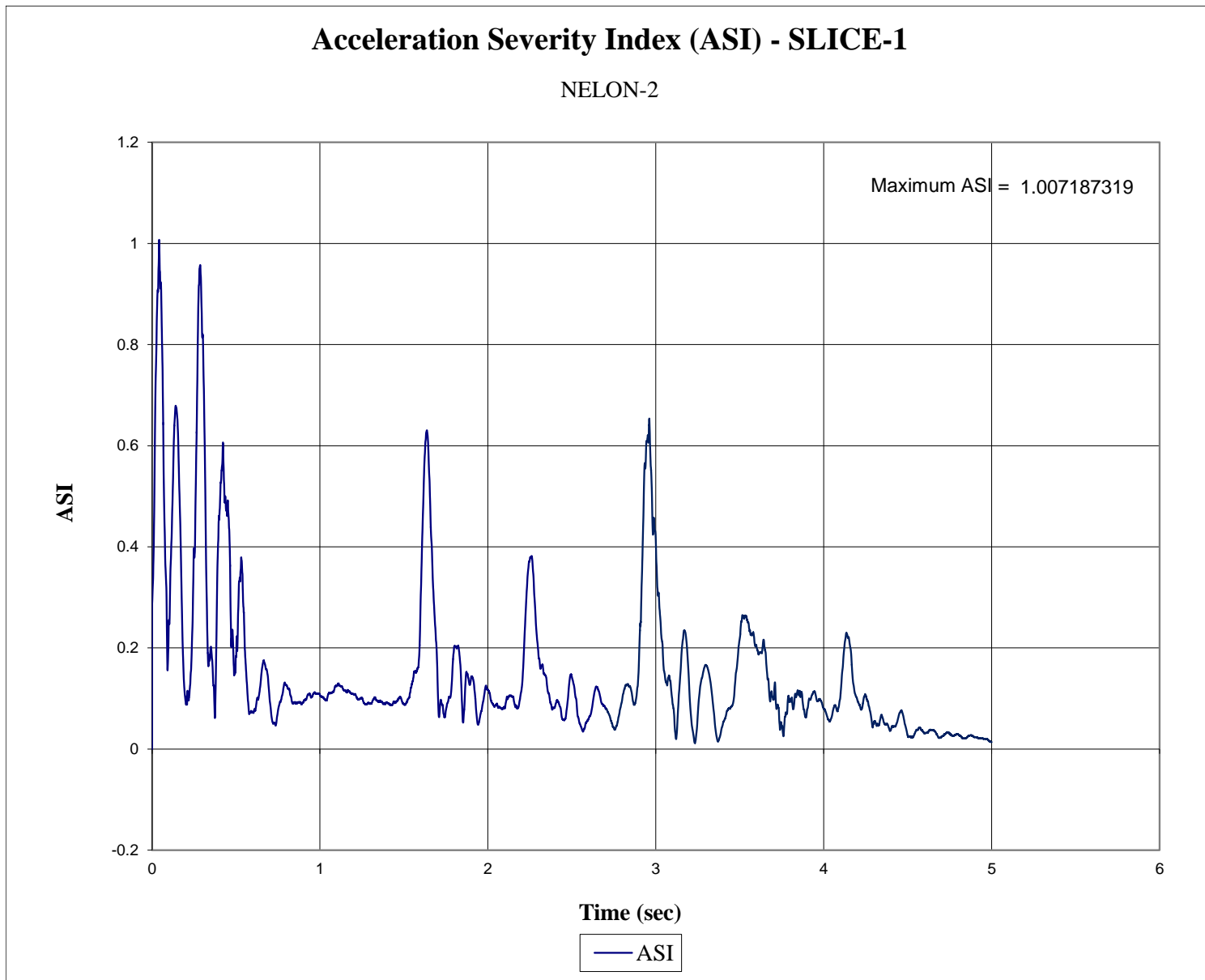


Figure E-8. Acceleration Severity Index (SLICE-1), Test No. NELON-2

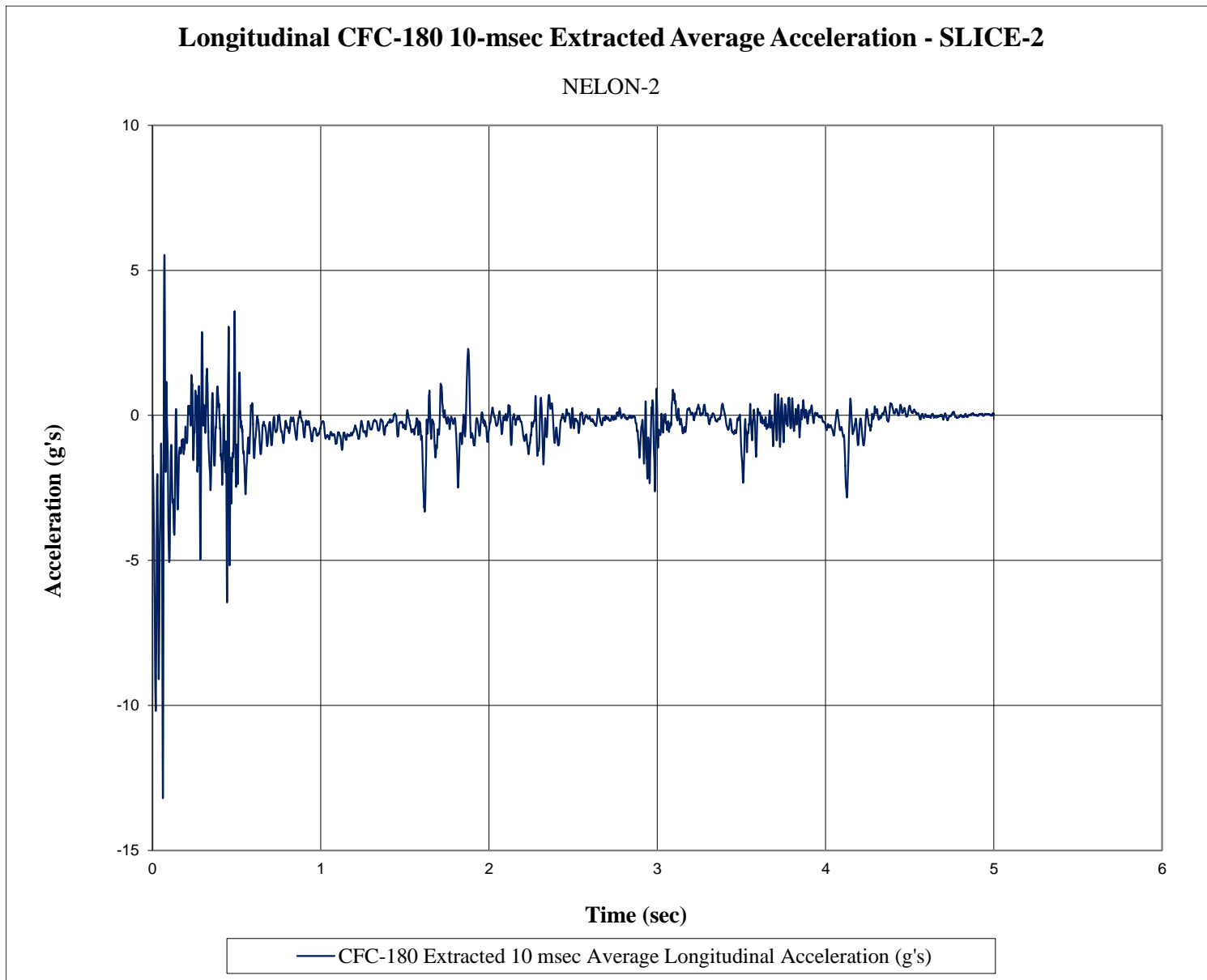


Figure E-9. 10-ms Average Longitudinal Deceleration (SLICE-2), Test No. NELON-2

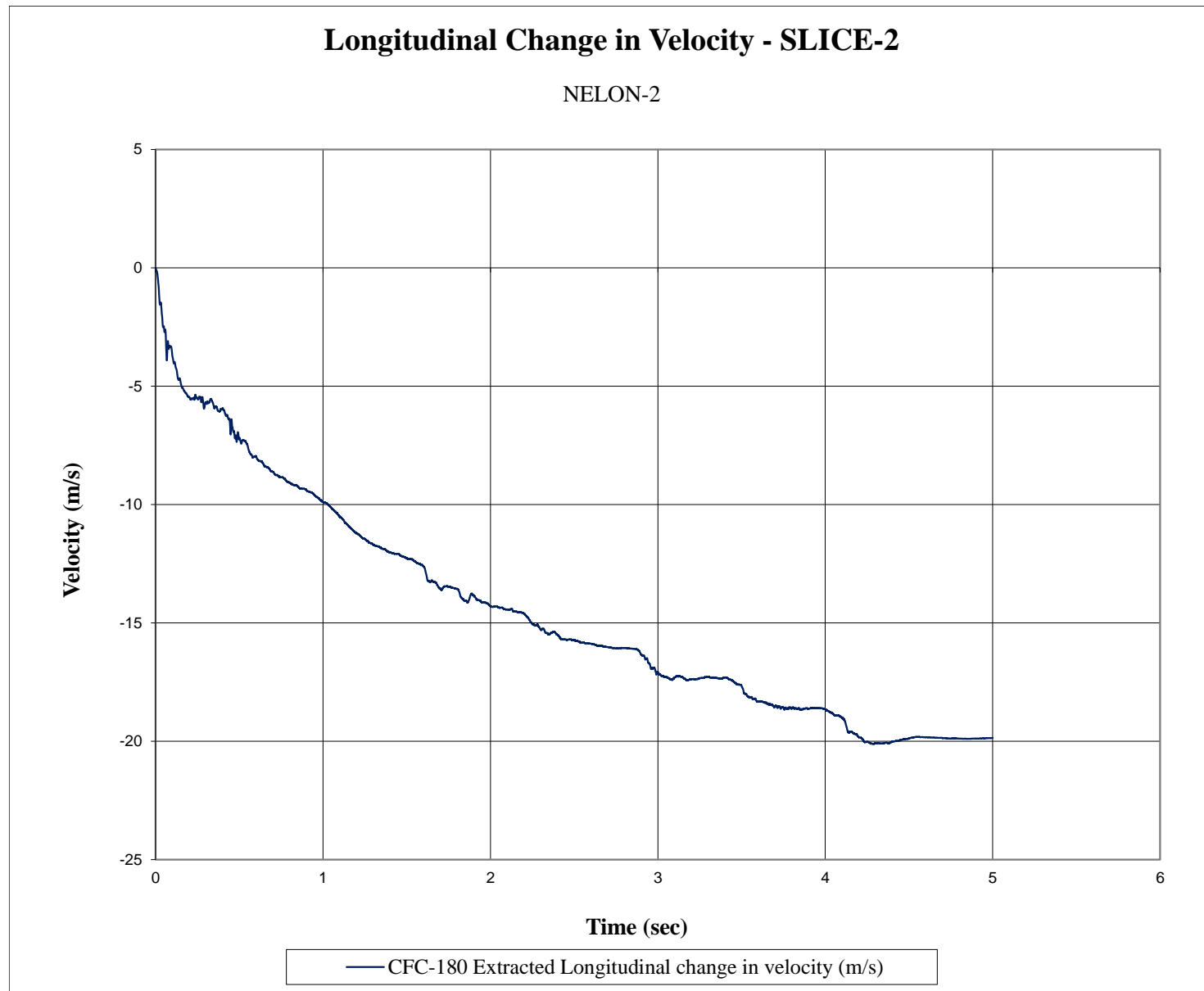


Figure E-10. Longitudinal Occupant Impact Velocity (SLICE-2), Test No. NELON-2

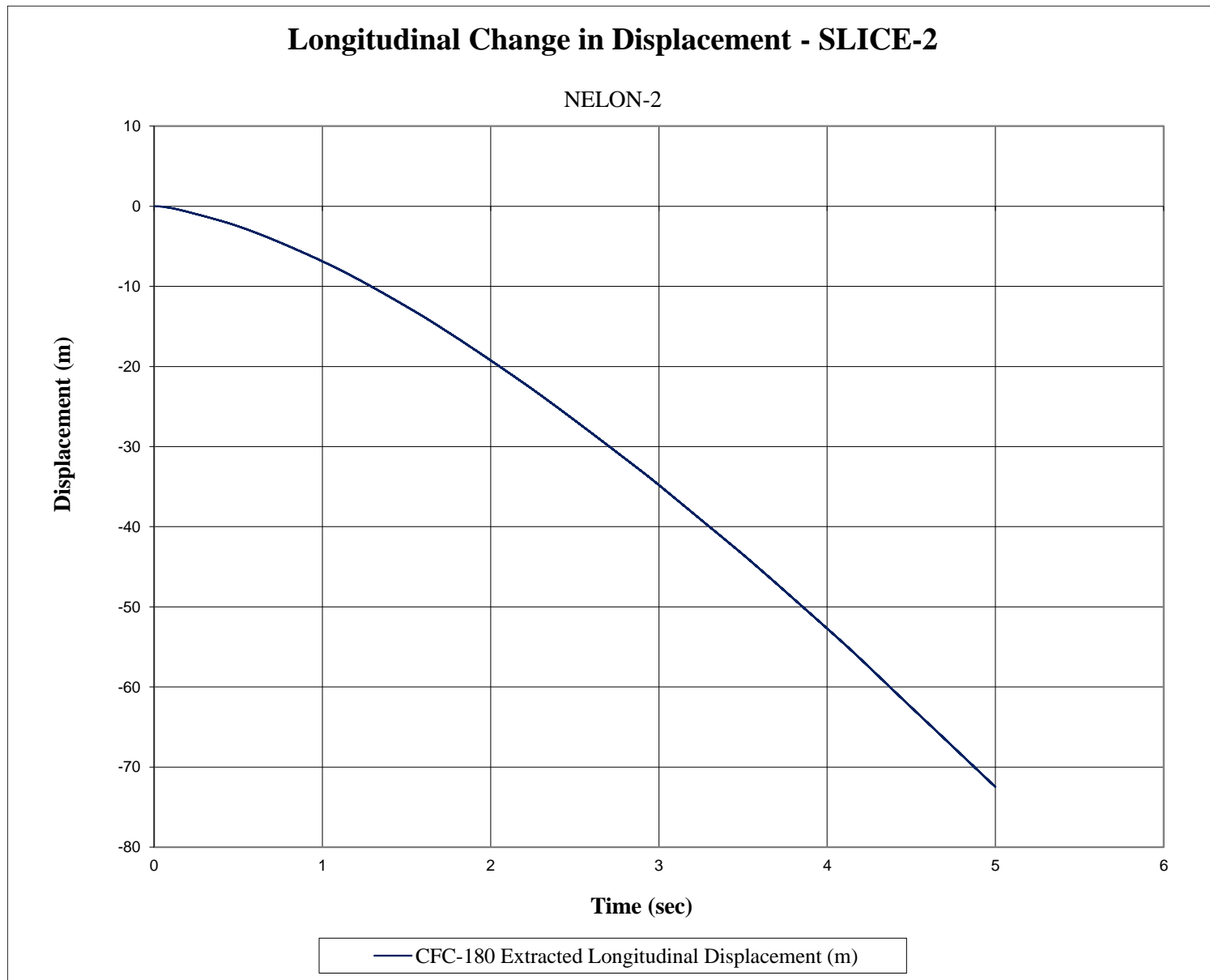


Figure E-11. Longitudinal Occupant Displacement (SLICE-2), Test No. NELON-2

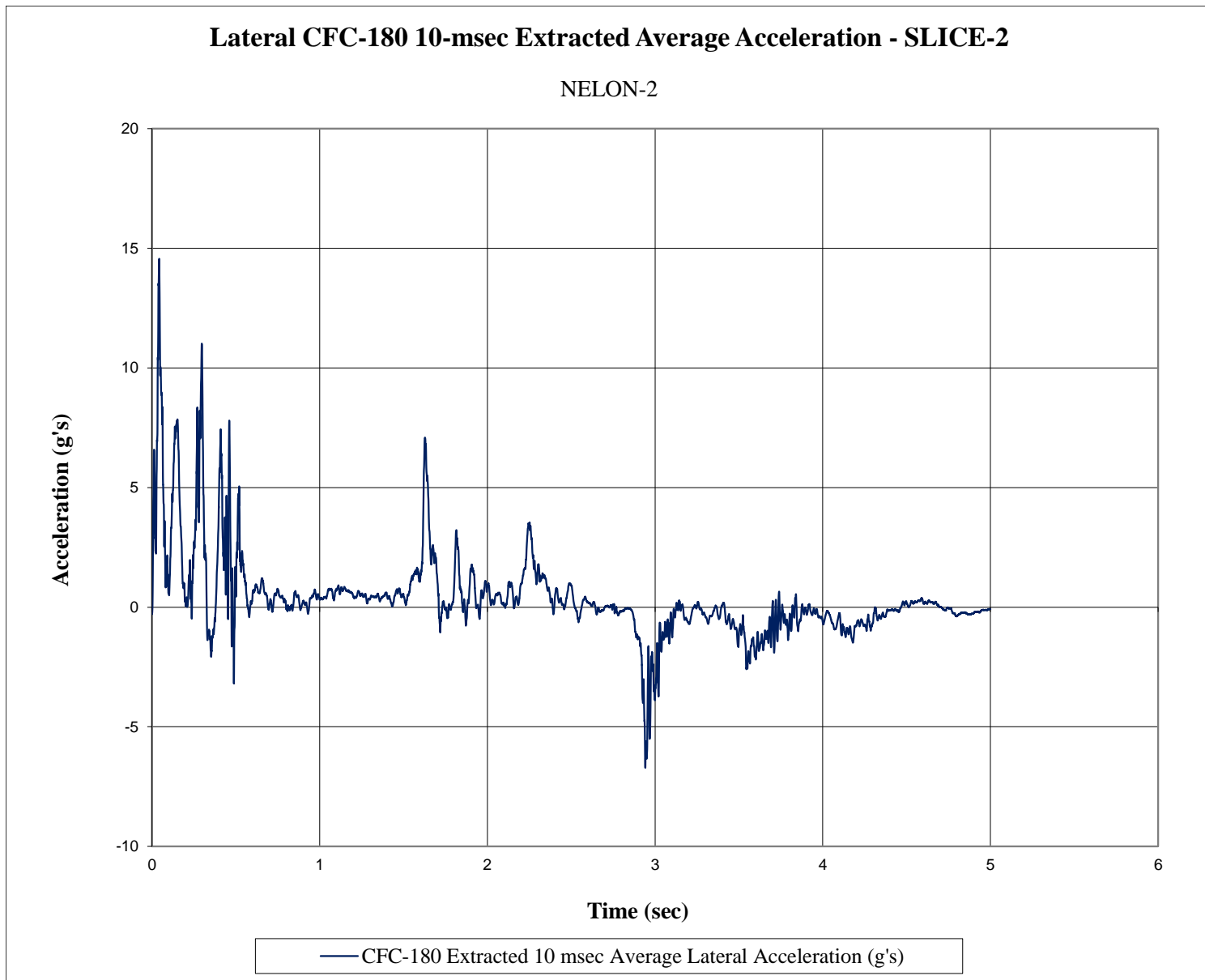


Figure E-12. 10-ms Average Lateral Deceleration (SLICE-2), Test No. NELON-2

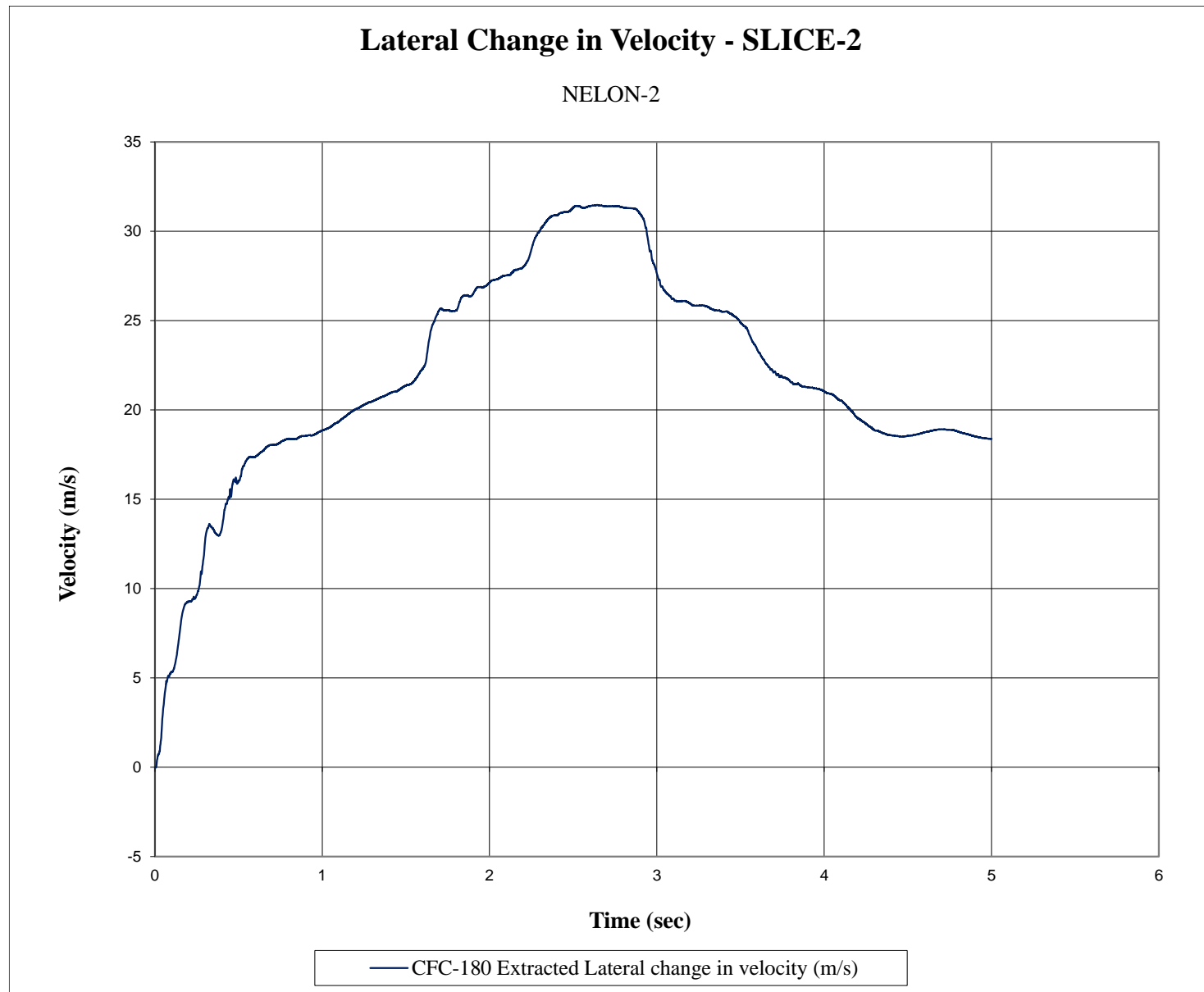


Figure E-13. Lateral Occupant Impact Velocity (SLICE-2), Test No. NELON-2

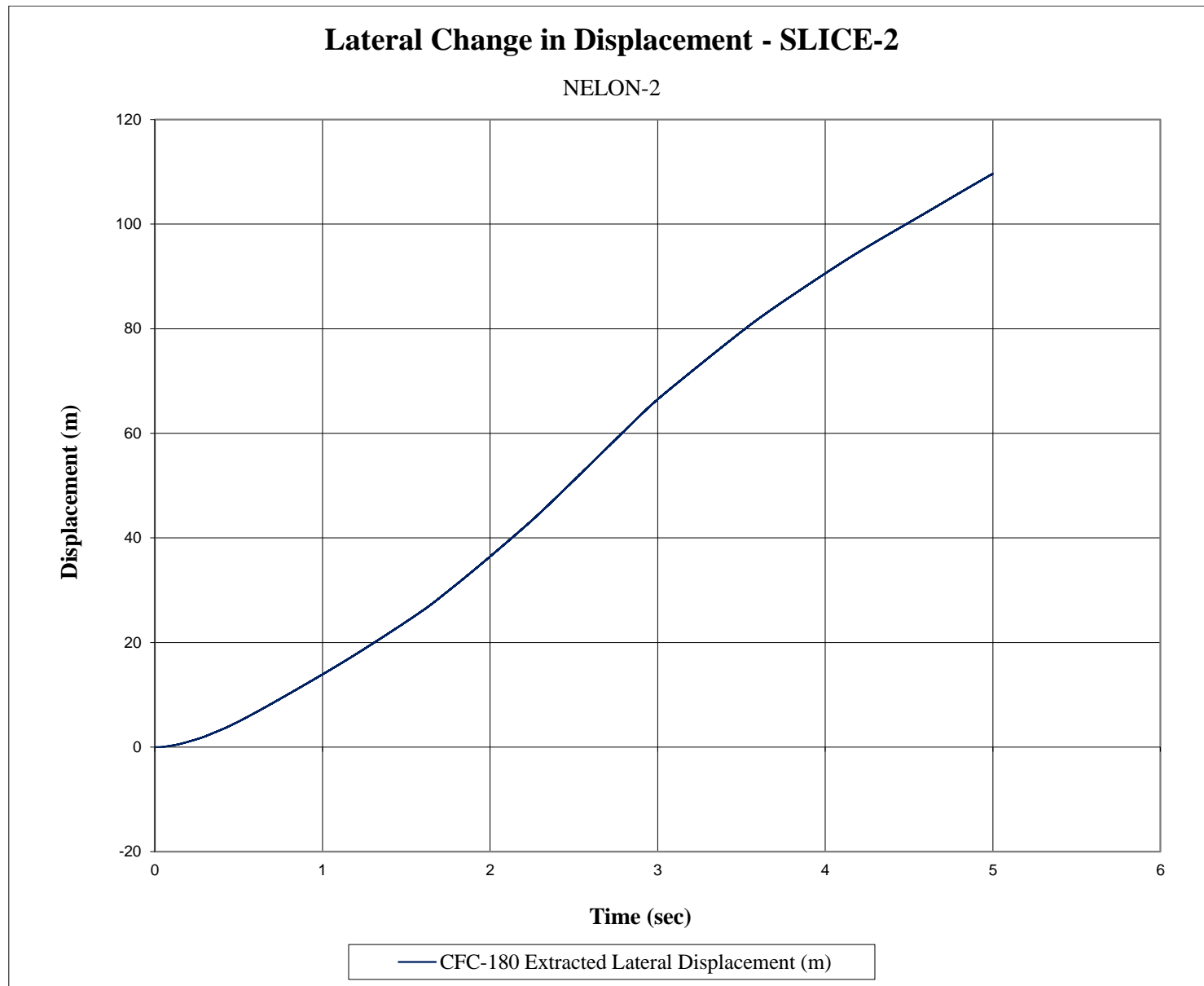


Figure E-14. Lateral Occupant Displacement (SLICE-2), Test No. NELON-2

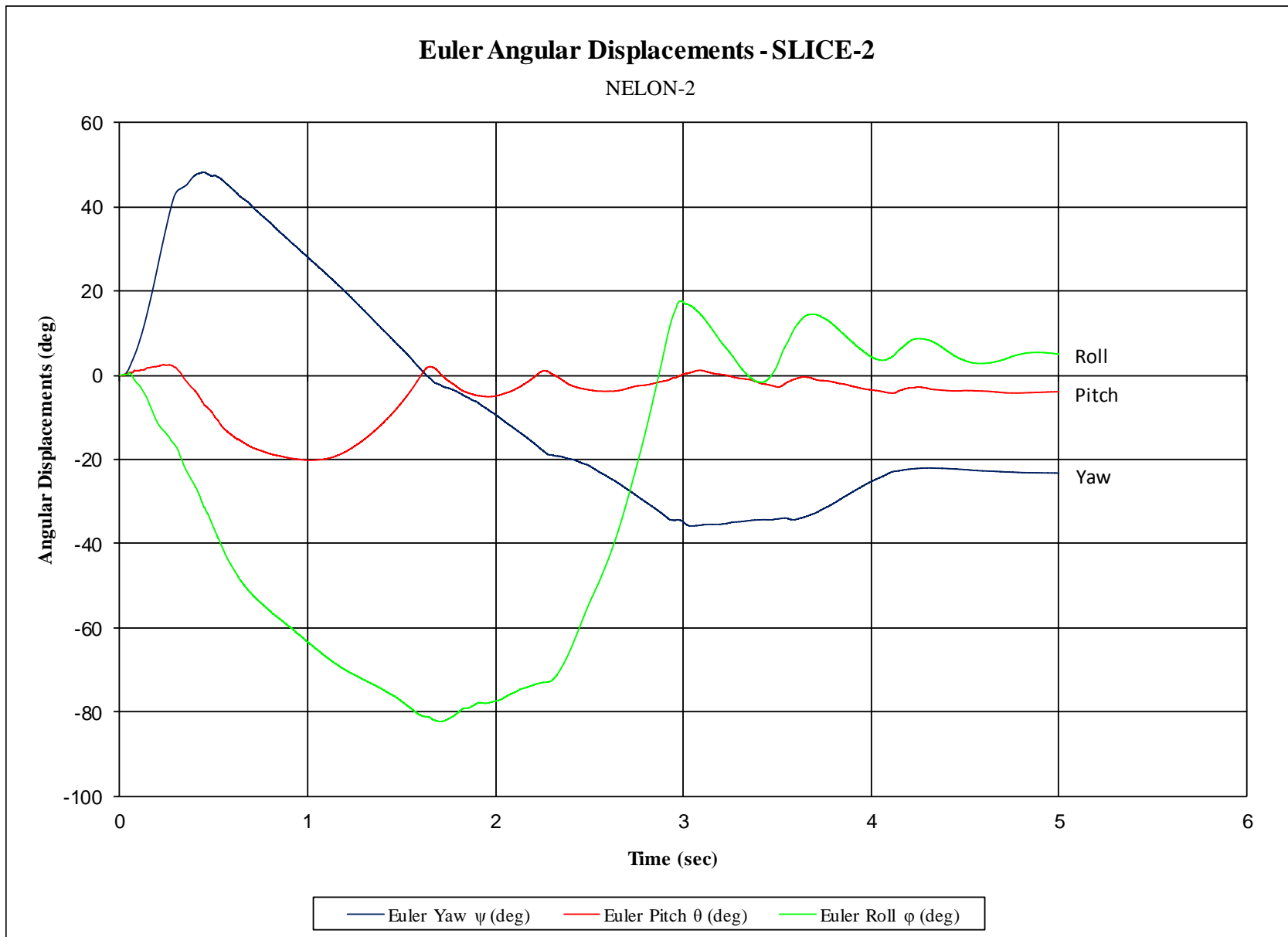


Figure E-15. Vehicle Angular Displacements (SLICE-2), Test No. NELON-2

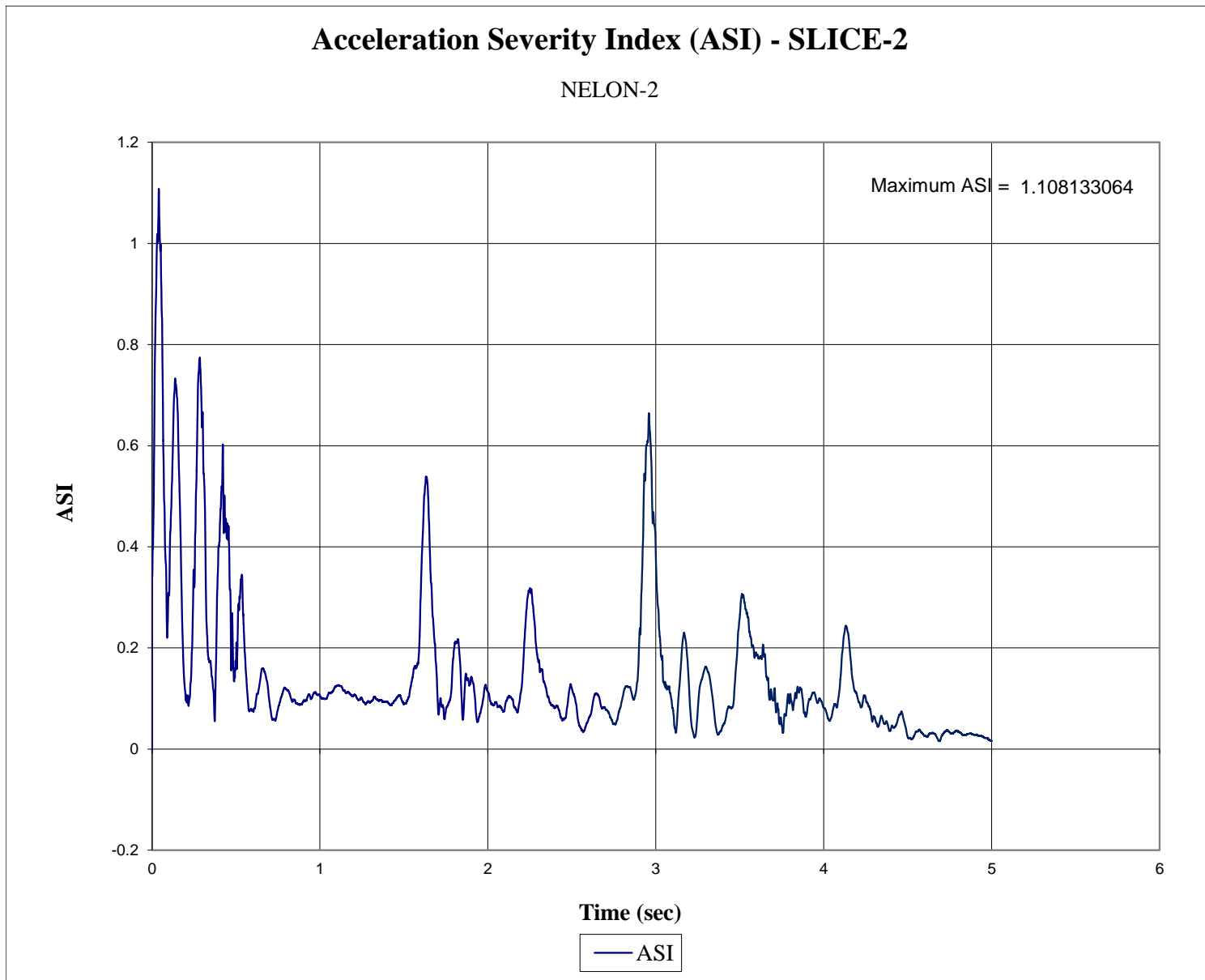


Figure E-16. Acceleration Severity Index (SLICE-2), Test No. NELON-2

END OF DOCUMENT